Coupling Fluid Temperature Control and Passive Cavitation Detection During Skin Sonoporation

Jeremy Robertson

Supervised by Dr Sid Becker

Submitted in partial fulfilment of the requirements of the degree of

Doctor of Philosophy in Mechanical Engineering

September 2018

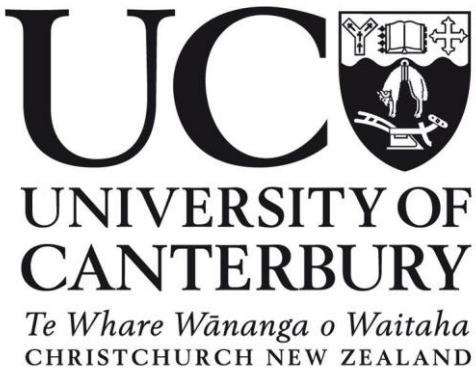

Acknowledgements

Dr Sid Becker – For making it all possible.

Dr Marie Squire – For being the most helpful person I have ever met.

Bradley Boyd – For the healthy distraction and collaboration.

Dr Nataša Pavšelj – For the helpful feedback and expert knowledge.

Mum – For being there. For setting the standard.

Dad – For being there. For understanding.

Charlotte – For being there (from 12,000 miles away).

Sarah – For being there. For the happy journal.

T & D – For the encouragement and support from where I'd rather be.

Claire – For being there.

Stacey – For being there.

Lewis – For being there.

Dr Barbara Zorec – For teaching me all there is to know about pig skin.

All my other friends and family – For being there and taking an interest.

N.T. – For the heavy.

UC Mechanical Engineering technical staff – For answering all of my silly questions.

UC Bioengineering postgrads – For the healthy distraction.

UC Chemistry staff – For allowing an engineer in your midst.

The staff at Ashburton Meat Processors – For the lovely fresh pigs' ears.

"When a book is finished it looks so orderly, and it looks like it was always the way it is. But of course there were so many dead ends, and there's so much on the cutting room floor."

Eleanor Catton

Abstract

Skin sonoporation refers to the creation of aqueous pathways in the stratum corneum with ultrasound. The mechanism responsible for the permeability increase that arises from sonoporation is inertial cavitation – the formation and collapse of gaseous cavities in the coupling fluid. *In vitro* skin sonoporation experiments are usually conducted in Franz diffusion cells – an apparatus designed for passive transdermal transport experiments. During skin sonoporation, the temperature of the coupling fluid often increases to a level which can cause burns. To mitigate temperature increases, previous studies have relied on duty cycles and replacement of the coupling fluid during ultrasound application. Reliance on these two methods has resulted in sonoporation protocols that are not clinically applicable: when using a duty cycle, 12 minutes of ultrasound can take up to 2 hours to administer; while coupling fluid replacement requires constant monitoring and disruptive manual intervention. This thesis introduces a circulation system which enables the coupling fluid to be set and maintained at a specified, safe temperature during continuous ultrasound application. With this new technology, duty cycles and fluid replacement are no longer required during *in vitro*, *in vivo* or clinical sonoporation. Using the temperature control system, a series of experiments were conducted to investigate the influence of coupling fluid temperature on post-sonoporation transport. Although the inertial cavitation activity decreased, the post-sonoporation transport increased as the specified coupling fluid temperature increased.

In other therapeutic ultrasound systems, passive cavitation detectors (PCDs) are used to monitor inertial cavitation activity (the main mechanism of permeability increase) to ensure it remains at the desired level during ultrasound application. Passive cavitation detectors

cannot be used to effectively monitor inertial cavitation activity in standard Franz diffusion cells as the donor chambers are too small to incorporate a transducer and hydrophone during sonoporation. Researchers have therefore had to assume that, for a given intensity, inertial cavitation activity always remains constant during ultrasound application. A modified diffusion cell setup that incorporates a transducer and PCD hydrophone during sonoporation is introduced. The PCD output was shown to increase with increasing ultrasound intensity (as inertial cavitation does) and decrease with increasing coupling fluid temperature (as inertial cavitation was shown to do). It can be concluded from these results that a PCD positioned in the coupling fluid can be used to monitor the inertial cavitation activity which occurs during skin sonoporation. Applying this system to clinical setups will be of great benefit as it will enable any changes in inertial cavitation activity to be detected and counteracted in real-time.

Acoustic reflections have been shown to significantly influence the ultrasound fields in cell sonoporation setups. The influence of acoustic reflection on the ultrasound field during skin sonoporation has not been investigated. A modified Franz diffusion cell setup was manufactured which allowed for passive measurement of the inertial cavitation at the skin aperture during sonoporation (with and without the suppression of reflections). When acoustic reflection was suppressed, the inertial cavitation dose (ICD) was lower than when the reflection was not supressed. It can be concluded from this result that the acoustic reflections within a low-frequency sonoporation setup can influence the inertial cavitation activity which occurs during ultrasound application. Therefore, for a given set input parameters, the same inertial cavitation activity that was obtained *in vitro* is not guaranteed in an *in vivo* or clinical scenario, due to differences in echoic conditions.

Forward

Chapter 1 contains the introduction which has two sections: Background, and Gaps in the Field and Thesis Objectives. Chapter 2 introduces a novel coupling fluid temperature control system developed specifically for sonoporation in Franz diffusion cells. The system enables the coupling fluid to be set and maintained at a specified temperature during continuous sonoporation. Chapter 3 introduces a passive cavitation detector (PCD) system capable of measuring the broadband noise emission that occurs during skin sonoporation in a Franz diffusion cell. Chapter 4 reports an investigation into the influence of acoustic reflection during ultrasound application in a Franz diffusion cell. Chapter 5 summarises the overall conclusions of the thesis and Chapter 6 suggests future work.

Two significant appendices are included in this thesis. Appendix A reports an initial attempt to employ both coupling fluid temperature control and a PCD during skin sonoporation. This was the first known study in which skin permeability (quantified by measuring caffeine transport with HPLC) was increased with ultrasound while the coupling fluid was circulated and cooled, a significant contribution to the field. The time saved by not needing to use duty cycles or fluid replacement meant that a full 10 repetitions could be run for each of the transport datasets – more than most previous studies have found it feasible to run. The work reported in Appendix A was vital in the development of the improved temperature control and PCD systems used in Chapters 2 and 3.

Appendix B reports an investigation conducted to find a combination of experimental parameters appropriate for the coupling fluid temperature study in Chapter 2. Appendix B also contains a demonstration of the novel temperature control system's ability to maintain a constant coupling fluid temperature during a long (30 minute) continuous application of ultrasound – another significant contribution to the field. The mean post-sonoporation calcein transport achieved with 30 minutes of sonoporation was almost twice that achieved with 10 minutes. Given this positive relationship between application time and transport, future researchers and clinicians will find it beneficial to use long application times. With the temperature control system, duty cycles and fluid replacement are no longer required. Therefore, it is now possible to apply long durations (≥30 minutes) of ultrasound in a reasonable, clinically practical time.

A list of completed conference and journal publications is provided at the end of the thesis, along with a list of journal papers in preparation. A full length journal paper based on the findings of Chapter 4 has been published already (in the Journal of Ultrasound in Medicine and Biology). A full length journal paper based off of the findings of Chapter 2 is under review (by the Journal of Ultrasound in Medicine and Biology). Three additional full length journal papers based off of the findings in Chapter 3, Appendix A, and Appendix B are in preparation.

Table of Contents

List of Figures

List of Tables

Abbreviations

SC	Stratum corneum
TDD	Transdermal drug delivery
HIFU	High-intensity focussed ultrasound
PCD	Passive cavitation detector
ICD	Inertial cavitation dose
HPLC	High-performance liquid chromatography

Nomenclature

I	Ultrasound intensity
m	Mass of water
C_p	Specific heat of water
A	Area of transducer face
T	Temperature
t	Time

L	Near field length
D	Transducer diameter
λ	Wavelength
C	Adjusted concentration
C_{RAW}	Measured concentration
V_{sample}	Sample volume
$V_{receiver}$	Receiver chamber volume
S	Sample number
I_S	Spectrofluorometer intensity
R	Reflection coefficient
Z_1	Acoustic impedance (material 1)
Z_2	Acoustic impedance (material 2)
N_{BL}	Baseline noise level
μ	Mean value of the noise floor
σ	Standard deviation of the noise floor
C_{CAF}	Caffeine concentration
A_C	Chromatogram peak area

1 Introduction

1.1 Background

1.1.1 Transdermal Drug Delivery

In transdermal drug delivery (TDD), a topically applied drug permeant diffuses through the skin before being absorbed into the bloodstream. The outermost layer of the skin, the stratum corneum (SC), is the greatest contributor to the skin's barrier function. Therefore, it is the permeability of the SC that dictates the rate at which topical permeants can diffuse through the skin (Becker, et al. 2014, Bommannan, et al. 1990, Marjukka Suhonen, et al. 1999, Tezel, et al. 2003b, Trommer and Neubert 2006). The SC is composed of flat Keratin fibre husks embedded in lipid layers which are arranged in lamellar sheets (Harding 2004, Menon, et al. 2012, Mitragotri, et al. 1996). Most transdermal transport of lipophilic solutes occurs through the SC space occupied by the lipid structures (Barry 2001, Kirjavainen, et al. 1999, Ogiso, et al. 1998, Prausnitz, et al. 2004), however, these lipid bilayers are a formidable barrier to any substances with molecular weights above 500 Da (Paliwal, et al. 2006). Despite the barrier presented by the SC, transdermal drug delivery is an attractive delivery method as there are no significant first pass metabolism effects from the liver, there is no pain during delivery, no chance of disease transmission by needle sharing, patients can self-administer, and a slow release of drugs is easily achieved (Boucaud, et al. 2001, Prausnitz and Langer 2008). There has been success with a number of commercialised passive TDD products for substances such as Fentanyl (for pain management) and Nicotine (Prausnitz and Langer 2008). However, techniques to temporarily increase the SC permeability must be developed if TDD is to

become a realistic delivery method for substances that do not diffuse passively. Researchers have used a variety of techniques to actively increase the permeability of the SC to transdermal transport by diffusion. These techniques have employed electric fields (Kost, et al. 1996, Prausnitz 1999, Wong, et al. 2006, Zorec, et al. 2013), ultrasound (Boucaud, et al. 2001, Cancel, et al. 2004, Johnson, et al. 1996, Park, et al. 2010, Tang, et al. 2001, Zorec, et al. 2015), chemical enhancement (Benson 2005, Lee, et al. 2010, Pathan and Setty 2009, Seto, et al. 2010), and microneedles (Chen, et al. 2010, Henry, et al. 1998b, Lanke, et al. 2009, Prausnitz and Langer 2008). This thesis is concerned with the application of ultrasound to the skin.

1.1.2 Ultrasound Enhanced Transdermal Drug Delivery

Under certain conditions, the application of ultrasound has been shown to enhance transdermal transport (Boucaud, et al. 2002, Cevc 1997, Kushner, et al. 2004, Lee, et al. 2004a, Lee, et al. 2004b, Mitragotri, et al. 1995a, Mitragotri and Kost 2004, Tachibana and Tachibana 1991, Tezel, et al. 2005). Ultrasound enhanced TDD can be classified into two categories (Ogura, et al. 2008): sonophoresis and sonoporation. In a sonophoresis experiment the ultrasound field and the permeant are applied to the skin simultaneously (Lee, et al. 2010, Merino, et al. 2003, Mitragotri, et al. 1996, Morimoto, et al. 2005, Polat, et al. 2012). Sonophoresis is thought to not only increase the skin permeability (due to structural alterations in the SC), but also enhance the permeant diffusion by convection (Mitragotri and Kost 2004). This thesis focuses on low-frequency (20 kHz to 100 kHz) sonoporation (also referred to as pre-treatment sonophoresis), which Zorec, et al. (2015) described as “the creation of aqueous pathways in the SC as a result of ultrasound application.” In a sonoporation experiment, ultrasound is applied to the skin for a set period of time to increase

its permeability. The ultrasound transducer is then removed and a permeant solution is applied to the temporarily permeabilized skin.

1.1.3 The Mechanism Behind Ultrasound Enhancement

Ultrasound intensity is defined as the ultrasonic power flowing through a unit area normal to the direction of propagation (O'Brien Jr 2007). When a threshold intensity is reached in an ultrasound field, cavitation nuclei in the coupling fluid (the medium between the transducer and skin) grow to form cavitation bubbles which then violently collapse upon compression (Helga, et al. 2015, Mitragotri and Kost 2004). This formation and violent collapse of bubbles is termed inertial cavitation (Chang, et al. 2001, Gaitan, et al. 1992, Lai, et al. 2006, Lawrie, et al. 2000, Miller 2007, Mitragotri and Kost 2004). The aggregate of all of the inertial cavitation collapses which occur in an ultrasound field is termed the inertial cavitation activity – the more collapse events that occur, the greater the inertial cavitation activity. Researchers have established that this inertial cavitation activity is the mechanism behind the skin permeability enhancement that occurs during ultrasound application (Alvarez-Román, et al. 2003, Lee, et al. 2010, Mitragotri, et al. 1995b, Tang, et al. 2002a, Tezel and Mitragotri 2003a, Tezel, et al. 2002, Tezel, et al. 2001, Ueda, et al. 2009, Ueda, et al. 1996, Wu, et al. 1998). When a cavitation bubble is far away from a solid boundary its collapse is symmetrical (Mitragotri and Kost 2004). When a bubble collapses near the skin surface, the movement of the portion of the bubble nearest to the skin is restricted, while the unrestricted portion of the bubble continues to collapse towards the skin. This results in an asymmetric collapse and the formation of a high-speed liquid jet (known as a micro jet) in the direction of the skin (Boyd and Becker 2018, Lauterborn and Ohl 1997, Tezel and Mitragotri 2003a, Wolloch and Kost 2010). These micro jets are thought to disrupt the SC structure by removing some portion of

the lipids and introducing defects to the lipid lamellae (Dahlan, et al. 2009, Mitragotri and Kost 2004, Smith 2007). Disruption of these lipid bilayers is known to result in an increase in skin permeability (Francoeur, et al. 1990, Gay, et al. 1994, Golden, et al. 1986, Potts and Francoeur 1990, Potts, et al. 1991). Cavitation induced lipid disruption was demonstrated in the study by Alvarez-Román, et al. (2003) which found, using infrared spectroscopy, that approximately 30 % of the intercellular lipids of the SC were removed during 20 kHz ultrasound application at an intensity of 15 W/cm^2 (the transducer was 5 mm from the skin and ultrasound was applied for 2 hours using a 10 % duty cycle). Similarly, Lee, et al. (2010) used a postfixation method to show that discrete elongated defects appeared in the lipid lamellae during 5 minutes of continuous ultrasound application at 0.8 W/cm^2 and 25 kHz. Lipid disruption was also demonstrated by Ueda, et al. (1996) who found that the leaching of lipids from the SC increased with increasing ultrasound application time (for a frequency of 150 kHz and an intensity of 0.11 W/cm^2).

Cavitation induced increases in skin permeability can be visualised by applying red dye to the skin after ultrasound application. As the amount of dye absorbed by the skin is dependent on the permeability – the areas which appear redder are known to be more permeable. These areas of increased permeability are known as local transport regions (LTRs) (Kushner, et al. 2008). By using this dye method, a number of studies have shown that post-ultrasound LTR formation is heterogeneous across the skin surface (Kushner, et al. 2008, Morimoto, et al. 2005, Schoellhammer 2015).

Tang, et al. (2002a) effectively demonstrated the importance of inertial cavitation to skin sonoporation by changing the coupling fluid from a low viscosity buffer solution to high

viscosity castor oil (thereby supressing cavitation). This suppression decreased permeability enhancement (the ratio of post-sonoporation skin permeability to pre-sonoporation skin permeability) by almost 100 %. In that study the frequency was 20 kHz, the intensity was 1.6 W/cm^2, the transducer was 8 mm from the skin and ultrasound was applied for 2 hours using a 10 % duty cycle.

1.1.4 *In vitro* Experimentation

Experimental studies that investigate the effects of low-frequency ultrasound on skin permeability have nearly always used glass Franz diffusion cells (Baji, et al. 2018, Han and Das 2013, Herwadkar, et al. 2012, Lavon, et al. 2005, Le, et al. 2000, Merino, et al. 2003, Mitragotri, et al. 2000a, Paliwal, et al. 2006, Rangsimawong, et al. 2018, Sarheed and Abdul Rasool 2011, Sarheed and Frum 2012, Smith, et al. 2003, Tang, et al. 2002a, Terahara, et al. 2002a, Terahara, et al. 2002b, Tezel and Mitragotri 2003a, Tezel, et al. 2001, Yin, et al. 2016). These consist of a donor and receiver chamber, clamped together with a skin sample in between. A cross-section of a standard Franz diffusion cell is shown in Fig. 1-1. Images of standard Franz diffusion cells are shown in Fig. 1-2. An ultrasound transducer is inserted into the donor chamber with the active face a set distance from the skin surface and parallel to the skin surface. The donor chamber fluid acts as the coupling fluid. The ultrasound waves propagate through this coupling fluid from the transducer to the skin.

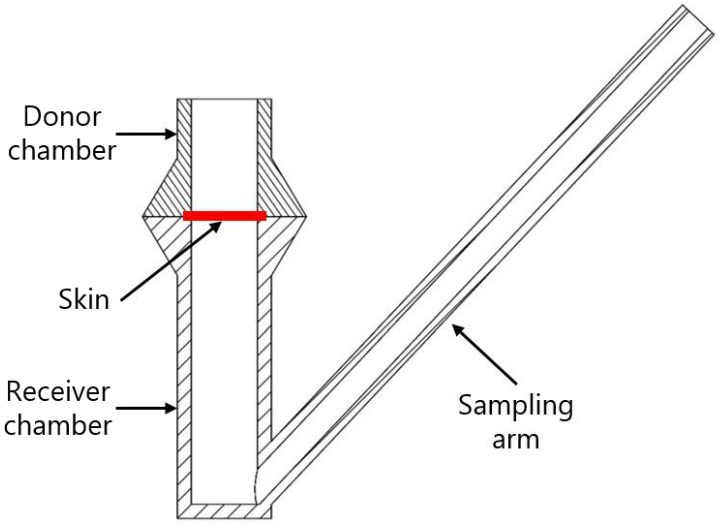

Fig. 1-1 Cross-section of a standard Franz diffusion cell

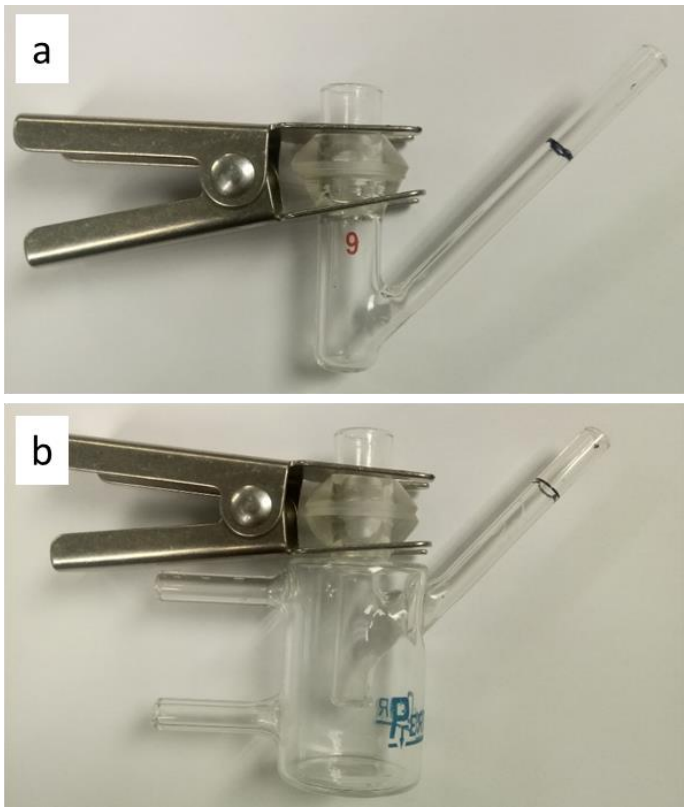

Fig. 1-2 Images of standard glass Franz diffusion cells (a) without receiver chamber water jacket and (b) with receiver chamber water jacket

Two methods are used to quantify the permeability increase achieved through ultrasound application in a diffusion cell: mass transport experiments, and electrical conductivity

experiments. In mass transport experiments a permeant molecule is added to the donor solution in some known concentration. The concentration of the permeant in the receiver solution is then measured to determine the amount that has diffused through the skin over a certain time period. The greater the concentration of the permeant in the receiver chamber after ultrasound application, relative to a control case without ultrasound, the greater the skin permeability increase achieved. Past studies have used permeants such as mannitol (Merino, et al. 2003, Mitragotri, et al. 2000a, Terahara, et al. 2002a, Terahara, et al. 2002b), glucose (Schoellhammer, et al. 2012), caffeine (Sarheed and Abdul Rasool 2011), ketoprofen (Herwadkar, et al. 2012), calcein (Lavon, et al. 2005), and bovine serum albumin (Han and Das 2013). Receiver chamber concentrations have been measured with techniques such as scintillation counting (Merino, et al. 2003, Mitragotri, et al. 2000a, Schoellhammer, et al. 2012, Terahara, et al. 2002a, Terahara, et al. 2002b), high-performance liquid chromatography (Han and Das 2013, Herwadkar, et al. 2012, Sarheed and Abdul Rasool 2011), and spectrophotometry (Lavon, et al. 2005).

Electrical conductivity experiments require less time than mass transport experiments as the skin's electrical properties may be immediately measured so that no lengthy transport diffusion times are required (Tezel, et al. 2001). Electrodes are placed into the donor and receiver chambers and an AC current is passed from one electrode, through the skin, to the other electrode. A conductivity value is then calculated from the measured current and the input voltage. Skin electrical conductivity can be used as a proxy for skin permeability as conductivity has been shown to increase with increasing permeability (Mitragotri, et al. 2000a). As this conductivity increase can be measured instantaneously (without having to wait for drug diffusion), it is often used as the measured variable in empirical studies

(Mitragotri, et al. 2000a, Tang, et al. 2002b, Terahara, et al. 2002a, Tezel, et al. 2001). However, the frequent use of electrical conductivity instead of mass transport has resulted in a relative scarcity of actual permeability data (Sarheed and Abdul Rasool 2011), which can only be obtained with mass transport experiments.

Previous sonoporation studies have used Franz diffusion cells to investigate the influences of five main experimental parameters on inertial cavitation activity and the permeability enhancement achieved. In their sonoporation study, Tezel, et al. (2002) investigated the influence of ultrasound frequency on skin conductivity enhancement (the ratio of post-sonoporation conductivity to pre-sonoporation conductivity). The conductivity enhancement achieved at 19.6 kHz was 3 times that achieved at 36.9 kHz and 23 times that achieved at 93.4 kHz. These results show that skin conductivity enhancement, an established proxy for permeability enhancement, increases with decreasing ultrasound frequency. Decreases in skin permeability enhancement with increasing ultrasound frequency were also shown by Tezel, et al. (2001), using electrical conductivity, and Merino, et al. (2003), using mass transport.

In their skin sonoporation study, Terahara, et al. (2002a) investigated the influence of ultrasound pre-treatment time on skin conductivity enhancement and mannitol permeability enhancement. Relative to its pre-sonoporation value, the mean conductivity increased 3-fold after 3 minutes of ultrasound application and 25-fold after 12 minutes of application. Likewise, the mean mannitol permeability increased 8-fold after 3 minutes of sonoporation and 14-fold after 12 minutes. These results indicate that skin permeability enhancement

increases with increasing exposure time. A similar result was found in the study by Mitragotri, et al. (2000a).

Herwadkar, et al. (2012) investigated the influence of duty cycle on the transdermal delivery of ketoprofen in their low-frequency study. They applied ultrasound at an intensity of 6.9 W/cm^2 with a duty cycle of either 100 *%* or 50 *%* (5 s on 5 s off). The total application time was the same for both duty cycles, meaning that the 100 *%* case took 2 minutes and the 50 *%* case took 4 minutes. There was a negligible difference in transdermal ketoprofen delivery between the two cases, meaning that duty cycle does not affect skin permeability increase. Similarly, Mitragotri, et al. (2000a) showed that, for a given total application time, the duty cycle does not affect the number of inertial cavitation events which occur at the skin aperture.

Terahara, et al. (2002a) showed that increasing the axial distance from the active face of the transducer to the skin surface decreases the electrical conductivity enhancement achieved. The conductivity enhancement achieved when the transducer was 2.5 mm from the skin surface was 3.5 times that achieved when it was 10 mm from the skin surface. In their low-frequency study, Herwadkar, et al. (2012) measured the transdermal delivery of Ketoprofen following 2 minutes of ultrasound application. They found that the transdermal transport was over 5 times greater following sonoporation at 0.3 cm than it was following sonoporation at 0.6 cm. From these results in can be concluded that permeability enhancement decreases as the transducer to skin distance increases.

In their low-frequency skin study, Tezel, et al. (2001) showed that the skin conductivity enhancement achieved with ultrasound increases with increasing ultrasound intensity if all other parameters remain constant. The skin conductivity was measured after insonation

(exposure to ultrasound) at five different frequencies. The conductivity enhancement increased as intensity increased, regardless of the frequency. Using a frequency of 58.9 kHz, the conductivity enhancement achieved at 1.3 W/cm^2 was 2.5 times that achieved at 0.8 W/cm^2. Increases in skin permeability enhancement with increasing intensity were also reported in the sonoporation studies by Tang, et al. (2002a) and Mitragotri, et al. (2000a).

Nearly all of the aforementioned sonoporation studies used off-the-shelf, glass Franz diffusion cells. These apparatus are regularly used because they are ready-made in standard sizes, easily obtainable, and are the established norm for transdermal experiments. However, in their sonoporation study, Zorec, et al. (2015) noted that, although Franz diffusion cells are considered the gold standard in passive diffusion studies, they are not ideal for studies which employ enhancement methods such as electroporation or sonoporation. Due to their glass construction, the geometry of standard Franz diffusion cells are difficult to customise without expensive glassblowing techniques and equipment. The difficulties associated with customising the geometry of standard glass Franz diffusion cells have made it impractical for sonoporation studies to incorporate custom systems for temperature control, cavitation monitoring, or the suppression of acoustic reflection – useful features which have been effectively incorporated into cell sonoporation and ultrasound ablation setups (Farny, et al. 2010, Hallow, et al. 2006, Hockham, et al. 2010, Kinoshita and Hynynen 2007, Montes and Hynynen 1995). The motivations behind incorporating systems for temperature control, passive cavitation monitoring, and the suppression of acoustic reflection in a sonoporation setup are discussed next.

1.2 Gaps in the Field and Thesis Objectives

1.2.1 The Problem of Coupling Fluid Temperature Increase During Sonoporation

When skin is sonoporated in a Franz diffusion cell, the donor chamber fluid acts as the coupling fluid. When the ultrasound waves travel through the coupling fluid a fraction of their energy is absorbed and converted to heat (Bacon and Carstensen 1990, O'Brien Jr 2007). At sufficiently high transducer induced pressure amplitudes, this heating may result in a significant, unwanted increase in the coupling fluid temperature (Tang, et al. 2002a, Terahara, et al. 2002a). Increases in coupling fluid temperature must be mitigated to maintain clinically relevant *in vitro* conditions: significant discomfort and blistering can occur when the skin is exposed to temperatures above 43 °C (Hao, et al. 2016, Lindeque, et al. 2013), while prolonged exposure to 44 °C has been shown to cause irreversible damage to epidermal cells (Moritz and Henriques 1947). Furthermore, second degree burns can occur within 4 minutes of the skin temperature reaching 51 °C (Williamson and Scholtz 1949).

In addition to causing burns and discomfort, increases in the temperature of the SC have also been shown to cause lipid phase transitions in the SC. Differential scanning calorimetry studies have shown that the SC lipids undergo multiple phase transitions between 10 °C and 50 °C (Akomeah, et al. 2004, Clarys, et al. 1998, Gay, et al. 1994, Golden, et al. 1986, Golden, et al. 1987, Silva, et al. 2006, Tang, et al. 2002a, Van Duzee 1975). These lipid phase transitions are known to result in increases in the skin's permeability to mass transfer (Gay, et al. 1994, Potts and Francoeur 1990). Therefore, the coupling fluid temperature increases which occur during sonoporation can affect the permeability of the SC.

Past studies have avoided excessive temperature increases by employing duty cycles and coupling fluid replacement (Baji, et al. 2018, Lavon, et al. 2005, Paliwal, et al. 2006, Polat, et al. 2011a, Rich, et al. 2014, Sarheed and Abdul Rasool 2011, Tang, et al. 2002a, Terahara, et al. 2002a, Tezel, et al. 2004, Tezel, et al. 2001). In their study concerning the role of cavitation in sonoporation, Tang, et al. (2002a) used a duty cycle (0.1 s on 0.9 s off) to reduce the heating rate. Despite this, the coupling fluid temperature still exceeded 37 °C after 10 minutes of ultrasound application. The authors of that study also periodically replaced the coupling fluid with new, room temperature solution to maintain the skin temperature below 40 °C. A duty cycle and periodic replacement were also employed in the study by Lavon, et al. (2005) which found that, with a 50 % duty cycle (0.5 s on 0.5 s off), the temperature of the coupling fluid increased by 3-5 °C every 5 minutes. To limit the temperature rise, the authors of that study replaced the coupling fluid every 5 minutes. Although these two methods are an effective way to mitigate increases in the coupling fluid temperature, they are impractical. Duty cycles increase the time required to run an experiment (by up to 10-fold in the case of a 10 % duty cycle), while fluid replacement requires constant monitoring and tedious manual intervention. Furthermore, these methods are not able to maintain the coupling fluid temperature at a specified constant value, they simply avoid excessive temperature increases. A novel system capable of maintaining a constant coupling fluid temperature during skin sonoporation would be of great benefit to the field: it would remove the need for duty cycles or fluid replacement and enable previously impossible investigations into the influence of coupling fluid temperature.

The first thesis objective is to devise an experimental setup that is able to maintain a constant coupling fluid temperature during sonoporation in a Franz diffusion cell. The system

used to maintain the temperature must not impact the inertial cavitation activity at the skin aperture. The system must also be easy to remove from one diffusion cell and apply to another so that multiple diffusion cells can be used within one set of diffusion experiments.

1.2.2 The Unknown Influence of Coupling Fluid Temperature on Inertial Cavitation in a Franz Diffusion Cell

Researchers have established that inertial cavitation is the primary mechanism behind skin sonoporation. Coupling fluid temperature is known to affect inertial cavitation activity in other ultrasound setups. In their high-intensity focussed ultrasound (HIFU) study, Hockham, et al. (2010) indicated that inertial cavitation activity can decrease with increasing coupling fluid temperature due to an associated increase in vapour pressure. In their low-frequency study involving a pressurised resonator, Bader, et al. (2012) showed that the inertial cavitation threshold (the pressure required to stimulate inertial cavitation) decreases with increasing temperature. A decrease in the cavitation threshold with temperature was also shown in the high frequency diagnostic ultrasound study by (Brabec and Mornstein 2007). The pressure required to achieve cavitation at 39 °C was 67 *%* less than the pressure required to achieve cavitation at 25 °C. From the studies of Hockham, et al. (2010), Bader, et al. (2012), and Brabec and Mornstein (2007), it is unclear how the coupling fluid temperature affects the inertial cavitation activity which impacts the skin in a low-frequency Franz diffusion cell setup. An experimental investigation is needed. This has not previously been investigated because the existing experimental systems are unable to set the coupling fluid at a variety of specific temperatures during ultrasound application. When objective one is met, and a desired coupling fluid temperature can be maintained, it will be helpful for researchers to know which

temperature will provide them with the greatest amount of inertial cavitation activity for a given set of input parameters. Therefore, **the second thesis objective** is to investigate the influence of coupling fluid temperature on the inertial cavitation activity that impacts the skin in a Franz diffusion cell. Meeting this objective will provide valuable knowledge to help researchers select the most effective coupling fluid temperature.

In their low-frequency sonoporation study, Terahara, et al. (2002a) used aluminium foil as a physical dosimeter. The number of pits in the foil were counted after ultrasound application at a variety of ultrasound intensities and transducer distances. Pitting was shown to increase with increasing intensity and decrease with increasing transducer distance. From these results the authors concluded that inertial cavitation activity at the skin surface increases with increasing intensity and decreases with increasing transducer distance. A foil pitting technique will be used to meet the second thesis objective.

1.2.3 The Unknown Influence of Coupling Fluid Temperature on Post-sonoporation Transport

Without a means to maintain the coupling fluid temperature at a set value during sonoporation, researchers have been unable to investigate the influence of coupling fluid temperature on post-sonoporation transport. The skin permeability increase achieved with sonoporation is known to be dependent on experimental parameters such as ultrasound frequency, ultrasound intensity, the distance between the transducer and the skin, and the ultrasound application time. Investigating the influences of these parameters was motivated by the desire to optimize ultrasound enhancement (Herwadkar, et al. 2012, Terahara, et al.

2002a, Tezel, et al. 2001). If such optimization is to be achieved then an understanding of all of the experimental parameters that affect post-sonoporation transport must be obtained. Therefore, an investigation into the influence of coupling fluid temperature (during sonoporation) on the post-sonoporation transport is needed.

The third thesis objective is to investigate the influence of coupling fluid temperature on the transdermal transport that follows sonoporation in a low-frequency Franz diffusion cell setup. This investigation will implement a version of the temperature control system developed in objective one in order to maintain three different coupling fluid temperatures over the duration of ultrasound application. The transdermal transport following sonoporation at each of these temperatures will then be compared to illustrate the influence of coupling fluid temperature. The results of this study could have important implications for future experimental and clinical sonoporation applications: if a higher coupling fluid is shown to increase the post-sonoporation transport, future researchers could use the temperature control system developed for objective one to further increase the post-sonoporation transport obtained with a given set of ultrasound input parameters.

1.2.4 The Need for Passive Cavitation Detection During Skin Sonoporation

In skin sonoporation studies, the ultrasound input parameters (frequency, intensity, application time, and transducer distance) are used to dictate the inertial cavitation activity to which the skin is exposed. Because these parameters are generally held constant during the experiments, researchers might assume that the inertial cavitation activity also remains constant during sonoporation. However, inertial cavitation activity is transient in nature (Rich 2017) and can change during the course of ultrasound application due to bubble dissolution,

the depletion of cavitation nuclei, interactions between bubbles, increased vapour pressure caused by heating, and shielding caused by pre-focal bubble activity (Hockham, et al. 2010). For example, in the HIFU study by Hockham, et al. (2010), repeated insonation of the same phantom resulted in a marked decrease in inertial cavitation activity due to depletion of cavitation nucleation sites.

Outside of skin sonoporation, experimental setups that use inertial cavitation often include passive cavitation detector (PCD) systems to monitor inertial cavitation activity during ultrasound application (Bian, et al. 2017, Bull, et al. 2013, Cleveland, et al. 2000, Farny, et al. 2010, Gateau, et al. 2011, Gyöngy and Coussios 2010, Hallow, et al. 2006, Helga, et al. 2015, Hockham, et al. 2010, King, et al. 2010, Liu, et al. 1998, Salgaonkar, et al. 2009). Monitoring the inertial cavitation activity with a PCD allows any changes in the inertial cavitation activity to be detected in real-time. The experimental inputs to the ultrasound field can then be adjusted to counteract these changes and ensure that the inertial cavitation activity remains at the required level throughout ultrasound application. The PCD output can also be used to detect and avoid potentially harmful exposure levels when applying therapeutic ultrasound (Rich 2017).

In a PCD system, a hydrophone, placed directly into the coupling fluid and aligned with the ultrasound beam, measures the ultrasound pressure fluctuations that are radiated by the cavitation bubbles during ultrasound application. The voltage vs. time data that this hydrophone records during ultrasound application is then filtered to isolate the broadband noise. The RMS value of the broadband noise is indicative of the magnitude of the inertial cavitation within the ultrasound field (Farny, et al. 2010, Hallow, et al. 2006, Helga, et al. 2015,

Liu, et al. 1998, Sundaram, et al. 2003). The broadband noise level can be seen at all frequencies within the spectrum that do not contain a subharmonic, ultraharmonic, or harmonic peak. Cell sonoporation studies, such as those conducted by Chen, et al. (2003) and Hallow, et al. (2006), have shown that it is the inertial cavitation dose (ICD), the time integral of broadband noise, as opposed to the magnitude of broadband noise emission at any one time, that best correlates with cavitation-induced enhancement of a bioeffect such as hemolysis or intracellular uptake. This is because the ICD includes a temporal component, therefore, any changes in inertial cavitation activity over the course of ultrasound exposure will be reflected by the ICD value.

While PCDs have been frequently employed in studies involving the insonation of media other than skin (Coussios and Roy 2008, Farny, et al. 2010, Liu, et al. 1998, McDannold, et al. 2006, Qiu, et al. 2010, Yao-Sheng, et al. 2010, Zhou, et al. 2008), they have rarely been used in low-frequency *in vitro* skin studies. This is due to the geometric constraints within the traditional Franz diffusion cell which makes it difficult to fit both a transducer and a hydrophone in the coupling fluid. In the study by Tang, et al. (2002a) a hydrophone was fixed to the outer surface of the bottom of a receiver chamber with epoxy. This allowed for the PCD data to be recorded during ultrasound application but did not directly capture the acoustic signal within the coupling fluid – where the important inertial cavitation activity is known is known to occur (Tang, et al. 2002a). Tezel and Mitragotri (2003a) were able to directly monitor the ultrasound field in the coupling fluid, but could not take measurements during skin insonation as the hydrophone was positioned where the skin sample would usually be positioned. In the high-frequency sonoporation study by Rich (2017), a PCD hydrophone was embedded in the receiver chamber of a diffusion cell. This setup enabled PCD data to be

recorded during sonoporation but limited the study to one diffusion cell as the hydrophone was fixed in place. This limitation was acceptable for that study as conductivity was used to quantify the permeability increase. However, a permanently embedded hydrophone would be impractical for mass transport studies which require the concurrent use of multiple diffusion cells. Placement of the hydrophone below the skin is also clinically impractical. A diffusion cell setup that allows for a PCD hydrophone to be positioned in the coupling fluid during sonoporation must be developed. Such a setup could enable real-time monitoring and control of the inertial cavitation activity that occurs in the coupling fluid during skin sonoporation.

The fourth thesis objective is to design and manufacture a diffusion cell setup that enables a PCD hydrophone to be positioned in the coupling fluid during sonoporation. In this setup it must be quick and easy to remove the PCD hydrophone from one diffusion cell and apply it to another so that multiple diffusion cells can be used within one set of diffusion experiments. The positioning of the PCD hydrophone, relative to both the skin aperture and the transducer, must be consistent from one repetition to the next. **The fifth thesis objective** is to assess the ability of the diffusion cell PCD setup (from objective four) to monitor the inertial cavitation activity that occurs during skin sonoporation. This will be achieved by varying experimental parameters (that are known to affect the inertial cavitation activity) to see if the PCD output responds accordingly.

In *in vitro* experiments the post-sonoporation transport is quantified by measuring the concentration of the permeant in the receiver chamber after a period of diffusion. However, measurement of post-sonoporation transport cannot easily be made in an *in vivo* or clinical

setting. Such a measurement would require either an invasive subcutaneous extraction, which would defeat the purpose of using non-invasive transdermal delivery, or a measurement of a bodily fluid such as urine (Mitragotri and Kost 2000), which cannot be collected on demand. If sonoporation is to become a clinically practical technique, clinicians must have some indication of the likely range of post-sonoporation transport during the application of ultrasound. In their cell sonoporation study, Hallow, et al. (2006) proposed that ICD has the potential to be a unifying parameter that correlates with ultrasound enhancement over a broad range of experimental conditions – meaning that monitoring it during ultrasound application can enable real-time feedback about the permeability increases that are occurring. As part of objective five, the correlation between the PCD output and the post-sonoporation transport will be assessed to investigate the potential of using PCD output, not just to monitor inertial cavitation activity, but also as an indicator of the post-sonoporation transport.

1.2.5 The Unknown Influence of Acoustic Reflection in a Franz Diffusion Cell

In vitro studies have investigated the influence of several parameters (frequency, intensity etc.) on skin permeability increase. However, little attention has been paid to the potential influence of acoustic reflection in skin sonoporation studies. This was noted by Smith (2007), who stressed the importance of reporting the echoic conditions of a transdermal insonation apparatus.

In vitro skin sonoporation and sonophoresis experiments in Franz diffusion cells involve ultrasound waves propagating within a finite volume of liquid. Therefore, there will always be acoustically reflective interfaces present in the experimental setup. An acoustically reflective

interface is an interface between two materials that have different acoustic impedances. For example, the interface where the coupling fluid meets the donor chamber wall or the interfaces where the receiver chamber wall meets the fluid surrounding the diffusion cell. Acoustic reflections occurring within *in vitro* insonation setups will always cause constructive and destructive interference. Zorec, et al. (2015) suggested that this interference may lead to a non-uniform sound field with parameters that are different from the field emitted by the transducer. Due to the reflection and interference that occurs within *in vitro* ultrasound setups, it is also possible for standing waves to occur (Barati, et al. 2007, Kinoshita and Hynynen 2007, Liu, et al. 1998).

While, to the author's knowledge, there are no published studies that explicitly investigate the influence of reflection in *in vitro* skin sonoporation or sonophoresis setups, some researchers have employed experimental methods intended to suppress these reflections. For example, in their low-frequency transdermal transport study, Merino, et al. (2003) placed a Teflon sheet at the bottom of the diffusion cell receiver chamber to "absorb ultrasound and thereby reduce multiple reflections in the diffusion cell". The same Teflon sheet placement was used in the low-frequency study by Alvarez-Román, et al. (2003) to absorb ultrasound and reduce multiple reflections. In their high-frequency *in vivo* study on transdermal transport through rat skin, Park, et al. (2012) avoided "strong reflection" by positioning their thermocouple outside of the direct beam of their transducer. Mitragotri, et al. (1995b) inserted a 1 mm thick Teflon sheet opposite the transducer in a high-frequency horizontal diffusion cell setup in an attempt to reduce multiple ultrasound reflections. Zorec, et al. (2013) sonoporated their skin samples on a rubber block to "avoid sound wave reflections." In their HIFU, *in vitro* study on transdermal transport through pig skin, Helga, et al. (2015)

inserted a polyurethane absorber opposite the transducer to “avoid reflections of the HIFU beam.”

Previous studies of the insonation of cells in cell culture plates have shown that acoustic reflection from the walls of the cell culture plates may strongly influence the inertial cavitation activity. For example, Kinoshita and Hynynen (2007) found that sonoporation could be doubled by facilitating the presence of a standing wave. Similarly, Jelenc, et al. (2012) showed that by suppressing the acoustic reflection with an acoustically absorbent lining, the maximum reflected pressure (at the cell suspension) was reduced by 81 %. These results motivate an important question: at ultrasound intensities relevant to skin sonoporation, do the acoustic reflections that occur within a skin sonoporation setup significantly influence the inertial cavitation activity? This is an important consideration for researchers looking to translate the results of *in vitro* studies (conducted in highly reflective diffusion cells) to *in vivo* or clinical setups that have different echoic conditions: if the echoic conditions affect the inertial cavitation activity, then different input parameters may be required in a clinical setup to achieve the same inertial cavitation activity that was obtained *in vitro*.

The sixth thesis objective is to devise an experimental setup that facilitates an investigation of the influence of acoustic reflection in a Franz diffusion cell. A modified Franz diffusion cell setup will be designed and manufactured to facilitate the measurement of inertial cavitation activity in the coupling fluid during ultrasound application. The echoic properties of this setup will then be altered to vary the acoustic reflections that occur. **The seventh thesis objective** is to investigate the influence of acoustic reflections on the inertial cavitation activity in this setup.

1.3 Summary

The identified gaps in the field are mostly due to the limitations of standard glass Franz diffusion cells. Franz diffusion cells were initially designed for passive transport experiments and are therefore poorly suited to sonoporation experiments. The donor chambers are too small to facilitate a PCD hydrophone, the glass construction makes it difficult to customise the geometry so that a coupling fluid cooling system can be incorporated, and the highly reflective acoustic boundaries likely cause unwanted interference in the ultrasound field. A key contribution of this thesis is the introduction of equipment made specifically for sonoporation experiments out of easily customisable, non-glass materials. This equipment enables experimental investigations that have previously been impossible.

2 Coupling Fluid Temperature Control During Skin Sonoporation

2.1 Abstract

Ultrasound induced heating during skin sonoporation can result in coupling fluid temperatures capable of causing burns. This study used a modified Franz diffusion cell along with a novel temperature regulation system to maintain the coupling fluid temperature at one of three set values (13 °C, 33 °C, or 46 °C) during the sonoporation of porcine skin. Following 10 minutes of sonoporation, a buffer solution containing calcein was applied to the skin and left to diffuse at room temperature for five hours. Periodic samples of the receiver fluid were taken at one hour intervals. The mean and median post-sonoporation transport of calcein increased with increasing coupling fluid temperature. The median transport achieved with a coupling fluid temperature of 46 °C was 2.3 times that achieved with a coupling fluid temperature of 33 °C which was 2.2 times that achieved with a coupling fluid temperature of 13 °C. Past studies have used duty cycles and fluid replacement to keep the coupling fluid below 37-40 °C during sonoporation. However, this study showed that temperature dependent increases in post-sonoporation transport can occur below 37-40 °C. Foil pitting experiments were used to investigate the influence of coupling fluid temperature on the inertial cavitation activity that occurred at the skin aperture. The mean number of pits after 1 s of ultrasound application at 10 °C was 2.0 times the mean number at 40 °C (p<0.05). It is then reasonable to conclude that, while the inertial cavitation activity decreased, the post-sonoporation transport increased with increasing coupling fluid temperature. This increase

was attributed to temperature dependent structural changes in the SC, which increased the SC permeability.

2.2 Introduction

Most published *in vitro* skin sonoporation experiments are conducted in Franz diffusion cells (Han and Das 2013, Herwadkar, et al. 2012, Lavon, et al. 2005, Mitragotri, et al. 2000a, Paliwal, et al. 2006, Tang, et al. 2002a, Terahara, et al. 2002a, Terahara, et al. 2002b). A transducer, inserted into the donor chamber, emits an ultrasound field which propagates through the coupling fluid towards the skin. When the ultrasound waves travel through the coupling fluid a fraction of their energy is absorbed and converted to heat (O'Brien Jr 2007). When the transducer amplitude is high enough, this heating may result in a significant, unwanted increase in the coupling fluid temperature (Tang, et al. 2002a, Terahara, et al. 2002a). Increases in coupling fluid temperature must be mitigated due to the discomfort, burns, and damage to epidermal cells which occur when the skin temperature exceeds 40 °C (Hao, et al. 2016, Lindeque, et al. 2013, Moritz and Henriques 1947, Williamson and Scholtz 1949).

The donor chambers of standard glass Franz diffusion cells do not have any inbuilt fluid cooling capability. Therefore, past sonoporation studies have avoided excessive temperature increases by employing duty cycles and coupling fluid replacement (Lavon, et al. 2005, Paliwal, et al. 2006, Polat, et al. 2011a, Tang, et al. 2002a, Terahara, et al. 2002a, Tezel, et al. 2004, Tezel, et al. 2001). In their study concerning the role of cavitation in sonoporation, Tang, et al. (2002a) used a duty cycle (0.1 s on 0.9 s off) to reduce the heating rate. Despite this, the

coupling fluid temperature still exceeded 37 °C after 10 minutes of ultrasound application. The authors of that study also periodically replaced the coupling fluid with new, room temperature solution to maintain the skin temperature below 40 °C. A duty cycle and periodic replacement were also employed in the study by Lavon, et al. (2005) which found that, with a 50 % duty cycle (0.5 s on 0.5 s off), the temperature of the coupling fluid increased by 3-5 °C every 5 minutes. To limit the temperature rise, the authors of that study replaced the coupling fluid every 5 minutes. Although these two methods are an effective way to mitigate increases in the coupling fluid temperature, they are impractical.

Duty cycles increase the time required to run an experiment – by up to 10-fold in the case of a 10 % duty cycle. In the study by Tang, et al. (2002a), more than 60 sonoporation experiments were conducted. In each of these experiments the ultrasound transducer was positioned in the donor chamber for 2 hours. However, because a duty cycle of 10 % was used to minimise thermal effects, only 12 minutes of ultrasound was applied during this time. Therefore, 60 experiments worth of ultrasound application took a total of 120 hours. If continuous ultrasound had been used, these same 60 experiments would have only taken 12 hours. A similar issue occurs with clinical sonoporation setups. Two pilot clinical studies with human subjects used duty cycles of 17 % to 38 % to minimise thermal effects during sonoporation (Maruani, et al. 2010, Maruani, et al. 2012). If these studies had been able to safely use continuous ultrasound, patient contact time could have been reduced by up to 83 % – resulting in a more clinically practical application protocol.

The method of fluid replacement requires constant monitoring and tedious manual intervention. In the study by Tezel, et al. (2004), a 13 °C increase in coupling fluid temperature

occurred after 2 minutes of sonoporation – even with a 50 % duty cycle. Every 2 minutes the transducer was turned off so that the coupling fluid could be replaced. Each sonoporation experiment lasted for 10 minutes. Therefore, the coupling fluid had to be replaced 4 times in each experiment. Approximately 25 experiments were conducted meaning that the coupling fluid had to be replaced around 100 times in total – a lot of work for the authors of the study.

Aside from being time-consuming and labour intensive, duty cycles and fluid replacement do not allow the coupling fluid temperature to be maintained at a specified level during ultrasound application. This is problematic as inertial cavitation activity can change with changes to the coupling fluid temperature (Bader, et al. 2012, Hockham, et al. 2010). Temperature variations of up to 20 °C have been reported in previous sonoporation studies (Tang, et al. 2002a, Terahara, et al. 2002a). Such changes in coupling fluid temperature during sonoporation can introduce a source of variability in both inertial cavitation activity and in the skin's lipid thermal behaviour. This variability makes comparison between studies difficult: while two studies may use the same ultrasound inputs, if their thermal variations are not the same, the permeability changes may differ.

The current study introduces a modified polypropylene Franz diffusion cell setup that can maintain a specified coupling fluid temperature during the continuous application of ultrasound. This setup is used to investigate the influence of coupling fluid on post-sonoporation transport – an investigation that was impossible with previous coupling fluid temperature control methods. Porcine skin is exposed to a continuous ultrasound field at an intensity of 55 W/cm^2 for 10 minutes. During ultrasound application, the coupling fluid is set and maintained at one of three temperatures (13 °C, 33 °C, or 46 °C) using a modified Franz

diffusion cell setup similar to that presented in my published study (Robertson and Becker 2018). Following ultrasound application, a buffer solution containing calcein is applied to the skin and left to passively diffuse for five hours. The transport of calcein is measured by taking periodic samples of the receiver fluid. The current study also contains an investigation into the influence of coupling fluid temperature on inertial cavitation activity in a Franz diffusion cell.

2.3 Materials and Methods

2.3.1 Modified Diffusion Cell

Modified Franz diffusion cells were used for this study. Unlike the standard glass diffusion cells used in previous studies, the custom geometry of these diffusion cells enabled the coupling fluid to be circulated and cooled during sonoporation. Each donor chamber had an outer diameter of 65 mm, an inner diameter of 61 mm, an aperture diameter of 9 mm, and a total volume of 96 mL. Each receiver chamber had a volume of 3.2 mL and an aperture diameter of 9 mm. A representative depiction of an assembled diffusion cell is shown in Fig. 2-1. Dimensions of the donor and receiver chambers are shown in Fig. 2-2.

The donor and receiver chambers were turned from solid polypropylene rods (Polystone, Dotmar EPP Pty Ltd., Christchurch, New Zealand) on a CNC lathe (Top-Turn CNC 406, Jashco Machine Manufacture Co. Ltd., Taichung, Taiwan). The receiver chamber sampling arms and donor chamber ports were then retrofitted by gluing (Loctite 401, Henkel AG, Düsseldorf, Germany) sections of carbon fibre tube (Carbon Fibre Tube Pultruded, MAKERshop, Auckland, New Zealand) into holes that were drilled into the polypropylene. The

tubing used for the sampling arms had an inner diameter of 3.5 mm and an outer diameter of 6 mm. The tubing used for the ports had an inner diameter of 2 mm and an outer diameter of 4 mm. The clamps that held the donor and receiver chambers together were 3-D printed from acrylonitrile butadiene styrene (ABS P430, Stratasys, Eden Prairie, MN, USA). A representative depiction of a clamp is shown in Fig. 2-3.

Fig. 2-1 Depiction of a diffusion cell (top) plan view, (middle) front view, and (bottom) isometric view

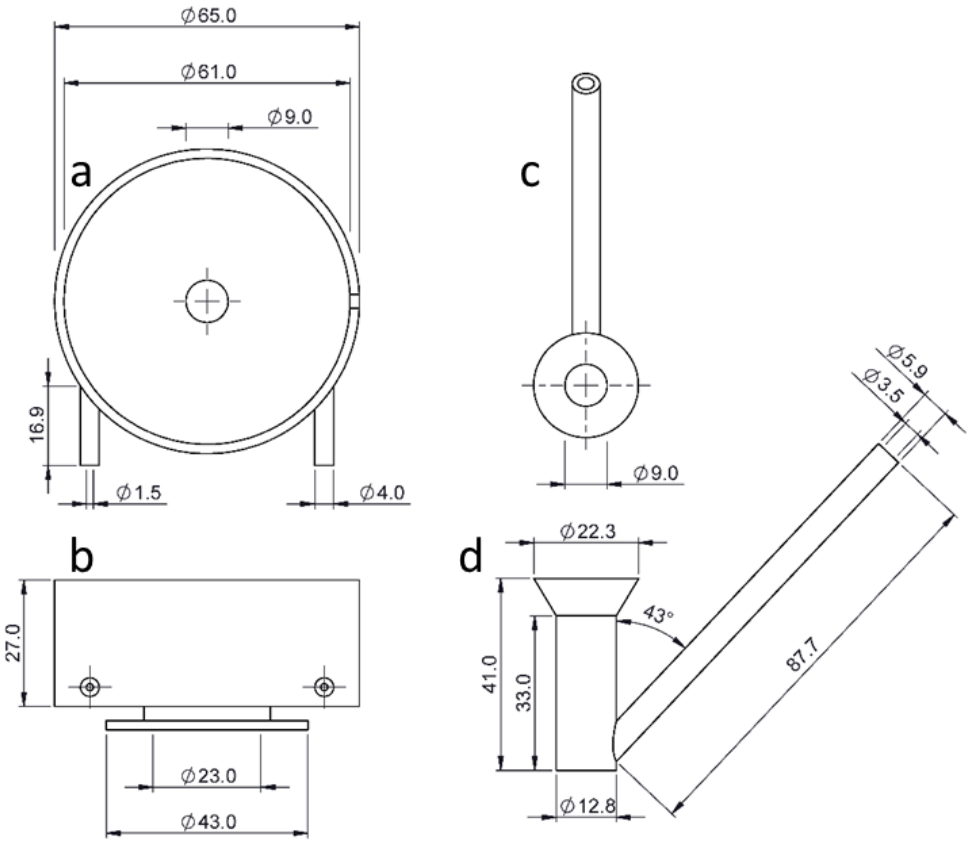

Fig. 2-2 Dimensions of the polypropylene donor and receiver chambers (a) donor chamber plan view, (b) donor chamber front view, (c) receiver chamber plan view, and (d) receiver chamber right view

Fig. 2-3 Depiction of a 3D printed ABS clamp

2.3.2 Chemicals

The permeant solution that was applied to the skin consisted of calcein (Calcein C0875, Sigma-Aldrich, St. Louis, MO, USA) dissolved in phosphate buffered saline (PBS) (Gibco PBS pH 7.4, Thermo Fisher Scientific, Waltham, MA, USA) at a concentration of 0.1 % w/v (1 g/L). This solution was made and stored at room temperature. Calcein is an easy to measure permeant which is commonly used in transdermal transport studies (Henry, et al. 1998a, Oh, et al. 2008, Prausnitz, et al. 1993, Vanbever and Preat 1999, Xie, et al. 2005). Deionised water was taken from a Labwater L991008 Deioniser (Suez Ltd, Thame, UK).

2.3.3 Porcine Skin

The *in vitro* skin models used in this study consisted of porcine ear skin. Porcine skin is commonly used in sonoporation and sonophoresis experiments (Lee and Zhou 2015, Merino, et al. 2003, Mitragotri, et al. 2000a, Paliwal, et al. 2006, Polat, et al. 2012, Sarheed and Abdul Rasool 2011, Schoellhammer, et al. 2012, Souza, et al. 2013, Tang, et al. 2002a, Terahara, et al. 2002a, Terahara, et al. 2002b, Tezel and Mitragotri 2003a, Tezel, et al. 2002, Tezel, et al. 2001, Zorec, et al. 2015) due to the established histological and physiological similarities between porcine and human skin (Dick and Scott 1992, Jacobi, et al. 2007). In some cases human skin itself has been used (Kushner, et al. 2008, Mitragotri, et al. 1995b, Smith, et al. 2003), however the complications associated with using cadaver skin makes it an impractical model for most studies.

Porcine ears were obtained from an abattoir (Ashburton Meat Processors Ltd, Ashburton, New Zealand) immediately after slaughter. These ears were not scalded or exposed to

detergent at the abattoir. Upon arrival at the laboratory, the ears were cleaned with cold tap water to remove the blood and soil. The skin was then removed from the ears using a dermatome (Dermatome 50 mm, Nouvag AG, Goldach, Switzerland) set to a thickness of 1 mm. This dermatome process, similar to that used in previous ultrasound studies (Boucaud, et al. 2001, Zorec, et al. 2015), achieved a consistent skin thickness close to full thickness. Full thickness skin, which is commonly used in sonoporation experiments (Merino, et al. 2003, Mitragotri, et al. 2000a, Terahara, et al. 2002a, Tezel, et al. 2002), is approximately 1-2 mm thick (Weimann and Wu 2002). Following the dermatome process, the pieces of skin were individually wrapped in Parafilm (PARAFILM, Sigma-Aldrich, St. Louis, MO, USA), placed in airtight plastic containers, and then transferred to a -20 °C freezer until use. The total time from slaughter to freezer was approximately 4 hours. All of the skin samples used for transport experiments were stored in the freezer no longer than 18 days.

2.3.4 Ultrasound Generation and Intensity Measurement

A continuous low-frequency (20 kHz) ultrasound field was generated with an ultrasonic processor (VC 505 Ultrasonic Processor, Sonics and Materials Inc., Newtown, CT, USA). This processor was fitted with a 13 mm replaceable tip. A replaceable tip was necessary as extended use resulted in cavitation damage (Fig. 2-4) which affected the flatness of the tip surface (a flat tip surface is necessary for the formation of a uniform ultrasound field). Following the manufacturer's instruction, compressed air was circulated through the ultrasonic processor to keep it cool during ultrasound application.

Fig. 2-4 New transducer tip (left) and used transducer tip displaying cavitation induced damage from extended use in sonoporation experiments (right)

The VC 505 ultrasonic processor allows the user to select the transducer tip displacement – quantified as a percentage of the maximum tip displacement (which is equal to 76 µm). For this study, the tip displacement was either 20 *%* or 60 *%*. The intensity of the ultrasound field with each of these tip displacements was determined using a common calorimetric approach (Merino, et al. 2003, Mitragotri, et al. 2000a, Mitragotri, et al. 2000b, Morimoto, et al. 2005, Mutoh, et al. 2003, Terahara, et al. 2002a) that was described in Section 2.4 of Robertson and Becker (2018). Briefly, the ultrasound transducer was positioned in a beaker of water embedded in a thermally insulating block of polystyrene. The transducer tip was 22 mm below the waterline of the beaker (the same depth used during sonoporation). The transducer was then operated at a variety of tip displacement amplitudes to vary the resulting ultrasound intensity. The intensity resulting from operation at each of the tip displacement amplitudes, I , was calculated from

$$I = \left(\frac{mC_P}{A} \right) \frac{\Delta T}{\Delta t} \tag{2.1}$$

where m is the mass of water in the beaker (0.2 kg), C_p is the specific heat of water (4.187 kJ/kgK), A is the active transducer face area (1.3 cm^2), and ΔT is the measured change in temperature that occurred during the 3 minutes (Δt) of ultrasound exposure. Each of these intensity measurements was run in triplicate. The intensities calculated for tip displacements of 20 *%* and 60 *%* were 13 W/cm^2 and 55 W/cm^2 respectively. These were spatial average, temporal average intensities as in the study by (Mitragotri, et al. 2000a). Note that Appendix B reports the series of transdermal transport experiments which were used to determine a tip displacement (60 *%*), application time (10 minutes), and transducer to skin distance (3 mm) capable of producing a significant increase in Calcein transport in the present setup.

The sonoporation intensity used in the present study (55 W/cm^2) was higher than other intensities used in the literature. However, variations in the calorimetry protocols between different studies makes comparison of intensity values difficult. A broad range of ultrasound intensities have been used by past sonoporation studies. Although most studies use Eq. 2.1 to determine intensity, each study uses different parameters (liquid, volume, vessel, application time, transducer depth, etc.) for their calorimetry experiments. In their low frequency sonoporation study, Sarheed and Abdul Rasool (2011) used an intensity of 3.7 W/cm^2. This value was calculated by measuring the temperature of 500 mL of distilled water before and after 15 minutes of ultrasound application. The water was contained in an insulated thermoflask. The depth of the transducer and transducer tip diameter were unspecified. Alternatively, in the study by Terahara, et al. (2002a), the intensities were between 2.4 W/cm^2 and 33 W/cm^2. These intensities were calculated by measuring the temperature of 150 mL of water before and after an unspecified duration of ultrasound

application. The water was contained in an uninsulated beaker. The transducer depth was varied between 0.5 cm and 8.5 cm. Note that transducer depth has a significant effect on the measured temperature increase (and the calculated intensity): because the entire transducer vibrates, not just the tip, more energy is transferred to the fluid when a greater portion of the transducer is submerged. An additional set of calorimetry experiments with the present setup showed that increasing the transducer depth from 5 mm to 40 mm increased the calculated intensity by 23 *%* (*p*=0.1). Yet another set of calorimetry protocols were used in the sonoporation study by Herwadkar, et al. (2012), which used an intensity of 6.9 W/cm^2. Calorimetry was performed with 50 mL of water in an insulated beaker. The application time and transducer depth were both unspecified. The important consideration for any sonoporation study is not so much the intensity value but the inertial cavitation activity which occurs at the skin surface. From the foil pitting experiments presented later in this chapter, and those shown in Appendix B, it is clear that an intensity of 55 W/cm^2 produces a significant amount of inertial cavitation activity in the present setup. Therefore, the intensity of 55 W/cm^2 was appropriate.

An alternative method for quantifying the strength of an ultrasound field is to measure its pressure with a hydrophone (Mitragotri, et al. 1996, Park, et al. 2007, Smith, et al. 2003, Tezel, et al. 2001). This method was not used in this thesis as the driving pressure is difficult to determine with a hydrophone when inertial cavitation is present in the ultrasound field: cavitation shifts the acoustic energy to frequencies other than the 20 kHz driving pressure (Liu, et al. 1998). A full set of hydrophone experiments were conducted to demonstrate this (Section A.3.1).

Any ultrasound field emitted from a planar piezoelectric transducer can be conceptually split into two parts: the near field, and the far field. The near field has its origin at the active face of the transducer and has an axial length, L, which can be calculated from the equation

$$L = \frac{D^2}{4\lambda} \tag{2.2}$$

where D is the diameter of the active face of the transducer and λ is the wavelength. Due to the significant spatial intensity fluctuations that occur in the near field, it is important to always ensure that the target medium is positioned far enough from the transducer face so as to be in the far more uniformly fluctuating and predictable far field during ultrasound application. For the 13 mm diameter transducer used in this thesis, the near field had a length of 0.58 mm. In the experiments described in this chapter the bottom of the tip was always positioned 3 mm from the surface of the skin. Therefore, the skin was well outside the near-field – which is common practice in low-frequency skin sonoporation (Herwadkar, et al. 2012, Mitragotri, et al. 2000a, Polat, et al. 2011a).

2.3.5 Measurement and Regulation of Coupling Fluid Temperature

The temperature of the coupling fluid was measured during each experiment using a wire type K thermocouple (Jaycar Electronics Pty. Ltd., Auckland, New Zealand). The location of the thermocouple (qualitatively depicted in Fig. 2-5) was chosen so that it was outside of the transducer beam and did not interfere with the ultrasound field near the skin. This position (8 mm above the bottom donor chamber wall and 7 mm from the transducer) was also chosen so that the thermocouple tip would not be damaged by cavitation. Preliminary temperature

measurements were conducted to assess the influence of the thermocouple position on the measured temperature. In these experiments, a second thermocouple was positioned directly over the skin (as shown in Fig. 2-6). The steady state temperatures measured by these thermocouples were compared under all of the experimental conditions used in this study.

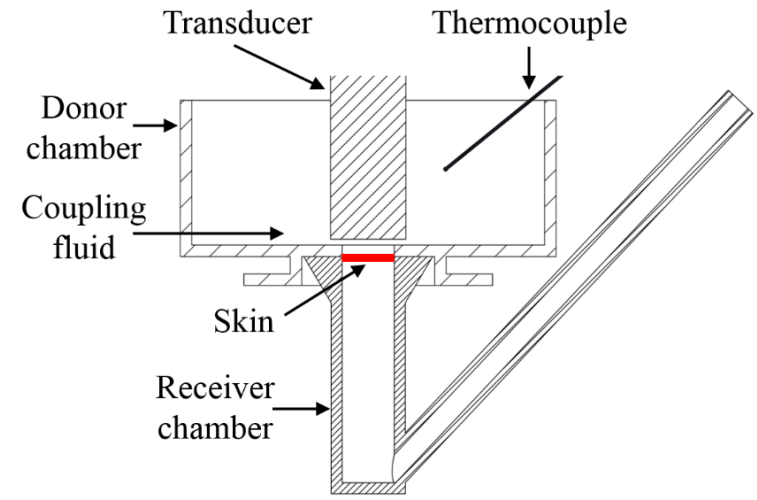

Fig. 2-5 Cross-section of the diffusion cell showing the positioning of the transducer and thermocouple during sonoporation

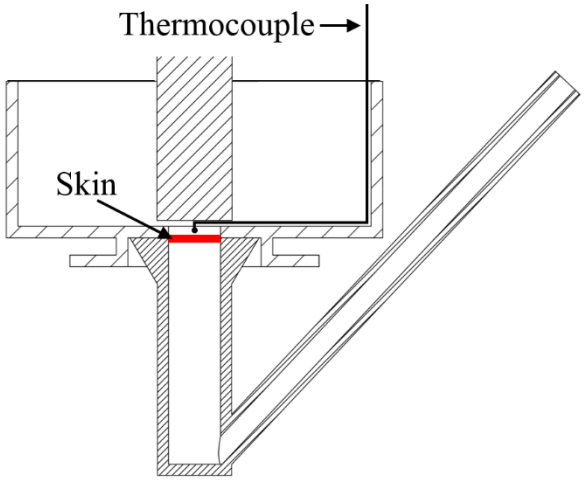

Fig. 2-6 Cross-section of the diffusion cell showing the thermocouple positioned directly above the skin surface

In this study, a temperature control system was used to set and maintain the coupling fluid temperature during sonoporation. This system was similar to the one I used in the published study (Robertson and Becker 2018), which forms the basis of Chapter 4. The coupling fluid (deionised water) was circulated out of the donor chamber via one of the two ports, through a heat exchanger, and back into the donor chamber via the other port (as shown in Fig. 2-7).

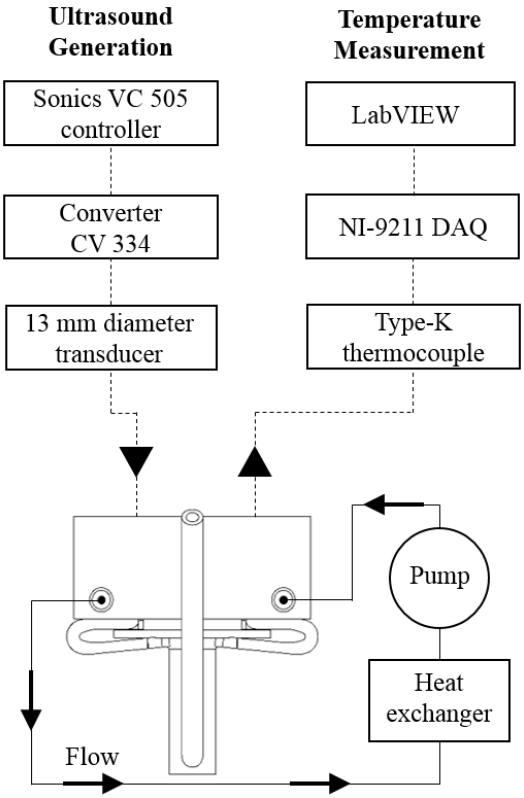

Fig. 2-7 System schematic. The solid lines represent the coupling fluid circuit. The dashed lines represent the signal inputs to the transducer and the signal outputs from the thermocouple.

A peristaltic pump (6-V Peristaltic Pump, Amazon, Seattle, WA, USA), driven by a power supply (MP3090, Powertech, Taiwan) maintained a constant flow rate of 0.14 L/min around this circuit. A peristaltic pump works by displacing fluid contained within a tube around a circular pump casing (Fig. 2-8). The only component that comes in contact with the fluid is the

inside of the tubing. This was a beneficial feature for the present study as it meant that the coupling fluid could not be contaminated by contact with other pump components. The heat exchanger consisted of an aluminium block submerged in a water bath (FP-50 Refrigerated/Heating Circulator, Julabo GmbH., Selbach, Germany). When the coupling fluid passed through channels milled within this block (shown in Fig. 2-9), the coupling fluid temperature tended towards the temperature of the water bath (which could be set to any temperature between 1 °C and 99 °C). The aluminium block was designed so that it could be easily taken apart for cleaning/sterilisation if required. The positioning of the aluminium block in the water bath is shown in Fig. 2-10.

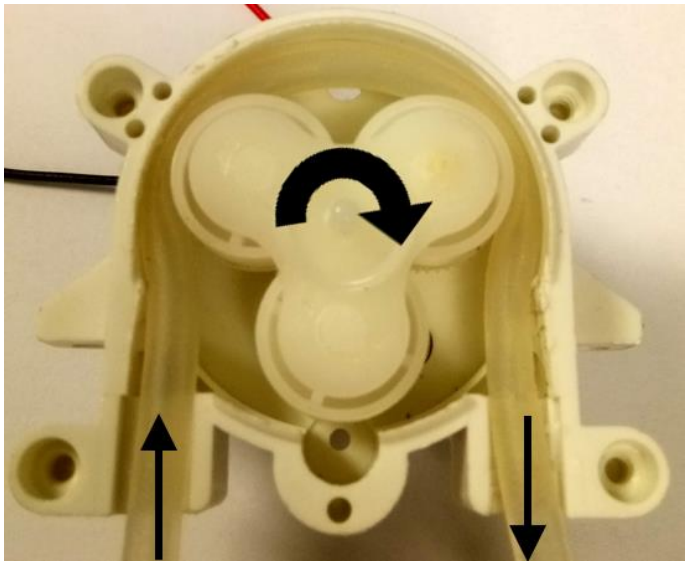

Fig. 2-8 Inner working of the 6 V peristaltic pump. The rotating wheels applied pressure to the pump tube which displaced the coupling fluid. The fluid flowed through the pump at 0.14 L/min.

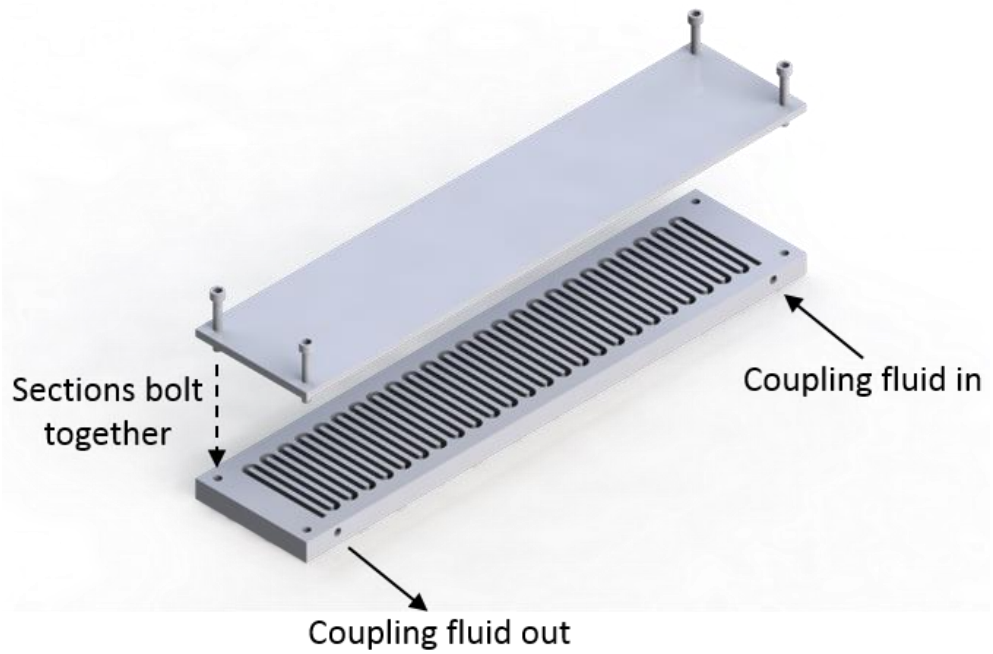

Fig. 2-9 Schematic of the heat exchanger that was positioned in water bath. The silicone tubing was inserted into the coupling fluid in and out holes. The two sections were bolted together with an O-ring in between to prevent leakage and to ensure that the coupling fluid followed the tortuous milled path.

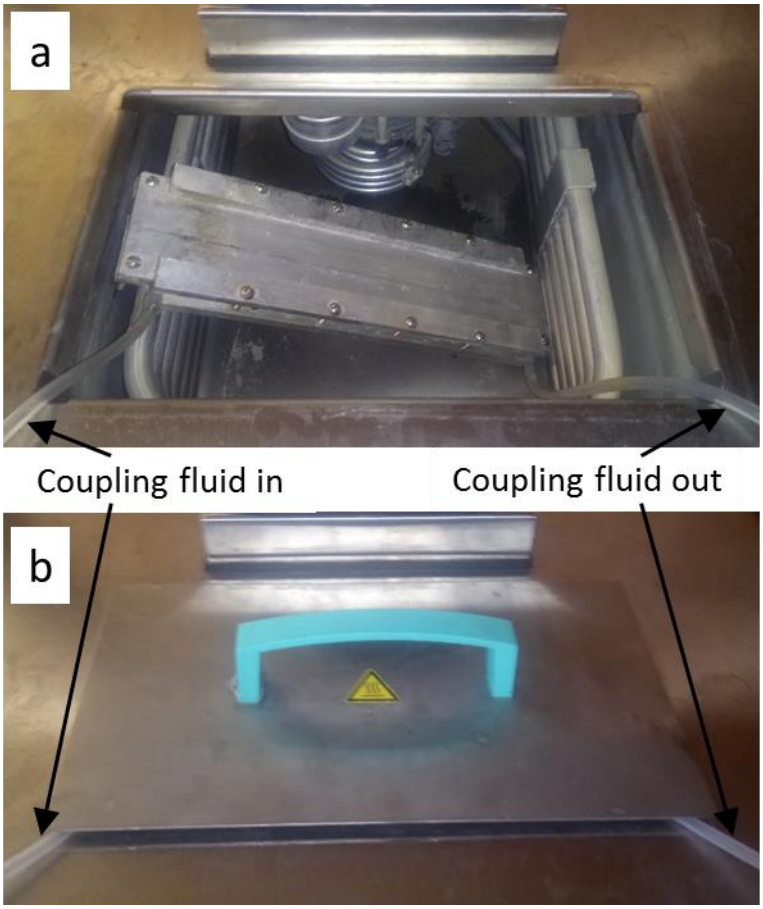

Fig. 2-10 Images of the heat exchanger positioned in the water bath of the refrigerated/heating circulator (a) with the lid off and (b) with the lid on

The temperature of the coupling fluid during ultrasound application was set by adjusting the water bath temperature. The components in the temperature regulation system were linked by silicone tubing (Silicone Tubing Clear Grade Inner Diameter 2.6 mm, Rubbermark Industries, Auckland, New Zealand) that could easily be removed from the donor chamber ports, allowing each of the seven diffusion cells to be integrated into and removed from the system. The coupling fluid circuit could easily be cleaned by pumping fresh deionised water through the heat exchanger, pump tubing, and linking tube. The custom built support structure that held the transducer, thermocouple and diffusion cells in place is described and shown in detail in Appendix Section A.2.7. The circulation of coupling fluid in the donor

chamber was shown to have a negligible effect on the inertial cavitation activity occurring at the skin aperture (this effect is quantified in Section 2.4.5).

The heat exchanger setup used in the present study was an improvement over an earlier iteration that was used in both Chapter 4 and Appendix A. That earlier iteration, described in detail in Section 4.3.2, provided sufficient cooling power for ultrasound intensities of 24 W/cm^2 and below, but was unable to maintain a constant coupling fluid temperature at higher intensities. The coupling fluid temperature increases which occurred during sonoporation at intensities above 24 W/cm^2 are shown in Section A.3.4 and discussed in Section A.4. The earlier heat exchanger iteration is mentioned here as researchers who intend to use low-intensity (<30 W/cm^2) sonoporation would find it to be an affordable and compact alternative to the present version, which requires a laboratory water cooler. Furthermore, as this earlier iteration used thermoelectric Peltier plates to cool the fluid, the cooling power could be quickly adjusted during sonoporation, which may be a helpful feature for some researchers.

An external, bidirectional heat pump could provide the coupling fluid temperature control required for continuous sonoporation or sonophoresis. However, this approach is not recommended as it would make it far more difficult to thoroughly clean the system, especially following a sonophoresis treatment (in which the circulating fluid contains a permeant substance). As the present heat exchanger can be separated from the other components, and taken apart, it is far easier to clean and/or autoclave than a bidirectional heat pump.

2.3.6 Transdermal Transport Experiments

In the present study, experiments were conducted to investigate the influence of coupling fluid temperature on the post-sonoporation transdermal transport of Calcein. These experiments began with filling one of the receiver chambers with room temperature (19 °C ± 1 °C) PBS (Fig. 2-11). A skin sample was then taken from the freezer and visually checked for any holes or areas of non-uniform thickness through which the calcein solution could easily diffuse. Any samples that displayed such imperfections were disposed of. Once an appropriate skin sample was selected, it was clamped between the filled receiver chamber and the donor chamber.

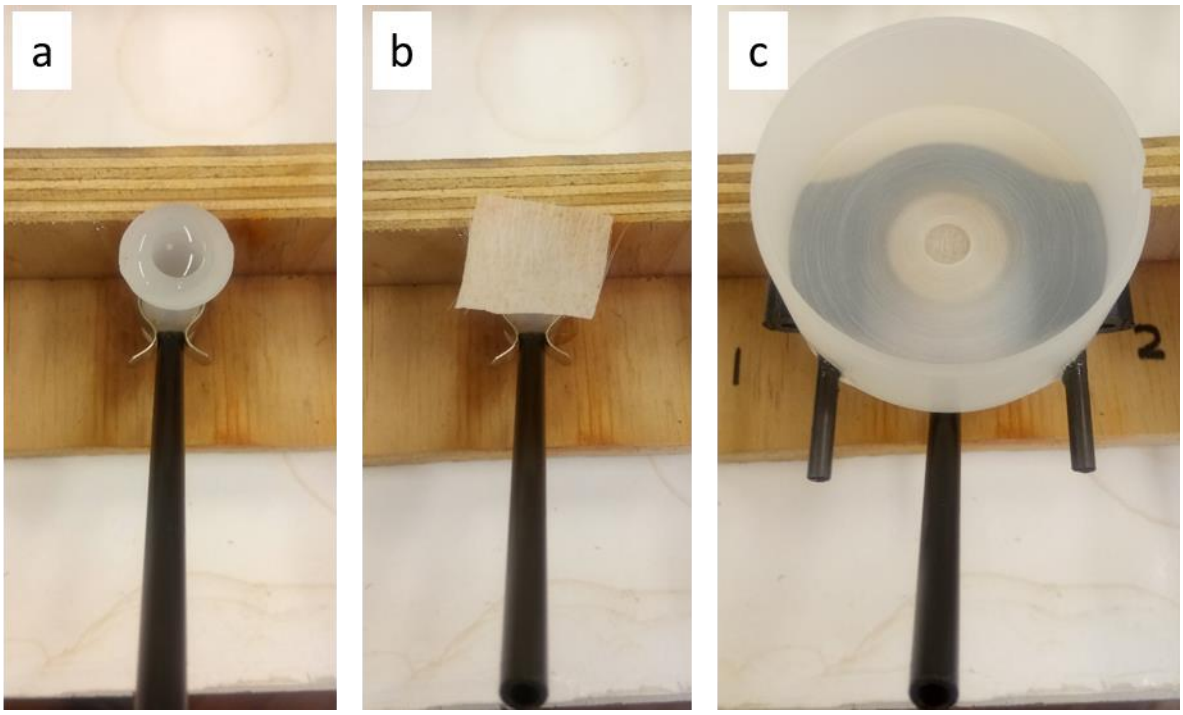

Fig. 2-11 Assembly of each diffusion cell involved (a) filling the receiver with PBS, (b) placing a skin sample on the filled receiver chamber, and (c) clamping the donor chamber on top

After ensuring that no air bubbles were present in the receiver chamber, the diffusion cell was mounted into the temperature regulation setup, which involved attaching the silicone tubing to the donor ports (shown in Fig. 2-12) and moving the thermocouple into position (note that full schematics of the support structure for the transducer, thermocouple, and diffusion cell are presented in Appendix A).

Fig. 2-12 Image of the silicone tubing attached to the donor chamber ports

Deionised water at room temperature was then added to the donor chamber and allowed to sit for three minutes to thaw the skin. The pump was then switched on in order to circulate the coupling fluid around the circuit (Fig. 2-7), thereby initiating temperature control. The water bath temperature required to achieve each of the coupling fluid target temperatures (13 °C, 33 °C or 46 °C) during sonoporation is shown in Table 2-1. Note that the present setup was capable of maintaining any coupling fluid temperature in the range of 10 °C to 70 °C

during continuous sonoporation. For each of the coupling fluid target temperatures, an additional set of experiments were run with coupling fluid circulation but without ultrasound. These three sets of experiments are termed 'controls'. Note that these are positive controls as opposed to true negative controls as some temperature effect may be expected. However, readers should note that the term 'control' is used for the sake of simplicity. The water bath temperatures required to achieve each of the coupling fluid target temperatures (13 °C, 33 °C or 46 °C) during the control experiments are also shown in Table 2-1.

Table 2-1 Water bath temperatures required to achieve the coupling fluid target temperatures for the control and sonoporation protocols.

Protocol	**Control**			**Sonoporation at 55 W/cm^2**		
Target temperature (°C)	**13**	**33**	**46**	**13**	**33**	**46**
Water bath temperature (°C)	13	35	50	1	25	40

With the temperature control system running, the coupling fluid was circulated for 10 minutes with continuous ultrasound application at 55 W/cm^2, or without ultrasound in the control case. The temperature of the coupling fluid was constantly monitored with the thermocouple during this time to ensure it remained at the desired target temperature. Following this 10 minute period, the coupling fluid was removed from the donor chamber and the diffusion cell was moved to a holding rack. A 0.5 mL volume of the calcein solution was then applied to the top of the skin so that its entire surface was submerged. This solution was left to diffuse for five hours at room temperature (19 °C ± 1 °C). During this time, 0.2 mL samples were taken from the receiver chamber every hour with a pipette (Calibra Digital 832 Macro Pipette, Socorex, Ecublens, Switzerland). The sampled volume was then replaced with an identical volume of fresh PBS. This dilution was later accounted for when calculating the

concentration of calcein in the receiver chamber. The adjusted concentration, C, was found with the equation

$$C = C_{RAW}\left(\frac{1}{1-(V_{sample}/V_{receiver})}\right)^{(s-1)} \quad (2.3)$$

where C_{RAW} is the measured concentration value (in mg/L), V_{sample} is the volume of the sample taken from the receiver chamber (0.2 mL), $V_{receiver}$ is the volume of the receiver chamber (3.2 mL), and s is the sample number (taken after 1, 2, 3, 4, or 5 hours). Note that each diffusion cell was washed with a surfactant cleaner (Jif, Unilever, France) in between each use to remove the calcein which had a tendency to adhere to the polypropylene.

2.3.7 Spectrofluorometry

The concentration of calcein in the receiver fluid was measured using a spectrofluorometer (Fluorolog-3, Horiba Ltd., Kyoto, Japan). A spectrofluorometer was used for this study as it provided a relatively quick way to measure calcein concentration, compared to the more time-consuming high-performance liquid chromatography (HPLC) method used in the earlier sonoporation study reported in Appendix A. The spectrofluorometer excitation and emission wavelengths were 488 nm and 513 nm respectively. These wavelengths are similar to those used to measure calcein in the literature (Alvarez-Román, et al. 2003, El Jastimi and Lafleur 1999, Morimoto, et al. 2005, Mueller, et al. 2004, Petronilli, et al. 1999). The software package FluorEssence (FluorEssence V3.5, Horiba Ltd., Kyoto, Japan) was used to control the spectrofluorometer and analyse its output. Each 0.2 mL sample was pipetted into a 1.2 mL

quartz crystal cuvette (Starna Ltd, Essex, UK). The remaining 1 mL of the cuvette was then filled with PBS. This dilution was accounted for by multiplying the measured spectrofluorometer intensity by six. The emission intensity values measured by the spectrofluorometer (at 513 nm) were converted to calcein concentrations, C_{RAW}, using the calibration curve described in Appendix B, which had the equation

$$C_{RAW} = 8.21\times10^{-10}(\mathrm{I}_S) + 4.04\times10^{-5} \tag{2.4}$$

where I_S is the measured spectrofluorometer emission intensity (CPS). A total of 210 individual spectrofluorometer measurements were required for this study. Between each measurement, the cuvette was cleaned with deionised water and dried with Kimwipes (Kimtech, Kimberly-Clarke, Irving, TX, USA) to ensure that all of the calcein was removed.

2.3.8 Measurement of the Receiver Fluid Temperature

Temperature increases during sonoporation are a result of absorption: as the ultrasound propagates through a fluid medium, a portion of the acoustic energy is absorbed by the fluid and converted to heat. This absorption can occur in both the donor and receiver fluids due to the propagation of the ultrasound field throughout the diffusion cell. To measure the heat transfer to or from the receiver fluid, a hole was drilled in the bottom of a spare receiver chamber which was not required for the transport experiments. A thermocouple was then inserted through this hole so that its tip was positioned 2 mm below the skin surface (Fig. 2-13). The hole in the bottom of the receiver chamber was then glued (Loctite 401, Henkel AG, Düsseldorf, Germany) to prevent any leakage and to ensure that the thermocouple

remained in position. Due to the use of polypropylene, this thermocouple position was easy to achieve with a standard drilling technique. With a glass receiver chamber this thermocouple position would have required specialist glass machining equipment – an illustration of the benefits of using polypropylene instead of glass. The thermocouple measured the temperature under each of the control and ultrasound experimental conditions. The thermocouple recorded data for a total of 30 minutes. The first 10 minutes of this corresponded to the 10 minutes of coupling fluid temperature regulation (for the control protocols) or the ten minutes of ultrasound application with coupling fluid temperature regulation (for the sonoporation protocols). An additional twenty minutes was also recorded to demonstrate the behaviour of the receiver chamber temperature immediately following calcein application.

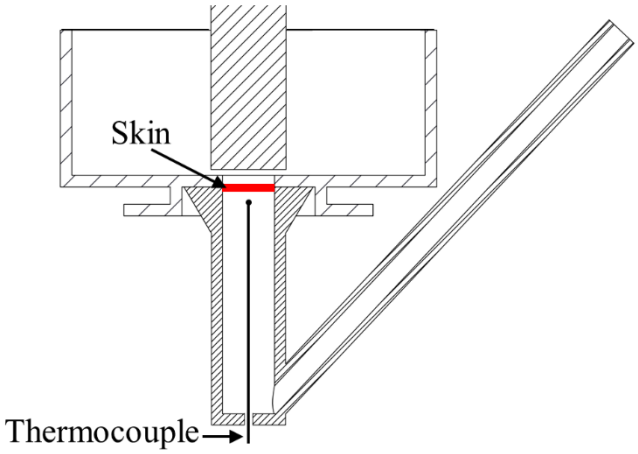

Fig. 2-13 Cross-section of the diffusion cell showing the positioning of the thermocouple used to measure the receiver fluid temperature. The tip of the thermocouple was 2 mm from the bottom surface of the skin.

2.3.9 Measurement of the Permeant Solution Temperature

Following the 10 minutes of coupling fluid circulation (with or without ultrasound), the coupling fluid was removed from the donor chamber. The calcein-buffer solution was then added to the donor chamber so that diffusion could begin. During the first 15 minutes of this diffusion, the temperature of the calcein-buffer solution was measured with a thermocouple which was positioned 1 mm above the skin surface (Fig. 2-14).

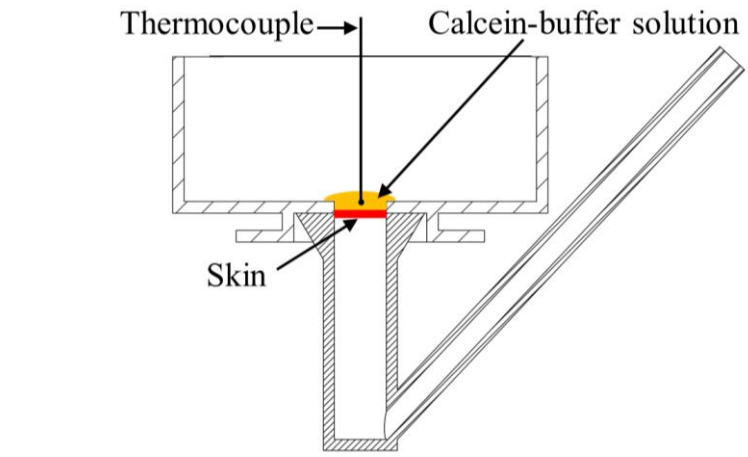

Fig. 2-14 Cross-section of the diffusion cell showing the positioning of the thermocouple used to measure the temperature of the 0.5 mL of calcein-buffer solution

2.3.10 Foil Pitting Experiments

The pitting of aluminium foil has previously been used to quantify the influence of different experimental parameters on the inertial cavitation activity that occurs during sonoporation (Mitragotri, et al. 2000a). This technique was used to investigate the influence of coupling fluid temperature on the inertial cavitation activity in the present setup. Ten pieces of foil were placed in a diffusion cell and exposed to 1 s of ultrasound (at an intensity of 55 W/cm^2) with the coupling fluid at 10 °C. This was repeated for another 10 foil samples that were exposed to ultrasound (at an intensity of 55 W/cm^2) with the coupling fluid at 40 °C. A third

set of 10 foil samples were exposed to ultrasound (at an intensity of 13.3 W/cm^2) with the coupling fluid at 10 °C. Finally, a fourth set of 10 foil samples were exposed to ultrasound (at an intensity of 13.3 W/cm^2) with the coupling fluid at 10 °C.

Foil pitting experiments were also used to investigate the influence of coupling fluid circulation on the inertial cavitation activity at the skin aperture. Ten pieces of 0.016 mm thick aluminium foil (Homebrand, Manukau, New Zealand) were exposed to ultrasound (at an intensity of 55 W/cm^2) for 2 s with and without coupling fluid circulation. The number of pits in each of the 20 pieces of foil were then counted to quantify the influence of circulation. In these experiments, the coupling fluid in the donor chamber was deionized water at 10 °C ± 1 °C. This temperature was achieved using the circulation system.

The length of time that a piece of foil is submerged in water prior to ultrasound application can affect the prevalence of air bubbles (nucleation sites) on the surface of the foil. Prior to each ultrasound application, the foil was submerged in the coupling fluid while the circulation system brought the coupling fluid to the specified temperature. The time required to achieve this temperature was consistent across each foil pitting dataset. Therefore, the effect of the submergence, on the prevalence of nucleation sites on the foil surface, was also consistent.

When counting the foil pits, any circular indent was counted as one pit. Two partially overlapping circular indents were counted as two pits. The duration of ultrasound exposure (either 1 s or 2 s) was short enough to avoid complete perforation of the foil, which would have made it impossible to quantify the number of individual pits.

2.4 Results

2.4.1 Coupling Fluid Temperature

This study employed a temperature regulation system to set and maintain the coupling fluid at one of three target temperatures (13 °C, 33 °C, and 46 °C) during 10 minutes of continuous ultrasound application. Temperature profiles are shown in Fig. 2-15 for regulated and unregulated continuous ultrasound application, application with a 50 % duty cycle, and application with a 10 % duty cycle. Unregulated continuous application resulted in the coupling fluid temperature exceeding 45 °C in just over 4 minutes. A 50 % duty cycle also resulted in the temperature increasing to above 40 °C. A 10 % duty cycle ensured that the temperature remained below 20 °C but an equivalent duration of only 1 minute of ultrasound was applied. When continuous application was used along with the novel temperature control system, the coupling fluid temperature increased to the target temperature of 13 °C and remained there for the duration. The temperature profiles for each of the three target temperatures (13 °C, 33 °C, and 46 °C) are shown in Fig. 2-16 for both the control and sonoporation protocols.

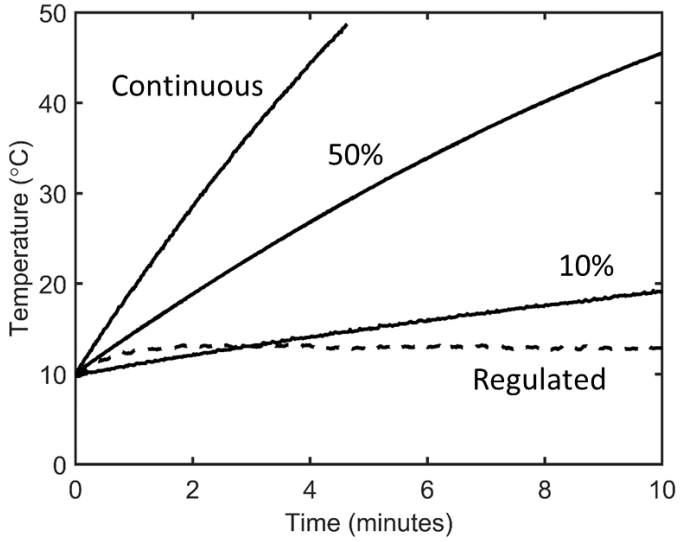

Fig. 2-15 Coupling fluid temperature as a function of time for continuous ultrasound application, a 50 % duty cycle, a 10 % duty cycle, and continuous application with temperature regulation

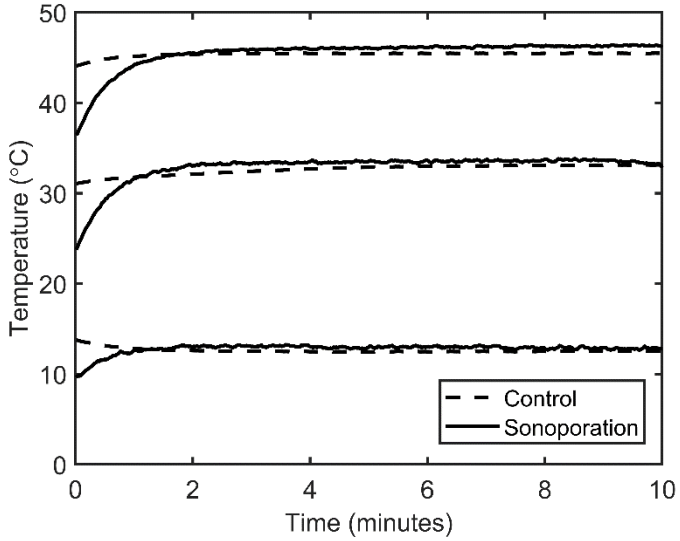

Fig. 2-16 Coupling fluid temperature profiles for the control and sonoporation protocols at target temperatures of 13 °C, 33 °C, and 46 °C

In the present study, the coupling fluid temperature was measured with a thermocouple that was positioned outside of the transducer beam. Preliminary temperature measurements were conducted to determine the difference in coupling fluid temperature by position. The

temperature measured outside of the beam was compared to the temperature measured directly over the skin surface. At steady state during sonoporation, the temperature over the skin surface was no more than 2 °C higher than the temperature outside of the beam (Fig. 2-17). This small difference had a negligible effect on the outcomes of the study. There was a negligible difference in the temperatures during the control protocols (in the absence of ultrasound).

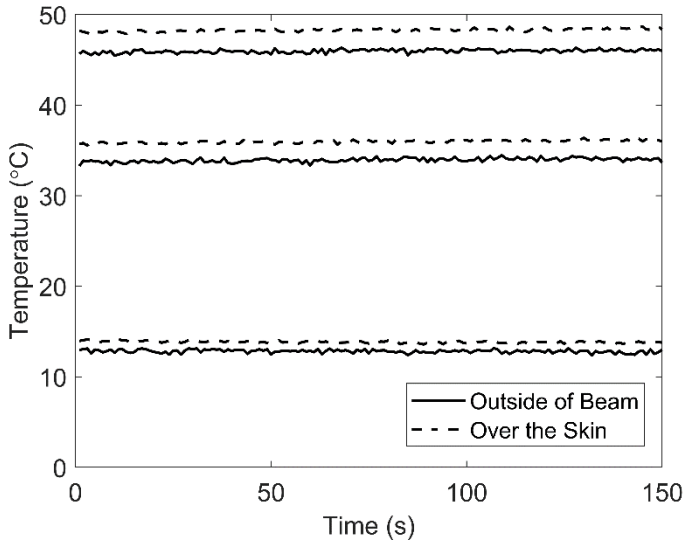

Fig. 2-17 The influence of thermocouple position on the thermocouple reading during sonoporation at an intensity of 55 W/cm^2 and steady state target temperatures of 13 °C, 33 °C, and 46 °C. The solid lines represent the temperatures recorded with the thermocouple outside of the transducer beam. The dashed lines represent the temperatures recorded with the thermocouple directly over the skin.

2.4.2 Transdermal Transport

Using the modified Franz diffusion cell, the coupling fluid temperature was maintained at 13 °C, 33 °C, or 46 °C for 10 minutes. During this period of temperature control, the skin was either exposed to continuous ultrasound at 55 W/cm^2 (the sonoporation protocol), or not (the control protocol). Following this 10 minutes, the coupling fluid was removed and buffer solution containing calcein at 0.1 w/v *%* was placed in the donor chamber for 5 hours. At the

end of each hour, a sample was taken from the receiver chamber. The protocol with ultrasound is termed sonoporation not sonophoresis as the calcein-buffer solution was not present during ultrasound application.

Seven repetitions of the control and sonoporation protocols were conducted for each coupling fluid target temperature to account for experimental variability. The receiver chamber concentrations for all seven repetitions are shown as a function of sampling time for each of the three control protocols (Fig. 2-18a, c, and e) and each of the three sonoporation protocols (Fig. 2-18b, d, and f). Most studies have presented sonoporation data using plots of the mean and standard deviation (Herwadkar, et al. 2012, Sarheed and Abdul Rasool 2011, Terahara, et al. 2002a). However, the variability within sonoporation datasets is often not normally distributed, therefore, presenting only the mean and standard deviation can be misleading. Consider the sonoporation study by Terahara, et al. (2002a) which presents an n=3 skin conductivity enhancement dataset with 100 *%* relative standard deviation. That dataset could have been normally distributed, but it is more likely that two data points were close together while the third was significantly different (making the mean value misleading). With this in mind, the variability of the datasets in Fig. 2-18 (which ranged from 49 *%* to 132 *%* relative standard deviation) is presented with boxplots. The crosses within each box represent the mean values, while the horizontal lines through the centre of each box represent the median values. Any data point that exceeded the upper quartile value by more than 1.5 times the interquartile range is shown as an outlier (represented by the “+” symbol). Note that 1.5 times the interquartile range is the common convention for outlier identification when using boxplots (Hubert and Vandervieren 2008, Krzywinski and Altman 2014, Spitzer, et al. 2014,

Whyte, et al. 2013). These outlier values were still considered when calculating each mean and median.

Following the control protocol, the mean and median receiver concentrations increased with time, regardless of the coupling fluid temperature. The mean concentrations after 5 hours were 30-60 times the mean concentrations after 1 hour. Similar increases in mean and median concentration occurred with time following the sonoporation protocols. The variability of these datasets (Fig. 2-18) was high, but similar to the variability shown in previous, well cited sonoporation studies. In the study by Terahara, et al. (2002a), 20 kHz ultrasound was applied to porcine skin at an intensity of 7.44 W/cm^2 for 12 minutes. A solution containing mannitol was then added to the donor chamber and left to diffuse for 24 hours. This protocol resulted in a 15-fold mean transport enhancement relative to a control case with no ultrasound. After only three repetitions (n=3), the relative standard deviation in the mannitol transport dataset was 93 *%* – similar to the variability in the present study (49 *%* to 132 *%*). Likewise, in the study by Terahara, et al. (2002b), 20 kHz ultrasound was applied to porcine skin at an intensity of 2.39 W/cm^2 for 12 minutes. This protocol resulted in an 8-fold mean mannitol transport enhancement after 24 hours of diffusion. That dataset, which contained five repetitions (n=5), had a relative standard deviation of 100 *%* – again similar to the variability in the present study.

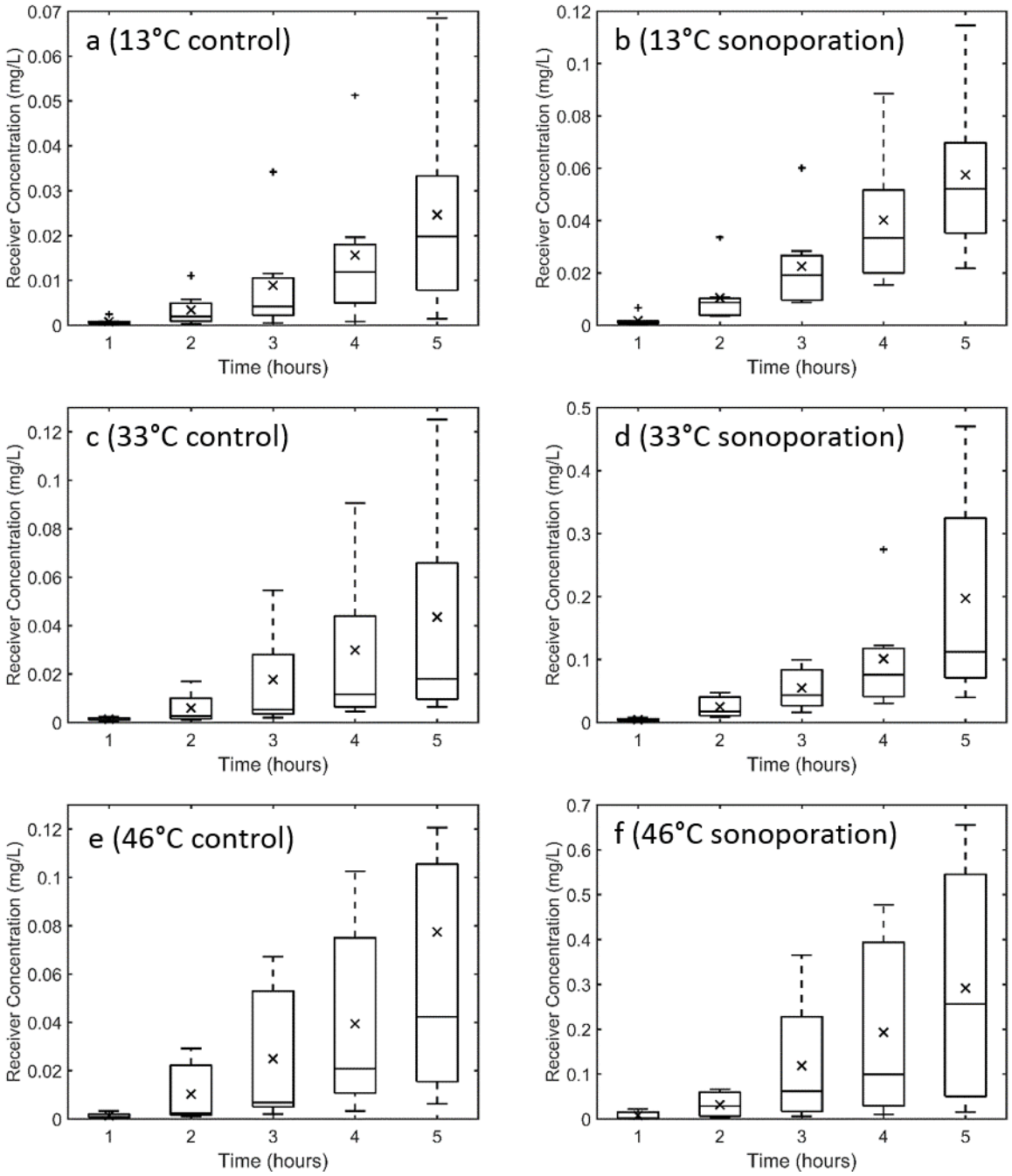

Fig. 2-18 Receiver chamber calcein concentration as a function of transport time following (a) control at 13 °C, (b) sonoporation at 13 °C, (c) control at 33 °C, (d) sonoporation at 33 °C, (e) control at 46 °C, and (f) sonoporation at 46 °C. The crosses within the boxes represent the mean values (n=7). The "+" symbols outside of the boxes represent outliers.

One of the key objectives of this study was to investigate the influence of coupling fluid temperature on post-sonoporation transport. To better illustrate this influence, the datasets from Fig. 2-18 were plotted as a function of coupling fluid temperature (Fig. 2-19). The first five subplots in Fig. 2-19 (a-e) present the receiver chamber concentration following the control (C) and sonoporation (S) protocols at each of the three coupling fluid temperatures (13 °C, 33 °C and 46 °C). The post-control receiver concentrations after five hours of transport are shown on their own (in Fig. 2-19f) so that the increase in mean post-control concentration with increasing coupling fluid temperature is visible.

Regardless of the diffusion time, an increase in coupling fluid temperature resulted in an increase in post-sonoporation transport. After five hours, an increase in coupling fluid temperature (from 13 °C to 33 °C) resulted in a 3.4-fold increase in the mean post-sonoporation calcein transport (p=0.07). A further 1.5-fold increase in mean post-sonoporation transport was found when the coupling fluid temperature was increased from 33 °C to 46 °C (p=0.7). An increase in transport with temperature also occurred post-control (Fig. 2-19f). After five hours, an increase in coupling fluid temperature (from 13 °C to 33 °C) resulted in a 1.8-fold increase in the mean post-control calcein transport (p=0.6). A further 1.8-fold increase in mean post-control transport was found when the coupling fluid temperature was increased from 33 °C to 46 °C (p=0.8). Note that these p-values were found using a Wilcoxon rank sum test. The non-parametric Wilcoxon rank sum test was deemed appropriate for the datasets in Fig. 2-19 due to their abnormal distributions (a Kolmogorov-Smirnov test showed that the data is not normally distributed at the 5 % significance level).

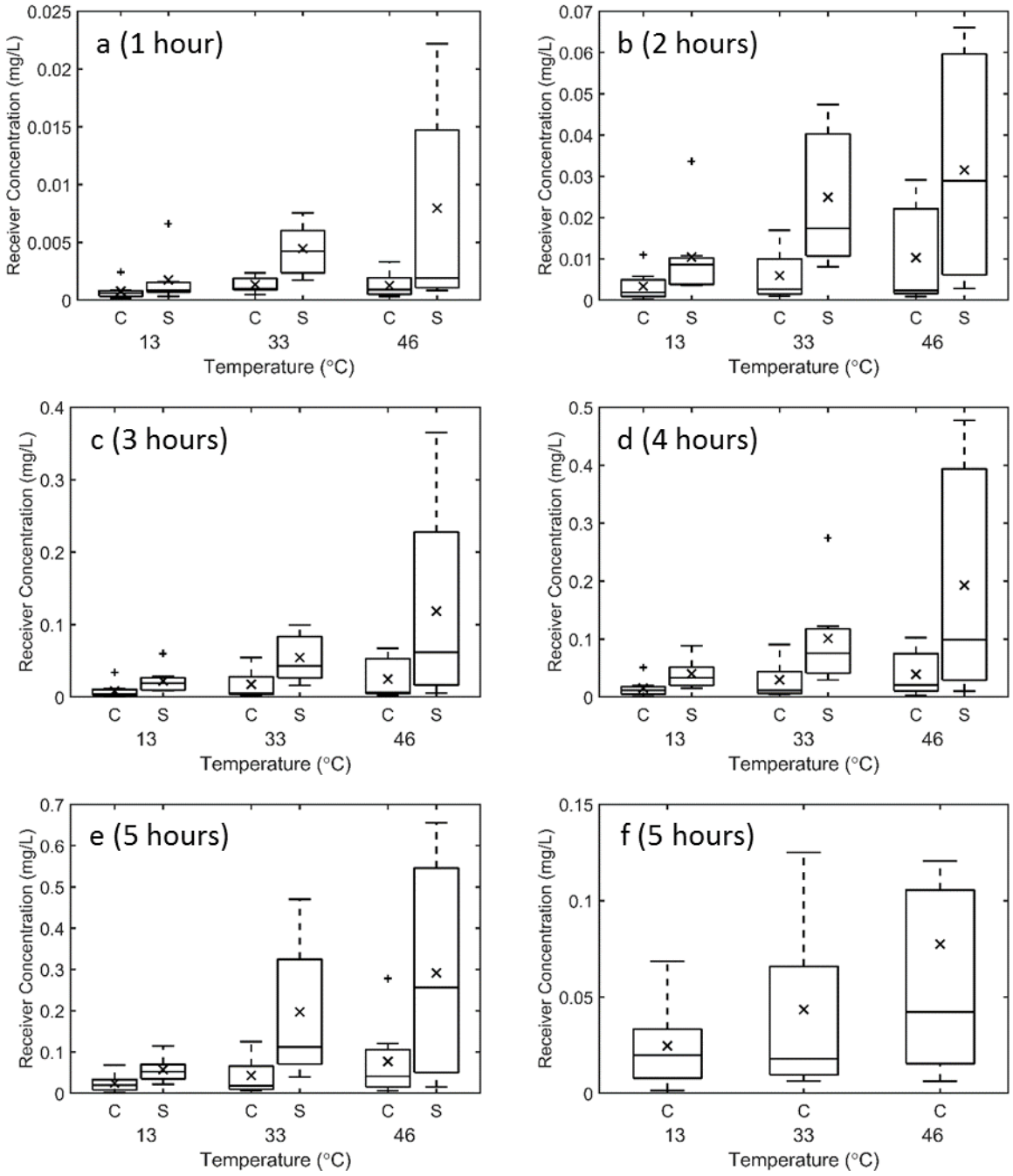

Fig. 2-19 Receiver chamber calcein concentration as a function of coupling fluid temperature after (a) 1 hour, (b) 2 hours, (c) 3 hours, (d) 4 hours, and (e) 5 hours of transport. Panel (f) is the concentration of the control case at 5 hours. The letters C and S denote control and sonoporation protocols. The crosses within the boxes represent the mean values (n=7). The "+" symbols outside of the boxes represent outliers.

2.4.3 Receiver Fluid Temperature

In a separate set of experiments, the receiver temperature was measured (for each of the three sonoporation and control protocols), to quantify its dependence on the coupling fluid temperature and the ultrasound field. A thermocouple, inserted through the bottom of the receiver chamber so that its tip was 2 mm below the skin, recorded data for 30 minutes. The first 10 minutes corresponded to the period of coupling fluid circulation. The following 20 minutes corresponded to the period immediately after calcein application when the diffusion cell was left at room temperature (19 °C ± 1 °C). Two important results are apparent from this receiver fluid temperature data: the receiver fluid temperature during and immediately following the 10 minutes of coupling fluid circulation increased with increasing coupling fluid temperature; and at each of the three coupling fluid target temperatures, the receiver fluid temperature was always higher for the sonoporation protocol than it was for the control protocol.

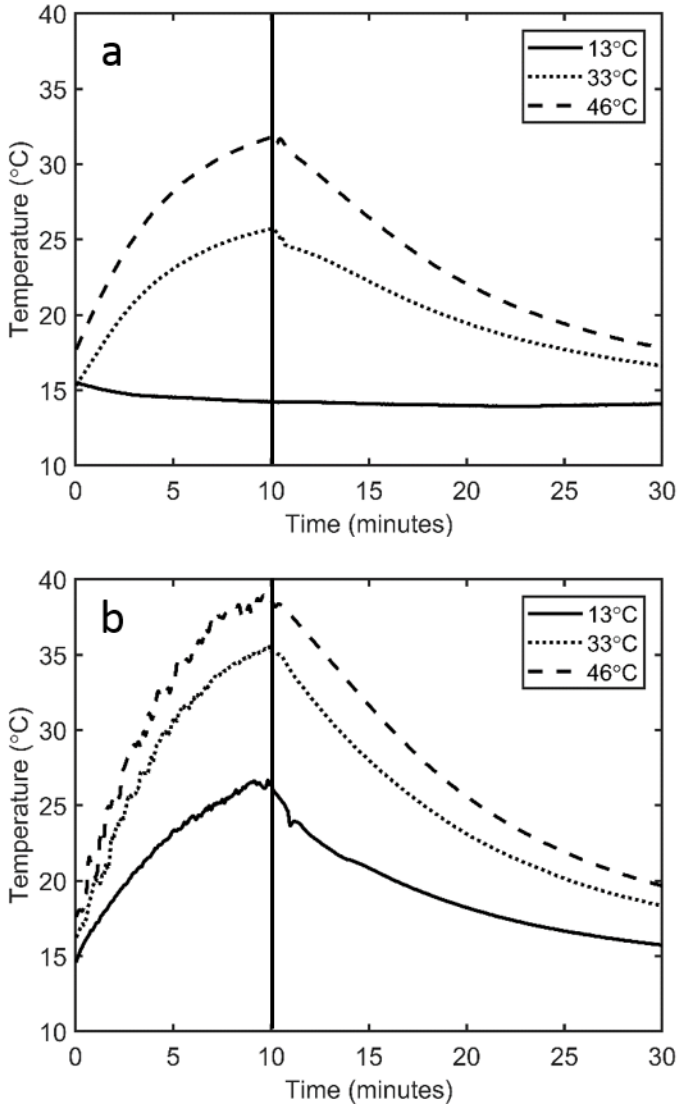

Fig. 2-20 Receiver chamber temperature as a function of time for each of the three coupling fluid target temperatures (a) without ultrasound and (b) with ultrasound. The temperature regulation system was run for the first ten minutes. The receiver fluid was then left to return back towards room temperature (19 °C ± 1 °C) for the remaining twenty minutes. The vertical lines depict the time at which the temperature regulation system was turned off.

2.4.4 Permeant Solution Temperature

The temperature of the calcein-buffer solution was measured during the first 15 minutes of diffusion to quantify its dependence on the coupling fluid temperature and the ultrasound field. Following the 10 minutes of sonoporation (or control), the coupling fluid was removed from the donor chamber and the calcein-buffer was applied to the skin. The room temperature during diffusion was always 19 °C ± 1 °C. In the first 15 minutes of diffusion, the maximum permeant temperature increased with increasing coupling fluid temperature, regardless of the protocol. It is also important to note that, for each of the three coupling fluid target temperatures, the permeant temperature was always higher following the sonoporation protocol than it was following the control protocol.

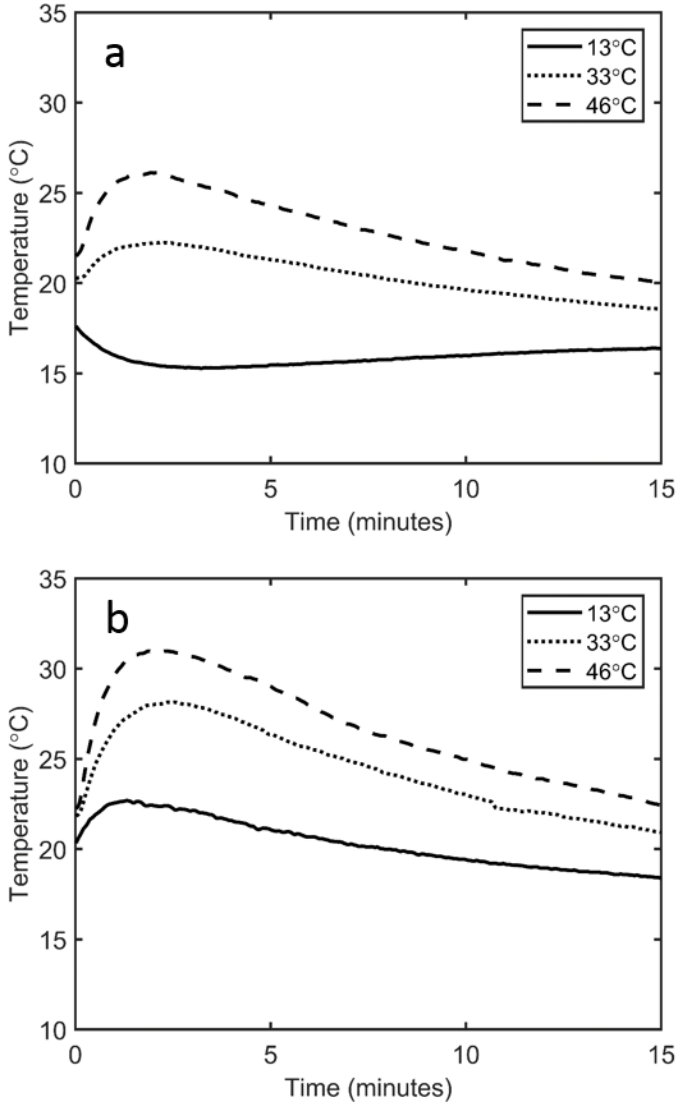

Fig. 2-21 Donor chamber fluid temperature following ten minutes of temperature control (a) without ultrasound and (b) with ultrasound. The 15 minutes shown corresponds to the time immediately after the coupling fluid was replaced with the calcein-buffer solution.

2.4.5 Foil Pitting

Foil pitting experiments were used to determine the influence of coupling fluid temperature on the inertial cavitation activity in the present setup. When the coupling fluid temperature was 10 °C, the mean number of pits after 1 s of ultrasound application (at an intensity of 55 W/cm^2) was 25.5 (Fig. 2-22). When the coupling fluid temperature was increased to 40 °C, the mean number of pits was 12.8 – representing a 50 *%* decrease (p<0.05). The same foil pitting experiment was repeated at an ultrasound intensity of 13 W/cm^2. When the coupling fluid temperature was 10 °C, the mean number of pits after 1 s of ultrasound application was 15.8 (Fig. 2-22). When the coupling fluid temperature was increased to 40 °C, the mean number of pits was 9.8 – representing a 38 *%* decrease (p<0.05).

A similar foil pitting experiment is reported in Appendix A. That study used a transducer to skin distance of 5 mm and an intensity of 34 W/cm^2 (compared to 3 mm and 55 W/cm^2 in the present study). In Appendix A, the mean number of pits following ultrasound application at 40 °C was 57 *%* less than the mean number at 25 °C (p<0.05), which was 65 *%* less than the mean number at 10 °C (Fig. A-13). These results are mentioned here to reinforce that an increase in coupling fluid temperature results in a decrease in pitting.

In the present study, foil pitting experiments were also used to determine the influence of coupling fluid circulation on the inertial cavitation activity at the skin aperture. Ten pieces of aluminium foil were exposed to ultrasound (at an intensity of 55 W/cm^2 and a transducer distance of 3 mm) for 2 s with and without coupling fluid circulation. The coupling fluid temperature was 10 °C ± 1 °C. Without coupling fluid circulation, the mean number of pits after ultrasound application was 36.6 and the median was 36.0 (Fig. 2-23). With coupling fluid

circulation, the mean number of pits was 35.7 and the median was 36.5. Therefore, circulation caused a 2 % decrease in the mean number of pits (p=0.85) and a 1 % increase in the median.

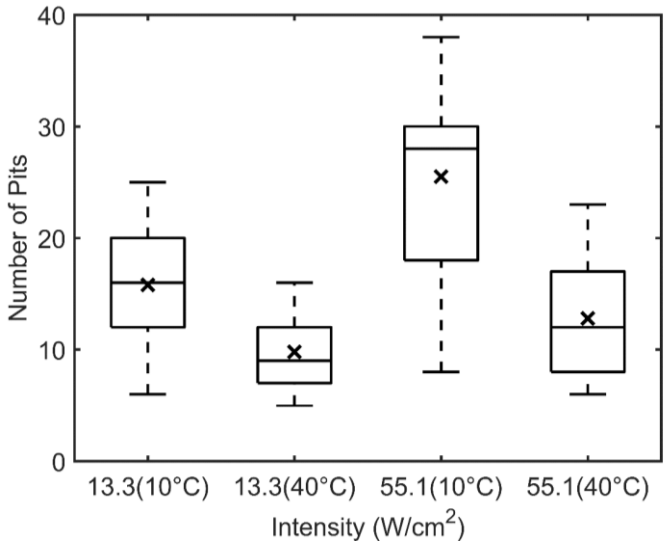

Fig. 2-22 Number of pits in aluminium foil after 1 s of ultrasound application for coupling fluid temperatures of 10 °C and 40 °C, and ultrasound intensities of 13 W/cm^2 and 55 W/cm^2. The transducer to skin distance was 3 mm. The crosses within the boxes represent the mean values (n=10).

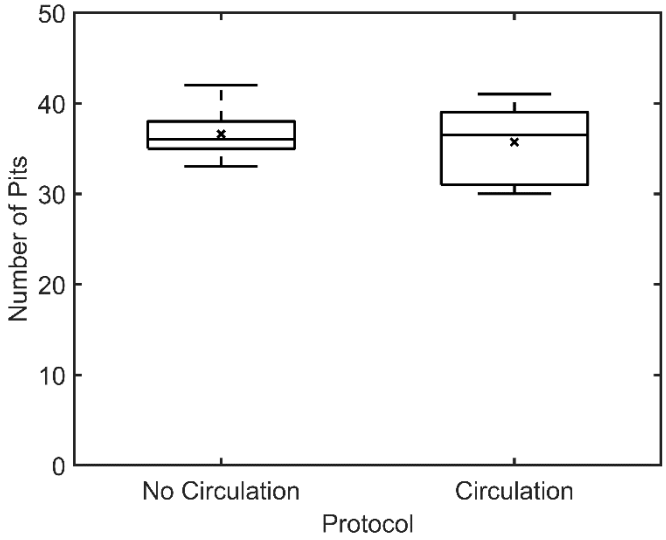

Fig. 2-23 The influence of coupling fluid circulation on the pitting of aluminium foil. Ultrasound was applied for 2 s at an intensity 55 W/cm^2. The transducer to skin distance was 3 mm. The crosses within the boxes represent the mean values (n=10).

2.5 Discussion

This study introduced a modified diffusion cell setup with an active temperature control system that circulated the coupling fluid through a heat exchanger. Foil pitting experiments showed that the circulation of the coupling fluid had a negligible influence on the inertial cavitation activity at the skin aperture. During 10 minutes of ultrasound exposure (55 W/cm^2), the system was able to maintain the steady state coupling fluid temperature to within ± 1 °C of each of the three target temperatures (13 °C, 33 °C, or 46 °C). The introduction of a system capable of maintaining the coupling fluid at a set temperature during sonoporation – without affecting inertial cavitation activity – is a significant contribution to the field as it removes the need for time consuming duty cycles or laborious periodic replacement of the coupling fluid. During the control cases (no ultrasound) the temperature control system was used to maintain the coupling fluid at the target temperatures for a duration of 10 minutes. Temperatures of the receiver chamber fluid and of the donor solution were taken for each sonoporation and control protocol to understand the thermal profile of the system.

The temperatures of the receiver chamber were recorded for each sonoporation and control protocol (see Fig. 2-20). In the absence of ultrasound during the control cases (Fig. 2-20a) the receiver fluid temperature decreased to a minimum of 13 °C when the coupling fluid temperature was 13 °C, and increased to maximums of 26 °C and 32 °C when the coupling fluid temperatures were 33 °C and 46 °C respectively. Therefore, in the absence of ultrasound, heat was conducted through the skin during coupling fluid circulation. This heat conduction implies that, in an *in vivo* or clinical transport setup without ultrasound, the temperature of the circulating fluid used to heat treat the skin prior to drug application would

affect, not just the SC temperature, but also the temperature of the tissue beneath the SC (the dermis and muscle tissue). During sonoporation, the receiver fluid always experienced continuous temperature increases (Fig. 2-20b), regardless of coupling fluid temperature. From an *in vivo* or clinical perspective, these temperature increases are important as they indicate that, during sonoporation, the underlying tissue can experience temperature increases even if the coupling fluid temperature is strictly controlled. The maximum receiver temperatures reached during sonoporation were 14 °C, 10 °C, and 7 °C higher than the temperatures reached during the control cases (for coupling fluid temperatures of 13 °C, 33 °C, and 46 °C). The only methodological difference between the control and sonoporation protocols was the presence of ultrasound. Therefore, the higher receiver temperatures which occurred during the sonoporation protocols must have been caused by absorption of the ultrasound energy. The ultrasound waves passed through the skin and were absorbed by the receiver fluid which resulted in a temperature increase. Increases in the receiver fluid temperature during sonoporation could be controlled in an *in vitro* setup by using a receiver chamber with a water jacket. However, this method of temperature control is not applicable to an *in vivo* or clinical setup. The results of Fig. 2-21 show that, in an *in vivo* or clinical setup, temperature increases in the underlying tissue could instead be mitigated by maintaining a low coupling fluid temperature during sonoporation. During sonoporation in the present study, the receiver fluid reached maximum temperatures of 27 °C, 36 °C, and 39 °C for coupling fluid temperatures of 13 °C, 33 °C, and 46 °C respectively. A lower coupling fluid temperature resulted in a smaller increase in the receiver fluid temperature. Therefore, future *in vivo* or clinical studies should consider maintaining a low coupling fluid temperature during sonoporation to minimize potentially harmful increases in the temperature of the underlying tissue.

During the sonoporation and control experiments, the coupling fluid in the donor chamber was held at one of three target temperatures (13 °C, 33 °C, or 46 °C) for 10 minutes. Following this 10 minute period, the donor chamber was emptied of coupling fluid and a 0.5 mL volume of 0.1 % w/v calcein in a phosphate buffer solution was applied to the skin surface with a pipette. The temperatures of the permeant solution were recorded for each protocol for 15 minutes after it was applied to the skin (Fig. 2-21). The temperature of the permeant was at ~17 ℃ before it was pipetted into the donor chamber.

Following the control protocol in which the coupling fluid was maintained at the lowest target temperature (13 °C), the calcein-buffer solution temperature decreased to 15 °C (Fig. 2-21a). This temperature decrease occurred because heat was conducted from the calcein-buffer to the donor chamber walls which had been cooled to 13 °C by the coupling fluid. Note that the donor chamber wall temperature was measured using an infrared thermometer (Cason CA380). Following the control protocol in which the coupling fluid was maintained above room temperature at 33 °C, the calcein-buffer solution increased to 22 °C (Fig. 2-21a). This temperature increase was due to heat conduction from both the donor chamber walls, which had been heated to 33 °C, and from the receiver chamber fluid, which had been heated to 26 °C. Heat conduction from the donor chamber walls and receiver fluid was also responsible for the increase in permeant temperature, to 26 °C (Fig. 2-21a), following the control protocol at 46 °C.

Following ultrasound application at all target temperatures, the permeant solution always experienced an initial increase in temperature (Fig. 2-21b). The initial permeant solution temperatures following ultrasound application always reached temperatures that were 3-8 °C

above those following the control protocols. For example, the maximum permeant temperature following the 33 °C control protocol was 22 °C, while the maximum temperature following the 33 °C sonoporation protocol was 28 °C. Following both the 33 °C control and 33 °C sonoporation protocols, heat was conducted from the donor chamber walls to the 0.5 mL of permeant solution. However, due to absorption, the receiver chamber fluid temperature was 10 °C higher following the 33 °C sonoporation protocol than it was following the 33 °C control protocol. Therefore, more thermal energy was stored in the system following sonoporation. This additional thermal energy passed from the receiver solution to the permeant via conduction through the skin. This is why the permeant solution had a higher temperature following the 33 °C sonoporation protocol than it did following the 33 °C control protocol. The same is true for the 13 °C and 46 °C cases.

Foil pitting experiments were conducted at coupling fluid temperatures of 10 °C and 40 °C. For an intensity of 55 W/cm^2, an increase in coupling fluid temperature corresponded to a 50 % decrease in the number of pits (p<0.05). It is reasonable to conclude from these data that, in the skin sonoporation experiments in this study, the skin was exposed to less inertial cavitation activity as the coupling fluid temperature was increased. This conclusion agrees with the assertion made in the HIFU study by Hockham, et al. (2010) which attributed the decrease in inertial cavitation activity to an increase in vapour pressure with increased coupling fluid temperature. An explanation is also given in the study by (Bader, et al. 2012): the cavitation threshold limits the energy that can be stored within the ultrasound field, which limits the maximum rarefactional pressure. The increase in temperature decreases the threshold for cavitation which decreases the maximum rarefactional pressure – decreasing the inertial cavitation activity which can be achieved for a given intensity. While inertial

cavitation activity decreased with increasing coupling fluid temperature, the results of the present study show that transdermal transport following sonoporation increased with coupling fluid temperature (Fig. 2-19).

The increases in transdermal transport with coupling fluid temperature, following both the control and sonoporation protocols (shown Fig. 2-19), were a result of temperature-dependent changes in the SC lipid structure. The SC lipids are known to undergo multiple phase transitions between 10 °C and 50 °C (Akomeah, et al. 2004, Clarys, et al. 1998, Gay, et al. 1994, Silva, et al. 2006, Tang, et al. 2002a), and these phase transitions are known to increase skin permeability (Gay, et al. 1994). Multiple phase transitions occurred throughout the coupling fluid temperature range (13 °C to 46 °C) used for both the control and sonoporation protocols. Therefore, these phase transitions provide a logical explanation for the increases in transport with temperature shown in Fig. 2-19. Differences in the calcein-buffer temperature (shown in Fig. 2-21) may also have contributed to the increase in transdermal transport with increasing coupling fluid temperature. An increase in the temperature of a permeant is known to result in an increase in the diffusivity of that permeant (Clarys, et al. 1998). This was demonstrated in the passive diffusion study by Akomeah, et al. (2004) which investigated the temperature dependence of methyl paraben transport through a cellulose membrane. The transport of methyl paraben through the cellulose membrane, measured after four hours of diffusion at a temperature of 23 °C, 30 °C, 37 °C, or 45 °C, increased with increasing temperature. The cellulose membrane had a temperature tolerance of 60 °C so its permeability was assumed to be constant in the 23 °C to 45 °C temperature range. Therefore, the increases in transport through the membrane with increasing temperature were due to an increase in the diffusivity of the permeant (methyl paraben). In

the present study, the maximum calcein-buffer temperature increased with increasing coupling fluid temperature, therefore, the diffusivity of the permeant in the first 15-20 minutes also increased with increasing coupling fluid temperature. However, this increased diffusivity could only affect the receiver chamber concentration measured at the end of the first hour of diffusion. Once the sample was taken at the end of the first hour, the coupling fluid temperature had already returned to room temperature and been at room temperature for 40-45 minutes. The temperature dependence shown in Fig. 2-19 for each subsequent hour could not have been influenced by increased diffusivity of the permeant alone. A significant dependence on coupling fluid temperature is shown across the full five hours in Fig. 2-19, therefore, although permeant diffusivity may have had some affect within the first 15-20 minutes, the dependence of transport on the coupling fluid temperature at the end of the five hours must have been due to a longer lasting effect – skin permeability increase due to phase transitions in the SC.

The increase in post-sonoporation transport with increasing coupling fluid temperature shown in Fig. 2-19 should be considered by researchers who wish to achieve a high degree of post-sonoporation transport in future *in vivo* or clinical studies. For a given set of ultrasound parameters (frequency, intensity, application time, and transducer distance) the post-sonoporation transport will increase with increasing coupling fluid temperature. Therefore, a temperature control system similar to the one introduced in this study could be used to maintain an elevated temperature during *in vivo* or clinical sonoporation so as to increase post-sonoporation transport. However, when using an increased coupling fluid temperature to increase post-sonoporation transport, researchers must still ensure that the temperatures

of the SC and underlying tissue remain at a safe level that will not cause burns or irreversible damage to epidermal cells.

The influence of coupling fluid temperature on the post-sonoporation transport has already been discussed – the post-sonoporation transport increased with increasing coupling fluid temperature (Fig. 2-20). Consider now the influence of coupling fluid temperature on the ultrasound enhancement (the ratio of the post-sonoporation to post-control transport at each coupling fluid temperature). Researchers have established that inertial cavitation is the primary mechanism behind the skin permeability enhancement that occurs during sonoporation (Tang, et al. 2002a, Tezel, et al. 2002, Tezel, et al. 2001). From the foil pitting experiments it was concluded that the skin was exposed to less inertial cavitation activity at higher coupling fluid temperature (Fig. 2-22). From this result, it would be logical to assume that increasing the coupling fluid temperature would lead to a decrease in the ultrasound enhancement – as this enhancement is caused by inertial cavitation activity which decreased with increasing coupling fluid temperature. However, a comparison of the control and sonoporation datasets in Fig. 2-19 indicates that the ultrasound enhancement was not diminished when the coupling fluid temperature was increased: for each of the five hours shown in Fig. 2-19a-e, the post-sonoporation transport datasets were always significantly greater ($0.026 \leq p \leq 0.16$) than the post-control transport datasets. Therefore, although the number of inertial cavitation collapses impacting the skin decreased by up to 50 % with increasing temperature, the cavitation induced permeability increase did not decrease. To make up for the lower number of collapses impacting the skin, the permeability increase caused by each cavitation collapse must then have increased with increasing coupling fluid temperature. In other words, increasing the skin temperature must have decreased the ability

of the SC lipids to withstand the disordering which is known to result from cavitation (Alvarez-Román, et al. 2003, Lee, et al. 2010, Ueda, et al. 1996). This temperature effect was previously postulated in the sonophoresis study by Merino, et al. (2003) which suggested that increasing the skin temperature may 'soften' the SC lipids for disruption by the ultrasound energy. Similarly, in their study on transdermal enhancement by laser-induced stress waves (LISW), Makoto, et al. (2002) suggested that an increase in the skin temperature during LISW exposure increased the fluidity of the SC lipids, making them more susceptible to disruption by the LISW. A similar effect may have occurred in the present study with increased coupling fluid temperature disordering the SC lipids thereby making them more susceptible to further disordering by inertial cavitation. The brittle-to-ductile phase transition which has been shown to occur in the SC between 20 °C and 40 °C (Papir, et al. 1975) could also make the SC lipids more susceptible to cavitation-induced disordering. This brittle to ductile transition was used in the ballistic particle delivery study by Kendall, et al. (2004) to explain why particle penetration depth increased by 2-fold when the ambient temperature was increased from 20 °C to 40 °C – the lipids were not able to resist the particles as well at higher temperature. A similar brittle to ductile change in the SC structure may also have compromised the SC lipids' ability to withstand disordering by the forces induced by inertial cavitation in the present study.

The ultrasound enhancements achieved in the present study are comparable to those achieved in sonoporation studies in the literature. The mean ultrasound enhancement (the ratio of the mean post-sonoporation to mean post-control transport) was 2.3 for the 13 °C case (significant at p=0.04). For the 33 °C case the mean enhancement was 4.5 (p=0.04). For the 46 °C case the mean enhancement was 3.8 (p=0.13). Direct comparisons with the

literature are difficult given the range of intensities, transducers, transducer to skin distances, application times, permeants, permeant diffusion times, skin models, skin processing protocols, and coupling fluid temperatures used in different studies. However, some approximate comparisons are possible and helpful in validating the results of the present study. In their low-frequency (20 kHz) sonoporation study, (Herwadkar, et al. 2012) applied ultrasound to hairless rat skin for 2 minutes at an intensity of 6.9 W/cm^2. The unspecified transducer tip was 3 mm from the skin surface during sonoporation. Ketoprofen (an anti-inflammatory drug) was then applied to the skin surface and left to diffuse for 24 hours. The concentration of Ketoprofen in the receiver chamber was then measured with HPLC. Relative to a passive control case, the mean enhancement achieved by (Herwadkar, et al. 2012) was approximately 3.3 (p=0.05), similar to the enhancements in the present study. In the sonoporation study by (Tang, et al. 2002a), 20 kHz ultrasound was applied to full thickness porcine skin for 2 hours (10 % duty cycle) at an intensity of 1.6 W/cm^2. The unspecified transducer tip was 8 mm from the skin surface. Relative to a passive control case, the electrical conductivity of the skin was enhanced by 2.5, similar to the enhancements in the present study. In the sonoporation study by Mitragotri, et al. (2000a), 20 kHz ultrasound was applied to full thickness porcine skin for 15 minutes (10 % duty cycle) at an intensity of 14 W/cm^2. The unspecified transducer tip was 10 mm from the skin surface. Relative to a passive control case, the electrical conductivity of the skin was enhanced by 5, again similar to the enhancements in the present study.

The present study was motivated by previous skin sonoporation studies that avoided excessive ultrasound related temperature rises by using duty cycles and by replacing the coupling fluid during US application (Lavon, et al. 2005, Paliwal, et al. 2006, Tang, et al. 2002a,

Terahara, et al. 2002a). Duty cycles do not allow for a constant coupling fluid temperature, they only slow the rate of heating. In the present setup, when the temperature control system was turned off, the coupling fluid temperature increased at a rate of 8.4 °C/min with continuous application at 55 W/cm^2, 3.5 °C/min with a 50 % duty cycle, and 0.9 °C/min with a 10 % duty cycle (Fig. 2-15). The other method that has been used to mitigate temperature rises – fluid replacement, also allows for changes in coupling fluid temperature during sonoporation. In the studies by Tang, et al. (2002a) and Terahara, et al. (2002a) the coupling fluid was at room temperature (~23 °C) at the beginning of sonoporation. The coupling fluid was then replaced during sonoporation when it reached approximately 40 °C. The temperature-dependent transport increases found in the present study show that even these temperature increases of 15-20 °C, reported by Tang, et al. (2002a) and Terahara, et al. (2002a), affect skin permeability. Therefore, the skin permeability enhancements that those studies reported may have been due to a combination of inertial cavitation and coupling fluid temperature increases. Future sonoporation studies should employ a circulation system to ensure that the coupling fluid temperature is the same during sonoporation and control experiments. This would remove any potential influence of coupling fluid temperature, thereby isolating the influence of inertial cavitation.

The temperature control system reported here is capable of maintaining a set steady state coupling fluid temperature for much longer than 10 minutes if required. In the present study, a 10 minute application time was used as it resulted in significant ($0.026 \leq p \leq 0.16$) permeability enhancements, without taking an excessive amount of time to run all 42 individual transport experiments. However, even greater permeability enhancement can be achieved by using longer application times (Mitragotri, et al. 2000a, Terahara, et al. 2002a). In Appendix B, the

mean and median receiver chamber calcein concentration following 30 minutes of sonoporation (at constant temperature) were shown to be twice those following 10 minutes of sonoporation (significant at p=0.38). The increase in skin permeability enhancement with ultrasound application time in Appendix B was due to inertial cavitation activity – the longer the skin was exposed to the ultrasound field, the more inertial cavitation events impacted the SC. Future, *in vitro*, *in vivo* or clinical studies that want to obtain a greater permeability increase by using an application time of 30 minutes, 1 hour, or more can do so with the present system without any concern for coupling fluid temperature increase. This long duration temperature control capability enables far greater ultrasound application times than have previously been feasible. Previously, when a duty cycle was used to control thermal effects, 30 minutes of ultrasound would have taken up to 5 hours to administer. This duration would be impractical in a clinical setting and tedious in a laboratory setting. With the present system, long durations of continuous ultrasound application are now possible.

This study focused on coupling fluid temperature control during skin sonoporation. However, it is interesting to consider the potential implications of employing such a system during sonophoresis, where coupling fluid temperature increases are also common (Alvarez-Román, et al. 2003, Merino, et al. 2003, Mitragotri, et al. 1996, Polat, et al. 2012). In sonophoresis, the permeant solution also acts as the coupling fluid. Using a coupling fluid temperature control system during sonophoresis would not only allow constant ultrasound application without the need for duty cycles or fluid replacement, but could also be used to maintain a higher diffusion coefficient than that which occurs at room temperature. The cooling system was designed so that dissolved permeants could easily be flushed and cleaned

from the tubing and heat exchanger. Therefore, the cooling system could easily be employed in a sonophoresis study.

The present study also showed that polypropylene can be used for *in vitro* sonoporation experiments. No cavitation damage occurred on any of the donor or receiver chamber surfaces. Also, the polypropylene was semi-transparent which made it easy to identify any air bubbles in the receiver chamber. Researchers conducting sonoporation (or sonophoresis) experiments would find polypropylene cells to be an affordable, easy to customise alternative to glass diffusion cells which are expensive and cannot be geometrically customised without the help of a glassblower.

2.6 Conclusions

A modified Franz diffusion cell along with a circulating temperature regulation system successfully maintained the coupling fluid temperature at either (13 °C, 33 °C, or 46 °C) during the sonoporation of porcine skin at 55 W/cm^2. Circulation of the coupling fluid did not affect the inertial cavitation activity at the skin aperture. The introduction of a system capable of maintaining a constant coupling fluid temperature during continuous sonoporation is a significant contribution to the field as it removes the need for replacement of the coupling fluid or time consuming duty cycles. In an experimental setting, use of the present temperature control system would reduce the time required to run each experiment and the labour required by the researcher. In a clinical setting, use of the present temperature control system could reduce the required patient contact time 10-fold relative to an application protocol that required a 10 % duty cycle to minimise thermal effects. Therefore this system

enables far more clinically practical sonoporation protocols than could previously have been achieved. Thesis Objective 1 (design and manufacture a system which enables the coupling fluid to be set and maintained at a variety of temperatures during skin sonoporation) has been fulfilled.

Increasing the coupling fluid temperature led to a decrease in foil pitting. An increase in coupling fluid temperature from 10 °C to 40 °C corresponded to a 38 % decrease in the number of pits (p<0.05). It is then concluded that, in all of the skin experiments in this study, the skin was exposed to less inertial cavitation activity when the coupling fluid temperature was higher. This agrees with the assertion made in the HIFU study by Hockham, et al. (2010) which attributed a decrease in inertial cavitation activity with increasing coupling fluid temperature to an increase in vapour pressure. Thesis Objective 2 (investigate the influence of coupling fluid temperature on the inertial cavitation activity that occurs in a low-frequency Franz diffusion cell setup) has been fulfilled.

Transdermal transport experiments showed that increasing the temperature at which the coupling fluid was maintained during sonoporation increased the post-sonoporation transport of calcein. Following 5 hours of diffusion, the median receiver chamber calcein concentration after sonoporation at a coupling fluid temperature of 46 °C was 2.3 times the concentration achieved after sonoporation at 33 °C, which was 2.2 times the concentration achieved after sonoporation at 13 °C. Past studies have used duty cycles and fluid replacement to keep the coupling fluid below 37-40 °C during sonoporation. However, this study shows that temperature dependent increases in post-sonoporation transport can occur above and below 37-40 °C. Thesis Objective 3 (use the coupling fluid temperature control

system to investigate the influence of coupling fluid temperature on post-sonoporation transport) has been fulfilled.

Two findings from this study have important implications for any future *in vivo* or clinical sonoporation studies that adopt this new method for coupling fluid temperature control. For a given set of experimental parameters (intensity, application time etc.), a higher coupling fluid temperature during sonoporation results in more post-sonoporation transport. However, a lower coupling fluid temperature during sonoporation results in a smaller increase in the temperature of the tissue underlying the SC. Given these two findings, future *in vivo* or clinical sonoporation studies that incorporate coupling fluid temperature control will need to carefully select their target coupling fluid temperature so as to find a balance between transport (which is greatest at high temperature) and safety (which is greatest at low temperature).

As a final reinforcement of the present study's contribution to the field, consider 12 skin sonoporation and sonophoresis studies from the literature (Boucaud, et al. 2002, Herwadkar, et al. 2012, Lavon, et al. 2005, Le, et al. 2000, Merino, et al. 2003, Mitragotri, et al. 2000a, Paliwal, et al. 2006, Sarheed and Abdul Rasool 2011, Smith, et al. 2003, Tang, et al. 2002a, Terahara, et al. 2002a, Terahara, et al. 2002b). From the information provided it was calculated that a total of 34 hours of ultrasound was applied across these 12 studies. However, due to the various duty cycles used, it took 210 hours to administer this 34 hours of ultrasound. Even without considering the time that would have been spent replacing coupling fluid, it is apparent that use of the temperature control system introduced in the present study would have saved approximately 176 hours across these 12 studies.

3 Passive Cavitation Detection During Skin Sonoporation

3.1 Abstract

Passive cavitation detectors (PCDs) have been effectively employed in high-intensity focused ultrasound (HIFU) and cell sonoporation studies to monitor variations in inertial cavitation activity during the course of ultrasound application. However, there are few published works that use PCDs in the fields of low-frequency skin sonoporation or sonophoresis. This is due to the geometric limitations imposed by the glass Franz diffusion cells that are commonly used for experimentation. This study uses the enlarged donor chamber of Chapter 2 so that a PCD hydrophone can be positioned in the coupling fluid during sonoporation. This PCD setup monitored the broadband noise emission as skin was sonoporated under four different coupling fluid temperature-intensity combinations. An inertial cavitation dose (ICD) value was then calculated for each sonoporation experiment by time-averaging the broadband noise emission over the 10 minutes of sonoporation. The mean ICD value increased with increasing intensity (as inertial cavitation does) and decreased with increasing temperature (as inertial cavitation was shown to do). Following sonoporation, a permeant was applied to the skin and left to diffuse passively for 2 hours. The post-sonoporation transport was then plotted against the ICD to determine whether the PCD output could be used, not just to monitor inertial cavitation activity, but as an indicator of the post-sonoporation transport. The poor correlation between ICD and post-sonoporation transport lead to the conclusion that the coupling fluid temperature must be held constant if

ICD is to be used as such an indicator. This is because an increase in coupling fluid temperature results in a decrease in ICD yet an increase in post-sonoporation transport.

3.2 Introduction

Experimental setups that use inertial cavitation often include PCD systems to monitor inertial cavitation activity during ultrasound application (Bian, et al. 2017, Bull, et al. 2013, Cleveland, et al. 2000, Farny, et al. 2010, Gateau, et al. 2011, Gyöngy and Coussios 2010, Hallow, et al. 2006, Helga, et al. 2015, Hockham, et al. 2010, King, et al. 2010, Liu, et al. 1998, Salgaonkar, et al. 2009). Inertial cavitation activity can change during the course of ultrasound application due to bubble dissolution, the depletion of cavitation nuclei, interactions between bubbles, increased vapour pressure caused by heating, and shielding caused by pre-focal bubble activity (Hockham, et al. 2010). Monitoring the inertial cavitation activity with a PCD allows any changes in the inertial cavitation activity to be detected in real-time. The experimental inputs to the ultrasound field can then be adjusted to counteract these changes and ensure that the cavitation activity remains at the desired level throughout ultrasound application. Furthermore, PCD output is seen as a potential unifying parameter that can correlate with permeability increase, meaning that monitoring it during ultrasound application can enable real-time feedback about the ultrasound effects that are occurring under a diverse range of experimental conditions (Hallow, et al. 2006).

While PCDs have been frequently employed in studies involving the insonation of media other than skin (Coussios and Roy 2008, Farny, et al. 2010, Liu, et al. 1998, Yao-Sheng, et al. 2010), they have rarely been used in low-frequency *in vitro* skin insonation studies. This is due

to the geometric constraints within the traditional Franz diffusion cell which make it difficult to fit both a transducer and a hydrophone in the coupling fluid. In the study by Tang, et al. (2002a) a hydrophone was fixed to the outer surface of the bottom of a receiver chamber with epoxy. This allowed for the PCD data to be recorded during skin insonation but did not directly capture the ultrasound field signal within the coupling fluid where important inertial cavitation activity is known to occur. Tezel and Mitragotri (2003a) were able to directly monitor the ultrasound field in the coupling fluid, but could not take measurements during skin insonation as the hydrophone was positioned where the skin sample would usually be positioned. Tezel, et al. (2002) placed their hydrophone perpendicular to the transducer in their low-frequency skin study, however, they did not specify the distance. Furthermore, they performed all of their PCD measurements in a separate chamber due to the geometrical constraints of a Franz diffusion cell. An *in vitro* skin apparatus that allows for a hydrophone to be positioned in the coupling fluid during skin sonoporation has not yet been reported. The lack of such an apparatus means that there is currently no way to monitor the inertial cavitation activity that occurs in the coupling fluid during skin sonoporation.

This study introduces a modified Franz diffusion cell setup that facilitates a PCD hydrophone in the coupling fluid during skin sonoporation. This PCD setup monitored the broadband noise emission as skin was sonoporated under four different coupling fluid temperature-intensity combinations. The dependence of the PCD output on the intensity and coupling fluid temperature is quantified to assess the ability of the PCD to respond to changes in inertial cavitation activity (brought on by changes in coupling fluid temperature and ultrasound intensity). The receiver chamber calcein concentration following sonoporation is

then plotted against the PCD output to assess the potential of using the PCD, not just to monitor inertial cavitation activity, but also as an indicator of post-sonoporation transport.

3.3 Materials and Methods

3.3.1 Modified Vertical Diffusion Cell

The diffusion cells used in this study were the same as those used in Chapter 2. The donor chambers had outer diameters of 65 mm, inner diameters of 61 mm and aperture diameters of 9 mm. The receiver chambers had volumes of 3.2 mL and aperture diameters of 9 mm. The diffusion cell is shown again in Fig. 3-1. The donor and receiver chambers were turned from solid polypropylene rods on a CNC lathe. The receiver chamber sampling arm and donor chamber ports were then added by gluing sections of carbon fibre tubing to the polypropylene. The donor and receiver chambers were held together with clamps 3-D printed from acrylonitrile butadiene styrene (ABS).

Fig. 3-1 Diffusion cell geometry (top) plan view, (middle) front view, and (bottom) isometric view

3.3.2 Coupling Fluid Temperature

The coupling fluid temperature was maintained at 10 °C or 37 °C during sonoporation. The system used to maintain the coupling fluid temperature during sonoporation was the same as that used in Chapter 2. Briefly, the coupling fluid was circulated out of one donor chamber port, through a heat exchanger, and back into the other donor chamber port. This circulation was maintained at a flow rate of 0.14 L/min using a peristaltic pump (6-V Peristaltic Pump, Amazon, Seattle, WA, USA). An overview of the temperature control circuit is shown in Fig. 3-2. The donor chamber, pump and heat exchanger were linked together by silicone tubing

(Silicone Tubing Clear Grade Inner Diameter 2.6 mm, Rubbermark Industries, Auckland, New Zealand). The heat exchanger consisted of an aluminium block submerged in a water bath (FP-50 Refrigerated/Heating Circulator, Julabo GmbH., Selbach, Germany). In this study, 10 °C was chosen for the lower temperature because anything colder has been shown to result in discomfort after extended exposure (Dunne, et al. 2013). The high coupling fluid temperature was set to 37 °C because it has been reported that exposure to temperatures over 40 °C can cause significant discomfort and irreversible damge to epidermal cells (Lindeque, et al. 2013, Moritz and Henriques 1947). The coupling fluid temperature was measured throughout sonoporation using a type K thermocouple (Jaycar Electronics Pty Ltd., Auckland, New Zealand). The positioning of the thermocouple in the coupling fluid is qualitatively depicted in Fig. 3-3.

3.3.3 Ultrasound

A VC 505 ultrasonic processor (Sonics and Materials Inc., Connecticut, USA), fitted with a 13 mm replaceable tip, was used to generate a 20 kHz ultrasound field. The tip of the transducer was 3 mm from the surface of the skin during sonoporation. Following the manufacturer's instructions, compressed air was circulated through the ultrasonic processor to keep it cool during ultrasound application. Two intensities were used in this study: 8.9 W/cm^2 and 36 W/cm^2 (spatial average, temporal average). These intensities were determined using a common calorimetric approach (Merino, et al. 2003, Mitragotri, et al. 2000a, Mitragotri, et al. 2000b, Morimoto, et al. 2005, Mutoh, et al. 2003, Terahara, et al. 2002a) that was described in Robertson and Becker (2018).

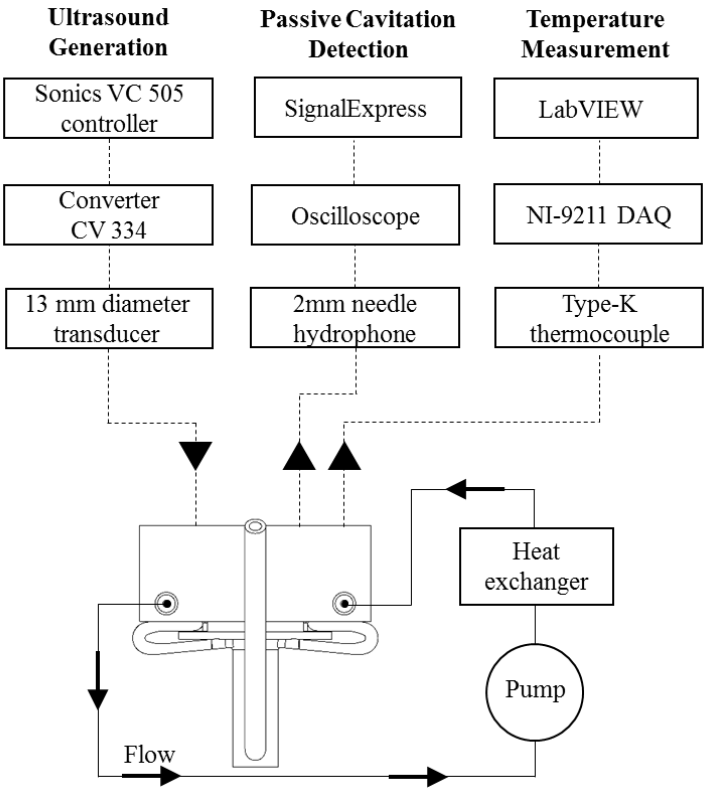

Fig. 3-2 System schematic. The dashed lines represent the signal inputs and outputs to and from the instruments in the coupling fluid. The solid lines represent the coupling fluid circuit.

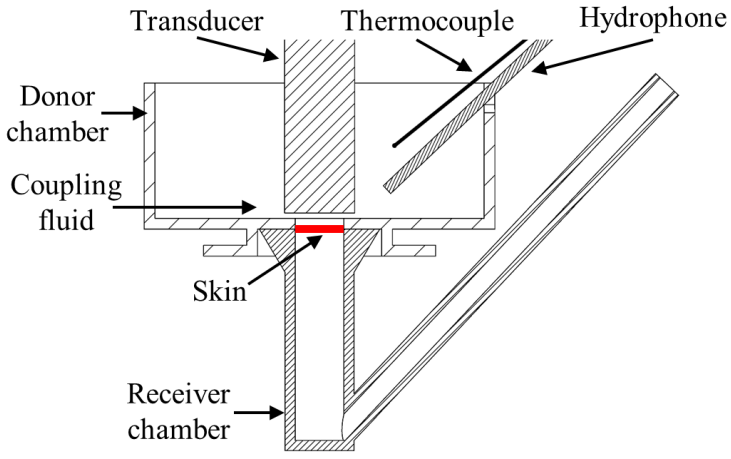

Fig. 3-3 Cross-section of the diffusion cell showing the positioning of the hydrophone, thermocouple, and transducer. The distance between the tip of the hydrophone and the bottom edge of the transducer was 5 mm.

3.3.4 Porcine Skin

The *in vitro* skin samples used in this study were harvested from porcine ears. The ears were collected from an abatoir (Ashburton Meat Processors Ltd, Ashburton, New Zealand) immediately after slaughter. The ears were not exposed to detergent or scalded at the abatoir. In the laboratory, the ears were cleaned with cold water to remove the blood and soil. The top layer of the skin was then removed with a dermatome (Dermatome 50 mm, Nouvag AG, Goldach, Switzerland), which was set to a thickness of 1 mm. The pieces of dermatomed skin were individually wrapped in parafilm (PARAFILM, Sigma-Aldrich, St. Loius, MO, USA) and placed in airtight plastic containers. These containers were stored in a -20 °C freezer until use. The total time from slaughter to freezer was approximately 3.5 hours. All of the skin samples used in this study were stored in the freezer no longer than one week.

3.3.5 Chemicals

The permeant solution used for the transport experiments was made by dissolving calcein (Calcein C0875, Sigma-Alfrich, St. Louis, MO, USA) in phosphate buffered saline (Gibco PBS, Thermo Fisher Scientific, Waltham, MA, USA) at a concentration of 0.1 % w/v (1 g/L). This solution was stored at room temperature. Deionised water was taken from a Labwater L991008 Deioniser (Suez Ltd, Thame, UK).

3.3.6 Hydrophone Alignment and Passive Cavitation Detection

One of the objectives for this study was to assess the ability of a PCD hydrophone to monitor the inertial cavitation activity occurring in a Franz diffusion cell during sonoporation. A hydrophone (2.0 mm Needle Hydrophone, Precision Acoustics Ltd., Dorchester, Dorset, UK)

was positioned in the coupling fluid during each of the sonoporation experiments described in Section 3.3.7. The manufacturer coated the hydrophone tip with a thin layer of silicone to protect the sensitive piezoelectric element from cavitation damage (Fig. 3-4). At the transducer driving frequency (20 kHz), the hydrophone had a sensitivity of -236.4 dBre1V/µPa. This sensitivity was measured by Neptune Sonar Ltd (East Yorkshire, UK). Note that the full list of calibrated sensitivity values, measured by Neptune Sonar, for frequencies between 5 kHz and 1000 kHz are shown in Appendix C.

Fig. 3-4 Image of the needle hydrophone showing the silicone coating, 2 mm diameter piezoelectric element and submersible preamplifier

The hydrophone was held in place by an aluminium sleeve. The mounting point of the sleeve was fixed relative to the diffusion cell and transducer. The complete schematics of the support structure for the transducer, hydrophone, and diffusion cell are presented in Appendix A. In the present study, the hydrophone tip was ~7 mm from the skin aperture during sonoporation. When in the "sonoporation position" (Fig. 3-5a), the hydrophone was able to record the pressure variations within the coupling fluid (a cross-section of Fig. 3-5a is shown in Fig. 3-3). Removal of the diffusion cell from the position shown in Fig. 3-5a was necessary as each experimental repetition was performed with a different diffusion cell. To enable a diffusion cell to be removed from the setup and replaced by the next one, the transducer was moved upwards on the clamp stand which held it in place and the hydrophone

sleeve was rotated out of the donor chamber (Fig. 3-5b). The diffusion cell could then be removed from its holder (Fig. 3-5c-d). To prepare for the next experimental repetition, another diffusion cell was inserted into the holder and the hydrophone sleeve was rotated back into the “sonoporation position”. The transducer was then lowered back down the clamp stand so that the setup again resembled Fig. 3-5a. This rotating alignment system ensured a consistent hydrophone position during sonoporation. An isometric view of the 3D printed ABS diffusion cell holder is shown in Fig. 3-6. An image of the transducer, hydrophone, thermocouple, and diffusion cell in place is shown in Fig. 3-7.

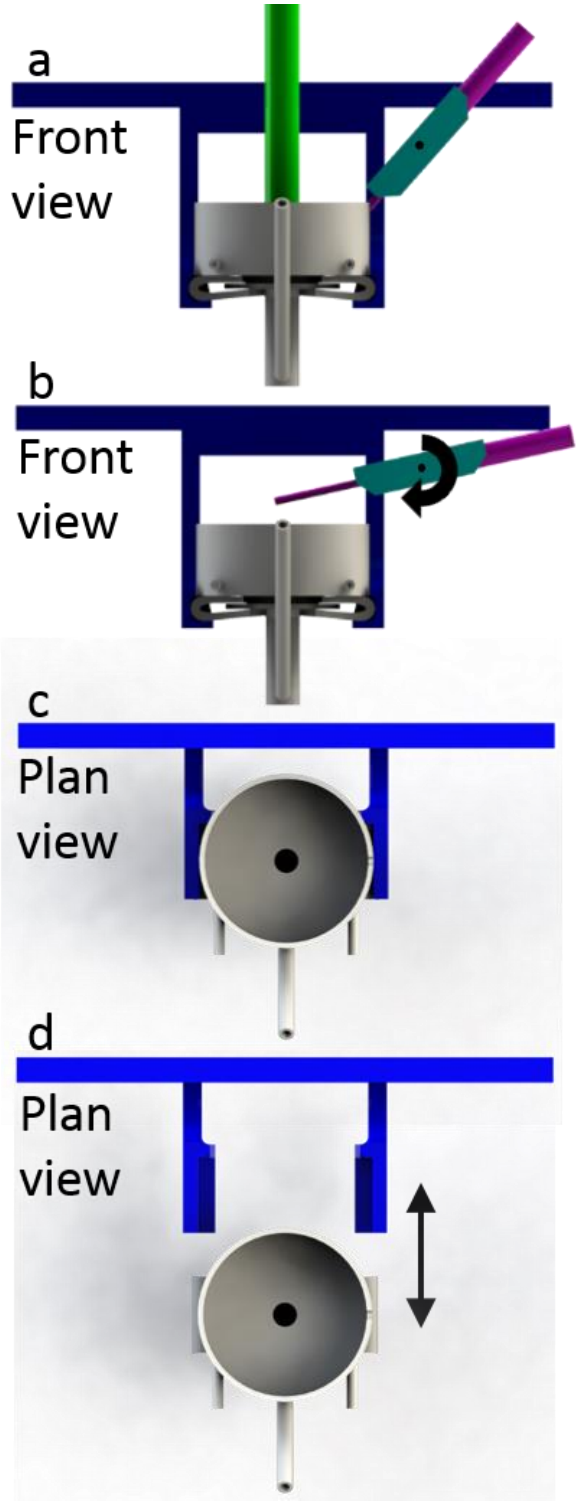

Fig. 3-5 Schematic of the disassembly process which began with the components in their sonoporation position (a). The transducer (green) was then removed allowing the hydrophone/thermocouple holder (aqua) to be rotated out of the donor chamber on its pivot mounting (b). The diffusion cell could then be removed from its holder (c and d). The diffusion cell for the succeeding experimental repetition was positioned by following this process in reverse (d to a). The hydrophone is shown in pink. The support frame is shown in blue.

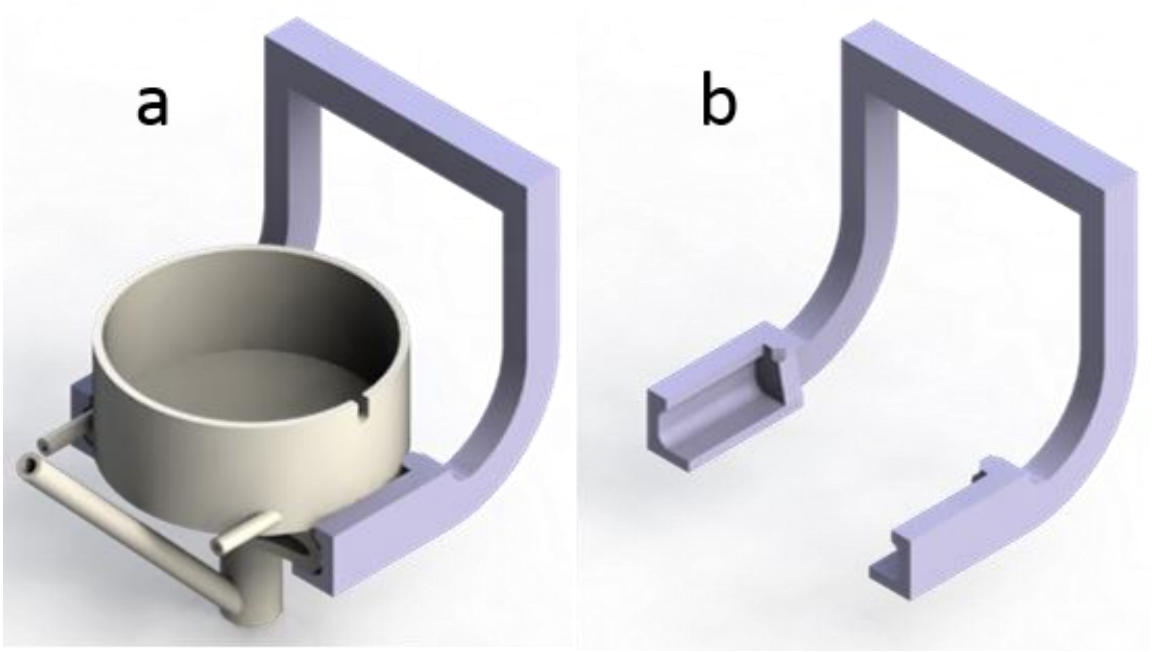

Fig. 3-6 Isometric view of the 3D printed ABS diffusion cell holder (a) with the cell in place and (b) without the cell

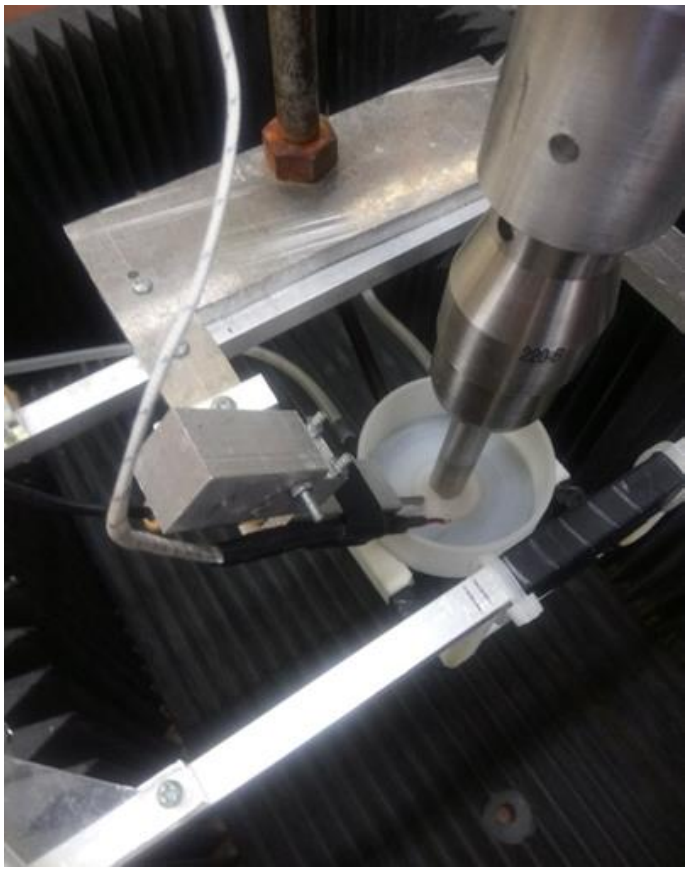

Fig. 3-7 Image of the transducer, hydrophone, thermocouple, and diffusion cell the sonoporation position

Outside of skin applications, studies involving a PCD have positioned the hydrophone so that it is confocal with the transducer (Choi, et al. 2014, Farny, et al. 2010, Helga, et al. 2015, Heymans, et al. 2017, Hockham, et al. 2010, Liu, et al. 1998). Due to the small distance between the transducer and the skin (3 mm) in the present study, it was not possible to position the hydrophone confocally. Instead, the hydrophone was focussed towards the gap between the transducer tip and the donor chamber (Fig. 3-3). The distance between the tip of the hydrophone and the bottom edge of the transducer was 5 mm. This positioning was as close to confocal as possible in the present setup. Increasing the transducer to skin distance from 3 mm to 5 mm would have enabled a perfectly confocal setup (with both the transducer and hydrophone aligned with the radial centre of the skin surface), as in the earlier PCD study reported in Appendix A. However, experiments reported in Appendix B showed that the median receiver chamber calcein concentration following 10 minutes of sonoporation at 3 mm was four times that following sonoporation at 5 mm (significant at p=0.3). Therefore, in the present study, perfect confocal alignment was sacrificed for an increase in skin permeability enhancement. Note that an increase in skin permeability enhancement with decreasing transducer distance was also found in the sonoporation studies by Herwadkar, et al. (2012) and Terahara, et al. (2002a), and is due to the greater number of inertial cavitation events which occur closer to the transducer tip, as shown with foil pitting experiments in Appendix B (Fig. B-14) and in the study by Terahara, et al. (2002a).

The voltage signal recorded by the hydrophone during sonoporation was passed through a pre-amplifier (HP Series Submersible Preamplifier, Precision Acoustics Ltd., Dorchester, Dorset, UK) and a DC coupler (DC Coupler, Precision Acoustics Ltd., Dorchester, Dorset, UK). The voltage signal was then read by an oscilloscope (TDS 2014B, Tektronix, Beaverton, OR,

USA) and transferred to a PC running SignalExpress (NI LabVIEW SignalExpress, National Instruments, Texas, USA) via a USB cable. The oscilloscope collected 2500 data points at a sampling rate of 1 MHz and then transferred these to the PC. The oscilloscope then collected another 2500 data points after a delay of around 1 to 2 s. This continued for the 10 minutes of sonoporation. Each set of 2500 data points was filtered using a digital infinite impulse response bandpass filter. The infinite impulse response bandpass filter was produced using MATLAB's 'designfilt' function (MATLAB, MathWorks, Natick, MA, USA). Six different passbands were used (2.5-7.5 kHz, 22.5-27.5 kHz, 29-31 kHz, 34-35 kHz, 70-90 kHz, and 92.5-97.5 kHz) to highlight the importance of PCD passband selection. Similarly, three different filter orders (4, 10, and 20) were used to highlight the importance of that parameter. Once each set of the 2500 data points had been filtered, the RMS value was calculated for the 2.5 ms time period associated with those data points. This RMS value then represented one noise amplitude data point. The inertial cavitation dose (ICD) was calculated by numerically integrating the noise amplitude over the 10 minutes of ultrasound application in each experiment. The ICD had units of V-s as in the cell sonoporation studies by Chen, et al. (2003) and Hallow, et al. (2006). This numerical integration was evaluated using the MATLAB 'trapz' function.

3.3.7 Transdermal Transport Experiments

One of the objectives of this study was to investigate whether a PCD can be used to monitor inertial cavitation activity during skin sonoporation. This study was also used to assess the potential of using PCD output to predict post-sonoporation transport. To assess this potential, the post-sonoporation transport had to be plotted against the ICD to see whether any correlation was apparent. To quantify the post-sonoporation transport, a calcein-buffer solution was applied to the skin immediately following sonoporation and left to passively diffuse for 2 hours. Seven repetitions of this transport experiment were conducted for each of the four coupling fluid temperature-intensity combinations (10 °C & 8.9 W/cm^2, 10 °C & 36 W/cm^2, 37 °C & 8.9 W/cm^2, and 37 °C & 36 W/cm^2).

Each transport experiment began with filling a receiver chamber with PBS. A skin sample was then taken from the freezer and visually checked for any holes or areas of non-uniform thickness through which the calcein solution could easily diffuse. Any samples that displayed such imperfections were disposed of. Once an appropriate skin sample was selected, it was clamped between the filled receiver chamber and the donor chamber. The silicone tubing was attached to the donor ports to complete the coupling fluid temperature control circuit. The diffusion cell was mounted into place and the transducer was positioned over the skin aperture. The thermocouple and PCD hydrophone were then positioned in the donor chamber. The donor chamber was filled with room temperature (19 °C ± 1 °C) deionised water and left to sit for 3 minutes to thaw the skin. After 3 minutes the circulation pump was turned on so that temperature control could begin. The water bath temperature required to maintain the coupling fluid target temperatures of 10 °C and 37 °C are shown in Table 3-1.

Table 3-1 Water bath temperatures required to maintain each coupling fluid temperature for the control and sonoporation protocols

Protocol	Control		Sonoporation (8.9 W/cm^2)		Sonoporation (36 W/cm^2)	
Target temperature (°C)	**10**	**37**	**10**	**37**	**10**	**37**
Water bath temperature (°C)	9	40	7	36	3	33

The coupling fluid was circulated for 10 minutes with ultrasound (the 8.9 W/cm^2 and 36 W/cm^2 sonoporation protocols) or without ultrasound (the control protocols). Note that the 37 °C control protocol is a positive control as opposed to a true negative control as some temperature effect may be expected. However, for the sake of simplicity, the term 'control' is used for both the 10 °C and 37 °C protocols that do not involve ultrasound. The water bath temperatures required to achieve the coupling fluid target temperatures (10 °C or 37 °C) during the control experiments are also shown in Table 3-1.

During the 10 minutes of fluid circulation, the coupling fluid temperature was constantly monitored with the thermocouple to ensure it remained at the desired target temperature. At the end of the 10 minutes, the donor chamber was emptied and the diffusion cell was moved to a holding rack. A 0.5 mL volume of the calcein solution was applied to the donor side of the skin. The calcein solution was then left to diffuse at room temperature (19 °C ± 1 °C) for 2 hours. After 2 hours a 1 mL sample was taken from the receiver chamber with a pipette (Calibra Digital 832 Macro Pipette, Socorex, Ecublens, Switzerland). Note that each diffusion cell was washed with a surfactant cleaner (Jif, Unilever, France) in between each use to remove the calcein which had a tendency to stick to the polypropylene.

3.3.8 Concentration Measurements

Following the two hours of diffusion, the receiver chamber calcein concentration was measured with a spectrofluorometer (Fluorolog-3, Horiba Ltd., Kyoto, Japan). The excitation wavelength was 488 nm. The emission wavelength was 513 nm. The software package FluorEssence (FluorEssence V3.5, Horiba Ltd., Kyoto, Japan) was used to control the spectrofluorometer and to record its output. The emission intensity values read by the spectrofluorometer (at 513 nm) were converted to calcein concentrations using the calibration curve described in Section B.3.1.

3.3.9 Detection of Sudden Changes in Inertial Cavitation Activity

A PCD can be a helpful tool to detect sudden, potentially unwanted changes in inertial cavitation activity in an ultrasound setup (Hockham, et al. 2010). The broadband noise emission in the present setup was monitored during 10 minutes of skin sonoporation (at an intensity of either 8.9 W/cm^2 or 36 W/cm^2). During sonoporation, the coupling fluid was maintained at (19 °C ± 1 °C). At the beginning of the 10 minute period, the coupling fluid was deionised water. A sudden suppression of inertial cavitation activity was then produced by adding carbonated water to the coupling fluid during sonoporation. The broadband noise emission was analysed to determine whether it decreased at the time the carbonated water was added (which would indicate that the PCD detected the sudden change).

The degree to which carbonated water supresses inertial cavitation activity was demonstrated with foil pitting experiments. This suppression is thought to be due to the large quantity of gas in the fluid. This gas significantly lowers the cavitation threshold. Such a

decrease in the cavitation threshold lowers the ultrasound energy that can be stored in the system (Bader, et al. 2012) – resulting in a decrease in the peak rarefactional pressure. This decrease in the peak rarefactional pressure causes a decrease in the inertial cavitation activity (Helga, et al. 2015). Previous studies have used castor oil to supress inertial cavitation (Robertson and Becker 2018, Tang, et al. 2002a). However, castor oil was not used in the present study as it would have been difficult to flush out of the silicone tubing through which the coupling fluid circulated. Ultrasound was applied to a piece of aluminium foil (at an intensity of 8.9 W/cm^2 for 15 s) with deionised water as the coupling fluid and again with carbonated water as the coupling fluid. Digital images were then taken of the two pieces of foil to depict the influence of carbonation on pitting. The aluminium foil (Homebrand, Manukau, New Zealand) was 0.016 mm thick.

The length of time that a piece of foil is submerged in water prior to ultrasound application can affect the prevalence of air bubbles (nucleation sites) on the surface of the foil. Prior to each ultrasound application, the foil was submerged in the coupling fluid while the circulation system brought the coupling fluid to the specified temperature. The time required to achieve this temperature was consistent across each foil pitting dataset. Therefore, the effect of the submergence, on the prevalence of nucleation sites on the foil surface, was also consistent.

3.4 Results

3.4.1 Coupling Fluid Temperature

This study employed the temperature control system described in Chapter 2 to set and maintain the coupling fluid at 10 °C or 37 °C during 10 minutes of continuous ultrasound application. Temperature profiles are shown in Fig. 3-8 for the 8.9 W/cm^2 sonoporation, and 36 W/cm^2 sonoporation protocols. The temperature control system successfully maintained the coupling fluid temperature at the desired value throughout the experiment.

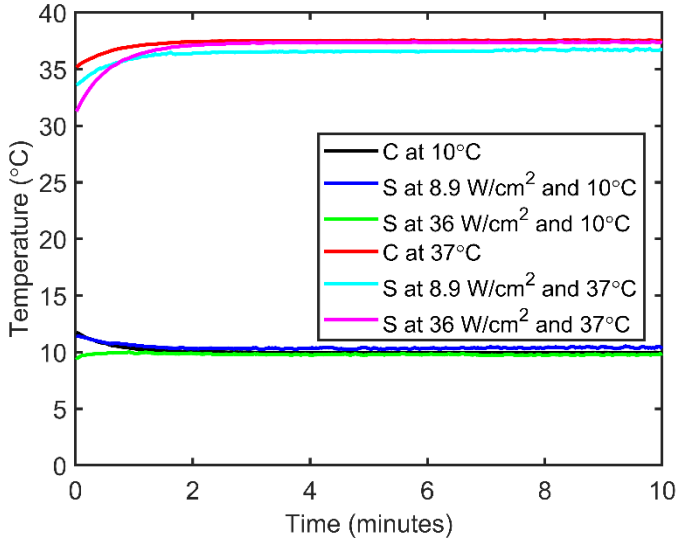

Fig. 3-8 Coupling fluid temperature profiles for the control (C), sonoporation (S) at 8.9 W/cm^2, and sonoporation at 36 W/cm^2 protocols at the target temperatures of 10 °C and 37 °C

3.4.2 Passive Cavitation Detection

One of the motivations of this study was to assess the ability of a PCD to monitor the inertial cavitation activity occurring in a Franz diffusion cell during sonoporation. A hydrophone, positioned in the coupling fluid of a modified Franz diffusion cell, recorded data during sonoporation. Four different combinations of coupling fluid temperature and ultrasound

intensity were used: 10 °C & 8.9 W/cm^2, 10 °C & 36 W/cm^2, 37 °C & 8.9 W/cm^2, and 37 °C & 36 W/cm^2. Seven experimental repetitions were run for each of these protocols. Examples of frequency transforms for each of the four sonoporation protocols are shown in Fig. 3-9. Examples of power spectra for each of the four sonoporation protocols are shown in Fig. 3-10. The driving frequency (20 kHz) is clearly represented in both Fig. 3-9 and Fig. 3-10, as are the higher harmonics, ultraharmonics, and subharmonics, to varying degrees. These figures are included to demonstrate that the 20 kHz sound field that was created by the transducer was monitored by the PCD hydrophone throughout the duration of ultrasound application (such monitoring was previously impossible with a standard glass Franz diffusion cell setup).

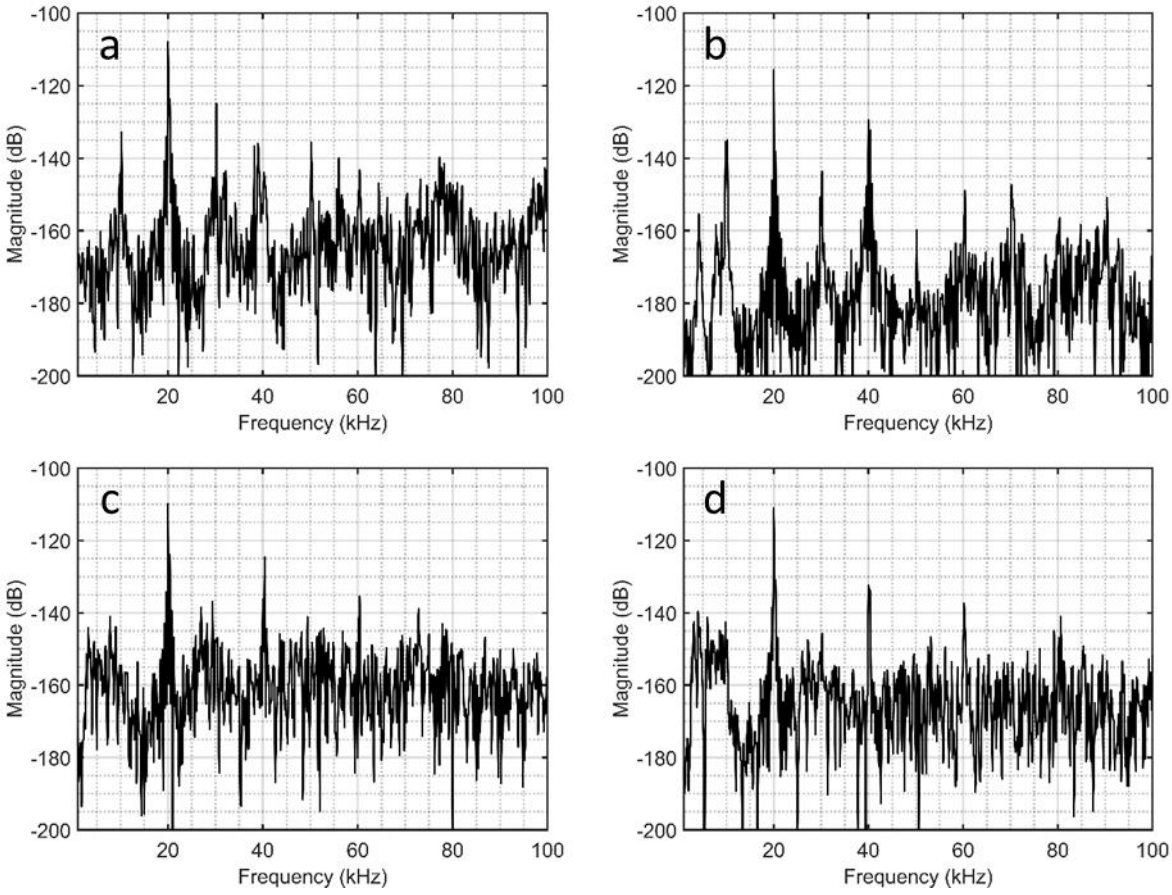

Fig. 3-9 Example frequency transforms for (a) 10 °C and 8.9 W/cm^2, (b) 37 °C and 8.9 W/cm^2, (c) 10 °C and 36 W/cm^2, and (d) 37 °C and 36 W/cm^2

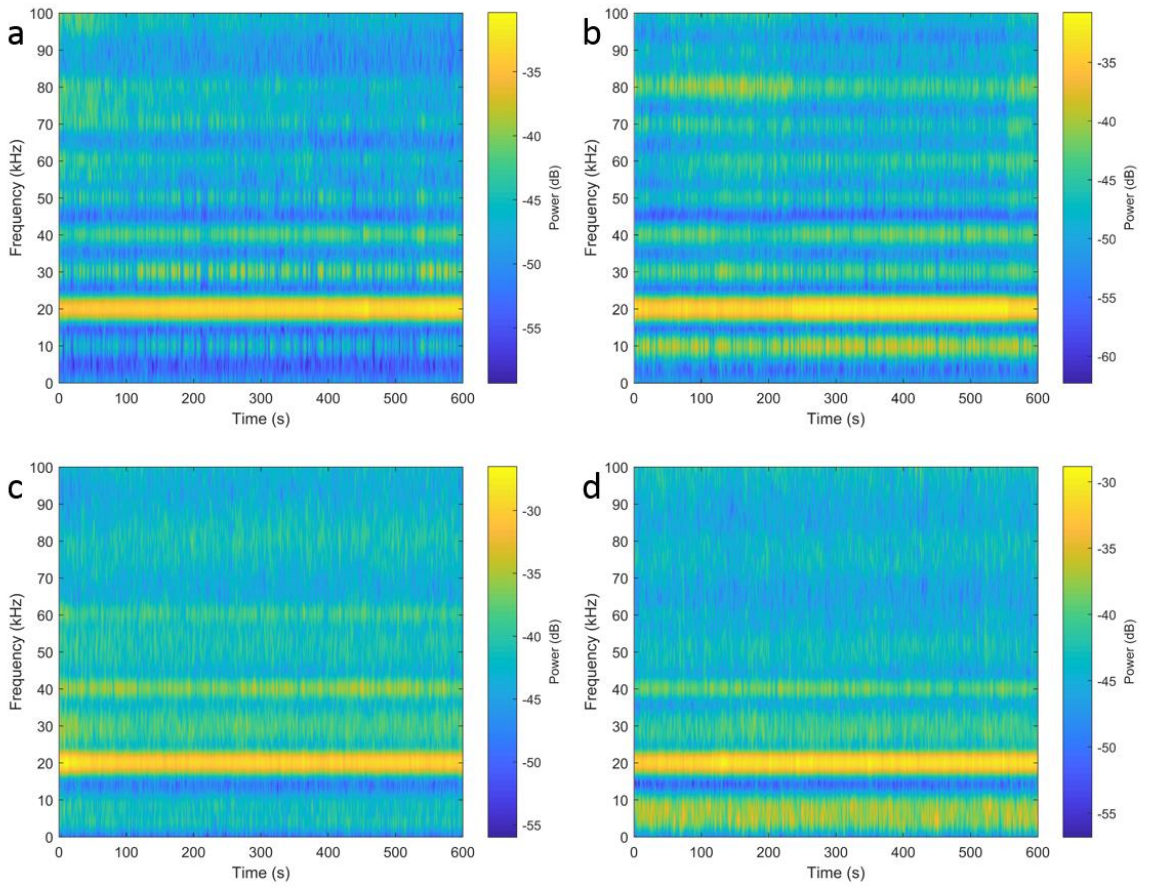

Fig. 3-10 Example power spectra for (a) 10 °C and 8.9 W/cm2, (b) 37 °C and 8.9 W/cm2, (c) 10 °C and 36 W/cm^2, and (d) 37 °C and 36 W/cm^2

Inertial cavitation activity is represented in the frequency spectrum by broadband noise which occurs between the subharmonic, harmonic, and ultraharmonic peaks (Yao-Sheng, et al. 2010). The hydrophone data was filtered to isolate this noise. This was achieved with a digital bandpass filter (described in Section 3.3.6). A filter order of 20 was chosen as it facilitated a complete isolation of the passband from any surrounding harmonics. The importance of filter order in this isolation can be shown with data from the present study. The magnitude responses for filters orders of 4, 10, and 20 are shown in Fig. 3-11 with the passband set to 22.5-27.5 kHz. When a filter order of 4 was used, the filter was unable to remove the harmonics at both 20 kHz and 40 kHz – the frequency spectra of the filtered signal

still showed distinct peaks at these frequencies (Fig. 3-12a). Similarly, a filter order of 10 was unable to entirely remove the 1st harmonic at 20 kHz from the frequency spectra of the filtered signal (Fig. 3-12b). Therefore, a filter order of 20 was used for this study as it facilitated a complete isolation of a 5 kHz wide passband from any surrounding harmonics (Fig. 3-12c).

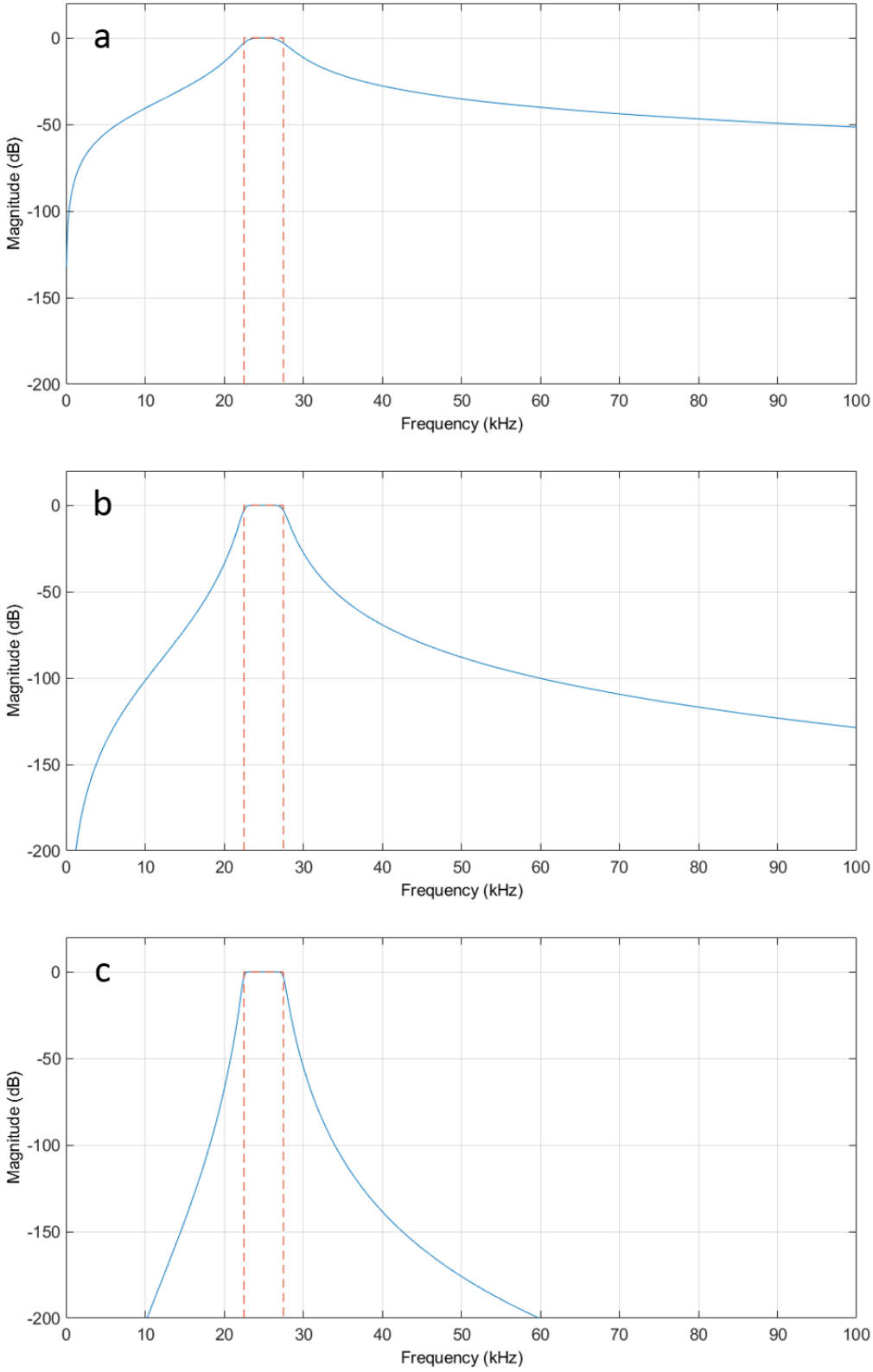

Fig. 3-11 Filter magnitude responses for the 22.5-27.5 kHz band for filter orders of (a) 4, (b) 10, and (c) 20

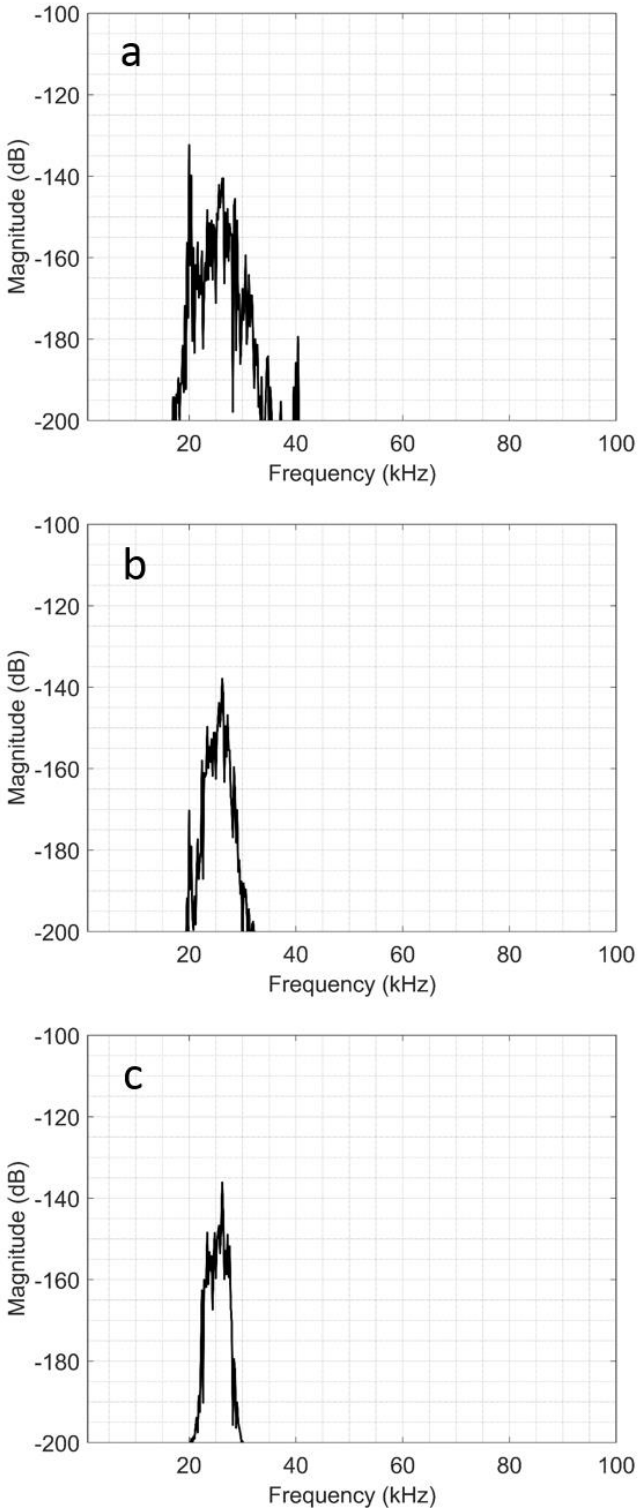

Fig. 3-12 Example frequency spectra after filtering with a passband of 22.5-27.5 kHz and filter orders of (a) 4, (b) 10, and (c) 20

Using a filter order of 20, the filtered signal from six different passbands was assessed to demonstrate the importance of passband selection. Examples of filtered noise data captured during sonoporation, for one of these bands (22.5 kHz-27.5 kHz), is shown in Fig. 3-13 for each of the four sonoporation protocols. Due to the variability in the broadband noise emission, moving averages are provided in Fig. 3-13 to aid interpretation of the data. The relative standard deviation in these datasets is between 16 % and 19 %. This degree of time-dependent variability in the broadband noise emission is similar to the variability in the highly cited PCD study by Hockham, et al. (2010).

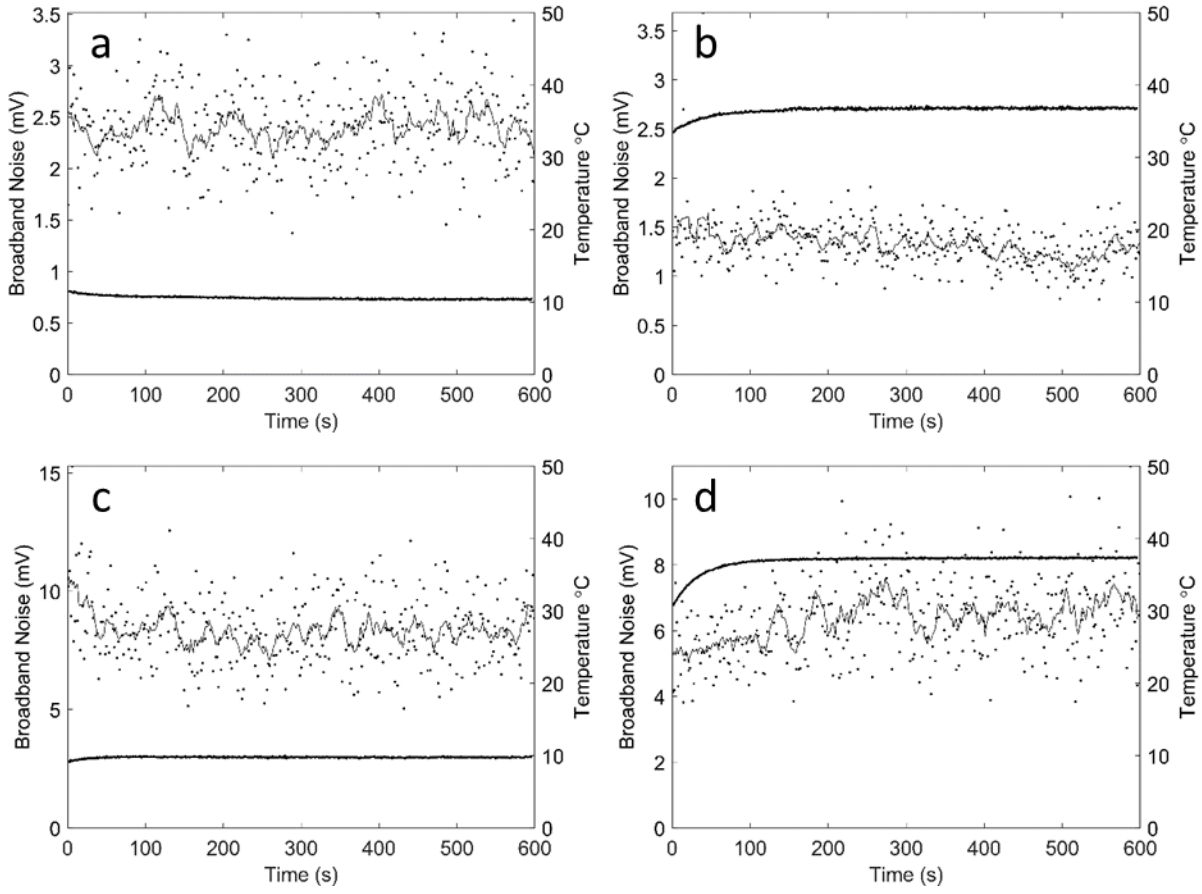

Fig. 3-13 Broadband noise as a function of time for coupling fluid temperature and intensities of (a) 10 °C and 8.9 W/cm^2, (b) 37 °C and 8.9 W/cm^2, (c) 10 °C and 36 W/cm^2, and (d) 37 °C and 36 W/cm^2. A moving average of the noise is also shown to aid interpretation of the data.

The choice of filter passband affects the response of a PCD to changes in inertial cavitation activity. There are no established protocols for selecting filter bandwidths or cut-off frequencies when using PCDs, except that no harmonic (n·f, *n*=1,2,3,4,5), subharmonic (f/2) or ultraharmonic (n·f/2, *n*=3,5,7,9) frequencies should be included as these are considered indicative of stable cavitation (Yao-Sheng, et al. 2010). Inertial cavitation activity is known to increase with increasing ultrasound intensity (Mitragotri, et al. 2000a, Tang, et al. 2002a, Terahara, et al. 2002a) and foil pitting experiments presented in Fig. 2-22 and Fig. A-13 showed that inertial cavitation activity at the skin aperture decreases with increasing coupling fluid temperature. The PCD hydrophone data collected in the present study was filtered with six different passbands to identify a passband in which the PCD output increased with increasing intensity and decreased with increasing coupling fluid temperature (as this would mean that that passband was responding to inertial cavitation activity). Two of these bands (29-31 kHz and 70-90 kHz) did include harmonics or ultraharmonics, while the other four (2.5-7.5 kHz, 22.5-27.5 kHz, 34-35 kHz, and 92.5-97.5 kHz) did not.

Cell sonoporation studies, such as those conducted by Chen, et al. (2003) and Hallow, et al. (2006), have shown that it is the ICD (as opposed to the magnitude of broadband noise emission at any instant) that best represents the effective inertial cavitation activity over the duration of ultrasound application. Each noise vs. time dataset was integrated over the duration of ultrasound application to obtain an ICD value. These ICD values are shown in Fig. 3-14 for the six different frequency bands. Boxplots were used in Fig. 3-14 to represent the variability in each dataset. The crosses within each box denote the mean values, while the horizontal lines within each box denote the median values. The horizontal lines at the top and bottom of each box represent the upper and lower quartiles, while the whiskers represent

the maximum and minimum values. Any data point that exceeded the upper quartile value by more than 1.5 times the interquartile range is shown as an outlier (represented by the "+" symbol). These outlier values were still considered in the calculation of the mean and median.

The influence of ultrasound intensity on the mean ICD value was dependent on the passband. The mean ICD value calculated using the 2.5-7.5 kHz passband increased with increasing intensity, regardless of coupling fluid temperature (Fig. 3-14a). The same was true for the ICD values calculated using the 22.5-27.5 kHz, 34-35 kHz, and 92.5-97.5 kHz passbands. However, ICD values calculated using the 29-31 kHz and 70-90 kHz passbands did not always increase with increasing intensity. The influence of the coupling fluid temperature on the mean ICD value was also dependent on the passband. The mean ICD values calculated using the 2.5-7.5 kHz passband increased with increasing coupling fluid temperature (Fig. 3-14a), regardless of the ultrasound intensity. The mean ICD values calculated with the five other passbands all decreased with increasing temperature, regardless of the ultrasound intensity. The passband used also influenced the variability in the ICD datasets.

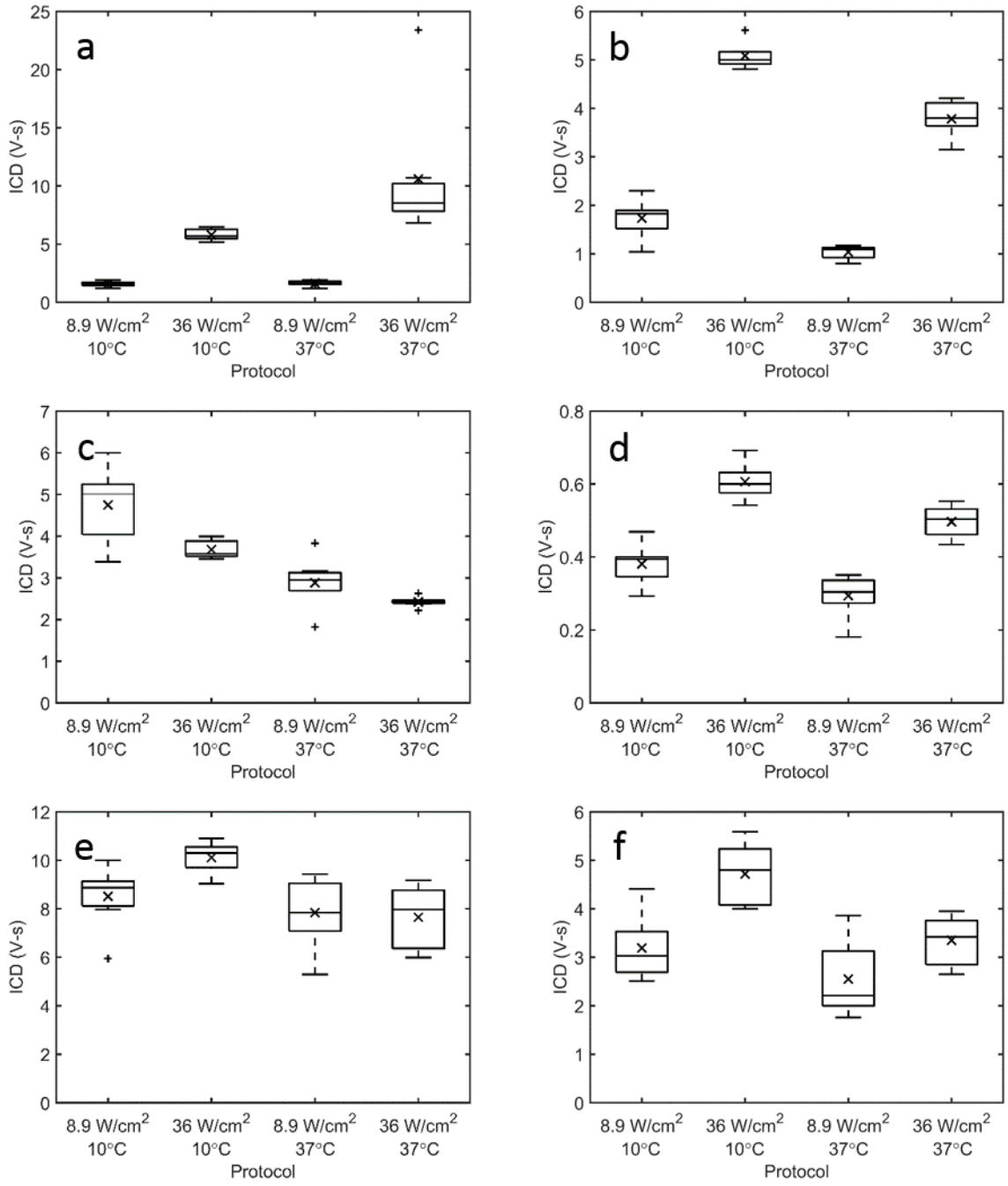

Fig. 3-14 Inertial cavitation dose as a function of temperature and intensity for frequency bands of (a) 2.5-7.5 kHz, (b) 22.5-27.5 kHz, (c) 29-31 kHz, (d) 34-35 kHz, (e) 70-90 kHz, and (f) 92.5-97.5 kHz (n=7). The influences of intensity and coupling fluid temperature on the ICD values were dependent on the passband used. The variability in the ICD datasets was also dependent on the passband used.

3.4.3 Transdermal Transport

Following the 10 minutes of sonoporation during which the PCD data was collected, a calcein-buffer solution was applied to the donor side of the skin. This solution was left to diffuse for 2 hours at room temperature. After 2 hours, samples were taken from the receiver chambers. The concentration of calcein in these samples was quantified using a spectrofluorometer.

Regardless of the intensity, the mean receiver calcein concentration was higher following sonoporation at 37 °C than it was following sonoporation at 10 °C (the same increase in transport with coupling fluid temperature occurred following the control protocol). Due to the variability, it is important to consider the *p*-values along with the mean values when comparing these datasets (shown as a function of temperature in Fig. 3-15). The mean receiver concentration following the control protocol at 37 °C was 4.4 times that following the control protocol at 10 °C (significant at p=0.05). The mean receiver concentration following the 8.9 W/cm^2 sonoporation protocol at 37 °C was 1.7 times that following the 8.9 W/cm^2 sonoporation protocol at 10 °C (p=0.32). Similarly, the mean receiver concentration following the 36 W/cm^2 sonoporation protocol at 37 °C was 1.7 times that following the 36 W/cm^2 sonoporation at 10 °C (p=0.46).

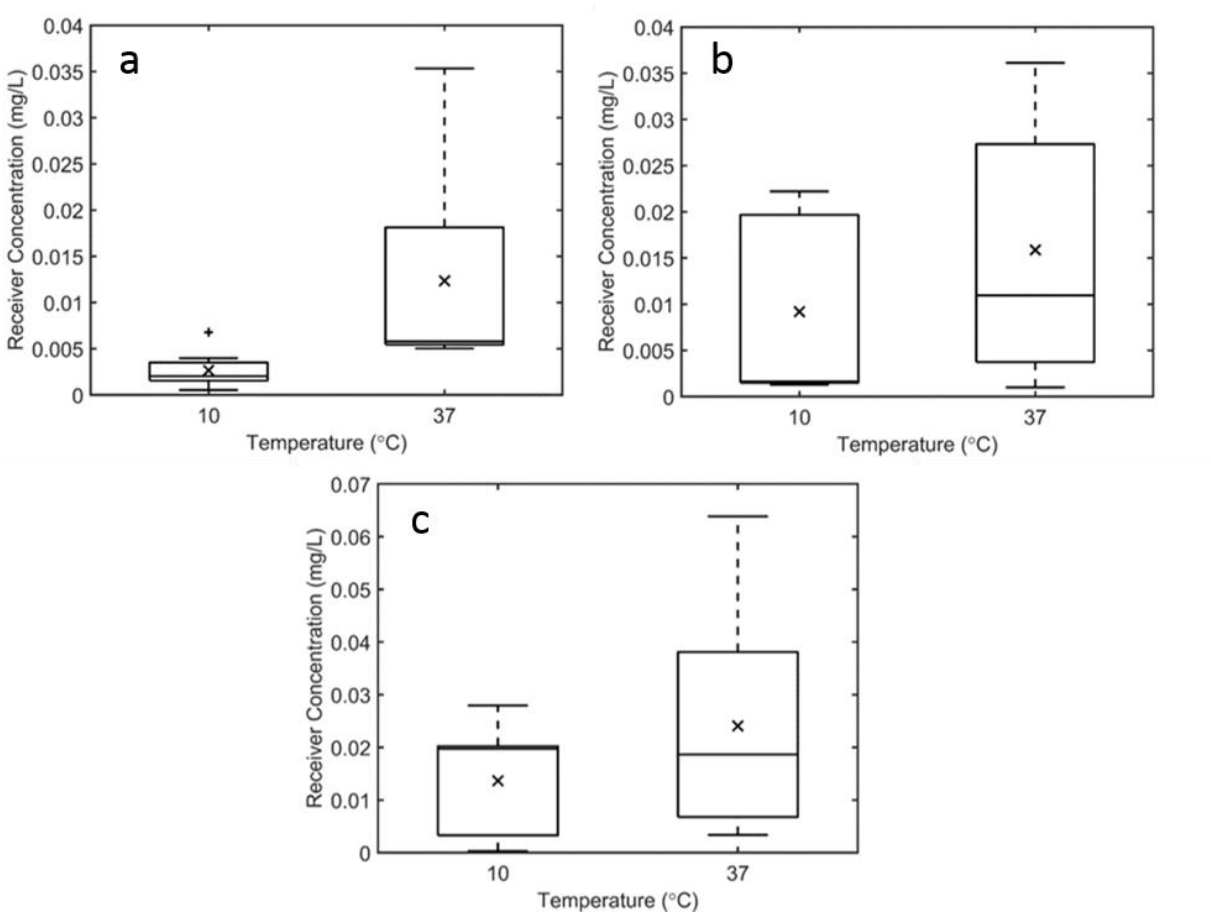

Fig. 3-15 Receiver chamber calcein concentration as a function of coupling fluid temperature following (a) control (b) sonoporation at 8.9 W/cm^2, and (c) sonoporation at 36 W/cm^2.The crosses within the boxes represent the mean values (n=7).

3.4.4 Transport-PCD Correlation

Beyond investigating whether a PCD can be used to monitor inertial cavitation activity during skin sonoporation, this study was also used to assess the potential of using PCD output to predict post-sonoporation transport. In their cell sonoporation study, Hallow, et al. (2006) found a strong correlation between ICD and cell permeability increase (the permeability increased with increasing ICD). This correlation lead them to suggest that PCD output could be used to provide real-time feedback about the bioeffects in ultrasound-mediated drug delivery applications.

If PCD output were to be used as an indicator of the cavitation-induced skin permeability increase, there would need to be a clear correlation between ICD and post-sonoporation transport. If such a correlation could be established, then the equation describing that correlation could enable the likely skin permeability increase to be calculated from the real-time PCD output. In a clinical setting, this kind of real-time feedback system could be used to adjust ultrasound intensity and/or application time, during sonoporation, to ensure that the ICD falls within a desired range. Ensuring that the ICD falls within a predetermined range of values would increase the likelihood that the permeability enhancement falls within a desired range. Therefore, this feedback system could be a valuable tool for increasing the consistency and predictability of treatment, especially as inertial cavitation activity is dependent on target rigidity (Kodama and Tomita 2000), and skin rigidity changes from person to person (Agache, et al. 1980, Owen, et al. 2016, Wolff, et al. 2011).

The first step to establishing a PCD based, real-time transport prediction system is to establish a correlation between ICD and the post-sonoporation transport. The correlation between the ICD output and the post-sonoporation transport was assessed in the present study by plotting the mean receiver calcein concentration against the mean ICD for the 22.5-27.5 kHz frequency band (Fig. 3-16). No correlation is apparent in Fig. 3-16 (the mean concentration did not always increase with increasing ICD). When the temperature of the coupling fluid was increased, at either intensity, the mean ICD decreased while the mean receiver chamber calcein concentration increased.

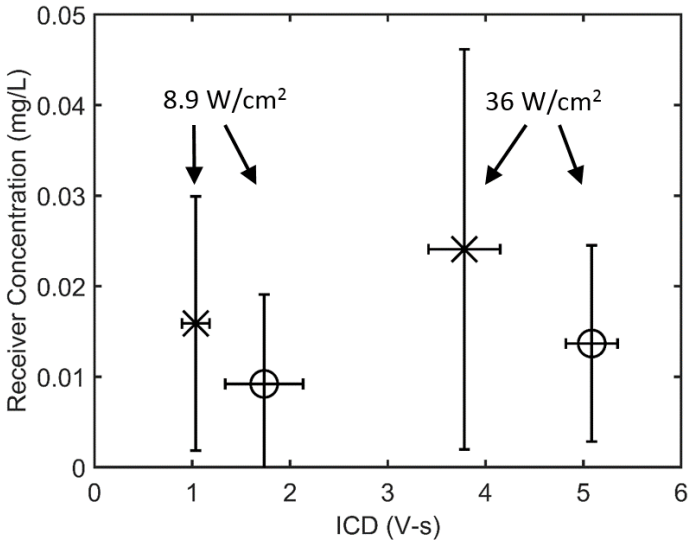

Fig. 3-16 Inertial cavitation dose and receiver chamber concentration for sonoporation at (○) 10 °C and (X) 37 °C. The vertical error bars represent the standard deviation in the concentration datasets while the horizontal error bars represent the standard deviation in the ICD datasets.

3.4.5 Foil Pitting

Foil pitting experiments were used to show that inertial cavitation activity at the skin aperture is supressed when carbonated water is used as the coupling fluid. Ultrasound was applied to aluminium foil for 15 s at an intensity of 8.9 W/cm^2. The coupling fluid was either carbonated water at room temperature (19 °C ± 1 °C) or deionised water at room temperature. When inertial cavitation was supressed, no pitting was visible on the aluminium foil after ultrasound application (Fig. 3-17a). After ultrasound application with deionised water as the coupling fluid, severe pitting and perforation were visible (Fig. 3-17b).

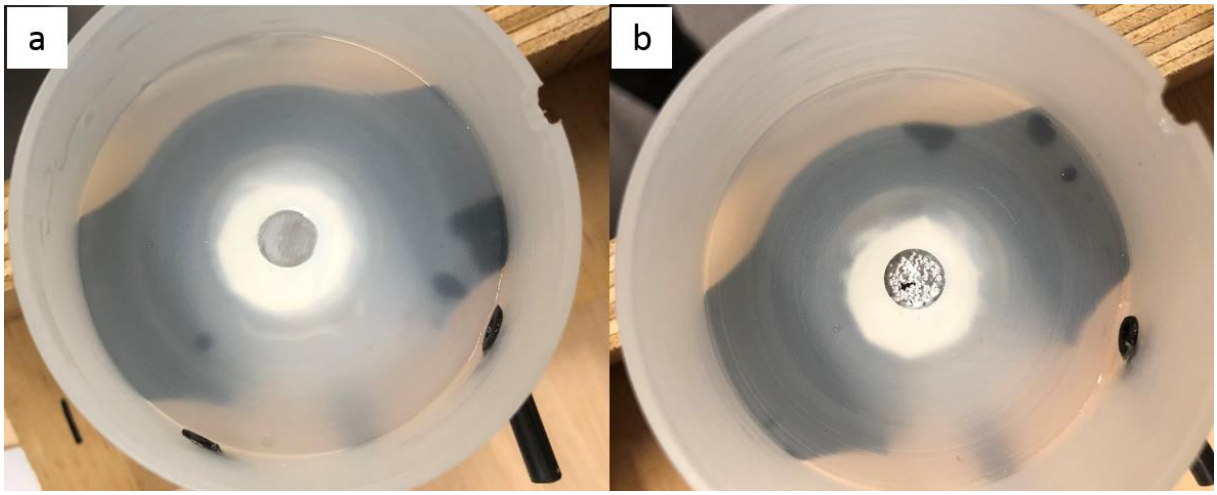

Fig. 3-17 Pitting of aluminium foil following sonoporation with (a) carbonated water and (b) deionised water as the coupling fluid. The transducer was positioned 3 mm from the surface of the foil and operated at an intensity of 8.9 W/cm^2 for 15 s.

3.4.6 Detection of Sudden Changes in Cavitation During Sonoporation

Inertial cavitation activity was supressed during skin sonoporation by adding carbonated water to the coupling fluid. The response of the PCD at the time the carbonated water was added was then analysed to assess the ability of the PCD to detect sudden changes in cavitation activity during sonoporation. Skin was sonoporated for 10 minutes at an intensity of 8.9 W/cm^2 or 36 W/cm^2. During sonoporation, the coupling fluid was maintained at (19 °C ± 1 °C) using the circulation system. The coupling fluid initially consisted entirely of deionised water. After 200 s of sonoporation at 8.9 W/cm^2, 20 mL of room temperature carbonated water was added to the donor chamber, displacing an equal amount of deionised water. The addition of this carbonated water resulted in a sudden reduction in the broadband noise emission (22.5-27.5 kHz) from a moving average value of approximately 1.7 mV to a value of approximately 0.7 mV (Fig. 3-18a). After a further 150 s of sonoporation, deionised water was slowly poured back into the donor chamber, displacing most of the carbonated water that had been added. This caused the moving average of the broadband noise to

increase from approximately 0.6 mV to approximately 1.2 mV within 50 s. After 300 s of sonoporation at 36 W/cm^2 carbonated water was added to the donor chamber. The addition of the carbonated water again resulted in a sudden reduction in broadband noise emission, this time from a moving average value of approximately 6 mV to a value of approximately 2 mV. Over the next 150 s the moving average then increased to approximately 4 mV as the ultrasound degassed the coupling fluid. More carbonated water was then added to the coupling fluid resulting in another sudden decrease in the moving average (to a value of approximately 0.5 mV). From these results it can be concluded that the output of the PCD always changed significantly at the same time that carbonated water was added or removed from the coupling fluid.

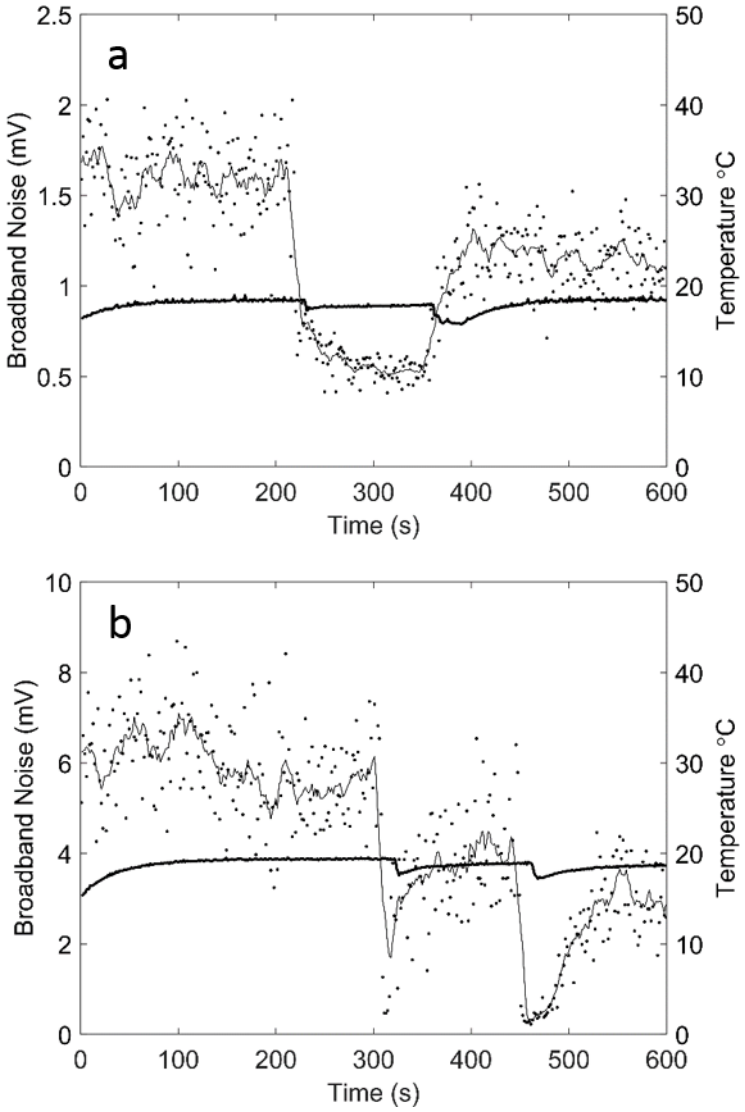

Fig. 3-18 Broadband noise emission (22.5-27.5 kHz) as a function of time with ultrasound intensities of (a) 8.9 W/cm^2 and (b) 36 W/cm^2. In (a) carbonated water was poured into the donor chamber at 200 s and deionised water was poured in at 350 s. In (b) carbonated water was poured into the donor chamber at 300 s and 450 s.

3.5 Discussion

A modified Franz diffusion cell setup allowed a PCD hydrophone to be positioned in the coupling fluid during sonoporation. The hydrophone signal was filtered to isolate the broadband noise which is indicative of inertial cavitation activity (Yao-Sheng, et al. 2010). The broadband noise was then time-integrated to obtain a single ICD value for each sonoporation

experiment. These ICD values were plotted as a function of the intensity (8.9 W/cm^2 or 36 W/cm^2) and of the coupling fluid temperature (10 °C or 37 °C) (Fig. 3-14).

One of the objectives of this study was to assess the ability of the PCD to monitor the inertial cavitation activity occurring in a Franz diffusion cell during sonoporation. When a passband of 22.5-27.5 kHz was used, the ICD increased with increasing ultrasound intensity and decreased with increasing coupling fluid temperature (Fig. 3-14b). Inertial cavitation activity is known to increase with increasing ultrasound intensity (Mitragotri, et al. 2000a, Tang, et al. 2002a, Terahara, et al. 2002a) and foil pitting experiments presented in Fig. 2-22 and Fig. A-13 lead to the conclusion that inertial cavitation activity at the skin aperture decreases with increasing coupling fluid temperature. Therefore, when a passband of 22.5-27.5 kHz was used, there was good agreement between the PCD output and the inertial cavitation activity. Even though the hydrophone was not perfectly confocal, this agreement supports the conclusion that a PCD hydrophone positioned in the coupling fluid can monitor inertial cavitation activity during skin sonoporation. This is the first key finding of this study and an important contribution to the field. Such a PCD system would be of great benefit in a clinical sonoporation setup as it would enable any changes in inertial cavitation activity to be detected and counteracted in real-time.

The ICD values produced using the 34-35 kHz and 92.5-97.5 kHz bands also increased with increasing intensity and decreased with increasing coupling fluid temperature (Fig. 3-14d and Fig. 3-14f). However, relative to the 22.5-27.5 kHz passband, using either of these bands would result in a PCD which was less sensitive to changes in inertial cavitation activity. Here the “sensitivity” of the PCD system is defined as the magnitude of the change in ICD value

when an experimental input is changed. The greater the sensitivity, the more effective a PCD is at responding to changes in inertial cavitation activity. The 34-35 kHz band was less sensitive to intensity than the 22.5-27.5 kHz band. When the intensity was increased from 8.9 W/cm^2 to 36 W/cm^2 (at a coupling fluid target temperature of 37 °C) the mean ICD value for the 34-35 kHz band experienced a 1.7-fold increase, compared to a 3.7-fold increase for the 22.5-27.5 kHz band. The relatively low sensitivity to changes in inertial cavitation activity with intensity makes the 34-35 kHz band less appropriate than the 22.5-27.5 kHz band. The 92.5-97.5 kHz band was a less appropriate option than the 22.5-27.5 kHz band for the same reason. Another reason for not using the 92.5-97.5 kHz band was that it resulted in more variable ICD values in comparison to the 22.5-27.5 kHz band. When the intensity was 8.9 W/cm^2 and the coupling fluid temperature was 37 °C, the relative standard deviation in the ICD value for the 92.5-97.5 kHz band was 0.3, compared to 0.1 for the 22.5-27.5 kHz band. The differences in sensitivity and variability produced with the 22.5-27.5 kHz, 34-35 kHz, and, 92.5-97.5 kHz bands highlight the importance of passband selection to the usefulness of a PCD.

The importance of passband selection is further illustrated by the undesirable response of the PCD when passbands containing harmonics and/or ultraharmonics are used. The 29-31 kHz band contained the ultraharmonic at 30 kHz. The mean ICD values calculated for this band decreased with increasing intensity at coupling fluid temperatures of both 10 °C and 37 °C. The 70-90 kHz passband contained the 4th harmonic at 80 kHz as well as the ultraharmonics at 70 kHz and 90 kHz. Using this band resulted in a decrease in the mean ICD with increasing intensity at a coupling fluid temperature of 37 °C (Fig. 3-14f). Inertial cavitation activity is known to increase with increasing ultrasound intensity. Therefore, the

decreases in ICD with intensity found using the 29-31 kHz and 70-90 kHz passbands reinforce the notion that PCD passbands should always exclude harmonics, subharmonics, and ultraharmonics (Yao-Sheng, et al. 2010). The 2.5-7.5 kHz frequency band could not be used to effectively monitor inertial cavitation activity in the present setup as its magnitude increased with increasing coupling fluid temperature (Fig. 3-14a). Even though this band did not include the subharmonic at 10 kHz, it may still have been influenced by the emissions from stable cavitation which occur at and near this frequency (Bull, et al. 2013), especially the f/4 subharmonic at 5 kHz (Fig. 3-9).

Along with investigating whether a PCD can be used to monitor inertial cavitation activity during skin sonoporation, this study was also used to assess the potential of using PCD output as an indicator of the cavitation-induced skin permeability increase, and therefore, as a predictor of post-sonoporation transport. Previously, researchers have relied on measurements of skin conductivity or mass transport to quantify the effect of sonoporation. Neither of these measurements are clinically applicable: a clinical conductivity measurement would require the placement of an electrode under the patient's skin, while a clinical mass transport measurement would require a sample of bodily fluid to be taken some time after ultrasound treatment. The input Intensity could be used to as a predictor, however, a predetermined intensity value cannot account for time-dependent or target dependent changes in inertial cavitation activity – PCD output can. If PCD output were to be used as an indicator of the cavitation-induced skin permeability increase, there would need to be a clear correlation between ICD and post-sonoporation transport. If such a correlation could be established, then the equation describing that correlation could enable the likely skin permeability increase to be predicted from the real-time PCD output. In a clinical setting, this

kind of real-time feedback system could be used to adjust ultrasound intensity and/or application time, during sonoporation, to ensure that the ICD falls within a desired range. Ensuring that the ICD falls within a predetermined range of values would increase the likelihood that the permeability enhancement falls within a desired range – which would make skin sonoporation a more predictable and consistent delivery method.

To assess the correlation between PCD output and post-sonoporation transport in the present study, the receiver chamber calcein concentration following sonoporation was plotted along with the ICD (22.5-27.5 kHz). This is shown in Fig. 3-16. No correlation between mean post-sonoporation transport and mean ICD is apparent in Fig. 3-16. An increase in mean ICD from 1.0 V-s to 1.7 V-s corresponded with a decrease in mean receiver concentration from 0.016 mg/L to 0.0092 mg/L. An increase in ICD from 1.7 V-s to 3.8 V-s resulted in an increase in mean transport from 0.0092 mg/L to 0.024 mg/L. A further increase in ICD to 5.1 V-s resulted in a decrease in mean transport from 0.024 mg/L to 0.014 mg/L. Therefore, in the present study, any prediction of post-sonoporation transport based on the ICD value alone would be inaccurate. One of the reasons for the poor correlation in Fig. 3-16 is that post-sonoporation transport is dependent on both inertial cavitation activity and coupling fluid temperature. Post-sonoporation transport increases with increasing coupling fluid temperature (as shown in Fig. 3-15 and Fig. 2-19), while ICD decreases with increasing coupling fluid temperature (Fig. 3-14b), due to the decrease in inertial cavitation activity (shown by the foil pitting data in Fig. 2-22 and Fig. A-12). Therefore, any future studies that attempt to use PCD output as an indicator of post-sonoporation transport must maintain a constant coupling fluid temperature during sonoporation. If the coupling fluid temperature is allowed to increase, then the resulting decrease in ICD could be misinterpreted as an

indication of decreased post-sonoporation transport. The need to maintain a constant coupling fluid temperature when attempting to use ICD as an indicator of post-sonoporation transport is the second key finding of this study.

An important potential application for passive cavitation detection in a clinical skin sonoporation system would be to detect sudden changes in inertial cavitation activity. Such a change could be brought on by a variety of unpredicted system malfunctions (for example, failure of the transducer, or degassing or leakage of the coupling fluid). In the present study, inertial cavitation activity was supressed during skin sonoporation by adding carbonated water to the coupling fluid. The response of the PCD at the time the carbonated water was added was then analysed to assess the ability of the PCD to detect sudden changes in the inertial cavitation activity during sonoporation. During sonoporation at intensities of both 8.9 W/cm^2 and 36 W/cm^2, the broadband noise emission decreased significantly at the times carbonated water was added (Fig. 3-18). Due to these significant decreases in broadband noise emission, which occurred at the times the inertial cavitation was suppressed, it can be concluded that, at both intensities, the PCD detected the sudden changes in inertial cavitation activity. Therefore, in a clinical setting, a PCD could be used as a single, real-time tool to detect sudden reductions in inertial cavitation activity that could arise from a variety of system malfunctions. The results of these carbonated water experiments further reinforce the previous conclusion that, even if not perfectly confocal, a PCD hydrophone positioned in the coupling fluid can monitor inertial cavitation activity during skin sonoporation.

The variability in the ICD values in the present study were significantly lower than those in Appendix A (which reports an earlier attempt to incorporate a PCD in a diffusion cell). The

lower variability shows that the hydrophone position used in the present study (7 mm from the skin aperture) resulted in superior PCD performance relative to that used in Appendix A (20 mm from the skin aperture). Also, the harmonic and ultraharmonic peaks in the frequency spectra of the present study are more pronounced than those in Appendix A – another indicator that the closer hydrophone position in the present study resulted in a superior PCD performance. This should be noted by any future *in vitro*, *in vivo*, or clinical skin sonoporation studies which attempt to use a PCD to monitor inertial cavitation activity – the hydrophone should be as close to the skin aperture as possible.

From the transport data in the present study (Fig. 3-15a) it can be concluded that pre-treating skin with warm circulating coupling fluid (without ultrasound), prior to drug application can increase the resulting transdermal transport. The mean receiver chamber calcein concentration following the control protocol at 37 °C was 4.4 times (p=0.05) that following the control protocol at 10 °C (Fig. 3-15a). A similar trend was shown in Chapter 2 (Fig. 2-19f): the mean receiver chamber calcein concentration following the control protocol at 33 °C was 1.8 times (p=0.6) that following the control protocol at 13 °C. Although not directly related to the purposes of this thesis, these temperature dependent increases are interesting as they show that briefly exposing excised skin to fluid above room temperature, but below the damaging 40 °C level, can increase permeability, relative to exposure at a low temperature (10-13 °C). *In vitro* studies that investigate the effects of temperature on transdermal transport usually apply heat treatment concurrent with drug application (Akomeah, et al. 2004, Clarys, et al. 1998, Ogiso, et al. 1998, Ohara, et al. 1995). The author is not aware of any studies that have investigated the effects of heat pre-treatment on the subsequent transdermal transport. Therefore, the temperature-dependent differences in

transport following the control protocols in this study, and Chapter 2, appear to be novel results. This finding has an important implication for clinical uses of passive transport systems as it indicates that the skin temperature prior to drug application can influence the subsequent passive diffusion. Skin temperature during passive diffusion has already been shown to increase drug transport. For example, in the study by Vanakoski, et al. (1996), human subjects were fitted with nicotine patches before entering a heated sauna bath. While in the sauna bath, the blood nicotine concentrations were measured at 15 minute intervals. The blood nicotine levels of the subjects in the sauna bath were significantly higher (p<0.01) during the time in the sauna than a control group who were not exposed to elevated temperatures. Similarly, Frölich, et al. (2001) reported a clinical case in which a patient fitted with a Fentanyl transdermal system experienced an overdose due to the simultaneous application of an upper-body warming blanket. Increases in skin temperature during passive diffusion have been shown to increase transdermal transport in numerous other studies too (Ashburn, et al. 2003, Newshan 1998, Prodduturi, et al. 2010, Shahzad, et al. 2015, Shomaker, et al. 2000, Tominaga and Tojo 2010). The specific conclusion from this study however, is that a higher skin temperature prior to the topical application of a permeant may increase the subsequent transport, even if the skin is not at an elevated temperature during diffusion. From a clinical perspective, this may mean that a patient who has been exposed to hot ambient conditions prior to permeant application will experience more transdermal transport than they would if their skin temperature was low prior to permeant application, even if their skin temperature is the same during diffusion in both cases. Further investigation is required if the full implications of pre-application skin temperature to the performance of passive transport systems is to be understood.

3.6 Conclusions

A custom sonoporation setup was designed and manufactured. This setup enabled a PCD hydrophone to be positioned in the coupling fluid of a Franz diffusion cell during sonoporation. Thesis objective 4 (design and manufacture a skin sonoporation setup that enables a PCD hydrophone to be positioned in the coupling fluid during sonoporation) has been fulfilled. Measurements of broadband noise emission with the novel setup showed that, even if not perfectly confocal, a PCD hydrophone positioned in the coupling fluid can be used to monitor the inertial cavitation activity which occurs during sonoporation in a Franz diffusion cell. The broadband noise emission was shown to increase with increasing intensity (as inertial cavitation does) and decrease with increasing coupling fluid temperature (as inertial cavitation was shown to do). The performance of the PCD in the present study was strongly dependent on the choice of passband and filter order. The introduction of a custom diffusion cell setup that facilitates a PCD capable of monitoring inertial cavitation activity during sonoporation is a significant contribution to the field. Thesis objective 5 (assess the ability of the PCD setup to monitor inertial cavitation activity during skin sonoporation) has been fulfilled.

The PCD was also shown to respond to sudden changes in inertial cavitation activity in the coupling fluid (brought on by the addition of carbonated water). The timely response of the broadband noise emission magnitude to these changes in inertial cavitation activity means that it could be an effective tool in a clinical setting. Any sudden, time-dependent changes in the inertial cavitation during sonoporation (from transducer malfunction, or coupling fluid

degassing or leakage, for example) could be immediately identified by the PCD system so that the problem could be addressed.

A second attempt was made to correlate the ICD values with the post-sonoporation transport (the first attempt is reported in Appendix A). This correlation was difficult given the variability in the transdermal transport datasets. However, the attempt at this correlation still lead to an important finding that will be of use to future studies – the coupling fluid temperature must be held constant if ICD is to be used to predict post-sonoporation transport. Otherwise a decrease in broadband noise emission, resulting from an increase in coupling fluid temperature that actually increases skin permeability, could be misinterpreted as an indicator of decreased post-sonoporation transport. This is another reason why future sonoporation studies should incorporate some version of the circulating temperature control system introduced in this thesis.

From the post-control transdermal transport data of the present study (as well as that from Chapter 2), it is reasonable to conclude that the skin temperature prior to the topical application of a permeant affects the passive transdermal transport. A higher pre-treatment temperature was shown to result in greater transdermal transport, even in the clinically relevant range of 10 °C to 37 °C. This could have important clinical implications for passive transdermal systems, however, further investigation is required if the full implications of pre-application skin temperature are to be understood.

4 Investigation of the Influence of Acoustic Reflection

4.1 Abstract

Prior to the work in Chapters 2 and 3, research was conducted to investigate the influence of acoustic reflection on inertial cavitation activity during low-frequency ultrasound exposure in a Franz diffusion cell. That investigation (which is described in this chapter) provided the initial idea of incorporating coupling fluid temperature control and a PCD into a Franz diffusion cell (which then became the key focuses of this thesis).

Two versions of a modified Franz diffusion cell setup were employed in this study. One version had acoustic conditions that were similar to a standard Franz diffusion cell surrounded by air, while the second was designed to greatly reduce the acoustic reflection by submerging the transmissive diffusion cell in a water bath. The temperature of the coupling fluid in both setups was controlled using a novel thermoelectric cooling system (an earlier version of the cooling system used in Chapters 2 and 3). At an ultrasound intensity of 13.6 W/cm^2 the mean and median inertial cavitation dose when the acoustic reflections were suppressed were found to be 16 *%* and 13 *%* lower than when reflections were not suppressed (significant at p=0.07). From the differences in ICD it can be concluded that the acoustic reflections, which occur in a low-frequency skin sonoporation setup, influence the inertial cavitation activity that occurs at the skin aperture. Therefore, for a given set input parameters, the same inertial cavitation activity that was obtained *in vitro* is not guaranteed in an *in vivo* or clinical scenario, due to differences in echoic conditions.

4.2 Introduction

In vitro experimental studies that investigate the effects of ultrasound on skin permeability employ Franz diffusion cells (Merino, et al. 2003, Mitragotri, et al. 2000a, Smith, et al. 2003, Terahara, et al. 2002a, Tezel, et al. 2001). These studies have considered the influences of parameters such as frequency (Tezel, et al. 2002), exposure time (Terahara, et al. 2002a), duty cycle (Herwadkar, et al. 2012), acoustic intensity (Tezel, et al. 2001), and the distance from the transducer to the skin (Terahara, et al. 2002a). However, little attention has been paid to the potential influence of acoustic reflection in skin sonoporation studies. This was noted by Smith (2007), who stressed the importance of reporting the echoic conditions of the transdermal insonation apparatus.

Previous studies of the insonation of cells in cell culture plates have shown that acoustic reflection from the walls of the cell culture plates may strongly influence the inertial cavitation activity. For example, Kinoshita and Hynynen (2007) found that sonoporation could be doubled by facilitating the presence of a standing wave. Similarly, Jelenc, et al. (2012) showed that by suppressing the acoustic reflection using an acoustically absorbent lining, the maximum reflected pressure (at the cell suspension) was reduced by 81 *%*. This motivates the question that is central to the present study: at ultrasound intensities relevant to skin sonoporation, do the acoustic reflections that occur within a Franz diffusion cell significantly influence the ICD?

While, to the author's knowledge, there are no published studies that explicitly investigate the influence of reflection in *in vitro* skin sonoporation setups, some researchers have

employed experimental methods intended to suppress these reflections. For example, in their high-frequency *in vivo* study on transdermal transport through rat skin, Park, et al. (2012) avoided “strong reflection” by positioning their thermocouple outside of the direct beam of their transducer. Mitragotri, et al. (1995b) inserted a 1 mm thick Teflon sheet opposite the transducer in a high-frequency horizontal diffusion cell setup in an attempt to reduce multiple ultrasound reflections. In their HIFU, *in vitro* study on transdermal transport through pig skin, Helga, et al. (2015) inserted a polyurethane absorber opposite the transducer to avoid reflections of the HIFU beam.

The presence of inertial cavitation has previously been shown to be observable with a PCD (Farny, et al. 2010, Hallow, et al. 2006, Helga, et al. 2015, Liu, et al. 1998). In a PCD setup, a hydrophone, placed directly into the coupling fluid and confocally aligned with the ultrasound beam, measures the ultrasound pressure fluctuations that are radiated by the cavitation bubbles during ultrasound application. The voltage vs. time data that this hydrophone records during ultrasound application is then filtered to isolate the broadband noise. The RMS value of the broadband noise is indicative of the magnitude of the inertial cavitation within the ultrasound field (Hallow, et al. 2006).

This study introduces a standard diameter Franz diffusion cell in which the transducer and the hydrophone were able to be simultaneously positioned in the coupling fluid. This allowed the ICD to be calculated from data taken directly from the actual donor cell during insonation. The diffusion cell setup also employed temperature control to mitigate the coupling fluid temperature increases brought on by continuous ultrasound application. This setup is used to investigate whether the acoustic reflections that occur within a Franz diffusion cell

significantly influence the ICD, and therefore, inertial cavitation activity at an intensity relevant to skin sonoporation.

4.3 Materials and Methods

4.3.1 Modified Franz Diffusion Cell

The modified Franz diffusion cell consisted of a donor chamber that was fixed to a receiver chamber with a specially designed acoustically transmissive clamp. The donor chamber had an inner diameter of 15 mm, an outer diameter of 19 mm and an aperture diameter of 9 mm – dimensions similar to a standard glass Franz diffusion cell (Zorec, et al. 2013). The total volume of the donor chamber was 6.7 mL. The receiver chamber also had a 9 mm aperture, and a volume of 3.2 mL. The donor, receiver, and clamp geometries are presented in Fig. 4-1. Dimensions of the donor chamber are shown in Fig. 4-2.

The donor chamber was 3D printed from VeroClear (VeroClear-RGD810, Stratasys Ltd, Minnesota, USA). The receiver chamber was turned from a solid polypropylene rod (Polystone, Dotmar EPP Pty Ltd, Christchurch, New Zealand) on a CNC lathe (Top-Turn CNC 406, Jashico Machine Manufacture Co. LTD, Taichung, Taiwan). A piece of carbon fibre tubing with an inner diameter of 3.5 mm (Carbon Fibre Tube Pultruded, MAKERshop, Auckland, New Zealand) was glued to the polypropylene receiver with Loctite 401 to form the sampling arm. To enable coupling fluid circulation and temperature control, two pieces of carbon fibre tubing with inner diameters of 2 mm were glued to the donor chamber to form ports (Carbon Fibre Tube Pultruded, MAKERshop, Auckland, New Zealand). The clamp was 3D printed from Acrylonitrile Butadiene Styrene (ABS P430, Stratasys Ltd, Minnesota, USA).

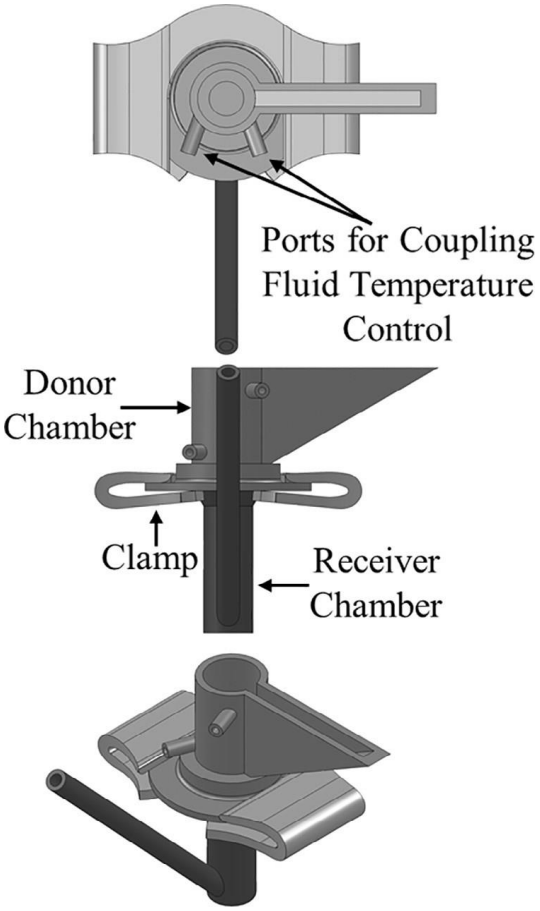

Fig. 4-1 Modified diffusion cell geometry (top) plan view, (middle) front view and (bottom) isometric view

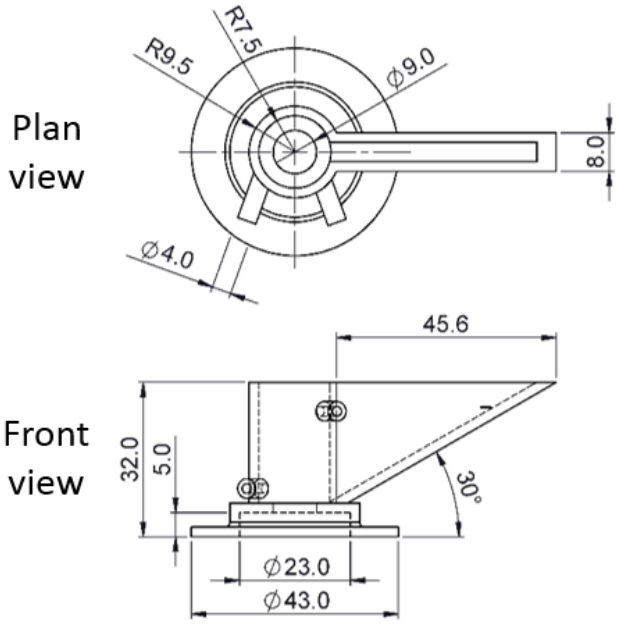

Fig. 4-2 Dimensions of the 3D printed VeroClear donor chamber. Dimensions of the receiver chamber are shown in Chapter 2.

A 16 mm diameter, 0.6 mm thick piece of polypropylene was inserted between the donor and receiver chambers. This acted as a skin phantom. Phantoms are often used in ultrasound studies as they remove the effects of physiological variations between different tissue samples (Helga, et al. 2015, Khokhlova, et al. 2006, Liao, et al. 2016, Maxwell, et al. 2010, Rifai, et al. 2010, Zell, et al. 2007). Like skin, polypropylene has a similar acoustic impedance to water. Therefore, the phantom provided the solid surface necessary for a-symmetrical bubble collapse without diminishing the intensity of the ultrasound waves that were transmitted through to the receiver fluid. The surface roughness of a material has been shown to influence the cavitation activity that arises when that material is insonated (Nour, et al. 2007). Therefore, the inertial cavitation activity that arises from the insonation of polypropylene may be different from that which arises from the insonation of skin under the same ultrasound conditions. However, the focus of this study was to assess the influence of the diffusion cell's acoustic conditions on the ICD. Therefore, the phantom was used as it provided a consistent target surface condition for inertial cavitation activity. Two polystyrene gaskets (Permagear Inc, Pennsylvania, USA) were placed between the donor and receiver chambers on each side of the phantom to prevent leakage.

4.3.2 Coupling Fluid Temperature Measurement and Control

The temperature of the coupling fluid was measured with a thermocouple (Wire Type K Thermocouple, Jaycar Electronics Pty Ltd, Auckland, New Zealand). The relative position of the thermocouple can be seen in Fig. 4-3. The readings from the thermocouple were passed to a NI-9211 DAQ module (National Instruments Ltd., Texas, USA) then on to a PC for processing in LabVIEW (National Instruments Ltd., Texas, USA). The thermocouple sampling frequency was 1 Hz.

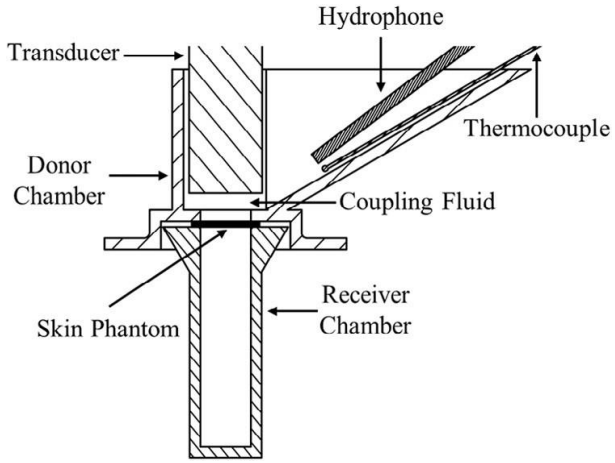

Fig. 4-3 Cross section of the diffusion cell revealing the positioning of the transducer, thermocouple and hydrophone

A constant coupling fluid temperature was maintained by circulating the fluid out of the donor chamber, through a custom built temperature controller and back into the donor chamber at a flow rate of 0.14 L/min. This circuit is depicted in Fig. 4-4. A peristaltic pump (6 V Peristaltic Pump, Amazon, Washington, USA) was used to achieve this flow rate. The components in the cooling circuit were linked by 2.6 mm inner diameter silicone tubing (Silicone Tubing Clear Grade, Rubbermark Industries Ltd., Auckland, New Zealand). This tubing could be easily removed from the donor chamber ports to allow for replacement of fluid between each experiment.

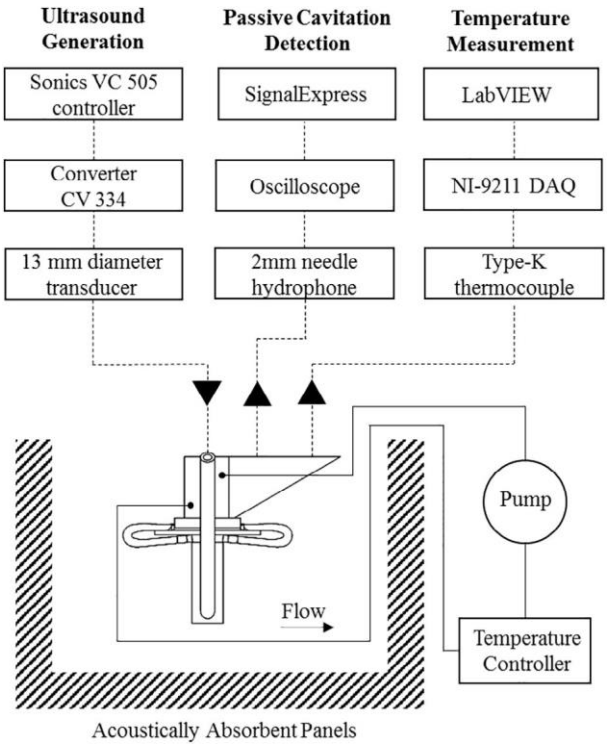

Fig. 4-4 System schematic. The solid lines represent the coupling fluid circuit. The dashed lines represent the signal inputs and outputs to and from the instruments in the coupling fluid.

The temperature controller consisted of six 12 V thermoelectric Peltier plates (Peltier 60 W, TecParts NZ Ltd., Tauranga, New Zealand) arranged around a block of aluminium (Fig. 4-5). The coupling fluid was cooled as it passed through a series of connected holes drilled in the aluminium block. The cooling rate was controlled by the power supply to the Peltier plates. The hot sides of the Peltier plates were connected to water cooled fins (Fig. 4-6). These fins were constructed from square cross-sectioned aluminium tubing that had a side length of 40 mm, a thickness of 3 mm, and an overall length of 300 mm. A thermally conductive paste (Heatsink Compound, Jaycar Electronics Pty Ltd, Auckland, New Zealand) was applied to both sides of each Peltier plate to ensure effective heat transfer. The coupling fluid temperature was maintained at 15 °C ± 1 °C. Researchers who intend to employ this temperature control

system in future studies should note that the Peltier plates can be sufficiently air-cooled (allowing a more compact setup) if the ultrasound intensity is below a certain threshold.

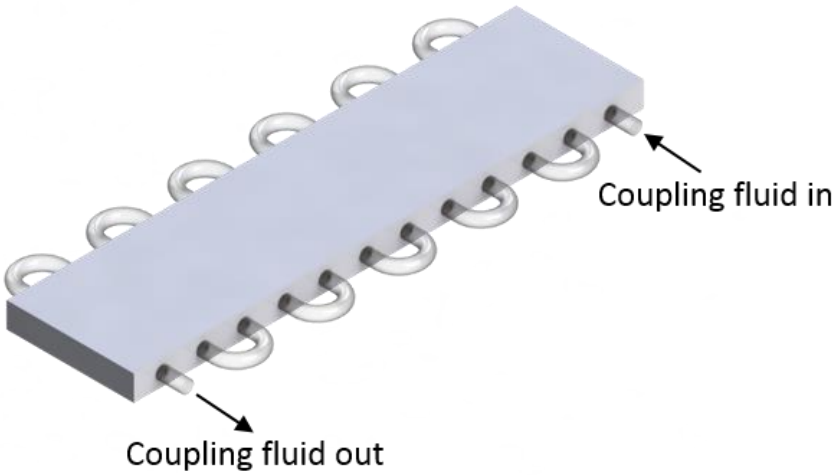

Fig. 4-5 Schematic of heat exchanger block. Sections of silicone tubing diverted the coupling fluid from one hole in the aluminium block to the next. Three Peltier plates were attached to each side of this block.

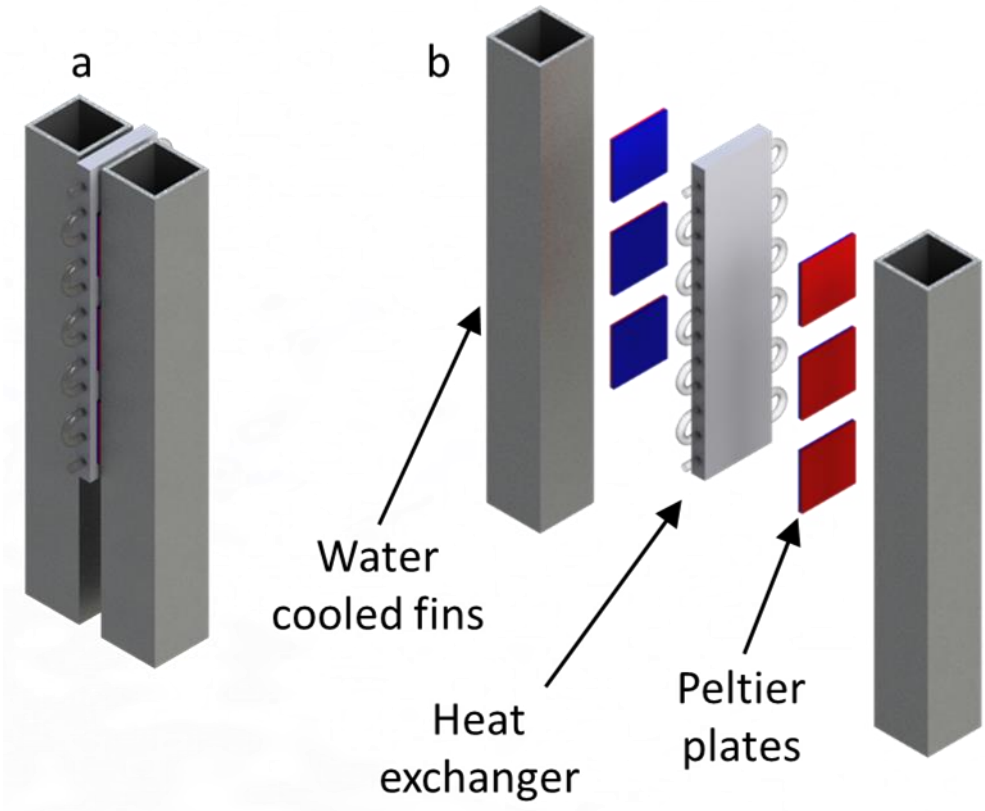

Fig. 4-6 Schematic of the temperature controller showing (a) the assembled components and (b) an exploded view of the components. The hot side of the Peltier plates are shown in red while the cold sides are shown in blue. Cool water was pumped through the hollow fins.

4.3.3 Ultrasound Field Generation

A 20 kHz ultrasound field was generated using an ultrasonic processor (VC 505, Sonics and Materials Inc., Connecticut, USA) with a 13 mm diameter replaceable tip. All of the experiments in this study used continuous ultrasound (a 100 % duty cycle). Following the manufacturer's instruction, compressed air was circulated through the ultrasonic processor to keep it cool during ultrasound application. Terahara, et al. (2002a) showed that the effectiveness of low-frequency skin sonoporation increases with decreasing distance between the transducer face and the target region. A distance of 5 mm was used for the experiments in the present study as this was the smallest distance that still allowed for the hydrophone to be confocal with the transducer.

The near-field to far-field transition distance, L , was determined from the relation (Sprawls 1995)

$$L = \frac{D^2}{4\lambda} \tag{3.1}$$

where D is the diameter of the active face of the transducer (13mm) and λ is the wavelength (73 mm), calculated with the speed of sound in water (at 15 °C) of 1466 m/s. For these parameters, the value of L was calculated to be 0.58 mm. Therefore, at the distance of 5 mm, the skin phantom was well outside the near-field, which is common practice in low-frequency skin sonoporation.

4.3.4 Determination of Ultrasound Intensity

The ultrasound intensity was determined using the calorimetric method (Merino, et al. 2003, Mitragotri, et al. 2000a, Mitragotri, et al. 2000b, Morimoto, et al. 2005, Mutoh, et al. 2003, Terahara, et al. 2002a). An intensity of 13.7 W/cm^2, which was achieved with a tip displacement setting of 20 *%* on the VC 505 ultrasonic processor, was used for all experiments in this study. This was a spatial average, temporal average intensity as in the study by (Mitragotri, et al. 2000a). This intensity level was chosen as both Terahara, et al. (2002a) and Mitragotri, et al. (2000a) achieved considerable skin conductivity increases with intensities between 5 and 15 W/m^2 when using the same diameter transducer tip that was used in this study.

4.3.5 Foil Pitting Experiments

Foil pitting experiments were used to investigate the influence of coupling fluid circulation on the inertial cavitation activity at the skin aperture in the present setup. Seven pieces of 0.016 mm thick aluminium foil (Homebrand, Manukau, New Zealand) were exposed to ultrasound (at an intensity of 13.7 W/cm^2) for 5 s with or without coupling fluid circulation. The number of pits in each of the 14 pieces of foil were then counted to quantify the influence of circulation. In these experiments, the coupling fluid in the donor chamber was deionized water at 15 °C ± 1 °C. This temperature was achieved using the circulation system.

The length of time that a piece of foil is submerged in water prior to ultrasound application can affect the prevalence of air bubbles (nucleation sites) on the surface of the foil. Prior to each ultrasound application, the foil was submerged in the coupling fluid while the circulation

system brought the coupling fluid to the specified temperature. The time required to achieve this temperature was consistent across each foil pitting dataset. Therefore, the effect of the submergence, on the prevalence of nucleation sites on the foil surface, was also consistent.

When counting the foil pits, any circular indent was counted as one pit. Two partially overlapping circular indents were counted as two pits. The duration of ultrasound exposure was short enough to avoid complete perforation of the foil, which would have made it impossible to quantify the number of individual pits.

4.3.6 Passive Cavitation Detector Alignment

The acoustic measurements were taken with a 2 mm needle hydrophone (2.0 mm Needle Hydrophone, Precision Acoustics Ltd, Dorchester, Dorset, UK), which had a sensitivity of -236.4 dBre1V/µPa at the transducer driving frequency of 20 kHz. Note that the full list of calibrated sensitivity values, measured by Neptune Sonar Ltd (East Yorkshire, UK), for frequencies between 5 kHz and 1000 kHz are shown in Appendix C. The manufacturer coated the tip of this hydrophone in silicone to reduce the potential of cavitation damage. A depiction of the relative position of the hydrophone in the diffusion cell is presented in Fig. 4-3. The hydrophone was pointed directly at the centre of the skin phantom so that it was confocal with the transducer. The tip of the hydrophone was 20 mm from the centre of the skin phantom further ensuring that the hydrophone tip was not damaged by cavitation. Note that the hydrophone was held in its fixed position using an aluminium sleeve (Fig. 4-7) that was fixed in place relative to the diffusion cell. In this way the hydrophone could be easily inserted and removed between experiments. Before each experiment, the hydrophone alignment was checked (with the transducer in place) by ensuring that a mark on the centre of the skin

phantom was visible when looking through the centre of the empty sleeve. Note that the support structure for the hydrophone, transducer, and diffusion cell used in this study was similar to that depicted in Section A.2.7.

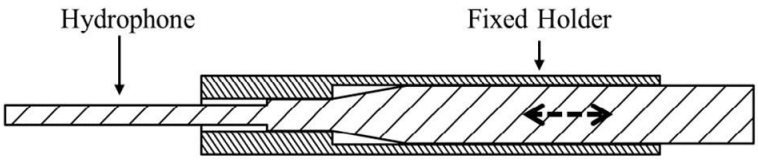

Fig. 4-7 Cross section of the hydrophone sleeve revealing the direction of hydrophone movement during removal and re-insertion.

The voltage signal measured by the hydrophone was recorded with an oscilloscope (TDS 2014B, Tektronix, Beaverton, OR, USA) connected via USB to a PC running SignalExpress (NI LabVIEW SignalExpress, National Instruments, Texas, USA). The oscilloscope collected 2500 data points at a sampling rate of 1 MHz and then transferred these to the PC. The oscilloscope then collected another 2500 data points after a delay of around 1 to 2 s. This continued for the 10 minute duration of insonation.

4.3.7 Determination of Inertial Cavitation Dose Using Broadband Noise Emission

Each set of 2500 data points was filtered so that the broadband noise (indicative of inertial cavitation) could be isolated from the harmonic and sub-harmonic peaks in the frequency spectrum. A digital bandpass filter isolated a band of noise between 92.5 and 97.5 kHz. When choosing the frequency range of this band, three factors were considered: that no harmonics or sub-harmonics should be included in the chosen filter band, as these are influenced by non-inertial cavitation (Yao-Sheng, et al. 2010); that the frequency band should be low enough to allow for a minimum of 10 data points per period to be sampled by the oscilloscope (to ensure

that the hydrophone signal was accurately represented); and that the variability in the broadband noise emission during ultrasound application should be as low as possible as no significant time-dependent variations are expected under the strictly controlled experimental conditions.

The infinite impulse response bandpass filter was produced using MATLAB's 'designfilt' function (MATLAB, MathWorks, Natick, MA, USA). A filter order of 20 was used as this was found to be the minimum order capable of providing the necessary reduction of the 5^{th} harmonic at 100 kHz and the ultraharmonic at 90 kHz.

Once each set of the 2500 data points had been filtered, the RMS value was calculated for the 2.5 ms time period associated with those data points. This RMS value then represented one noise amplitude data point. The ICD was calculated by numerically integrating the noise amplitude over the 10 minutes of ultrasound application in each experiment. Therefore, the ICD had units of V-s as in the cell sonoporation studies by Chen, et al. (2003) and Hallow, et al. (2006). This numerical integration was evaluated using the MATLAB 'trapz' function.

4.3.8 Acoustic Reflection Experiments

Two sets of experiments were devised to investigate the influence of acoustic reflections on ICD. In one set of experiments, the diffusion cell was surrounded by air to replicate the echoic conditions within a traditional Franz diffusion cell. In the second set of experiments, acoustic reflection was greatly reduced by submerging the acoustically transmissive diffusion cell in a water bath so that the water line was 5 mm below the top of the donor chamber (Fig. 4-8). The water bath was 794 mm long, 396 mm wide, and 362 mm high. The walls of the

water bath were made from 12 mm thick acrylic sheets. To further reduce reflection, the interior walls of one half of the water bath (the half containing the diffusion cell) were lined with acoustically absorbent panels (SA-J35, Hangzhou Applied Acoustic Institute, Hangzhou, Zhejiang, China). These panels have been shown to decrease low-frequency ultrasound reflection by 20 dB (Jelenc, et al. 2012). The panels were 300 mm wide, 300 mm long, and had a thickness that varied from 10 mm to 35 mm due to their wedged front surface. The unlined half of the water bath was used for the coupling fluid temperature control system.

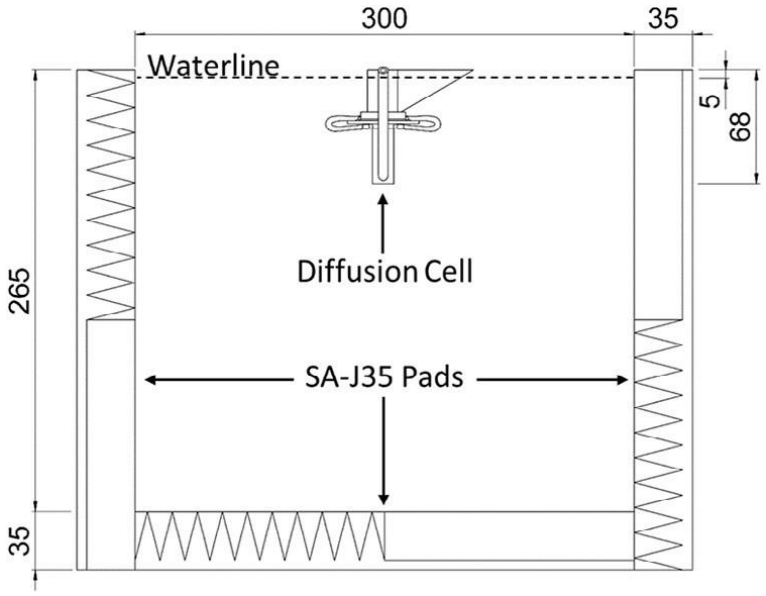

Fig. 4-8 Section view of the diffusion cell in the water bath, which was lined with acoustically absorbent SA-J35pads.The overall height of the diffusion cell is shown along with the waterline, which was 5 mm below the top of the donor chamber.

The proportion of ultrasound that was reflected (R) at the interface of the diffusion cell and surrounding medium in each of the two setups can be approximated by the relation (Cracknell 1980)

$$R = \left(\frac{Z_2 - Z_1}{Z_2 + Z_1} \right)^2 \tag{3.2}$$

where Z_1 is the acoustic impedance of the material that the acoustic wave is propagating from (the coupling fluid) and Z_2 is the acoustic impedance of the material the acoustic wave is propagating into (the surrounding medium). Given the acoustic impedance values for polypropylene (2.4 MRayl), water (1.5 MRayl), and air (400 Rayl), the R values are calculated as 0.99 for the setup surrounded by air and 0.05 for the setup submerged in water (note that the acoustic impedance of the 3D printed VeroClear donor chamber was approximated to be equal to that of polypropylene). These values indicate that the proportion of ultrasound that was reflected back into the coupling fluid was approximately 20 times greater for the cell surrounded by air.

Seven repetitions of the experiments were conducted for each of the two setups (n=7). Each experiment consisted of 10 minutes of ultrasound exposure. This application time was chosen to reflect those of published low-frequency skin sonoporation studies (Sarheed and Abdul Rasool 2011, Terahara, et al. 2002a, Tezel, et al. 2001). The coupling fluid (deionised water) was replaced between each experimental repetition. Deionised water was taken from a Labwater L991008 Deioniser (Suez Ltd, Thame, UK). The same phantom was used in each experimental repetition as no cavitation damage was observed on its surface.

4.4 Results

4.4.1 Coupling Fluid Temperature

Under certain conditions, the application of ultrasound in a diffusion cell has been shown to result in an increase in coupling fluid temperature due to absorption (Ahmadi, et al. 2012,

O'Brien Jr 2007): the fluid medium absorbs a portion of the ultrasound energy, converting it into heat. A constant coupling fluid temperature was maintained by circulating the fluid through a thermoelectric cooling device during the application of ultrasound at an intensity of 13.7 W/cm^2. The effectiveness of the cooling device was apparent when the coupling fluid temperature without circulation was compared to the coupling fluid temperature with circulation over 10 minutes of insonation (Fig. 4-9). In the absence of temperature control, the coupling fluid temperature increased to 50 °C within 110 s. With circulation, the temperature was able to be maintained at 15 °C ± 1 °C.

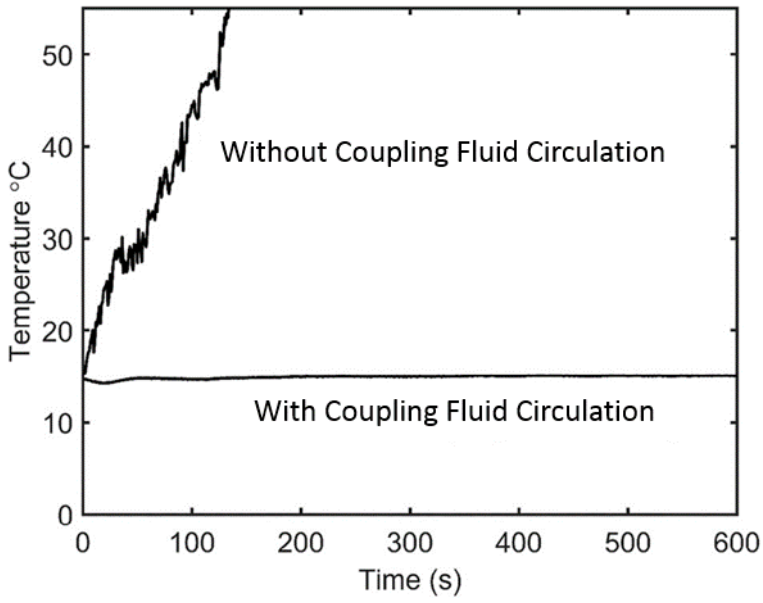

Fig. 4-9 Transient behaviour of the coupling fluid temperature with and without coupling fluid circulation during ultrasound application at an intensity of 13.7 W/cm^2.

4.4.2 Foil Pitting Experiments

Foil pitting experiments were used to investigate the influence of coupling fluid circulation on the inertial cavitation activity at the skin aperture in the present setup. Seven pieces of aluminium foil were exposed to ultrasound (at an intensity of 13.7 W/cm^2 and a transducer

distance of 5 mm) for 5 s with and without coupling fluid circulation. The coupling fluid temperature was 15 °C ± 1 °C. Without coupling fluid circulation, the mean number of pits after ultrasound application was 13 and the median was 12 (Fig. 4-10). With coupling fluid circulation, the mean number of pits was 12 and the median was 11. Therefore, circulation caused a 4 *%* decrease in the mean number of pits (*p*=0.9) and an 8 *%* increase in the median. Given the *p*-value, the difference between the two datasets is negligible.

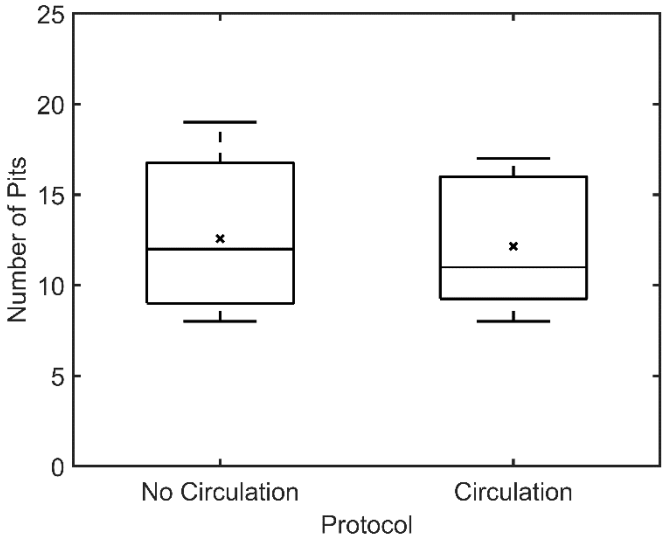

Fig. 4-10 The influence of coupling fluid circulation on the pitting of aluminium foil. Ultrasound was applied for 5 s at an intensity 13.7 W/cm^2. The transducer to skin distance was 5 mm. The crosses within the boxes represent the mean values (n=7).

4.4.3 Passive Cavitation Detection

The amplitude of the broadband noise has been reported to be an effective indicator of the presence of inertial cavitation in insonation setups (Farny, et al. 2010, Hallow, et al. 2006, Helga, et al. 2015, Liu, et al. 1998). To demonstrate the relationship between inertial cavitation and broadband noise in the current setup, the standard configuration (with air as the surrounding medium) was used to capture the PCD frequency spectra under three

different insonation conditions. First, the frequency spectrum in the absence of any applied ultrasound (0 W/cm^2) was captured to quantify the noise floor (Fig. 4-11a). The noise floor in the frequency band of interest (92.5 to 97.5 kHz) had a magnitude of around -250 dB (relative to 1V). Next, two frequency spectra resulting from insonation at 13.7 W/m^2 were captured. For one of these, the coupling fluid was deionised water, while for the other, the coupling fluid was castor oil. Castor oil has a similar acoustic impedance to water (1.4 MRayl for castor oil and 1.54 MRayl for water) but a much higher viscosity (0.65 Pa s for castor oil and 0.00089 Pa s for water) (Polat, et al. 2011b). Therefore castor oil subdues inertial cavitation activity (Tang, et al. 2002a) without removing the harmonic and sub-harmonic peaks in the frequency spectrum. With this in mind, frequency spectra corresponding to insonation without inertial cavitation suppression and insonation with inertial cavitation suppression are presented in Fig. 4-11b and Fig. 4-11c respectively. When inertial cavitation was not suppressed, the broadband noise emission magnitude in the frequency band of interest was around -160 dB, far greater than the noise floor of -250 dB. When inertial cavitation was suppressed using castor oil as the coupling fluid, the broadband noise emission magnitude was approximately -220 dB. Although this magnitude is still somewhat higher than the noise floor, it is significantly lower than the deionised water case. It is then reasonable to conclude that broadband noise emission, within this frequency range, did represent the inertial cavitation activity in the present diffusion cell setup.

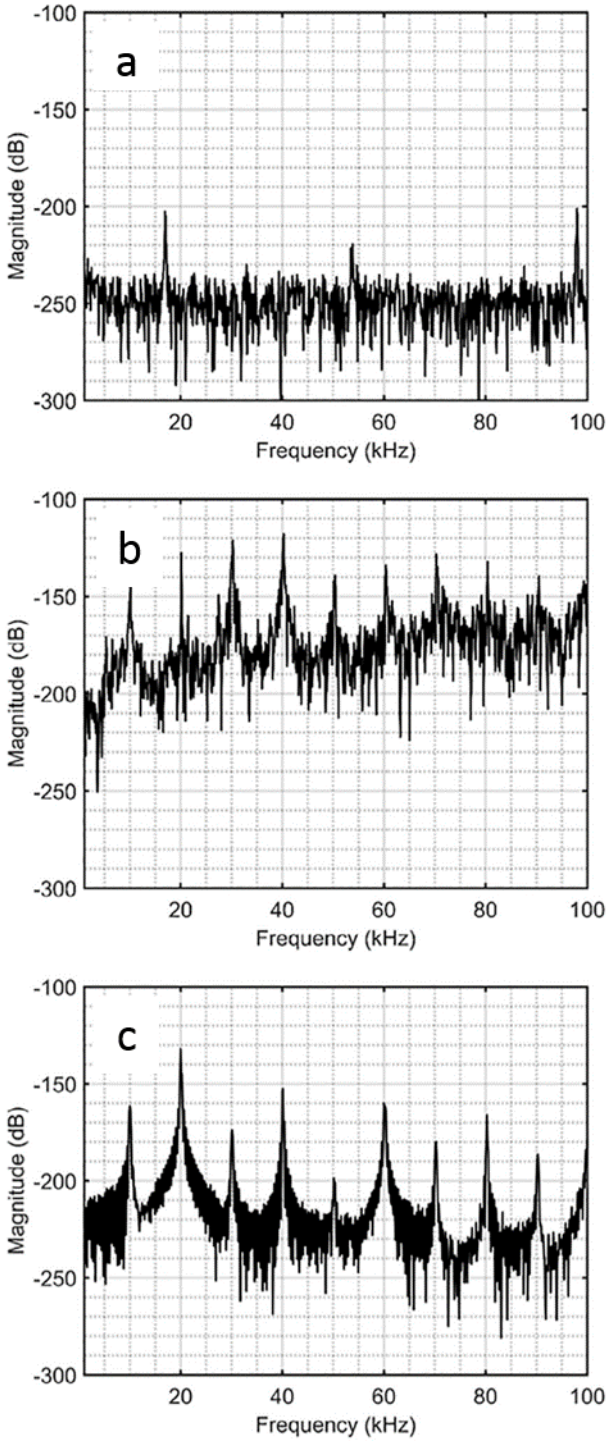

Fig. 4-11 Passive cavitation detector frequency spectra in (a) the absence of ultrasound, (b) the presence of ultrasound with deionised water as the coupling fluid and (c) the presence of ultrasound with castor oil as the coupling fluid.

The 92.5-97.5 kHz passband was used for the PCD in this study as it resulted in relatively consistent broadband noise emission over the 10 minutes of ultrasound application.

Examples of broadband noise emission are shown in Fig. 4-12 for passbands of 2.5-7.5 kHz, 22.5-27.5 kHz, 32.5-37.5 kHz, and 92.5-97.5 kHz. There is no reason to suspect that the inertial cavitation activity varied dramatically during the 10 minutes of ultrasound application under the strictly controlled experimental conditions. Therefore, the temporal variations which sometimes occured in the 2.5-7.5 kHz, 22.5-27.5 kHz, 32.5-37.5 kHz passbands made those passbands inappropriate for use in the present study. These temporal variations were likely a result of fluctuations in nearby harmonic, subharmonic, or ultraharmonic peaks.

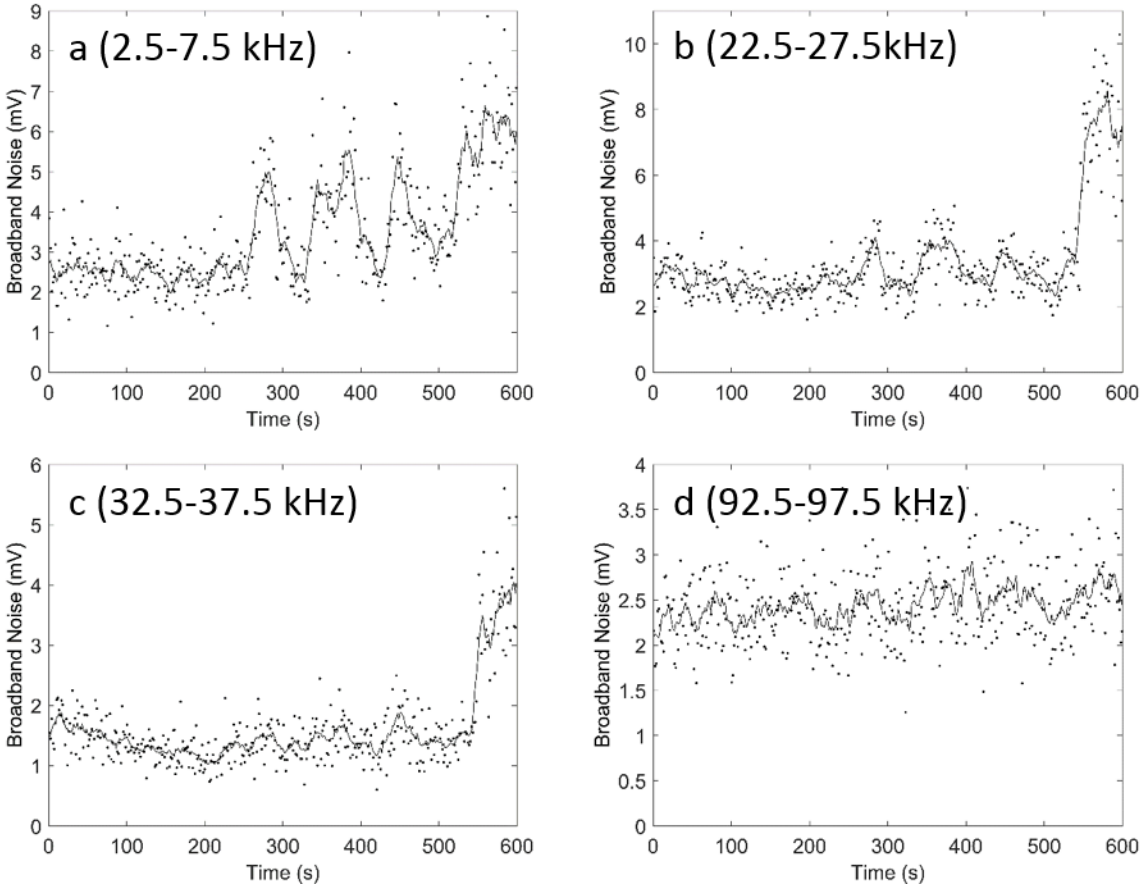

Fig. 4-12 Examples of broadband noise data for four different frequency bands (a) 2.5-7.5 kHz, (b) 22.5-27.5 kHz, (c) 32.5-37.5 kHz, and (d)92.5-97.5 kHz. The solid line is a moving average intended to aid interpretation of the data. The moving average value was calculated by taking the mean of the current, four preceding, and four succeeding data points.

Both temperature and broadband noise emission (92.5-97.5 kHz) were monitored over 10 minutes of ultrasound application in a diffusion cell surrounded by air and in a diffusion cell submerged in water. The broadband noise data for one of the seven repetitions that was collected when the cell was surrounded by air is presented in Fig. 4-13a. The broadband noise data for one of the seven repetitions that was collected when the cell was submerged in water is presented in Fig. 4-13b. Transient temperature data is not shown here, but the coupling fluid temperature was always maintained at 15 °C ± 1 °C.

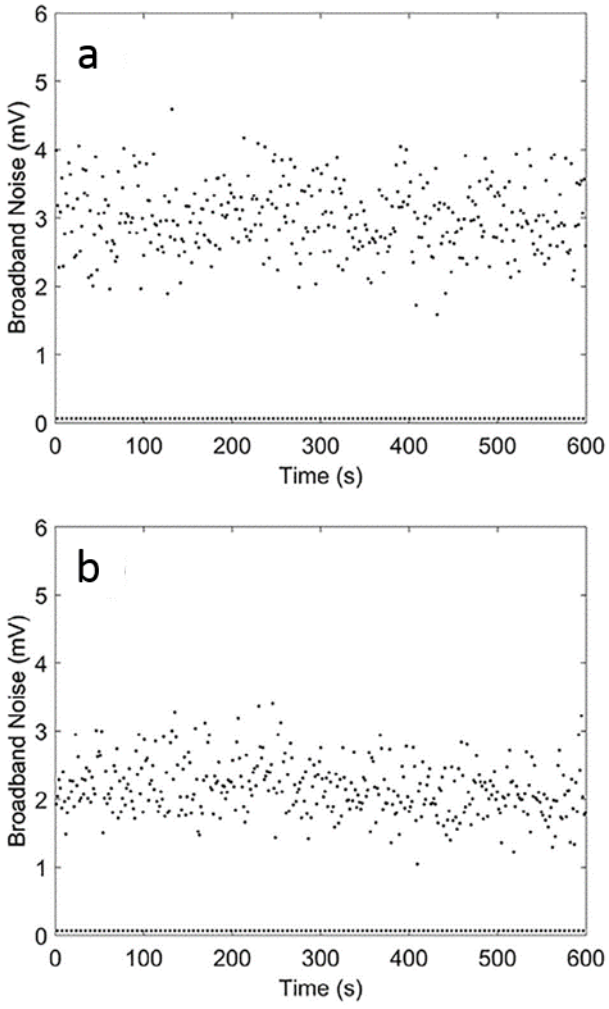

Fig. 4-13 Examples of the broadband noise data captured over 10 min of continuous ultrasound application at an intensity of 13.7 W/cm^2 with the coupling fluid maintained at 15 ± 1 °C in (a) a diffusion cell surrounded by air and (b) a diffusion cell submerged in water. The dashed lines at the very bottom depict the baseline noise level.

In the study by Bull, et al. (2013), a simple method was used to determine whether broadband noise emission exceeded a threshold level representative of statistically significant inertial cavitation activity. The '100 % occurrence threshold' methodology dictates that all filtered broadband noise readings must be above a minimum baseline level in order for the inertial cavitation threshold to be surpassed. This baseline noise level, N_{BL}, was determined from the relation,

$$N_{BL} = \mu + 4\sigma \tag{3.3}$$

where μ is the mean value of the noise floor and σ is the standard deviation of the noise floor. The baseline noise level for the present setup is depicted by the dashed lines at the bottom of Fig. 4-13a and Fig. 4-13b. All of the broadband noise emission data in Fig. 4-13a and Fig. 4-13b was well above this threshold. Therefore, the level of the broadband noise observed during each of the seven repetitions in each of the two diffusion cells was due to inertial cavitation activity as opposed to other potential sources of noise such as electromagnetic interference.

4.4.4 The Influence of Acoustic Reflection

The broadband noise emission data was converted to an ICD value for each of the seven repetitions conducted in each of the two diffusion cell setups. Fig. 4-14 displays boxplots of the ICD data. The central horizontal line in each of the boxes represents the median value, the cross represents the mean value, the top and bottom horizontal line of each box

represents the upper and lower quartiles, and the whiskers represent the maximum and minimum values in each set.

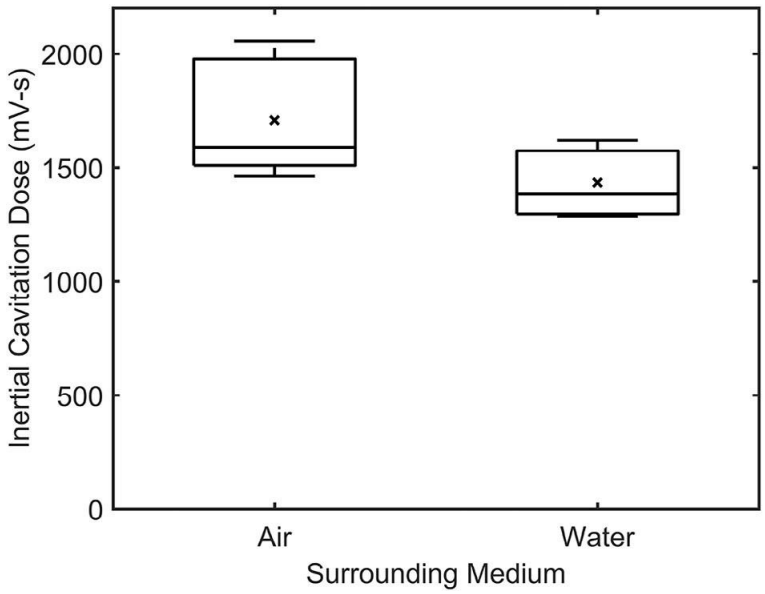

Fig. 4-14 Inertial cavitation dose calculated for the diffusion cell setup surrounded by air and the diffusion cell setup submerged in water (n = 7). Ultrasound was applied at an intensity of 13.7 W/cm^2 continuously for 10 min. The coupling fluid was maintained at 15±1 °C.

There was a difference between the median and mean dose values for the two setups. When the surrounding medium was air, the median and mean values were 1590 mV-s and 1709 mV-s respectively. When the surrounding medium was water, the median and mean values were 1385 mV-s and 1433 mV-s respectively. Therefore, the suppression of acoustic reflection resulted in a 13 % decrease in the median ICD and a 16 % decrease in the mean ICD (significant at p=0.07).

There was also a difference in the degree of variability for the two cases. When the surrounding medium was air, the standard deviation was 255 mV-s. When the surrounding

medium was water, the standard deviation was 149 mV-s. This difference in variability was anticipated because an increase in the mean ICD has been reported to result in an increase in standard deviation (Chen, et al. 2003). Note that three other temporally stable frequency bands investigated (62.5-67.5 kHz, 72.5-77.5 kHz, and 82.5-87.5 kHz) also showed decreases in mean ICD, between 8 *%* and 18 *%* ($0.05<p<0.26$) with the suppression of reflection.

4.5 Discussion

At an ultrasound intensity of 13.6 W/cm^2, the ICD was influenced by the acoustic reflections in the diffusion cell setup. It can then be concluded that the inertial cavitation which occurs in a sonoporation setup is influenced by the echoic conditions of that setup. Therefore, differences in echoic conditions should be considered when translating the results of *in vitro* studies (conducted in highly reflective Franz diffusion cells) to *in vivo* or clinical setups that have vastly different degrees of acoustic reflection. For a given set of experimental parameters, the same inertial cavitation activity that which was obtained *in vitro* is not guaranteed in an *in vivo* or clinical scenario*,* due to the differences in acoustic reflection within the setups. However, it is unclear from the results in Fig. 4-14 whether the acoustic reflections within a diffusion cell would influence the transport results of an *in vitro* skin sonoporation study by a statistically significant amount, especially considering the relatively small difference in mean ICD and the high degree of variability in most sonoporation studies (Mitragotri, et al. 2000a, Schoellhammer, et al. 2012, Terahara, et al. 2002a, Tezel, et al. 2001), as in Fig. 2-18, Fig. 3-15, Fig. A-22, and Fig. B-10 of this thesis. Future *in vitro* studies that want to supresses reflection, as was attempted in the studies which inserted a thin polymer absorber at the bottom of the receiver chamber (Alvarez-Román, et al. 2003, Merino,

et al. 2003, Mitragotri, et al. 1995b), should use the setup introduced in the present study. The acoustically transmissive polymer components allow the vast majority of the ultrasound energy (~95 %) to pass through the diffusion cell into the acoustically lined water bath. Using the present setup would ensure that the ultrasound field was far closer to an *in vivo* or clinical case than that achieved with any glass setup.

The present study was in part motivated by the results of cell sonoporation studies which found that acoustic reflections can have a strong influence on inertial cavitation activity. An experiment was conducted to investigate whether acoustic reflections in experimental conditions associated with skin sonoporation would also influence inertial cavitation. The influence of acoustic reflections found in the present study was minor in comparison to that found in a study which investigated the influence of acoustic reflections in a cell sonoporation setup. Kinoshita and Hynynen (2007) found that cell sonoporation was halved when acoustic reflections were suppressed. One explanation for the much smaller influence of reflection in the present study compared to the cell sonoporation study may be related to the different setup geometries used in the experiments. The setup geometry affects the intensity of the reflected ultrasound waves in the target region, due to the distance that the reflected waves must travel before returning to the target region from the point of reflection. The target region in the setup of Kinoshita and Hynynen (2007) was the cell culture plate, while the target region in the present setup was the coupling fluid near the surface of the phantom. The main acoustically reflective interface in the cell culture plate was the top of the cell culture plate (which was within the target region), whereas the main acoustically reflective interface in the Franz diffusion cell was the bottom of the receiver chamber which was outside the target region (by approximately 40 mm in this case). As the reflected wave fronts had to travel a

shorter distance in the study by Kinoshita and Hynynen (2007) than they did in the present study, they caused a greater amount of acoustic interference, and therefore, lead to a greater increase in the peak rarefactional pressure in the target region.

The PCD passband that was used in Chapter 3 (22.5-27.5 kHz) was found to be inappropriate for the setup in the present study. The broadband noise emission found with the 22.5-27.5 kHz passband sometimes varied significantly during the 10 minutes of ultrasound application (Fig. 4-12c). Similar temporal variations were found in the broadband noise emission using passbands of 2.5-7.5 kHz and 32.5-37.5 kHz. The passband that displayed the least amount of temporal variation was 92.5-97.5 kHz, which is why it was used for the present study. The differences in temporal variations in broadband noise emission for different passbands again lead to the conclusion that, instead of just arbitrarily selecting a passband, care should be taken to select a PCD passband that is appropriate for a specific ultrasound setup (a point previously discussed in Section 3.5). The importance of tailoring the PCD passband to the setup highlights an advantage of using a digital filter instead of the analog filtering setups that are often used in PCD systems (Farny, et al. 2010, Helga, et al. 2015, Hockham, et al. 2010, Tang, et al. 2002a, Tezel, et al. 2002). In the present study, the voltage data from the hydrophone was saved before filtering. This enabled the broadband noise emission from a number of passbands to be analysed, from one set of voltage data, so that the most appropriate band for this specific setup could be selected.

In the present setup, the pitting of aluminium foil was negligibly affected by circulation of the coupling fluid. From this result it concluded that the inertial cavitation at the skin aperture was unaffected by circulation. This finding is beneficial for any researcher who wishes to use

a small diameter Franz diffusion cell with temperature control (as opposed to the large diameter setups used in Chapters 2 and 3, and Appendices A and B). If the present small diameter setup were to be used to control coupling fluid temperature during sonoporation, the circulation would not affect the inertial cavitation activity which impacted the skin.

The present study contains the first known use of the 3D printed material VeroClear in a sonoporation or sonophoresis setup. No cavitation damage was observed on any of the VeroClear donor chamber's surfaces at the end of this study (which involved more than 2.5 hours of ultrasound application at an intensity shown to cause significant pitting in aluminium foil). The ability of this translucent material to withstand inertial cavitation damage demonstrates that it can be used as an alternative to glass in future studies. The rapid manufacturing process also enables more complex custom geometries than are possible with glass. The high cost of the material was the only reason it was not used in place of Polypropylene in the experiments reported in Chapters 2, 3, Appendix A, and Appendix B.

4.6 Conclusions

A modified Franz diffusion cell setup with variable echoic properties was developed. The reflectivity of one version of this setup was approximately 20 times greater than that of a second version that supressed reflection. Thesis objective 6 (design and manufacture a Franz diffusion cell setup with variable echoic properties) has been fulfilled.

A PCD hydrophone was positioned confocally with the transducer during ultrasound application. A coupling fluid circulation and cooling system enabled the continuous

application of ultrasound (at an intensity relevant to skin sonoporation) for a period of 10 minutes without any notable increase in the temperature of the coupling fluid. The confocal hydrophone position allowed for PCD data to be captured during the application of ultrasound. This enabled ICD to be employed as a means for quantifying inertial cavitation behaviour. This setup was used to investigate the effect of acoustic reflection on the ICD during low-frequency insonation at an intensity applicable to skin sonoporation (13.6 W/cm^2). When acoustic reflection was suppressed, the median and mean ICD were 13 *%* and 16 *%* lower respectively than when the reflection was not supressed (significant at p=0.07). These results show that, at an intensity of 13.6 W/cm^2, a frequency of 20 kHz, and a transducer distance of 5 mm, the acoustic reflections within a low-frequency Franz diffusion cell skin sonoporation setup can influence inertial cavitation during ultrasound application. Therefore, differences in echoic conditions should be considered when translating the results of *in vitro* studies (conducted in highly reflective Franz diffusion cells) to *in vivo* or clinical setups that have vastly different echoic properties. For a given set input parameters, the same inertial cavitation activity that was obtained *in vitro* is not guaranteed in an *in vivo* or clinical scenario*,* due to differences in echoic conditions. Thesis objective 7 (investigate the influence of acoustic reflection on inertial cavitation activity during ultrasound application in a Franz diffusion cell) has been fulfilled.

The present study represents an initial inquiry into the influence of acoustic reflections in skin sonoporation setups. While the intensity and frequency used in this study are applicable to skin sonoporation (Mitragotri, et al. 2000a, Terahara, et al. 2002a), further investigation of the influence of acoustic reflections in Franz diffusion cells should consider a range of frequencies, intensities and target materials if a complete understanding of the underlying

physics is to be obtained. The novel transmissive (low reflection) diffusion cell setup introduced in this study provides an important basis for the methodologies and setups required for these further investigations, and is therefore in itself an important contribution to the field.

5 Conclusions

This section contains a summation of the conclusions from Chapters 2, 3, and 4 as they pertain to thesis objectives 1-7.

1) Design and manufacture a system which enables the coupling fluid to be set and maintained at a variety of temperatures during skin sonoporation.

In Chapter 2.4.1, a modified Franz diffusion cell along with a circulating temperature regulation system successfully maintained the coupling fluid temperature at either (13 °C, 33 °C, or 46 °C) during the sonoporation of porcine skin. Foil pitting experiments showed that this temperature regulation system had a negligible effect on the inertial cavitation at the skin aperture. **Thesis objective 1 has been fulfilled**. The ability to maintain a constant coupling fluid temperature during sonoporation removes the need for time consuming duty cycles or tedious periodic replacement of the coupling fluid. Therefore, the coupling fluid temperature control system used in this study represents a significant contribution to the field. In an experimental setting, use of the present temperature control system would reduce the time required to run each experiment and the labour required by the researcher. In a clinical setting, use of the present temperature control system could reduce the required patient contact time 10-fold relative to an application protocol that required a 10 % duty cycle to minimise thermal effects. Therefore this system enables far more clinically practical sonoporation protocols than could have previously been achieved. This system could easily be adopted by other skin sonoporation or sonophoresis researchers.

2) Investigate the influence of coupling fluid temperature on the inertial cavitation activity that occurs in a low-frequency Franz diffusion cell setup.

In foil pitting experiments, reported in Chapter 2.3.10, increasing the coupling fluid temperature decreased the number of pits. For an intensity of 55 W/cm^2 and a transducer distance of 3 mm, an increase in coupling fluid temperature from 10 °C to 40 °C corresponded to a 50 *%* decrease in the number of pits (p<0.05) after 1 s of ultrasound application. For an intensity of 13 W/cm^2 and a transducer distance of 3 mm, an increase in coupling fluid temperature from 10 °C to 40 °C corresponded to a 38 *%* decrease in the number of pits (p<0.05). Additional foil pitting experiments (shown in Fig. A-13) were conducted with an ultrasound intensity of 34 W/cm^2 and a transducer distance of 5 mm. An increase in coupling fluid temperature from 10 °C to 25 °C resulted in a 57 *%* decrease in the mean number of pits (p<0.05), while an increase from 25 °C to 40 °C resulted in a further 65 *%* decrease (p<0.05) after 5 s of ultrasound application. From these decreases in pitting it can be concluded that increasing the coupling fluid temperature results in a decrease in the inertial cavitation activity that impacts the skin in a Franz diffusion cell. This agrees with the assertion made in the HIFU study by Hockham, et al. (2010) which attributed decreasing inertial cavitation activity to an increase in vapour pressure with increasing coupling fluid temperature. **Thesis objective 2 has been fulfilled.**

3) Investigate the influence of coupling fluid temperature on post-sonoporation transport.

Transdermal transport experiments, reported in Chapter 2.4.2, showed that increasing the temperature at which the coupling fluid was maintained during sonoporation increased the post-sonoporation transport of calcein. Following 5 hours of diffusion, the median receiver chamber calcein concentration after sonoporation at a coupling fluid temperature of 46 °C was 2.3 times the concentration achieved after sonoporation at 33 °C (p=0.07), which was 2.2 times the concentration achieved after sonoporation at 13 °C (p=0.7). Past studies have used duty cycles and fluid replacement to keep the coupling fluid below 37-40 °C during sonoporation. However, the results of this study show that temperature dependent increases in post-sonoporation transport can occur above and below 37-40 °C.

In the transdermal transport experiments in Chapter 3.4.3 the post-sonoporation transport also increased with increasing coupling fluid temperature, in the range of 10 °C to 37 °C. This reinforces the transport-temperature relationship found in Chapter 2.4.2. **Thesis objective 3 has been fulfilled.**

Two findings from objective 3 have important implications for any future *in vivo* or clinical sonoporation studies that adopt the circulating coupling fluid temperature control method. For a given set of experimental parameters (intensity, application time etc.), a higher coupling fluid temperature during sonoporation results in more post-sonoporation transport. However, a lower coupling fluid temperature during sonoporation results in a smaller increase in the temperature of the tissue underlying the SC. Given these two findings, future *in vivo* or clinical sonoporation studies that incorporate coupling fluid temperature control will need to carefully select their target coupling fluid temperature so as to find a balance

between transport (which is greatest at high temperature) and safety (which is greatest at low temperature).

4) Design and manufacture a skin sonoporation setup that enables a PCD hydrophone to be positioned in the coupling fluid during sonoporation.

A modified Franz diffusion cell setup was designed and manufactured. This setup enabled a PCD hydrophone to be positioned in the coupling fluid in a repeatable manner during sonoporation. The custom hydrophone and diffusion cell support structures allowed for the easy removal and reinsertion of multiple diffusion cells. **Thesis objective 4 has been fulfilled.**

5) Assess the ability of the PCD setup from 4) to monitor inertial cavitation activity during skin sonoporation. Also assess the potential for using the PCD output as a real-time indicator of the post-sonoporation transport.

From measurements of broadband noise emission (Chapter 3.4.2) it can be concluded that, even if not perfectly confocal, a PCD hydrophone positioned in the coupling fluid can be used to monitor the inertial cavitation activity which occurs during sonoporation in a Franz diffusion cell. The broadband noise emission was shown to increase with increasing intensity (as inertial cavitation does) and decrease with increasing coupling fluid temperature and carbonation (as inertial cavitation was shown to do). The introduction of a diffusion cell setup that facilitates a PCD capable of monitoring inertial cavitation activity during sonoporation is a significant contribution to the field.

Two attempts were made to correlate PCD output with the post-sonoporation transport (in Chapter 3.4.4 and in the earlier study reported in Appendix A.3.3). This correlation was difficult given the variability in the transdermal transport datasets. However, the attempts at this correlation still lead to an important finding – that the coupling fluid temperature must be held constant if ICD is to be used as an indicator of post-sonoporation transport. Otherwise a decrease in broadband noise emission, resulting from an increase in coupling fluid temperature that actually increases skin permeability, could be misinterpreted as an indicator of decreased post-sonoporation transport. **Thesis objective 5 has been fulfilled.**

6) Design and manufacture a Franz diffusion cell setup with variable echoic properties.

A modified Franz diffusion cell setup with variable echoic properties was developed. This diffusion cell consisted of a custom made VeroClear donor chamber which was clamped to a polypropylene receiver chamber using an acoustically transmissive clamp. The acoustically transmissive support structure for this setup allowed it to be submerged in a water tank which was lined with acoustically absorbent panels. The reflectivity of the setup when the surrounding medium was air was approximately 20 times greater than when it was submerged in water. Like the modified diffusion cells used in Chapters 2 and 3, this setup incorporated coupling fluid temperature control and a PCD. **Thesis objective 6 has been fulfilled.**

7) Use the setup from 6) to conduct a preliminary investigation into the influence of acoustic reflection during ultrasound application in a Franz diffusion cell.

The incorporation of a PCD enabled the ICD to be employed as a means for quantifying inertial cavitation behaviour. The reflection setup was used to investigate the effect of acoustic reflection on the ICD during low-frequency insonation at an intensity applicable to skin sonoporation (13.6 W/cm^2). When acoustic reflection was suppressed, the median and mean ICD were 13 *%* and 16 *%* lower respectively than when the reflection was not supressed (significant at p=0.07). It can be concluded from these results that the acoustic reflections within a low-frequency Franz diffusion cell influence inertial cavitation activity at the skin aperture during ultrasound application. Therefore, differences in echoic conditions should be considered when translating the results of *in vitro* studies (conducted in highly reflective Franz diffusion cells) to *in vivo* or clinical setups that have vastly different echoic properties. For a given set of experimental parameters, the same inertial cavitation activity that was obtained *in vitro* should not be expected in an *in vivo* or clinical scenario. **Thesis objective 7 has been fulfilled.**

*

This thesis contains the first known uses of polypropylene, 3D printed VeroClear, and 3D printed ABS components in skin sonoporation or sonophoresis setups. After numerous hours of exposure to 20 kHz ultrasound at a variety of intensities, neither the polypropylene or VeroClear donor chambers showed any signs of cavitation damage. The ability of these semi-transparent materials to withstand cavitation damage means that they could be used in place

of glass in future sonoporation studies. Relative to glass, both 3D printed VeroClear and polypropylene allow for customisation and built for purpose components. The ability to make custom diffusion cell setups was important for this thesis as every experiment required functionality that cannot be had from standard glass diffusion cells. The polypropylene components used in this thesis were also very affordable relative to the expensive off the shelf glass components often employed in transdermal studies.

6 Future Work

It would be beneficial to employ a coupling fluid temperature control system during sonophoresis. In sonophoresis, the permeant solution also acts as the coupling fluid. Therefore, using a coupling fluid temperature control system during sonophoresis would not only allow constant ultrasound application without the need for duty cycles or fluid replacement, but could also be used to maintain a higher permeant diffusion coefficient than that which occurs at room temperature. The coupling fluid would simply need to be maintained in the safe but elevated range of 30-35 °C. The temperature control system reported in this thesis was designed so that dissolved permeants could easily be flushed and cleaned from the tubing and heat exchanger. Therefore, the system could easily be employed in a sonophoresis study.

The temperature control system developed for this thesis is capable of maintaining a variety of coupling fluid temperatures during sonoporation at a wide range of ultrasound intensities. However, it required a laboratory water cooler. Although water coolers like this are common in most research facilities, they are heavy. If coupling fluid cooling was to be incorporated into a clinical sonoporation or sonophoresis device, it would be helpful to use a more portable setup that didn't require such a large and heavy piece of equipment. A worthwhile future project could involve the development of a lightweight, portable coupling fluid temperature control system, based on the same circulating technique employed in this thesis.

It would also be helpful to incorporate a feedback loop into the temperature control system so that the user does not have to manually set the water bath temperature (or the thermoelectric power supply). Implementing this would require a LabVIEW program which had thermocouple temperature as an input and heat exchanger cooling power as an output. This feedback would allow the user to change the transducer tip displacement mid-experiment without having to manually change the water bath temperature (or the thermoelectric power supply) in order to maintain the same coupling fluid temperature. For such a feedback system to be helpful, the delay between changing the transducer tip displacement and restabilising the desired steady coupling fluid temperature would need to be minimal.

A chemical dosimeter could be used to further investigate the influence of coupling fluid temperature on inertial cavitation activity in a low-frequency sonoporation setup. Terephthalic acid (TA) is a common chemical dosimeter that fluoresces when exposed to cavitation (Barnett 1996, McLean and Mortimer 1988, Price and Lenz 1993, Tang, et al. 2002a). Using a coupling fluid containing TA, skin could be sonoporated at variety of temperatures between 10 °C and 37 °C. The fluorescence of the coupling fluid after sonoporation could then be measured with a spectrofluorometer. The influence of coupling fluid temperature on fluorescence and foil pitting could then be compared. Terephthalic acid could also be used to further investigate the influence of acoustic reflection on the inertial cavitation activity in a Franz diffusion cell. The influence of acoustic reflection on the fluorescence could then be compared to the PCD data from Chapter 4.

Appendix A Temperature Control and Passive Cavitation Detection During Skin Sonoporation – Preliminary Caffeine Study

A.1 Abstract

This study was conducted prior to those in Chapters 2 and 3 and presents the first attempt to employ a PCD system to monitor inertial cavitation activity during constant temperature skin sonoporation in a Franz diffusion cell. Three different ultrasound intensities were employed to create three different magnitudes of inertial cavitation activity. The broadband noise emission was measured during skin sonoporation at each of these intensities. Following sonoporation, a caffeine solution was applied to the skin and left to diffuse for 20 hours. The correlation between the post-sonoporation receiver chamber caffeine concentration and ICD was then assessed. The correlation was poor which means that the PCD output could not be used as an effective real-time indicator of post-sonoporation caffeine transport in the present setup. However, from this preliminary study it was hypothesised that moving the hydrophone closer to the skin aperture would result in a more accurate PCD. Therefore, the hydrophone to aperture distance was decreased by 13 mm for the PCD study in Chapter 3 (and the performance of the PCD was improved significantly). The heat exchanger used in this study was insufficient at high intensity but provided a good basis for the improved system used later. Two key findings were made in this study using foil pitting experiments with a transducer distance of 5 mm: circulation of the coupling fluid causes only a small difference in the inertial cavitation activity that impacts the skin, while increasing the coupling fluid temperature results in a significant decrease in the activity that impacts the skin. This was the

first known study in which skin permeability (quantified by measuring caffeine transport with HPLC) was increased with ultrasound while the coupling fluid was circulated and cooled, a significant contribution to the field. The time saved by not needing to use duty cycles or fluid replacement meant that a full 10 repetitions could be run for each of the transport datasets – more than most previous studies have found it feasible to run.

A.2 Materials and Methods

A.2.1 Modified Diffusion Cell

The diffusion cells used in this study were the same as those used in Chapters 2 and 3. The donor chambers had outer diameters of 65 mm, inner diameters of 61 mm and aperture diameters of 61 mm. The receiver chambers had volumes of 3.2 mL and aperture diameters of 9 mm. The diffusion cell is shown again in Fig. A-1. The donor and receiver chambers were turned from solid polypropylene rods on a CNC lathe. The receiver chamber sampling arm and donor chamber ports were then added by gluing sections of carbon fibre tubing to the polypropylene. The donor and receiver chambers were held together with clamps 3-D printed from acrylonitrile butadiene styrene (ABS).

A.2.2 Chemicals

Caffeine (ReagentPlus) was purchased from Sigma-Aldrich (St Louis, MO, USA). Phosphate buffered saline (PBS) (pH 7.4) was purchased from Thermofisher (Waltham, MA, USA). The caffeine solution was prepared by dissolving the caffeine powder in room temperature PBS at a concentration of 0.5 % w/v (5 g/L), as in the study by Sarheed and Abdul Rasool (2011). Deionised water was taken from a Labwater L991008 Deioniser (Suez Ltd, Thame, UK).

A.2.3 Porcine Skin

Porcine ears were obtained from Ashburton Meat Processors Ltd (Ashburton, New Zealand) immediately after slaughter. The ears were cleaned with cold tap water to remove the blood and soil. The top 1 mm of the skin was removed from each ear using a dermatome (Dermatome 50 mm, Nouvag AG, Goldach, Switzerland). The dermatomed pieces of skin were flash frozen in liquid nitrogen using the technique described by Han and Das (2013) then immediately transferred to a -20 °C freezer for storage. Prior to each set of experiments, the skin was removed from the freezer and thawed in a container of deionized water at room temperature. Each piece of skin was then visually assessed for uniform thickness and integrity before being mounted in a diffusion cell.

Fig. A-1 Diffusion cell (top) plan view, (middle) front view, and (bottom) isometric view

A.2.4 Ultrasound Generation and Intensity

A low-frequency (20 kHz) ultrasound field was generated using a VC 505 ultrasound processor (Sonics and Materials Inc., Connecticut, USA). This unit was operated with a 13 mm diameter replaceable tip. An application time of 10 minutes was used for all of the skin sonoporation experiments in this study. The transducer face was positioned 5 mm from the surface of the skin as this was the smallest distance that allowed for a confocal hydrophone (shown in Fig. A-3). The ultrasound intensities (23.8 W/cm^2, 34.2 W/cm^2, and 39.4 W/cm^2) were determined with the commonly used calorimetric method (Merino, et al. 2003,

Mitragotri, et al. 2000a, Mitragotri, et al. 2000b, Morimoto, et al. 2005, Mutoh, et al. 2003, Terahara, et al. 2002a). This method is described in (Robertson and Becker 2018). Following the manufacturer's instruction, compressed air was circulated through the ultrasonic processor to keep it cool during ultrasound application.

A.2.5 Ultrasound Pressure Measurement

Throughout this thesis, the ultrasound field strength is reported as an intensity, measured with calorimetry. Alternatively, the field strength can also be reported as a pressure (Mitragotri, et al. 1996, Park, et al. 2007, Smith, et al. 2003, Tezel, et al. 2001, Zorec, et al. 2015). To measure pressure, a hydrophone was positioned a set distance from the ultrasound transducer and pointed directly at the transducer face. Both the transducer and hydrophone were situated in a water bath. The water bath was 794 mm long, 396 mm wide, and 362 mm high. The walls of the water bath were made from 12 mm thick acrylic sheets. The interior walls of the water bath were lined with acoustically absorbent panels (SA-J35, Hangzhou Applied Acoustic Institute, Hangzhou, Zhejiang, China). These panels have been shown to decrease low-frequency ultrasound reflection by 20 dB (Jelenc, et al. 2012). The RMS voltage signal from the hydrophone was then converted to a pressure using a sensitivity provided by the manufacturer. The pressure measurement technique is effective when no cavitation is present in the ultrasound field. However, when cavitation is present, the ultrasound energy moves to a broader spectrum, away from the driving frequency which is being measured (Liu, et al. 1998). This leads to an inaccurate pressure measurement. To demonstrate this inaccuracy, the hydrophone output was measured for a range of tip displacements used throughout this thesis. The needle hydrophone was positioned 40 mm from the transducer (Fig. A-2). This distance was necessary to prevent cavitation damage to the sensitive

hydrophone tip. The hydrophone voltage signal was measured for 2.5 ms. An RMS voltage was then calculated over this 2.5 ms. Ten RMS values were measured for transducer displacements of 20 %, 30 %, 40 %, 50 %, and 60 %. These RMS voltages were converted to RMS pressure values.

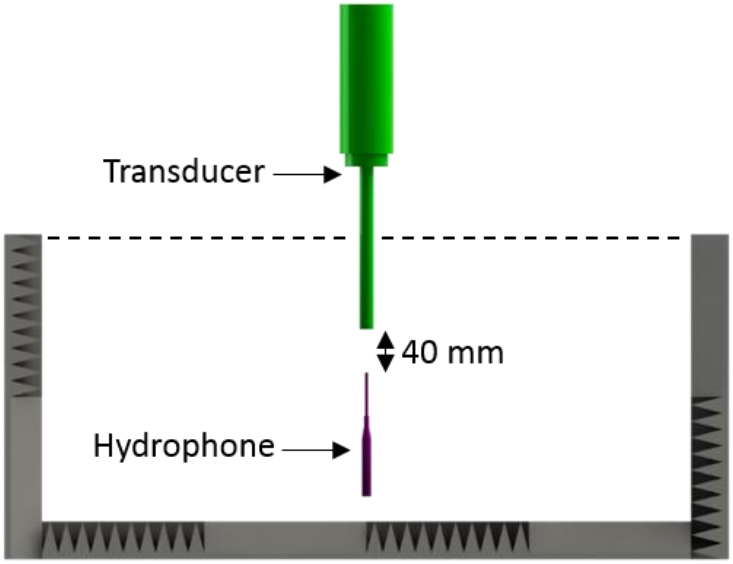

Fig. A-2 Cross-section of the ultrasound pressure measurement setup in a water bath lined with acoustically absorbent SA-J35 panels. The dotted line depicts the water line. The hydrophone and transducer were concentrically aligned. Their active tips were separated by 40 mm. The acrylic tank walls are not shown.

A.2.6 Temperature Measurement and Control

The temperature of the coupling fluid was measured with a thermocouple (Wire Type K thermocouple, Jaycar Electronics Pty Ltd, Auckland, New Zealand). The thermocouple was not positioned within the beam of the transducer, where it would have best represented the temperature of the coupling fluid near the skin surface, as this would have partially obscured the skin surface, and resulted in cavitation damage to the thermocouple tip. Instead the thermocouple was positioned outside of the transducer beam (Fig. A-3). The difference in the temperatures recorded in these two positions was found to be less than 1.5 °C during

sonoporation at 39.4 W/cm^2. The readings from the thermocouple were passed (Fig. A-4) to a NI-9211 DAQ module (National Instruments Ltd., Texas, USA) then on to a PC for processing in LabVIEW (National Instruments Ltd., Texas, USA). The thermocouple sampling frequency was 1 Hz. The accuracy and precision of the thermocouple was checked against a calibrated thermometer (3040 Precision Thermometer with Immersion Probe, Prema Semiconductor, Mainz, Germany). Three beakers were filled with water at either 16 °C, 29 °C, or 43 °C (as measured by the thermometer). Three measurements of these temperatures were then taken with the thermometer in quick succession. The thermocouple temperature reading differed from the thermometer reading by a maximum of 1 °C over this temperature range. Note that this process was repeated, with the same result, for two other thermocouples that were used for experiments in other parts of this thesis.

Continuous application of ultrasound at the intensities used in this study results in significant increases in coupling fluid temperature. A circulating, thermoelectric system, described in Section 4.3.2, was used to mitigate this temperature increase during skin sonoporation. Between experimental repetitions, the silicon tubing was removed from the donor chamber ports of one diffusion cell and connected to the next diffusion cell.

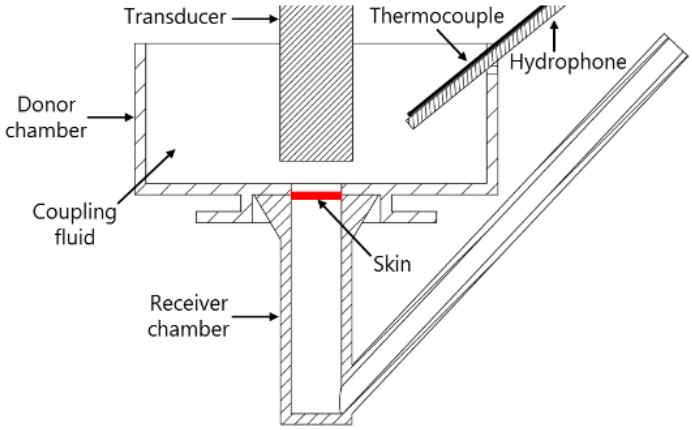

Fig. A-3 Cross section of the diffusion cell showing the positioning of the transducer, hydrophone, and thermocouple.

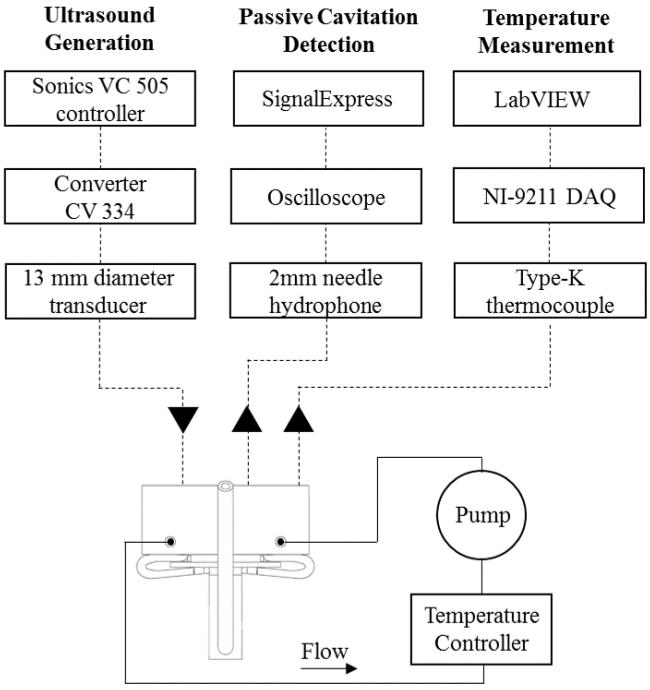

Fig. A-4 System schematic. The solid lines represent the coupling fluid circuit. The dashed lines represent the signal inputs and outputs to and from the instruments in the coupling fluid.

A.2.7 Passive Cavitation Detection

The PCD hydrophone was positioned in the coupling fluid so that it was confocal with the ultrasound transducer (Fig. A-3). This needle hydrophone (2.0 mm Needle Hydrophone,

Precision Acoustics Ltd, Dorchester, Dorset, UK) had a sensitivity of -236.4 dBre1V/µPa at the transducer driving frequency. Note that the full list of calibrated sensitivity values, measured by Neptune Sonar Ltd (East Yorkshire, UK), for frequencies between 5 kHz and 1000 kHz are shown in Appendix C. The position of the hydrophone was kept consistent over all of the experimental repetitions by using an aluminium sleeve that was fixed relative to the transducer and diffusion cell. A support structure for the transducer, diffusion cell, and hydrophone was built to make the removal of one diffusion cell and reinsertion of another as simple and repeatable as possible. This support structure (shown in Fig. A-5) was constructed from aluminium, laser cut acrylic and 3D printed ABS components. The support structure was fixed in position on top of the water bath used for the experiments in Chapter 4 (Fig. A-6).

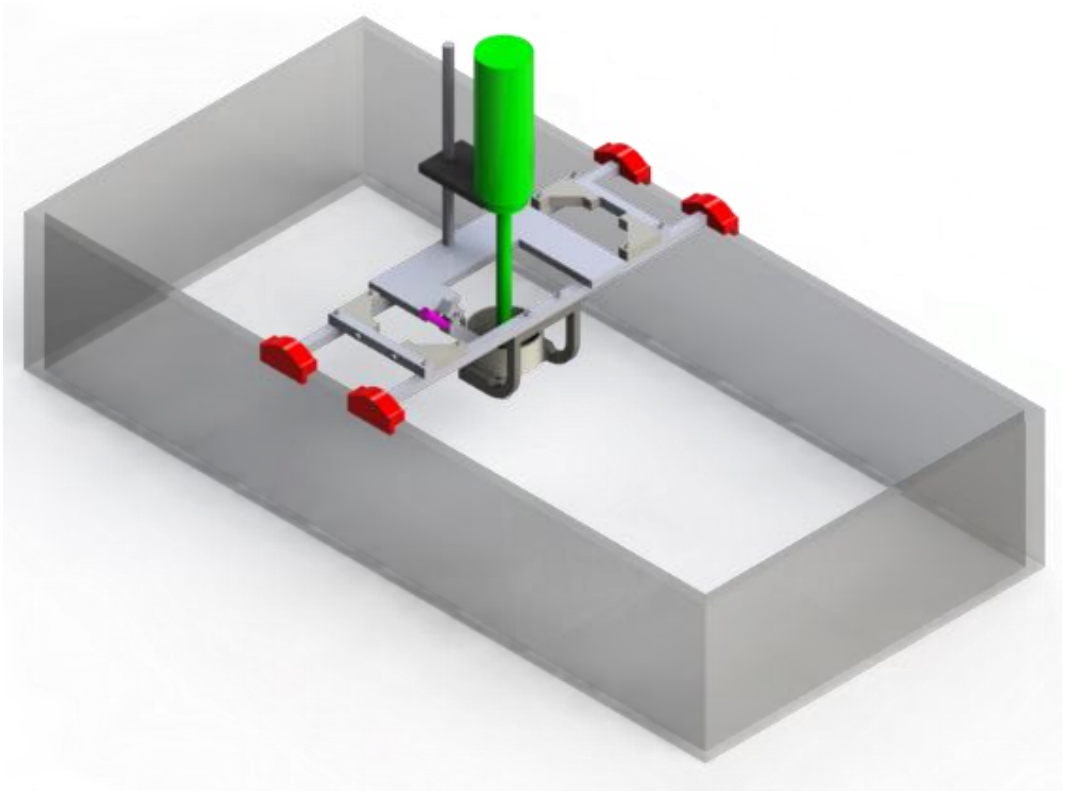

Fig. A-5 Overview of the experimental setup. The transducer is shown in green. The Hydrophone is shown in pink. The frame that holds the transducer, hydrophone and diffusion cell is supported by the walls of a Perspex tank. The 3D printed frame feet (shown in red) held the frame in position on the tank.

Fig. A-6 Image of the entire experimental setup including the tank, diffusion cell support assembly, water cooler, DAQ, power supply, ultrasound driver, oscilloscope, and PC

During sonoporation, the components were positioned as in Fig. A-7. Once one sonoporation experiment (described in section A.2.8) was completed, the transducer was removed from the donor chamber by sliding it up the clamp stand to the position shown in Fig. A-8. The hydrophone was then slid upwards out of the aluminium sleeve (note that the thermocouple has held by a similar sleeve and was removed in the same way). With these components out of the way, the diffusion cell was then slid horizontally out of its holder (Fig. A-9). The next diffusion cell was then inserted into the holder so that the transducer and

hydrophone could be returned back to their exact sonoporation positions. An isometric view of the diffusion cell holder is shown in Fig. A-10. This holder was 3D printed from ABS (ABS P430, Stratasys Ltd, Minnesota, USA).

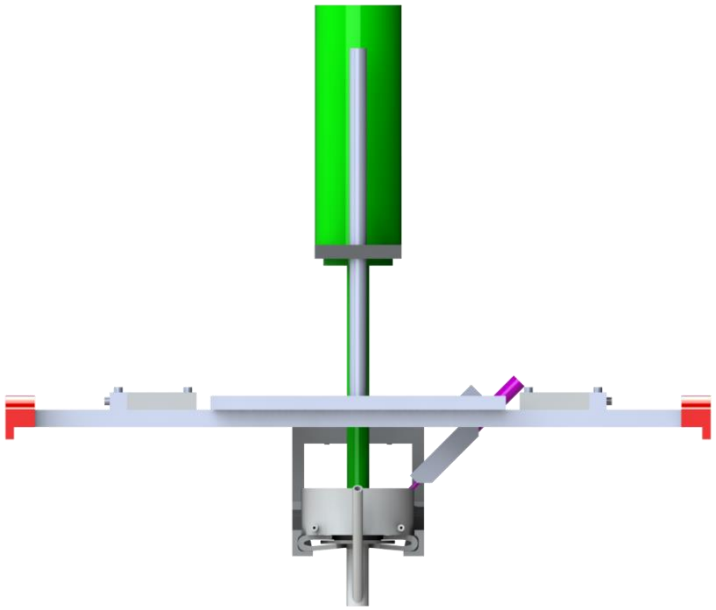

Fig. A-7 Schematic showing the hydrophone, transducer, and diffusion cell in their sonoporation positions (front view).

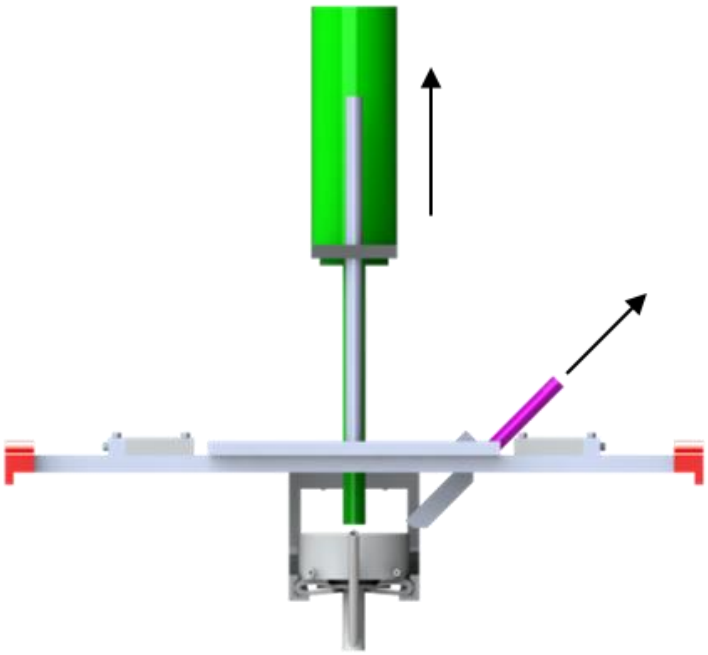

Fig. A-8 Schematic showing the hydrophone, transducer and diffusion cell in their swap positions (front view).

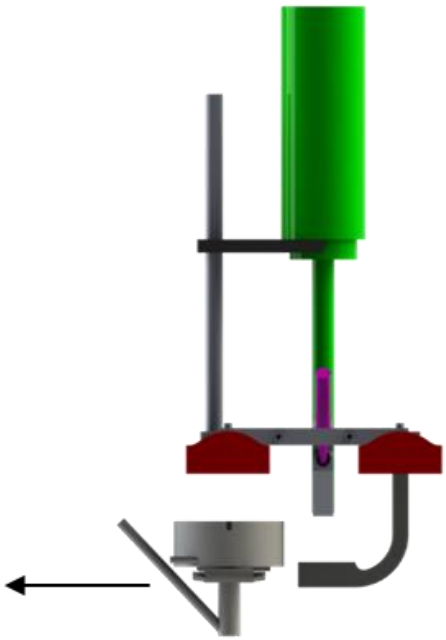

Fig. A-9 Schematic showing the removal of a diffusion cell from the experimental setup (right view).

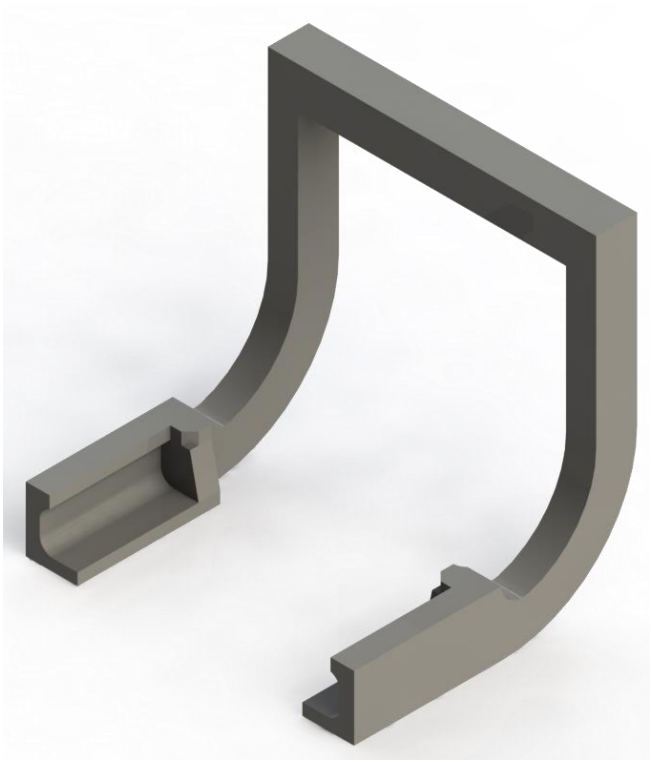

Fig. A-10 Isometric view of the 3D printed ABS diffusion cell holder

The method used to process the raw hydrophone data was described in Robertson and Becker (2018) and Section 4.3.7. Briefly, the voltage signal measured by the hydrophone was recorded with an oscilloscope (TDS 2014B, Tektronix, Beaverton, OR, USA) connected via USB to a PC running SignalExpress (NI LabVIEW SignalExpress, National Instruments, Texas, USA). The voltage data was filtered to isolate the broadband noise emission between 92.5 kHz and 97.5 kHz. An RMS value of this filtered data was calculated every 1-2 s. All of the RMS values were then integrated over the 10 minutes of ultrasound application to calculate a single ICD value for each ultrasound application. Therefore, each ICD value represents the time-averaged broadband noise emission for a specific sonoporation experiment.

A.2.8 Transdermal Transport Experiments

Prior to the ultrasound application, a piece of skin was mounted onto each of the ten diffusion cells. The receiver fluid consisted of PBS while the donor chamber fluid was deionized water. One at a time, each diffusion cell was positioned in the support structure along with the transducer, hydrophone and thermocouple. The temperature control system was then switched on to lower the coupling fluid (deionized water) to 10 °C. Continuous ultrasound was then applied for 10 minutes. During this time, the temperature control system was used to keep the coupling fluid temperature as close to 10 °C as possible. Following sonoporation of each skin sample, fresh room temperature deionized water was added to the donor chamber to keep the skin hydrated while the other skin samples were sonoporated. After all ten of the skin samples had been individually sonoporated, the deionized water was removed from each of the donor chambers and the caffeine-buffer solution was applied. This solution was allowed to diffuse for a period of 20 hours. During this time the donor chambers were covered with Parafilm (Bemis, WI, USA) to prevent evaporation of the fluid. This process

was repeated for three different ultrasound intensities (23.8, 34.2, and 39.4 W/cm^2). In addition to these experiments, two control cases were also investigated. For the first control case, the ten diffusion cells were set up in the same manner described above, however, no ultrasound was applied. The coupling fluid was simply maintained at 10 °C for ten minutes. For the second control case, no ultrasound was applied and the coupling fluid was maintained at 25 °C for ten minutes. Note that these are positive controls as opposed to true negative controls as some temperature effect may be expected. However, the term 'control' is used for the sake of simplicity. After each 20 hour diffusion period, a 2 mL sample was removed from each receiver chamber via the sampling arm.

A.2.9 Chromotography

The samples taken from the receiver chambers were pipetted into 2 mL chromatography vials (THC09150838, Thermo Fisher Scientific, MA, USA). The chromatography vials were then mounted into an HPLC system (Ultimate 3000, Thermo Fisher Scientific, MA, USA). The solid phase consisted of a Poroshell 120 column (EC-C18, DKSH NZ Ltd, Palmerston North, New Zealand). This column was maintained at 40 °C. The mobile phase consisted of 10 % acetonitrile in water. The flow rate was 0.8 mL/min. The injection volume was 1 µL. The retention time was 3.5 minutes and the reproducibility relative standard deviation was 1 %.

Each receiver fluid sample was injected into the liquid phase before passing through the column and into the UV detector. The peak corresponding to caffeine in each chromatogram was identified by its UV spectrum. The area under the caffeine peak was representative of the caffeine concentration. The software package Chromeleon (Thermo Fisher Scientific, MA, USA) was used to operate the HPLC system and to process the chromatic output. A 'blank'

consisting of Milli-Q water was run in between each caffeine sample to ensure that any caffeine residue from the proceeding sample had passed through the HPLC system. The caffeine peak areas from the chromatograms were converted to caffeine concentrations using a calibration curve. This curve was produced by measuring the peak areas (in triplicate) resulting from six different known concentrations of caffeine in PBS.

A.2.10 Physical Dosimeter Experiments

The pitting of aluminium foil under ultrasound application has previously been used to determine the influence of ultrasound parameters on inertial cavitation activity (Mitragotri, et al. 2000a). In the present study, the influence of coupling fluid circulation on the inertial cavitation activity at the skin aperture was investigated with foil pitting. Ten pieces of 0.016 mm thick aluminium foil (Homebrand, Manukau, New Zealand) were insonated (at an intensity of 34.2 W/cm^2) for 5 s with and without coupling fluid circulation. The number of pits in each of the 20 pieces of foil were then counted to quantify the influence of circulation. In these experiments, the coupling fluid in the donor chamber was deionized water at 10 °C ± 1 °C. This temperature was achieved using the circulation system.

Aluminium foil was also used to investigate the influence of coupling fluid temperature on the inertial cavitation activity at the skin aperture. Ten pieces of aluminium foil were insonated for 5 s at coupling fluid temperatures of 10 °C, 25 °C, and 40 °C. The coupling fluid circulation system was used to achieve these temperatures but was then switched off so that no circulation occurred during ultrasound application.

The length of time that a piece of foil is submerged in water prior to ultrasound application can affect the prevalence of air bubbles (nucleation sites) on the surface of the foil. Prior to each ultrasound application, the foil was submerged in the coupling fluid while the circulation system brought the coupling fluid to the specified temperature. The time required to achieve this temperature was consistent across each foil pitting dataset. Therefore, the effect of the submergence, on the prevalence of nucleation sites on the foil surface, was also consistent.

When counting the foil pits, any circular indent was counted as one pit. Two partially overlapping circular indents were counted as two pits. The duration of ultrasound exposure was short enough to avoid complete perforation of the foil, which would have made it impossible to quantify the number of individual pits.

A.3 Results

A.3.1 Measuring Ultrasound Pressure

Hydrophone measurements were conducted to determine the influence of increasing transducer tip displacement on the measured pressure in a cavitating ultrasound field. The hydrophone was positioned in front of the transducer, which was operated at tip displacements of 20 %, 30 %, 40 %, 50 %, and 60 %. The RMS hydrophone voltage was converted to an RMS pressure. The mean RMS pressure was highest at a tip displacement of 20 % (1166 kPa). The mean value then decreased with increasing tip displacement (Fig. A-11). The mean RMS value at a tip displacement of 30 % was 1047 kPa, a 10 % decrease (p<0.05). At 40 %, the mean value was 954 kPa, at 50 % it was 911 kPa, and at 60 % it was 906 kPa.

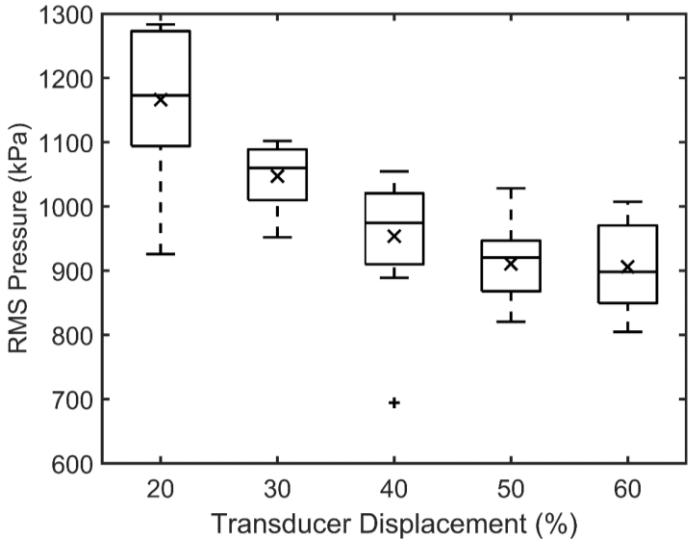

Fig. A-11 RMS pressure as a function of transducer tip displacement. The crosses within the boxes represent the mean values (n=10).

A.3.2 Foil Pitting

Foil pitting experiments were used to determine the influence of coupling fluid circulation on the inertial cavitation activity at the skin aperture. Ten pieces of aluminium foil were exposed to ultrasound (at an intensity of 34.2 W/cm^2 and a transducer distance of 5 mm) for 5 s with and without coupling fluid circulation. The coupling fluid temperature was 10 °C ± 1 °C. Without coupling fluid circulation, the mean number of pits after ultrasound application was 28.8 and the median was 28.5 (Fig. A-12). With coupling fluid circulation, the mean number of pits was 25.3 and the median was 27. Therefore, circulation of the coupling fluid caused a 12 *%* decrease in the mean and a 5 *%* decrease in the median (p=0.40).

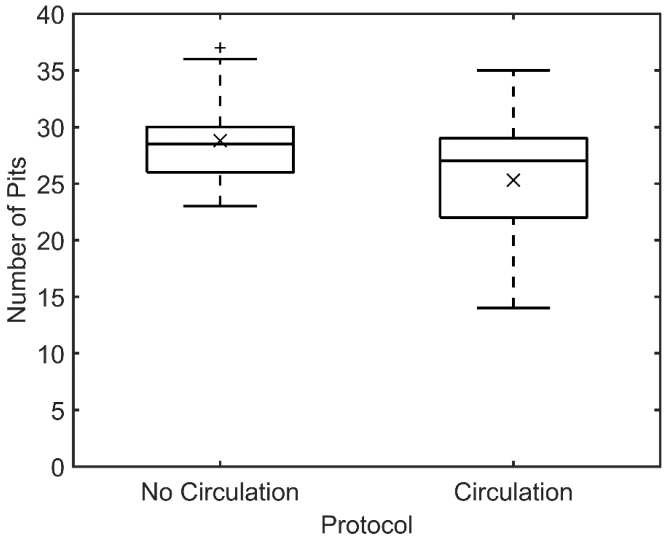

Fig. A-12 The influence of coupling fluid circulation on the pitting of aluminium foil. Ultrasound was applied for 5 s at an intensity 34.2 W/cm^2. The transducer to skin distance was 5 mm. The crosses within the boxes represent the mean values (n=10).

Foil pitting experiments were also used to investigate the influence of coupling fluid temperature on the inertial cavitation activity that occurs at the skin aperture. Ten pieces of aluminium foil were exposed to ultrasound for 5 s at coupling fluid temperatures of 10 °C, 25 °C, and 40 °C. The mean and median number of pits following ultrasound application at 10 °C were 23.4 and 24.5 respectively. At 25 °C the mean and median were both 10.0. At 40 °C the mean and median were both 3.5. Therefore, an increase in coupling fluid temperature from 10 °C to 25 °C resulted in a 57 *%* decrease in the mean number of pits (p<0.05), while an increase from 25 °C to 40 °C resulted in a further 65 *%* decrease (p<0.05).

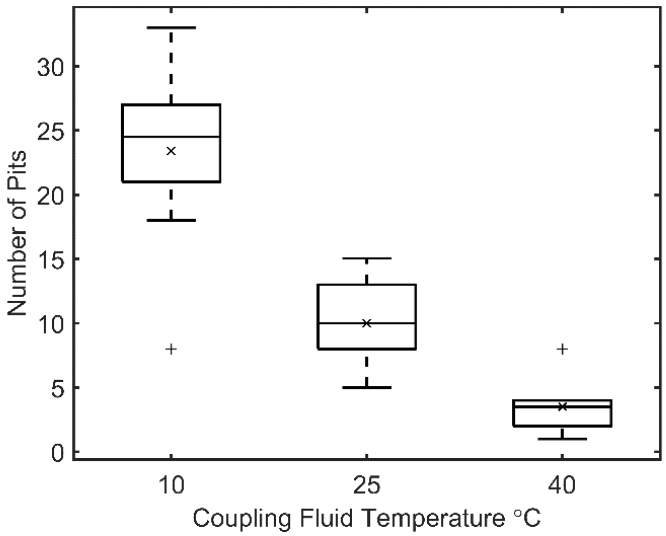

Fig. A-13 The influence of coupling fluid temperature on the pitting of aluminium foil. The crosses within the boxes represent the mean values (n=10).

A.3.3 Transdermal Transport and Inertial Cavitation Dose

Skin sonoporation experiments were conducted at three different ultrasound intensities (23.8 W/m^2, 34.2 W/m^2, 39.4 W/m^2). Each skin sample was sonoporated continuously for 10 minutes (control experiments were also conducted in which no ultrasound was applied during these 10 minutes). A caffeine-buffer solution was then applied to the SC (donor side) of the skin and left to diffuse at room temperature for 20 hours. The concentration of caffeine in the receiver chambers at the end of this period was measured using HPLC. Example chromatograms for caffeine concentration measurements following control and sonoporation experiments are shown in Fig. A-14 and Fig. A-15 respectively. The concentration of caffeine in each receiver fluid sample was proportional to the area under the peak which occurred at 1.25 minutes in the chromatograms. This peak was identified from its UV spectrum which showed a distinct peak at 273 nm (Fig. A-16 and Fig. A-17), known to correspond to caffeine (Fernandez, et al. 2000, Franeta, et al. 2002, Rodrigues, et al. 2007, Vichare, et al. 2010). The caffeine peak occurred at a time of 1.25 minutes in all of the

chromatograms used in this study which means that the liquid HPLC phase passed through the solid phase consistently throughout the experiments. This consistency is important to the validity of the concentration data as it means that the condition of the HPLC column was not degraded throughout the study. Between each HPLC caffeine measurement, a 'blank' consisting of milli-Q water was run through the column to ensure that all of the caffeine from the proceeding measurement was removed. An example chromatogram for one of these 'blank' runs is shown in Fig. A-18. No peaks are apparent in this chromatogram so all of the caffeine was removed from the HPLC system between runs. This is further reinforced by analysing the UV spectrum of the 'blank' around 1.25 minutes (Fig. A-19). No UV peak is apparent at 273 nm, which again shows that all of the caffeine was removed from the HPLC system between runs. The area of the caffeine peak in each chromatogram was converted to a caffeine concentration value using a calibration curve produced for this study (Fig. A-20). This curve was produced by measuring the peak areas (in triplicate) resulting from six different known concentrations of caffeine in PBS. A linear trendline was applied to the calibration curve. This line had an R^2 value of 0.99. Using this trendline, the caffeine concentration C_{CAF} (mg/L) could be found with the equation

$$C_{CAF} = 17.6(\mathrm{A}_C) \tag{A.1}$$

where A_C is the peak area in the chromatogram (mAU-s).

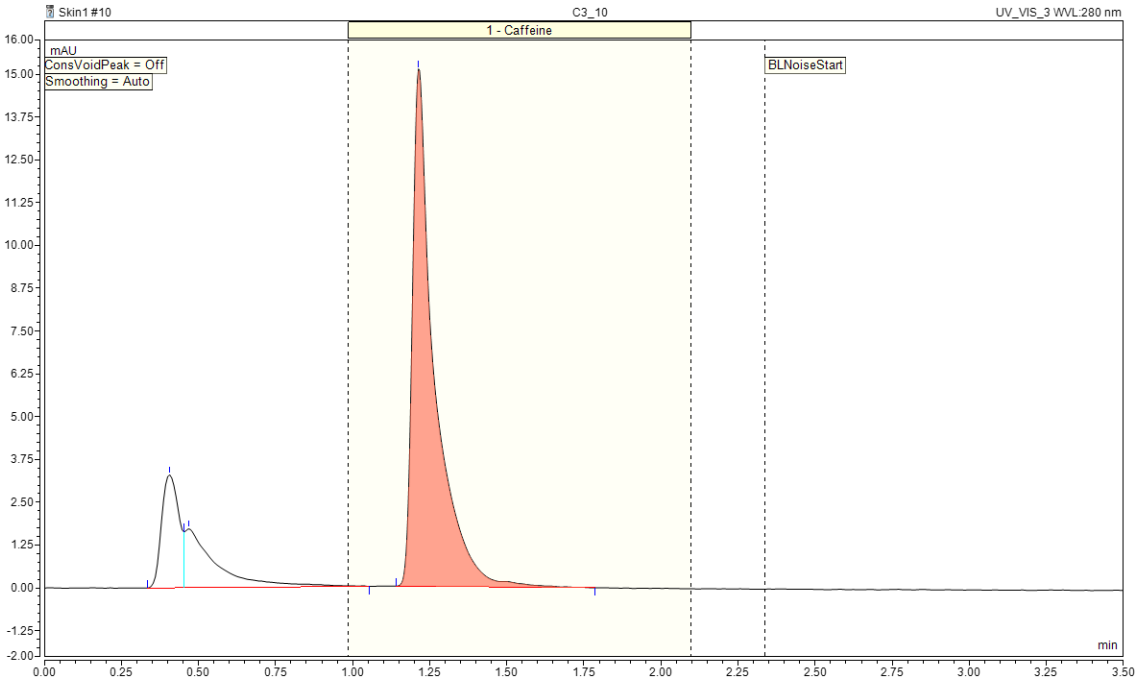

Fig. A-14 Example chromatogram for a receiver fluid sample following control at 10 °C

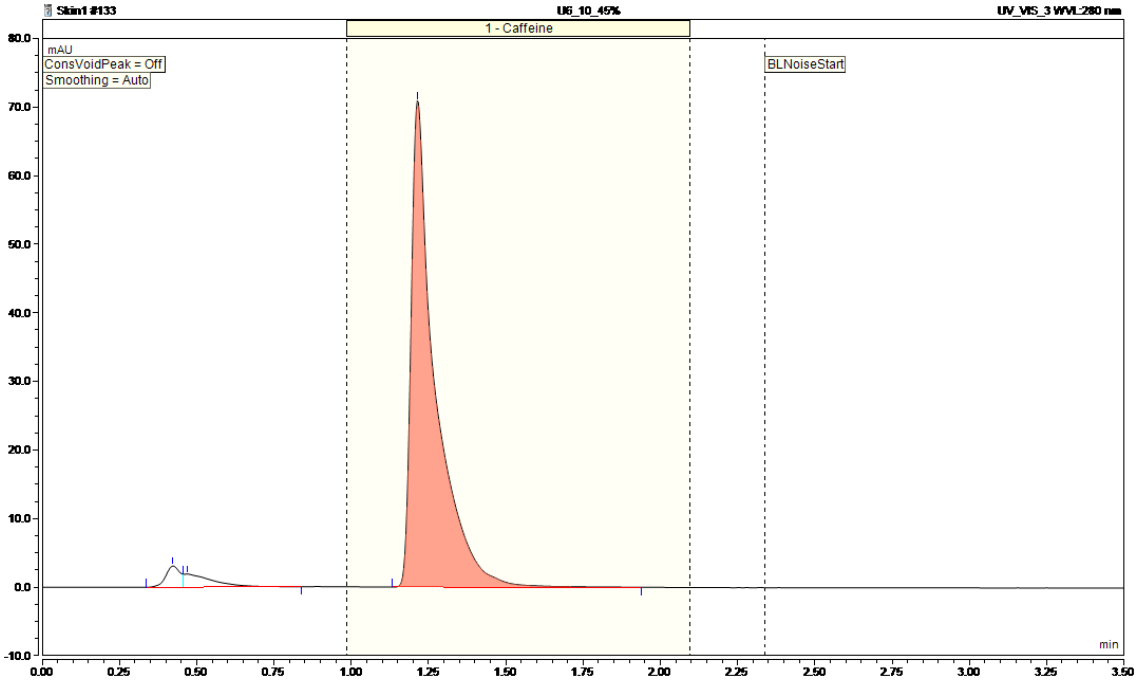

Fig. A-15 Example chromatogram for a receiver chamber fluid sample following sonoporation at 39 W/cm²

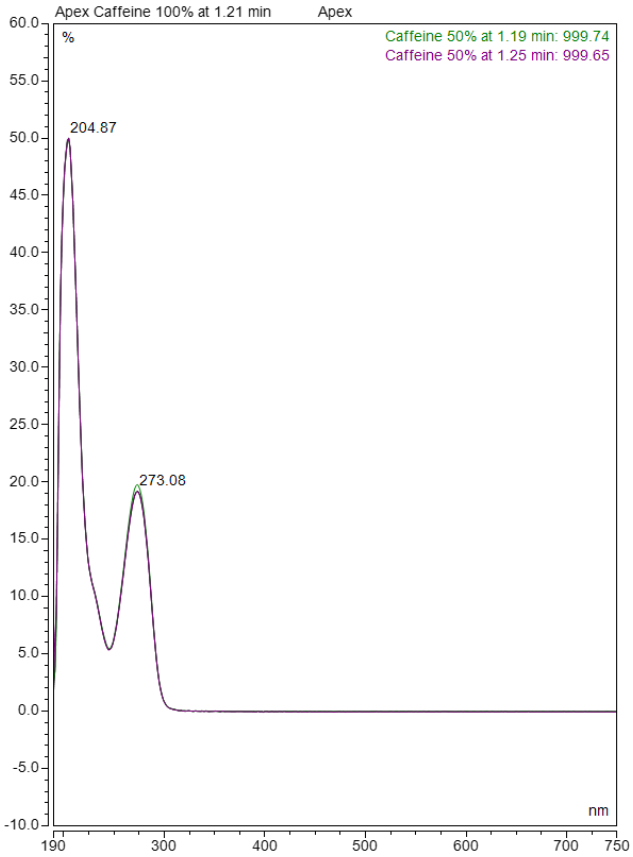

Fig. A-16 UV spectrum for the caffeine peak shown in Fig. A-14

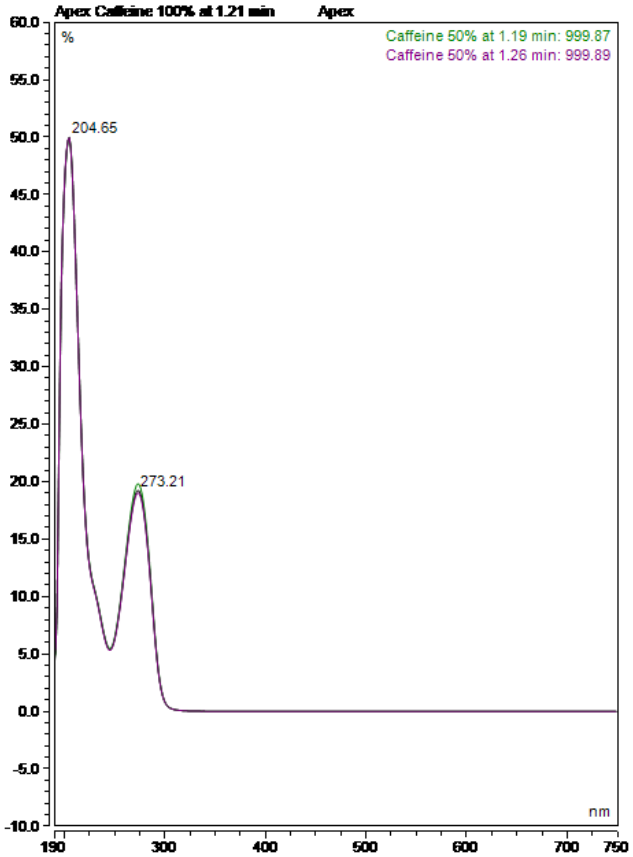

Fig. A-17 UV spectrum for the caffeine peak shown in Fig. A-15

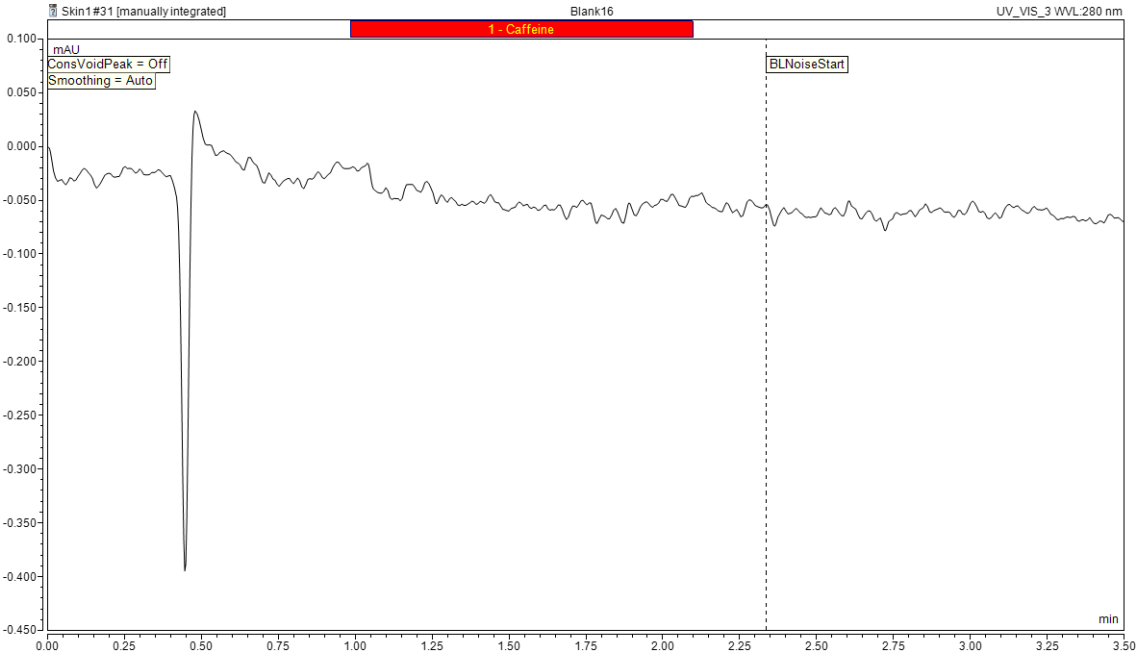

Fig. A-18 Example chromatogram for a Milli-Q water 'blank'

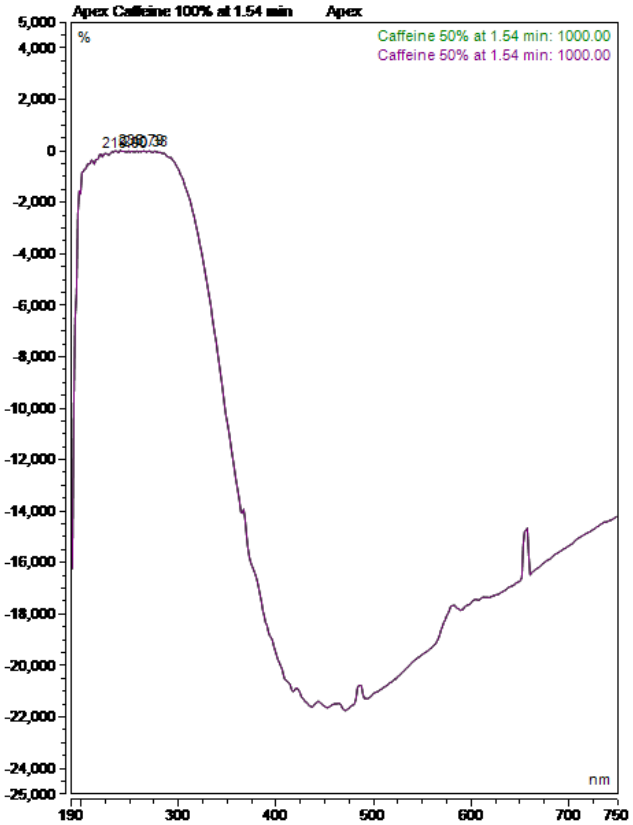

Fig. A-19 UV spectrum for the caffeine region in the Milli-Q water chromatogram shown in

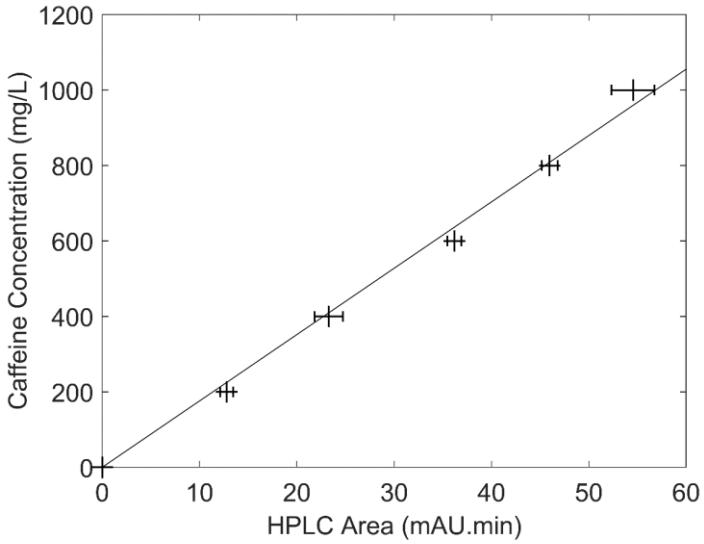

Fig. A-20 Caffeine HPLC calibration curve with an R^2 value of 0.99 (*n*=3)

The receiver chamber concentrations following the control experiments (at 10 °C and 25 °C) are shown in Fig. A-21. Following diffusion for 20 hours, the mean and median receiver caffeine concentrations for the control at 10 °C were 31.6 mg/L and 27.6 mg/L respectively. For the control at 25 °C, the mean and median receiver caffeine concentrations were 42.5 mg/L and 34.9 mg/L respectively. Therefore, an increase in coupling fluid temperature from 10 °C to 25 °C resulted in an increase in the mean receiver concentration of 26 *%* (*p*=0.4).

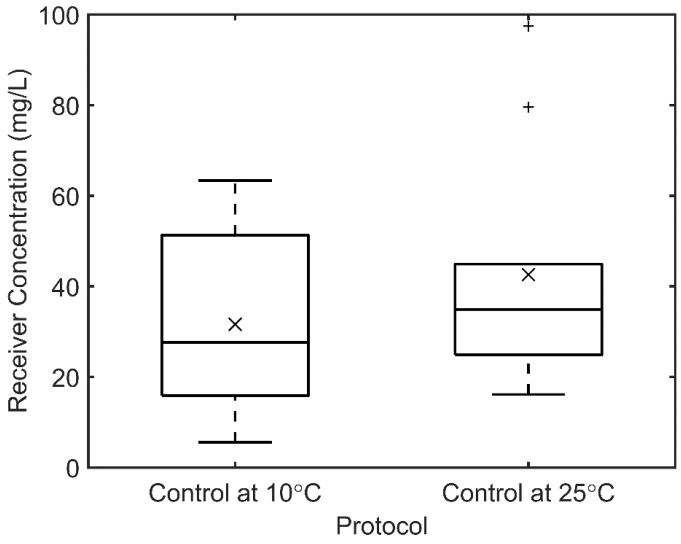

Fig. A-21 Receiver chamber caffeine concentration after 10 minutes of exposure to 10 °C or 25 °C deionized water and 20 hours of passive caffeine diffusion (n=10)

Ultrasound was applied to skin samples at three different intensities. Application at 23.8 W/cm^2 resulted in mean and median receiver caffeine concentrations of 45.9 mg/L and 15.6 mg/L respectively (shown in Fig. A-22). Application at 34.2 W/cm^2 resulted in mean and median receiver caffeine concentrations of 111.4 mg/L and 95.2 mg/L. Application at 39.4 W/cm^2 resulted in mean and median receiver caffeine concentrations of 116.6 mg/L and 108.7 mg/L. When these values are compared to those from the two control cases, it is apparent that no enhancement was achieved at an intensity of 23.8 W/cm^2 while ultrasound at 34.2 W/cm^2 and 39.4 W/cm^2 resulted in mean values that were 3.5 (p<0.05) and 3.7 (p<0.05) times the mean of the 10 °C control case. Note that these p-values were found using a Wilcoxon rank sum test as a Kolmogorov-Smirnov test rejected the null hypothesis that the data is normally distributed at the 5 % significance level in all of the data sets shown in Fig. A-21 and Fig. A-22.

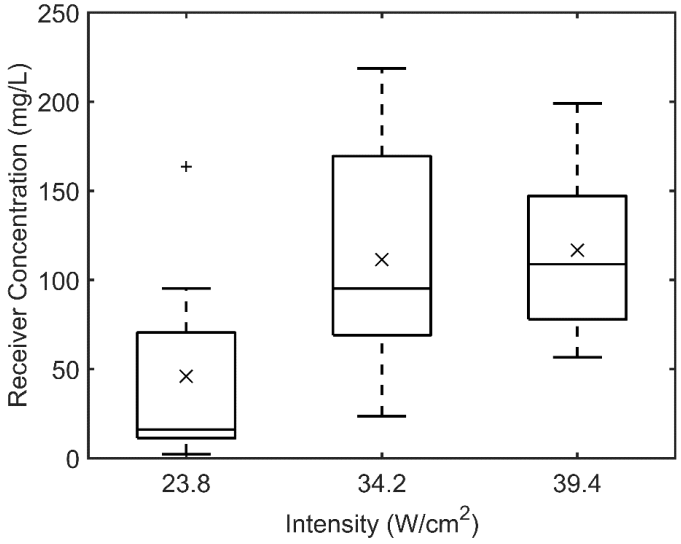

Fig. A-22 Receiver chamber concentration after 10 minutes of ultrasound exposure to various intensities. The coupling fluid temperature was maintained between 10 °C and 20 °C (n=10).

During each ultrasound exposure, a hydrophone positioned in the coupling fluid recorded the pressure variations in the ultrasound field. Examples of frequency spectra for the PCD data recorded during sonoporation at each of the three intensities are shown in Fig. A-23. The driving frequency at 20 kHz is pronounced in each of these spectra, as are various higher harmonics and ultraharmonics. The PCD hydrophone data was filtered to isolate the broadband noise between 92.5 kHz and 97.5 kHz. Examples of the broadband noise emission recorded during sonoporation at each of the three intensities is shown in Fig. A-24.

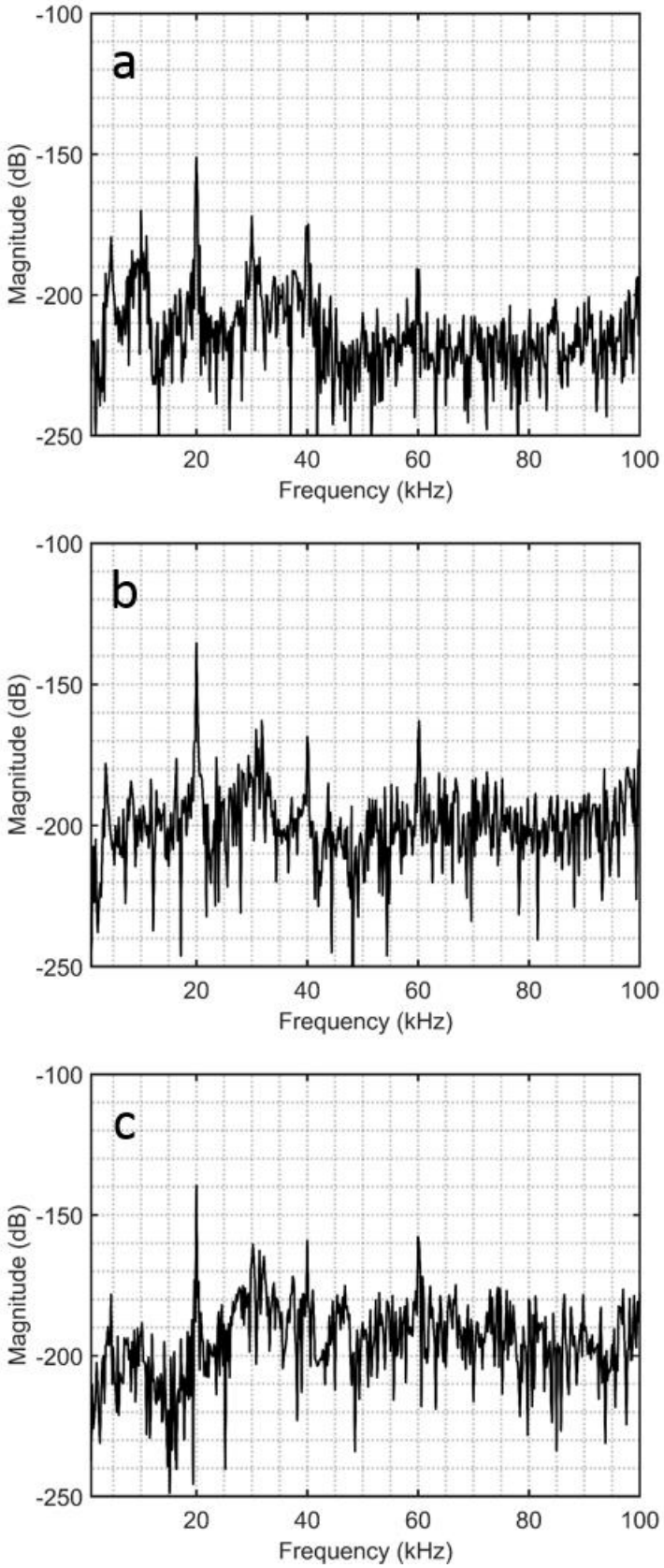

Fig. A-23 Example frequency spectra from PCD data captured during sonoporation at intensities of (a) 23.8 W/cm^2, (b) 34.2 W/cm^2, and (c) 39.4 W/cm^2

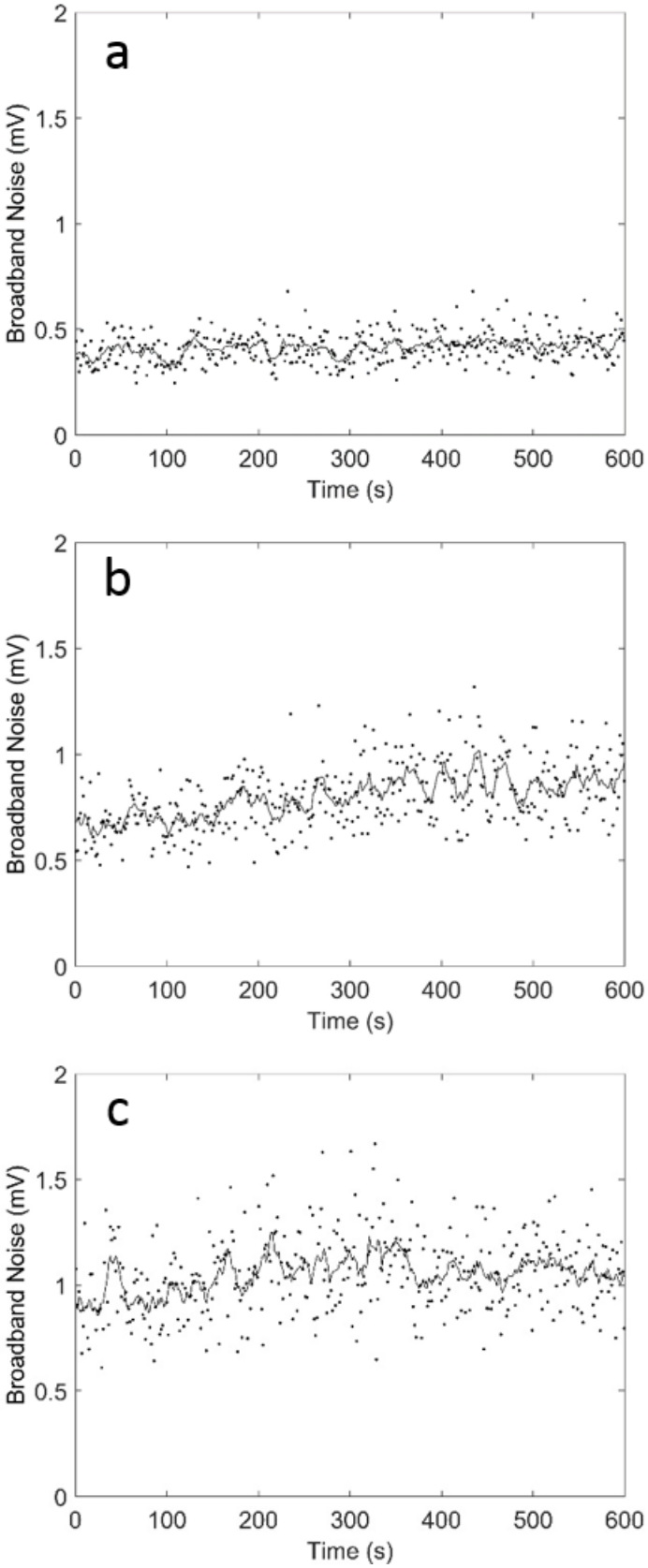

Fig. A-24 Broadband noise (92.5-97.5 kHz) as a function of time for intensities of (a) 23.8 W/cm^2, (b) 34.2 W/cm^2, and (c) 39.4 W/cm^2. A moving average of the noise is also shown to aid interpretation of the data.

The broadband noise emission was time-integrated over the 10 minutes of ultrasound application to obtain the ICD. The mean and median ICD increased with increasing intensity. Sonoporation at 23.8 W/cm^2 resulted in a mean ICD of 269 mV-s and a median of 226 mV-s (Fig. A-25). The mean value increased to 507 mV-s for an intensity of 34.2 W/cm^2. The median for this intensity was 328 mV-s. When the ultrasound intensity was 39.4 W/cm^2 the mean and median ICD values were 547 mV-s and 637 mV-s respectively.

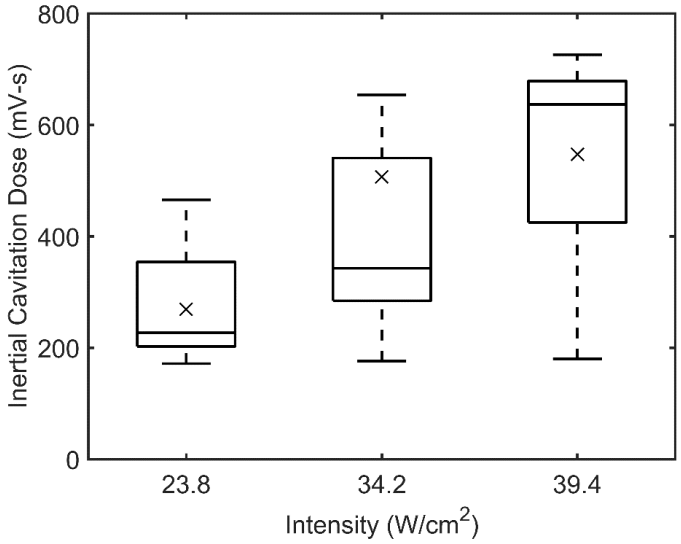

Fig. A-25 Inertial cavitation dose as a function of ultrasound intensity (n=10)

If PCD output were to be used as a real-time indicator of the likely post-sonoporation transport, there would need to be a clear correlation between ICD and receiver chamber caffeine concentration. If such a correlation could be established, then the equation describing that correlation could enable the likely post-sonoporation transport to be calculated from the real-time PCD output. To better assess the correlation between the receiver chamber caffeine concentration and the corresponding ICD values, each receiver concentration value from Fig. A-22 was plotted as a function of its ICD value from Fig. A-25.

This direct comparison is shown in Fig. A-26. The values from the 23.8 W/cm^2 dataset are represented by the 'o' symbols. The values from the 34.2 W/cm^2 dataset are represented by the 'Δ' symbols. The values from the 39.4 W/cm^2 dataset are represented by the '□' symbols. No correlation is evident in Fig. A-26: the receiver chamber caffeine concentration did not increase with increasing ICD.

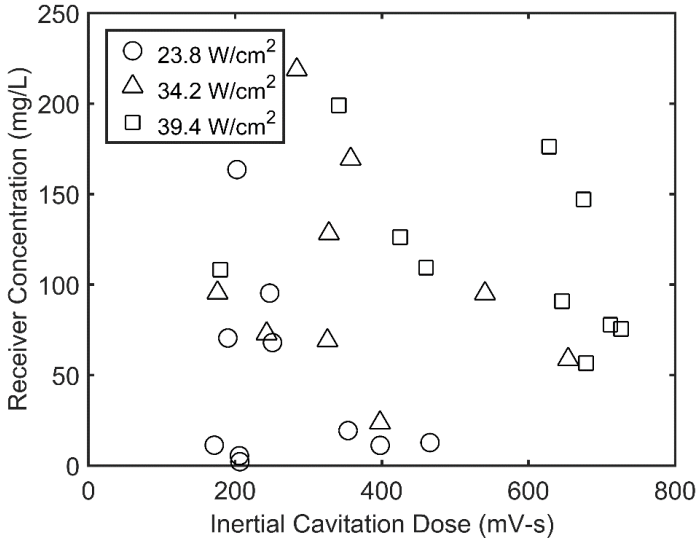

Fig. A-26 Receiver chamber caffeine concentration as a function of ICD

A.3.4 Coupling Fluid Temperature

The coupling fluid temperature was recorded during each of the sonoporation experiments. The temperature control system was supposed to maintain a constant steady state coupling fluid temperature of 10 °C ± 1 °C during sonoporation at each intensity. However, due to the insufficient power of the thermoelectric temperature controller used for this study, the coupling fluid temperature increased above 11 °C during sonoporation at 34.2 W/cm^2 and 39.4 W/cm^2 (Fig. A-27). The maximum coupling fluid temperature recorded during each sonoporation experiment is shown in Fig. A-28 as a function of ultrasound intensity. During

sonoporation at 34.2 W/cm^2, the coupling fluid temperature reached a mean maximum of 13.7 °C. During sonoporation at 39.4 W/cm^2, the coupling fluid temperature reached a mean maximum of 15.8 °C.

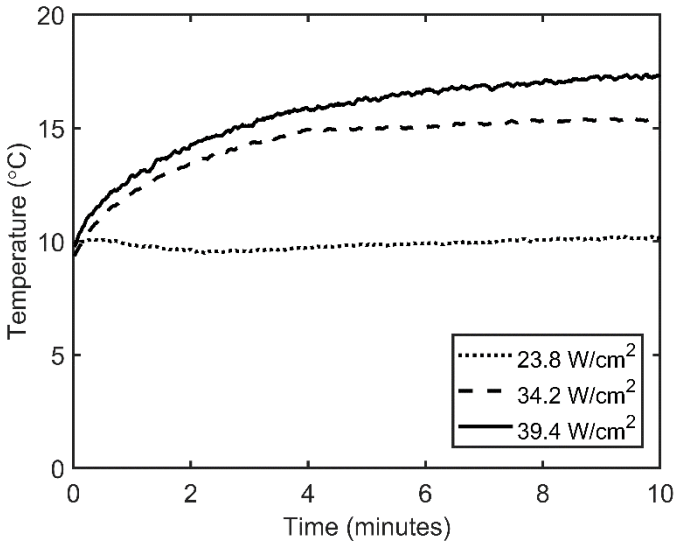

Fig. A-27 Example temperature profiles measured during sonoporation for each ultrasound intensity

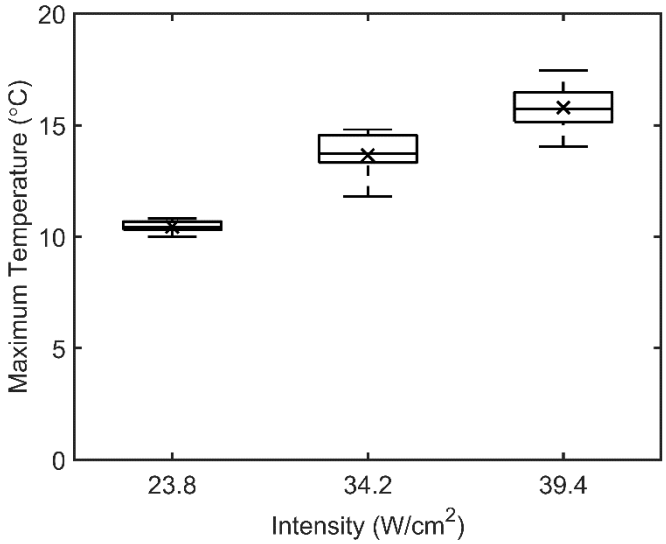

Fig. A-28 Maximum coupling fluid temperatures reached during sonoporation (n=9-10)

The coupling fluid temperature increase without coupling fluid circulation was also measured for each of the three sonoporation protocols. At the lowest intensity, the coupling fluid temperature still exceeded the 40 °C threshold (above which burns and damage are known to occur) within the 10 minutes (Fig. A-29). The maximum temperature was 44 °C. During sonoporation at 34.2 W/cm^2, the 40 °C threshold was exceeded after 5 min and 40 s. The maximum coupling fluid temperature was 55 °C. During sonoporation at 39.4 W/cm^2, the 40 °C threshold was exceeded after 4 min and 47 s. The maximum temperature was 61 °C. From this temperature data it is apparent that a time-consuming duty cycle would have been required if the circulating temperature control system was not available.

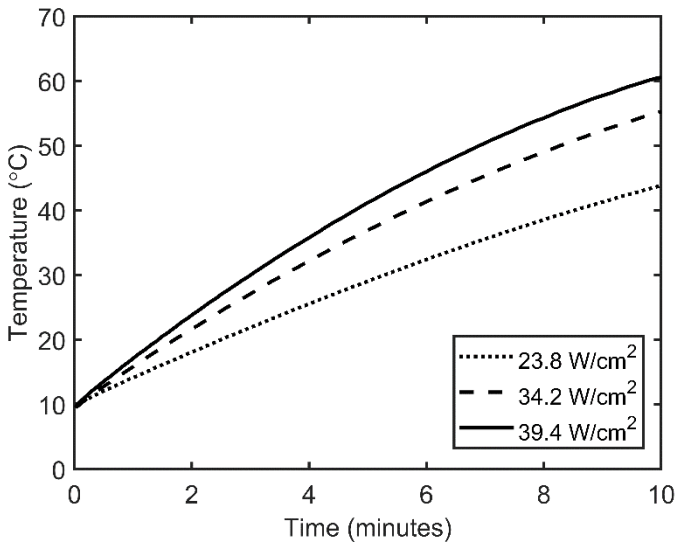

Fig. A-29 Temperature profiles measured during sonoporation with no coupling fluid circulation

A.4 Discussion

This appendix describes an initial attempt to employ both a coupling fluid temperature control system and a PCD system during sonoporation. The receiver chamber caffeine concentration following 10 minutes of sonoporation at intensities of 23.8 W/cm^2, 34.2 W/cm^2, and 39.4 W/cm^2 were measured using HPLC. The concentration values were determined from the HPLC chromatograms using a calibration curve produced for this study.

The ultrasound intensity values in this thesis were determined using a common calorimetric method. To demonstrate why this method is commonly used to quantify the ultrasound field strength, an attempt was made to use the alternative, pressure measurement method. The transducer was positioned in an acoustically lined water tank. The hydrophone was positioned below the transducer so that its tip was parallel with and directly facing the transducer tip. The distance between the transducer and hydrophone tips was kept at 40 mm to prevent cavitation damaging the sensitive piezoelectric hydrophone tip. The transducer was operated at tip displacements from 20 % to 60 %. The pressure value calculated from the hydrophone voltage output decreased consistently over this tip displacement range (Fig. A-11) – the mean calculated pressure at a tip displacement of 60 % was only 78 % of that at a tip displacement of 20 %. This decrease in calculated pressure with increasing tip displacement occurred as a result of increasing inertial cavitation activity: cavitation shifts the acoustic energy to frequencies other than the 20 kHz transducer frequency (Liu, et al. 1998). Increasing the tip displacement increased the inertial cavitation activity between the transducer and hydrophone which shifted the acoustic energy further away from the driving frequency, decreasing the measured incident pressure. This shift in acoustic energy makes

the hydrophone pressure measurement method an ineffective way to quantify the ultrasound field strength when cavitation is present.

Foil pitting, a common experimental tool in sonoporation studies, was used to investigate the influence of coupling fluid circulation on the inertial cavitation activity that occurs at the skin aperture. When the transducer was 5 mm from the aperture, circulation resulted in a 5 *%* decrease in the median number of pits after 5 s of ultrasound application at 34.2 W/cm^2 (significant at p=0.40). From this small difference in pitting it can be concluded that, when the transducer distance is 5 mm, coupling fluid circulation has only a small effect on the inertial cavitation activity which impacts the skin. This small difference is acceptable and far outweighed by the benefits of employing coupling fluid temperature control during sonoporation – namely, not needing to use duty cycles or manual fluid replacement.

Foil pitting experiments were also used to investigate the influence of coupling fluid temperature on the inertial cavitation activity that occurred at the skin aperture. For a transducer distance was 5 mm, an increase in coupling fluid temperature from 10 °C to 25 °C resulted in a 57 *%* decrease in the mean number of pits (p<0.05) after 5 s. An increase from 25 °C to 40 °C resulted in a further 65 *%* decrease in the mean number of pits (p<0.05). It is then reasonable to conclude that, for the skin sonoporation experiments in this study, the skin was exposed to less inertial cavitation activity when the coupling fluid temperature was higher.

The influence of coupling fluid temperature on inertial cavitation further reinforces the need for a temperature control system that can be used during skin sonoporation. A

thermoelectric coupling fluid temperature control system (Section 4.3.2) was employed in an attempt to maintain a steady state temperature of 10 °C ± 1 °C during sonoporation at 23.8 W/cm^2, 34.2 W/cm^2, and 39.4 W/cm^2. During sonoporation at 23.8 W/cm^2, the thermoelectric system was able to maintain the temperature within the desired range. However, when the intensity was increased to 34.2 W/cm^2 and 39.4 W/cm^2, the thermoelectric system could not provide the necessary cooling power and the temperature increased to mean maximum values of 13.7 °C and 15.8 °C after 10 minutes. This insufficient temperature control led to the development of the improved cooling system which was used for the sonoporation experiments in Chapters 2 and 3, and Appendix B. This improved system was described in Section (2.3.5). Relative to the system used in this study, the improved system had more cooling power and more consistent cooling power (the Peltier plates used in the present study had a tendency to lose power over time).

Without circulation and cooling, the coupling fluid exceeded the safe 40 °C threshold within 10 minutes, regardless of the intensity (Fig. A-29). So although the thermoelectric system was not always able to maintain a constant coupling fluid temperature in the present study, it was still a significant improvement over a system without cooling – duty cycles or fluid replacement were not required. The time saved by not needing to use duty cycles or fluid replacement made it relatively easy to run 10 repetitions for each of the five caffeine transport datasets. A shortcoming of some previous *in vitro* skin sonoporation and sonophoresis studies has been the low number of repetitions within each dataset. The study by Terahara, et al. (2002a) reports an investigation into the influence of ultrasound pre-treatment time on the enhancement of mannitol transport. For each of the four pre-treatments times, only three repetitions were conducted. If that study had not had to use a

50 % duty cycle and fluid replacement to keep the temperature below 40 °C, the time saved could have been used to run a greater number of repetitions. Similarly, in the sonoporation study by Herwadkar, et al. (2012), each transport dataset consisted of only around three repetitions. Again, if a 50 % duty cycle had not been used then a greater number of repetitions could have been completed in the same amount of time. Likewise, in the sonophoresis study by (Mitragotri, et al. 1996), only three repetitions were used to determine the transdermal transport of Salicylic acid as a function of application time over five hours. If a coupling fluid cooling system had have been used, instead of a 10 % duty cycle and fluid replacement, then the length of each experiment could have been reduced and a greater number of repetitions could have been completed within the same timeframe. Sonoporation and sonophoresis datasets with $n \leq 4$ were also reported in several other studies in the literature (Boucaud, et al. 2002, Kushner, et al. 2004, Morimoto, et al. 2005, Rangsimawong, et al. 2018, Ueda, et al. 2009). As mentioned in Chapter 2, future studies should employ one of the temperature control systems introduced in this thesis to reduce the time required for each experiment. This saved time could then be put to better use by producing more repetitions, which would enable more reliable conclusions to be drawn from each dataset.

Due to the higher coupling fluid temperatures reached during sonoporation at 34.2 W/cm^2, and 39.4 W/cm^2 in the present study, control experiments were run at both 10 °C and 25 °C to determine the influence of increased coupling fluid temperature on the receiver chamber caffeine concentration. An increase from 10 °C to 25 °C resulted in only a 1.3-fold increase in the mean receiver concentration (significant at p=0.4). Therefore, it can be assumed that the far smaller increases of 3 °C to 6 °C that occurred during sonoporation at 34.2 W/cm^2 and

39.4 W/cm^2 had negligible influences on the post-sonoporation receiver chamber caffeine concentration.

Sonoporation at 23.8 W/cm^2 had no discernible influence on receiver chamber caffeine concentration relative to the control cases. However, when the intensity was increased to 34.2 W/cm^2, the mean receiver chamber caffeine concentration after 20 hours of diffusion increased to 3.5 times that of the 10 °C control case (p<0.05). A further increase in intensity to 39.4 W/cm^2 resulted in a mean receiver concentration that was 3.7 times that of the 10 °C control case (p<0.05). These increases in receiver concentration can be attributed to the increase in skin permeability enhancement known to occur with increasing sonoporation intensity (Terahara, et al. 2002a). This increase in permeability enhancement with increasing intensity is caused by an associated increase in inertial cavitation activity (Tang, et al. 2002a), the main mechanism behind sonoporation (Tezel, et al. 2002).

The ultrasound-induced increases in transdermal transport achieved in the present study are comparable to those of the most similar study in the literature – Sarheed and Abdul Rasool (2011). That study also applied continuous ultrasound to porcine skin for 10 minutes, with a transducer to skin distance of 5 mm, then allowed a caffeine solution to diffuse for 24 hours (similar to the 20 hours in the present study). However, they used a lower intensity (3.7 W/cm^2), a smaller transducer tip (3 mm), and lacked sufficient coupling fluid temperature control. With that setup and those protocols, Sarheed and Abdul Rasool (2011) achieved a 1.5-fold mean caffeine transport enhancement relative to a passive permeation case. Therefore, the results of the present study are comparable. The caffeine transport enhancements achieved with intensities of 34.2 W/cm^2 and 39.4 W/cm^2 in the present study

were, respectively, 2.3 and 2.5 times that achieved by Sarheed and Abdul Rasool (2011). These greater enhancements are reasonable given the aforementioned positive relationship between intensity and post-sonoporation transport.

In the present study, the inertial cavitation activity was monitored during sonoporation with a PCD. A hydrophone, positioned in the coupling fluid, responded to the pressure fluctuations that occurred in the ultrasound field. The hydrophone output was filtered to isolate the broadband noise (known to be indicative of inertial cavitation activity). The broadband noise recorded over the 10 minutes of sonoporation was time integrated to produce a single ICD value for each sonoporation experiment. When the ultrasound intensity increased, the mean ICD value increased. For sonoporation at 23.8 W/cm^2, the mean value was 269 mV-s. This increased by 1.9-fold (p=0.089) to 507 mV-s at 34.2 W/cm^2. A further 1.1-fold increase (p=0.10) to 547 mV-s then occurred when the intensity was increased to 39.4 W/cm^2. Note that an outlier occurred in the 34.2 W/cm^2 ICD dataset. This outlier had a value of 1761 mV-s. This value was considered an outlier as it exceeded the upper quartile by more than 1.5 times the interquartile range (a standard outlier criteria when using box plots). This value was not represented in Fig. A-25 but was considered in the calculation of the mean and median values in the 34.2 W/cm^2 dataset. This outlier explains how a p-value of 0.10 occurred between the 34.2 W/cm^2 and 39.4 W/cm^2 datasets when the mean value only increased 1.1-fold. The increases in ICD with increasing intensity (shown in Fig. A-25) indicate that the output of the PCD system was affected by the inertial cavitation activity that occurred during sonoporation.

In the cell sonoporation study by Hallow, et al. (2006), ICD was touted as a potential unifying parameter that can be used as a real-time indicator of a desired ultrasound-induced bioeffect. If PCD output were to be used as a real-time indicator of the likely post-sonoporation transport, there would need to be a clear correlation between ICD and receiver chamber caffeine concentration. If such a correlation could be established, then the equation describing that correlation could enable the likely post-sonoporation transport to be calculated in real-time from the PCD output. The ultrasound intensity or application time could then be adjusted during sonoporation to ensure that the required ICD, and therefore, post-sonoporation transport were always achieved. In the study by Hallow, et al. (2006), a strong correlation was found between the ICD and the desired bioeffect (uptake into viable human prostate cancer cells). To better assess the correlation between the post-sonoporation transport and the corresponding ICD values in the present study, each receiver concentration value was plotted as a function of its corresponding ICD value (Fig. A-26). Despite the increase in both receiver chamber caffeine concentration and ICD with increasing intensity (Fig. A-22 and Fig. A-25), no correlation is apparent in Fig. A-26. There is no clear separation between the intensity groups and no apparent correlation within each intensity group - the PCD output could not be used as an effective real-time indicator of post-sonoporation caffeine transport in the present setup.

The poor correlation shown in Fig. A-26 indicates that the PCD system used in this study did not represent the effective inertial cavitation events that occurred during skin sonoporation. However, this may be misleading. There are several features of the methodology that may have contributed to the poor correlation between caffeine transport and ICD. There was a significant amount of variability in both the receiver chamber calcein concentration and ICD

datasets. The variability in the ICD datasets may be improved by moving the hydrophone closer to the skin aperture (as in Chapter 3) and maintaining more strict control of the coupling fluid temperature (which was shown to affect inertial cavitation activity in Fig. A-13).

Some variability in the concentration datasets was expected given the variability in other transdermal transport studies in the literature (Merino, et al. 2003, Terahara, et al. 2002a, Terahara, et al. 2002b). However, this variability could potentially be reduced by using a molecule with a larger molecular weight than caffeine. The small size of the caffeine molecules (194 g/mol) meant that any physiological variation between skin samples may have resulted in large differences in caffeine transport. Using a larger molecule, for example calcein (623 g/mol), should reduce the impact of physiological variations as its molecular weight means that it cannot diffuse in large quantities without ultrasound enhancement. Using calcein may also have the added benefit of increasing the permeability enhancement relative to the control case – the transport of larger molecules that diffuse more slowly through the skin is enhanced more by ultrasound than the transport of smaller molecules (Mitragotri, et al. 1995b).

The long caffeine residence time (20 hours) may also have contributed to the poor correlation shown in Fig. A-26. This long residence time resulted in highly hydrated skin samples. Skin hydration is known to significantly affect skin permeability (Alonso, et al. 1995, Verdier-Sévrain and Bonté 2007, Wu, et al. 2006, Zhai, et al. 2002). Therefore, reducing the residence time should decrease the effects of hydration which may isolate the effects of inertial cavitation and improve the correlation between transport and PCD output.

A.5 Conclusions

Circulation of the coupling fluid through the donor chamber (at a flow rate of 0.14 L/min) resulted in a 5 *%* decrease in the median number of pits after 5 s when the transducer was 5 mm from the aperture (significant at p=0.4). This small decrease in pitting is acceptable considering the possibility circulation provides for coupling fluid temperature control during sonoporation. Foil pitting experiments were also used to investigate the influence of coupling fluid temperature on the inertial cavitation activity that occurred at the skin aperture. An increase in coupling fluid temperature from 10 °C to 25 °C resulted in a 57 *%* decrease in the mean number of pits (p<0.05), while an increase from 25 °C to 40 °C resulted in a further 65 *%* decrease (p<0.05). It is then concluded that, for the experimental parameters used in this study, increasing the coupling fluid temperature results in a decrease in the inertial cavitation activity that impacts the skin.

This study included a first attempt at incorporating both coupling fluid temperature control and passive cavitation detection during skin sonoporation. The potential of both systems was apparent. The temperature control system was able to maintain a constant coupling fluid temperature during sonoporation at 23.8 W/cm^2, and was able to maintain safe coupling fluid temperatures at all three intensities – time consuming duty cycles and fluid replacement were not required. The PCD system was able to monitor the broadband noise emission within the coupling fluid during skin sonoporation. However, neither system functioned to the required standard. The temperature control system was unable to maintain a constant coupling fluid temperature at intensities of 34.2 W/cm^2 and 39.4 W/cm^2. No correlation between the ICD and transdermal transport values was identified despite both of these variables increasing

with increasing intensity. The poor correlation means that the PCD output could not be used as an effective real-time indicator of post-sonoporation caffeine transport in the present setup.

The shortcomings of the systems used in this study were important in informing the materials and methods used in Chapters 2 and 3. Improvements made to the temperature control system following this study resulted in a system capable of maintaining a variety of coupling fluid temperatures during sonoporation at 55 W/cm^2 (Chapter 2). Researchers intending to adopt a circulating temperature controller in their own studies should note the difference in performance of the temperature control systems used in Chapter 2 and the present study – the water bath heat exchanger used in Chapter 2 is a more powerful and consistent option than the thermoelectric heat exchanger used in the present study. Moving the hydrophone closer to the skin aperture following the present study resulted in a significant reduction in the variability of the ICD values found in Chapter 3. The lower variability indicates that, for the large diameter diffusion cell setup, the hydrophone position used in Chapter 3 (7 mm from the skin aperture) resulted in superior PCD performance relative to that used in the present study (20 mm from the skin aperture). Also, the harmonic and ultraharmonic peaks in the frequency spectra of Chapter 3 are more pronounced than those in the present study – another indicator that the closer hydrophone position in resulted in a superior PCD performance. This should be noted by any future *in vitro*, *in vivo*, or clinical skin sonoporation studies which attempt to use a PCD to monitor inertial cavitation activity – the hydrophone should be as close to the skin aperture as possible. Despite its shortcomings, this is the first known study in which transdermal transport was enhanced with sonoporation while the coupling fluid was circulated and cooled, a significant contribution to the field.

Appendix B The Influence of Transducer Distance and Application Time – Initial Calcein Study

B.1 Abstract

Following the caffeine sonoporation study reported in Appendix A, a larger permeant molecule was required for the experiments reported in Chapter 2. Preliminary experiments were attempted with Testosterone but abandoned due to its poor solubility in water. Eventually Calcein was selected as an appropriate permeant. Calcein has a molecular weight of 623 g/mol and has been used as a model drug in many transdermal transport studies in the literature (Henry, et al. 1998a, Oh, et al. 2008, Prausnitz, et al. 1993, Vanbever and Preat 1999, Xie, et al. 2005). This Chapter reports a series of sonoporation experiments with Calcein. These experiments were conducted to find a combination of experimental parameters that resulted in a significant enhancement in Calcein transport relative to a control case. It can be concluded from the results that, in a sonoporation setup with circulating coupling fluid, the post-sonoporation transport increases with increasing ultrasound application time and decreases with increasing transducer to skin distance. Of the five combinations of experimental parameters investigated in this study, that which involved an application time of 10 minutes, an intensity of 55 W/cm^2 and a transducer to skin distance of 3 mm was deemed most appropriate for use in the coupling fluid temperature study (Chapter 2). Although the present study did not directly address any of the thesis objectives, it does contain the first known example of calcein transport enhancement using continuous sonoporation with coupling fluid temperature control. This study also demonstrates the circulation system's ability of to maintain a constant coupling fluid temperature during a long

(30 minute), continuous application of ultrasound – another significant contribution to the field.

B.2 Materials and Methods

B.2.1 Modified Diffusion Cell

Modified diffusion cells were used to conduct the transdermal transport experiments. The diffusion cells were the same as those used in Chapters 2, 3, and Appendix A. A description of these cells was given in Section 2.3.1. The geometry of the cells was shown in Fig. 2-1.

B.2.2 Chemicals

The permeant solution that was applied to the skin consisted of calcein (Calcein C0875, Sigma-Aldrich, St. Louis, MO, USA) dissolved in phosphate buffered saline (PBS) (Gibco PBS pH 7.4, Thermo Fisher Scientific, Waltham, MA, USA) at a concentration of 0.1 % w/v (1 g/L). This solution was made and stored at room temperature. Deionised water was taken from a Labwater L991008 Deioniser (Suez Ltd, Thame, UK).

B.2.3 Porcine Skin

The *in vitro* skin models used in this study consisted of porcine ear skin. The ears were obtained from an abattoir (Ashburton Meat Processors Ltd, Ashburton, New Zealand) immediately after slaughter. These ears were not scalded or exposed to detergent at the abattoir. Upon arrival at the laboratory, the ears were cleaned with cold tap water. The skin was then removed from the ears using a dermatome (Dermatome 50 mm, Nouvag AG, Goldach, Switzerland) set to a thickness of 1 mm. Following the dermatome process, the

pieces of skin were individually wrapped in Parafilm (PARAFILM, Sigma-Aldrich, St. Louis, MO, USA), placed in airtight plastic containers, and then transferred to a -20 °C freezer until use.

B.2.4 Ultrasound Generation and Intensity

A low-frequency (20 kHz) ultrasound field was generated with an ultrasonic processor (VC 505 Ultrasonic Processor, Sonics and Materials Inc., Newtown, CT, USA). This processor was fitted with a 13 mm replaceable tip. Following the manufacturer's instruction, compressed air was circulated through the ultrasonic processor to keep it cool during ultrasound application. The intensity of the ultrasound field was determined using the same calorimetric approach described in Section 4.3.4. Two intensities were used in this study: a low intensity (13 W/cm^2) and a high intensity (55 W/cm^2). The low intensity was generated with a tip displacement setting of 20 %. The high intensity was generated with a tip displacement setting of 60 %.

B.2.5 Coupling Fluid Temperature Measurement and Control

The temperature measurement and control system was the same as that used in Chapters 2 and 3. Briefly, a peristaltic pump circulated the coupling fluid out of one donor chamber port, through a heat exchanger, and back into the other donor chamber port. The heat exchanger consisted of an aluminium block submerged in a water bath (FP-50 Refrigerated/Heating Circulator, Julabo GmbH., Selbach, Germany). The coupling fluid temperature tended towards the temperature of the water bath as it passed through channels milled within the aluminium block (shown in Fig. 2-9). This system ensured that the steady state coupling fluid temperature was always 12 °C ± 1 °C during sonoporation, as

measured by the thermocouple in the coupling fluid. A cross-section of the diffusion cell setup is shown again in Fig. B-1. The system schematic is shown again in Fig. B-2.

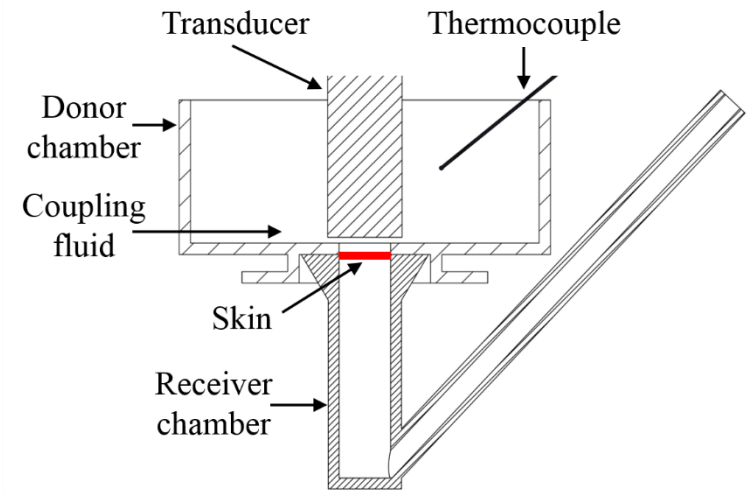

Fig. B-1 Cross-section of the diffusion cell showing the positioning of the transducer and thermocouple

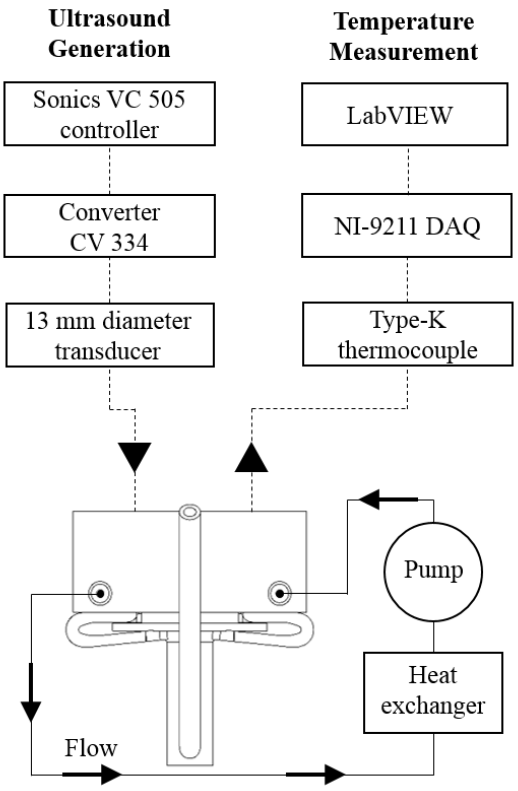

Fig. B-2 System schematic. The solid lines represent the coupling fluid circuit. The dashed lines represent the signal inputs to the transducer and the signal outputs from the thermocouple.

The location of the thermocouple (qualitatively depicted in Fig. 2-5) was chosen so that it was outside of the transducer beam and did not interfere with the ultrasound field near the skin. This position (8 mm above the bottom donor chamber wall and 7 mm from the transducer) also prevented cavitation damage to the thermocouple tip. Preliminary temperature measurements were conducted to assess the influence of the thermocouple position on the measured temperature. In these experiments, a second thermocouple was positioned directly over the skin (as shown in Fig. B-3). The steady state temperatures measured by these thermocouples were then compared.

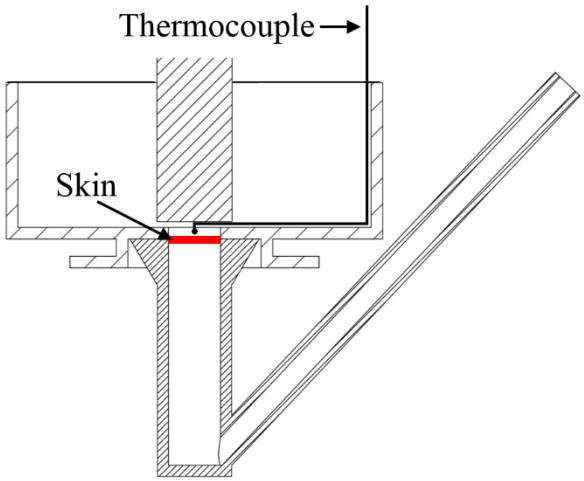

Fig. B-3 Cross-section of the diffusion cell showing the thermocouple positioned directly above the skin surface

B.2.6 Measurement of Receiver Chamber fluid Temperature

Ultrasound-induced temperature increases are a result of absorption. This absorption can occur in both the donor and receiver fluids due to the propagation of the ultrasound field throughout the diffusion cell. To measure the heat transfer to the receiver fluid, a hole was drilled in the bottom of a spare receiver chamber which was not required for the transport experiments. A thermocouple was then inserted through this hole so that its tip was positioned 2 mm below the skin surface (Fig. B-4). The hole in the bottom of the receiver chamber was then glued to prevent any leakage and to ensure that the thermocouple remained in position. The thermocouple measured the temperature during ultrasound application.

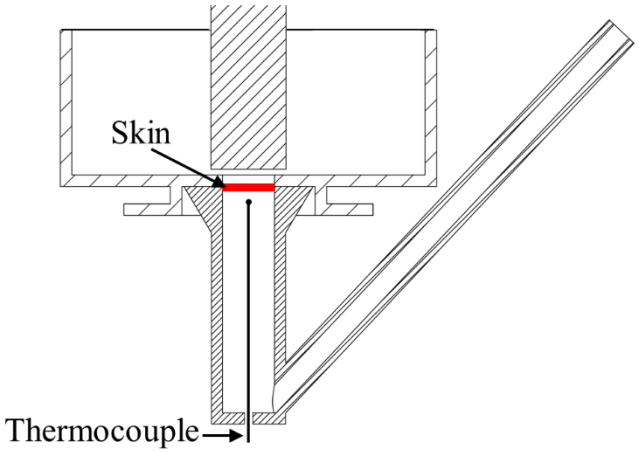

Fig. B-4 Cross-section of the diffusion cell showing the positioning of the thermocouple used to measure the receiver fluid temperature. The tip of the thermocouple was 2 mm from the bottom surface of the skin.

B.2.7 Transdermal Transport Experiments

Transdermal transport experiments were conducted to investigate the influence of intensity, ultrasound application time, and transducer to skin distance on the transport enhancement achieved with sonoporation. These experiments began with filling one of the receiver chambers with PBS. A skin sample was then taken from the freezer and visually checked for any holes or areas of non-uniform thickness through which the calcein solution could easily diffuse. Any samples that displayed such imperfections were disposed of. Once an appropriate skin sample was selected, it was clamped between the filled receiver chamber and the donor chamber. After ensuring that no air bubbles were present in the receiver chamber, the diffusion cell was mounted into the temperature regulation setup, which involved attaching the silicone tubing to the donor ports and moving the thermocouple into position. Room temperature (19 °C ± 1 °C) deionised water was then added to the donor chamber and allowed to sit for three minutes to thaw the skin. Temperature control was then initiated by switching on the circulation pump. With the temperature control system running,

the coupling fluid was circulated for 10 minutes with or without ultrasound. The temperature was constantly monitored with the thermocouple during this time to ensure it remained at 12 °C ± 1 °C. After 10 minutes of circulation, the coupling fluid was removed from the donor chamber and the diffusion cell was moved to a holding rack. A 0.5 mL volume of the calcein solution was then applied to the top of the skin so that its entire surface was submerged. This solution was then left to diffuse for one hour at room temperature (19 °C ± 1 °C). After 1 hour, a 1 mL volume was taken from the receiver chamber. Six different combinations of ultrasound parameters were used during the 10 minutes of coupling fluid circulation. These are shown in Table B-1. Seven transport experiments were conducted using each combination of ultrasound parameters. Note that each cell was washed with a surfactant cleaner (Jif, Unilever, France) in between each use to remove the calcein which had a tendency to stick to the polypropylene.

Table B-1 Combinations of experimental parameters used.

Combination	a (control)	b	c	d	e	f
Ultrasound Intensity (W/cm^2)	0	13.3	55.1	55.1	55.1	55.1
Transducer to skin distance (mm)	5	5	5	5	3	3
Ultrasound application time (min)	0	10	10	30	10	30

B.2.8 Concentration Measurements and Calibration Curve

The concentration of calcein in the receiver fluid was measured using a spectrofluorometer (Fluorolog-3, Horiba Ltd., Kyoto, Japan). The excitation and emission wavelengths were 488 nm and 513 nm respectively. These wavelengths are similar to those used in the literature (Alvarez-Román, et al. 2003, El Jastimi and Lafleur 1999, Morimoto, et al. 2005, Mueller, et al. 2004, Petronilli, et al. 1999). The software package FluorEssence (FluorEssence V3.5, Horiba

Ltd., Kyoto, Japan) was used to operate the spectrofluorometer and analyse its output. The fluorescence values read by the spectrofluorometer were converted to calcein concentrations using a calibration curve. This curve was produced by measuring (in triplicate) the fluorescent intensity of nine different known concentrations of calcein in PBS. Each sample was pipetted into a 1.2 mL quartz crystal cuvette (Starna Ltd, Essex, UK). This cuvette was cleaned with deionised water and Kimwipes (Kimtech, Kimberly-Clarke, Irving, TX, USA) between each measurement to ensure that all of the calcein was removed.

B.2.9 Foil Pitting Experiments

In the present study, aluminium foil was used as a physical dosimeter to investigate the influence of transducer to skin distance on the on the inertial cavitation activity at the skin aperture with circulating coupling fluid. Ten pieces of 0.016 mm thick aluminium foil (Homebrand, Manukau, New Zealand) were insonated (at an intensity of 55 W/cm^2) for 2 s with the transducer 3 mm, 5 mm, or 7 mm from the skin surface. The number of pits in each of the 30 pieces of foil were then counted to quantify the influence of transducer distance. In these experiments, the coupling fluid in the donor chamber was deionized water at 12 °C ± 1 °C. This temperature was achieved using the circulation system.

The length of time that a piece of foil is submerged in water prior to ultrasound application can affect the prevalence of air bubbles (nucleation sites) on the surface of the foil. Prior to each ultrasound application, the foil was submerged in the coupling fluid while the circulation system brought the coupling fluid to the specified temperature. The time required to achieve this temperature was consistent across each foil pitting dataset. Therefore, the effect of the submergence, on the prevalence of nucleation sites on the foil surface, was also consistent.

When counting the foil pits, any circular indent was counted as one pit. Two partially overlapping circular indents were counted as two pits. The duration of ultrasound exposure was short enough to avoid complete perforation of the foil, which would have made it impossible to quantify the number of individual pits.

B.3 Results

B.3.1 Calcein Calibration

A calibration curve was produced so that receiver chamber calcein concentration could be calculated from the spectrofluorometer output. Examples of spectrofluorometer outputs are shown when no calcein was present (Fig. B-5) and when calcein was present (Fig. B-6). The emission intensity value at 513 nm was proportional to the concentration of calcein in the receiver chamber. A linear trendline was applied to the calibration curve (Fig. B-7). This line had an R^2 value of 0.99. Using this calibration, the calcein concentration C_{RAW} could be found with the equation

$$C_{RAW} = 8.21\times10^{-10}(\mathrm{I}_S) + 4.04\times10^{-5} \quad \text{(B.1)}$$

where I_S is the fluorescent intensity emitted by the calcein. The maximum emission intensity of the spectrofluorometer was approximately 20 MCPS. Therefore, any samples that approached this value (in this Appendix or in Chapters 2 or 3) were diluted with PBS. This dilution was later accounted for when calculating the concentration.

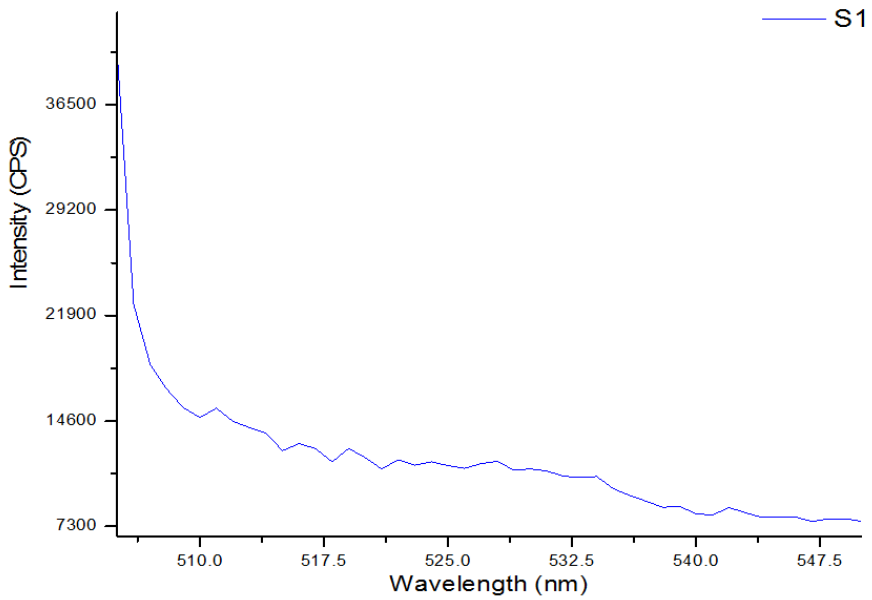

Fig. B-5 Example fluorometer output with no calcein. The excitation wavelength was 488 nm. The emission wavelength was 513 nm.

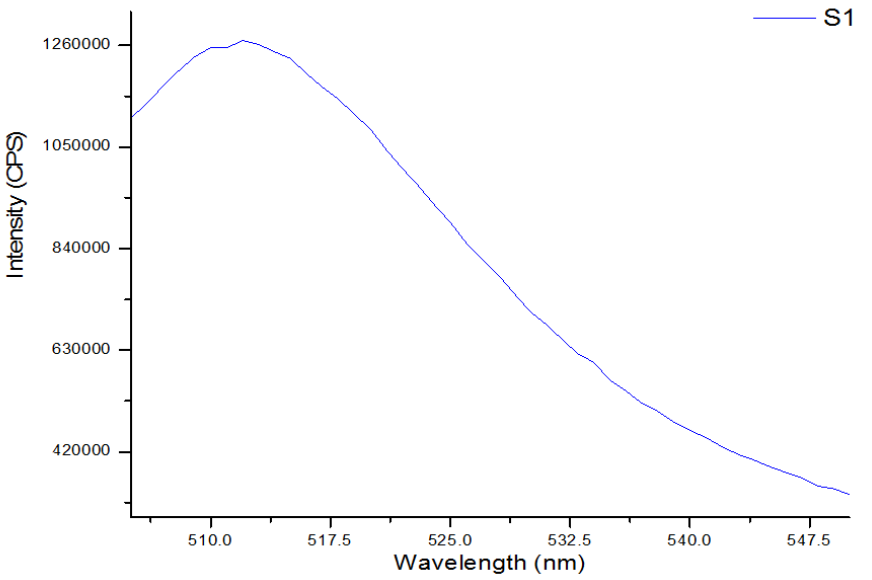

Fig. B-6 Example fluorometer output with calcein. The excitation wavelength was 488 nm. The emission wavelength was 513 nm.

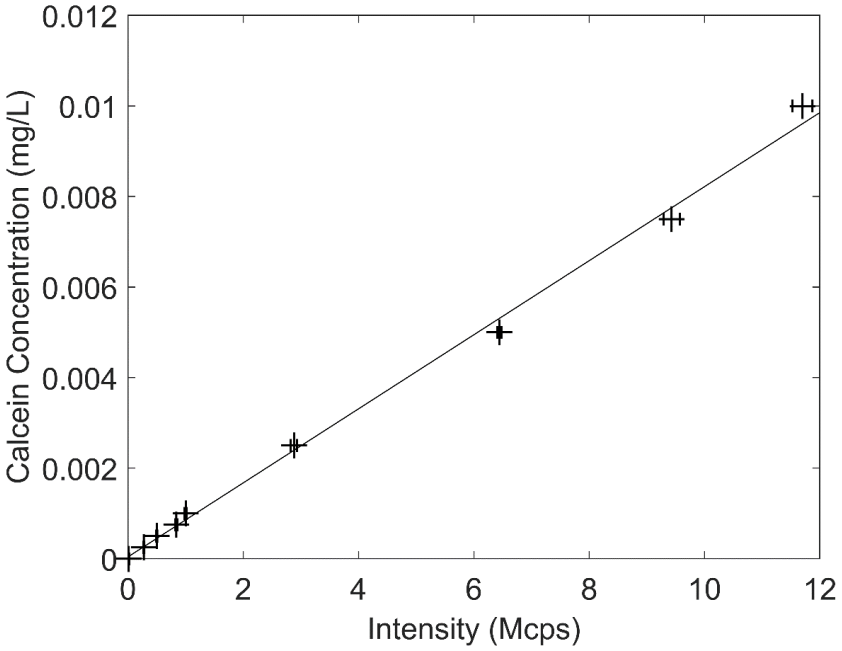

Fig. B-7 Calcein fluorometry calibration curve with an R^2 value of 0.99 (n=3)

B.3.2 Transdermal Transport

Transdermal transport experiments were conducted to find a combination of experimental parameters that resulted in a significant enhancement in Calcein transport relative to a control case (without ultrasound). With the steady state coupling fluid temperature at 12 °C ± 1 °C, skin was sonoporated under a variety of different experimental conditions (Table B-1). The calcein-buffer solution was then applied to the skin and left to diffuse at room temperature for 1 hour. The fluorescence of the receiver chamber fluid was then measured and converted to concentration using the calibration curve (Fig. B-7).

Initially, the transducer to skin distance was set to 5 mm, as it was for the caffeine sonoporation experiments in Appendix A. At this distance, skin was sonoporated for 10 minutes at both 13 W/cm^2 and 55 W/cm^2. Relative to the control case (with no ultrasound), sonoporation at 13 W/cm^2 resulted in a 1.8-fold increase in the mean receiver

chamber calcein concentration (Fig. B-8). However, the median decreased by 0.7-fold and the *p*-value was 0.8. Sonoporation for 10 minutes at 55 W/cm^2 resulted in a 3.8-fold increase in the mean receiver concentration (p=0.46) but a 0.7-fold decrease in the median value. Note that these *p*-values were found using a Wilcoxon rank sum test as a Kolmogorov-Smirnov test rejected the null hypothesis that the data was normally distributed at the 5 *%* significance level. Skin was also sonoporated for 30 minutes at 55 W/cm^2 with a transducer to skin distance of 5 mm. Relative to the control case, this protocol resulted in a 6-fold increase in the mean receiver concentration (p=0.26) and a 1.1-fold increase in the median (Fig. B-9).

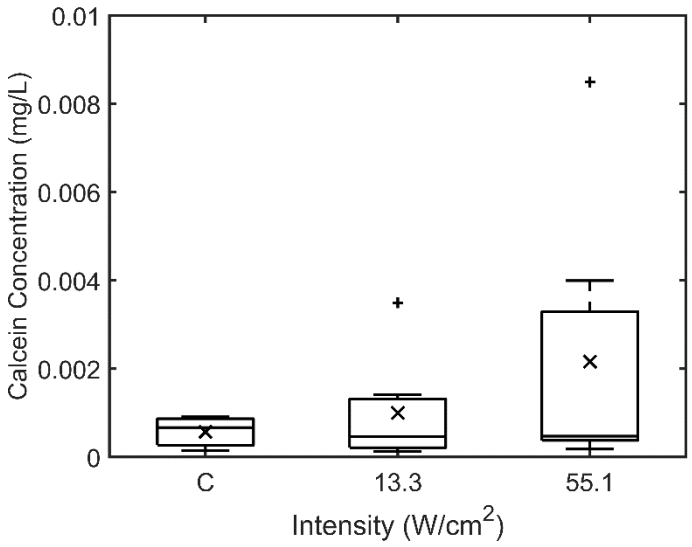

Fig. B-8 Receiver chamber calcein concentration as a function of ultrasound intensity. The transducer to skin distance was 5 mm. The ultrasound application time was 10 minutes. The post-sonoporation diffusion time was 1 hour (n=7).

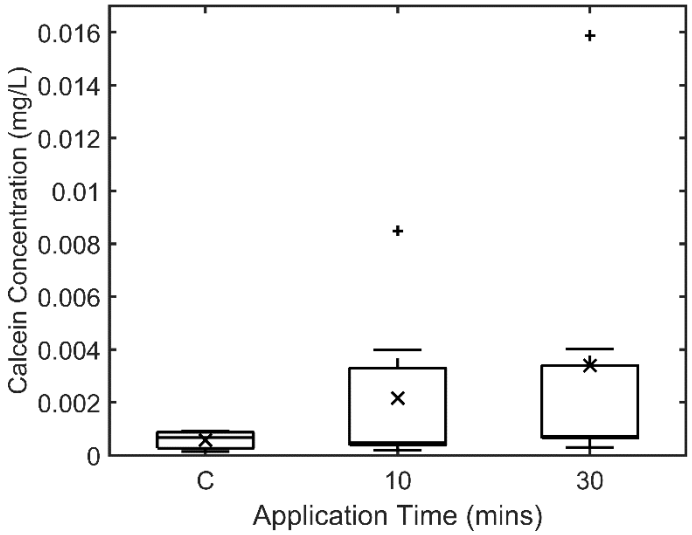

Fig. B-9 Receiver chamber calcein concentration as a function of ultrasound application time. The ultrasound intensity was 55 W/cm^2. The transducer to skin distance was 5 mm. The post-sonoporation diffusion time was 1 hour (n=7).

With the transducer to skin distance set to 3 mm, skin was sonoporated for 10 or 30 minutes at an intensity of 55 W/cm^2. Relative to the control case, 10 minutes of sonoporation resulted in a 3.8-fold increase (p<0.05) in mean receiver chamber concentration. The median value increased by 2.8-fold (Fig. B-10). Sonoporation for 30 minutes resulted in a 7.1-fold increase in the mean receiver concentration (p<0.05) and a 5.8-fold increase in the median.

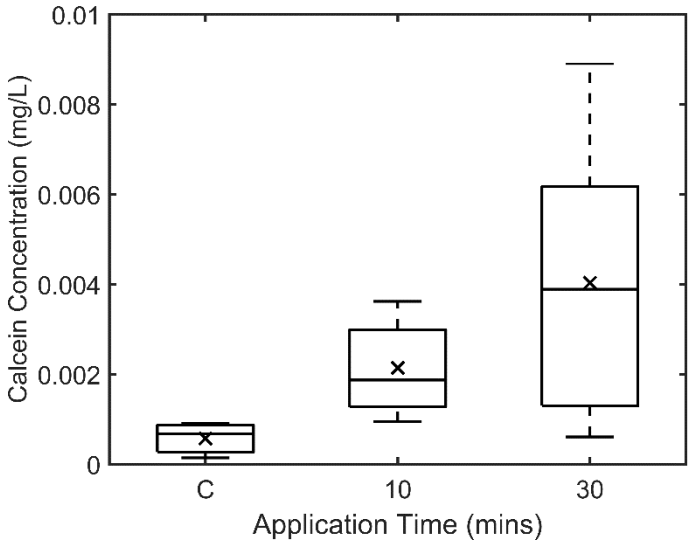

Fig. B-10 Receiver chamber calcein concentration as a function of ultrasound application time. The ultrasound intensity was 55 W/cm^2. The transducer to skin distance was 3 mm. The post-sonoporation diffusion time was 1 hour (n=7).

B.3.3 Donor Temperature

This study employed a temperature regulation system to set and maintain the coupling fluid at 12 °C ± 1 °C during 10 minutes or 30 minutes of continuous ultrasound application. The coupling fluid temperature was measured with a thermocouple that was positioned outside of the transducer beam. Preliminary temperature measurements were conducted to determine the difference in coupling fluid temperature outside of the transducer beam and directly over the skin surface. At steady state, when the transducer was 3 mm from the skin surface, the temperature over the skin surface was at most 2 °C higher during sonoporation (Fig. B-11). When the transducer was 5 mm from the skin surface, the temperature over the skin surface was at most 1 °C higher than the temperature outside of the beam. These small differences illustrate that the thermocouple outside of the beam undervalued the temperature over the skin surface by 1-2 °C during sonoporation. This undervaluing was too small to have an influence on the results of the study and was therefore ignored.

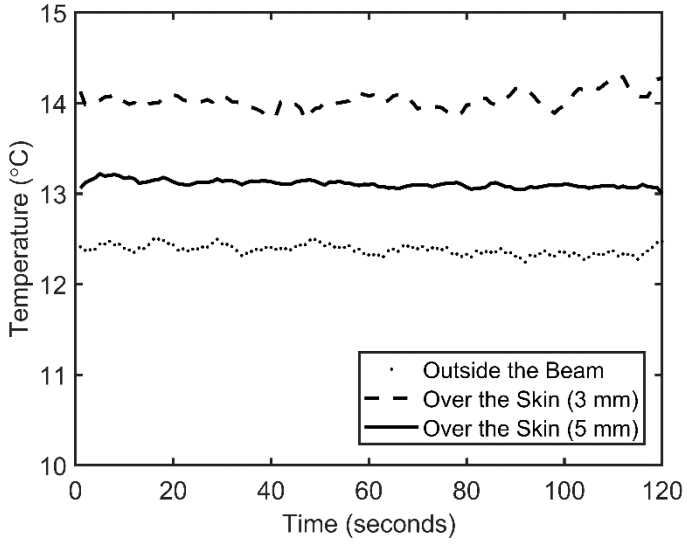

Fig. B-11 The influence of thermocouple position on the steady state thermocouple reading during sonoporation with a tip displacement of 60 % and a target temperature of 12 °C. The dotted line represents the temperature recorded with the thermocouple outside of the transducer beam. The dashed and solid lines represent the temperatures recorded with the thermocouple directly over the skin when the transducer was 3 mm and 5 mm from the skin.

B.3.4 Receiver Temperature

The temperature of the receiver fluid was measured during each of the high intensity sonoporation protocols to quantify its dependence on the transducer to skin distance. A thermocouple, inserted through the bottom of the receiver chamber so that its tip was 2 mm below the skin, recorded data for the duration of ultrasound application. When the transducer was 5 mm from the skin surface, the receiver temperature after 10 minutes of sonoporation was 25 °C (Fig. B-12). When the transducer was 3 mm from the skin surface, the temperature after 10 minutes was 30 °C. Therefore, the transducer to skin distance had only a minor influence on the receiver chamber temperature during 10 minutes of sonoporation at 55 W/cm^2.

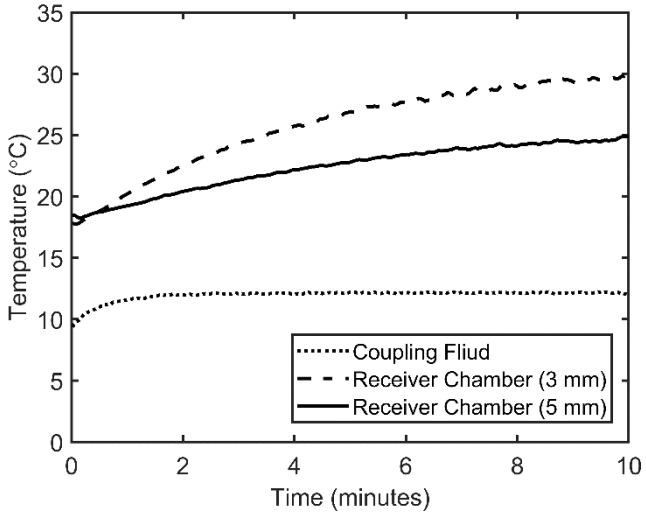

Fig. B-12 Receiver chamber temperatures during 10 minutes of sonoporation (55 W/cm^2) for transducer distances of 3 mm and 5 mm. Coupling fluid temperature is also shown.

When the transducer was 5 mm from the skin surface, the receiver temperature after 30 minutes of sonoporation was 26 °C (Fig. B-13). When the transducer was 3 mm from the skin surface, the temperature after 30 minutes was 31 °C. Therefore, the transducer to skin distance had only a minor influence on the receiver chamber temperature during 30 minutes of sonoporation at 55 W/cm^2.

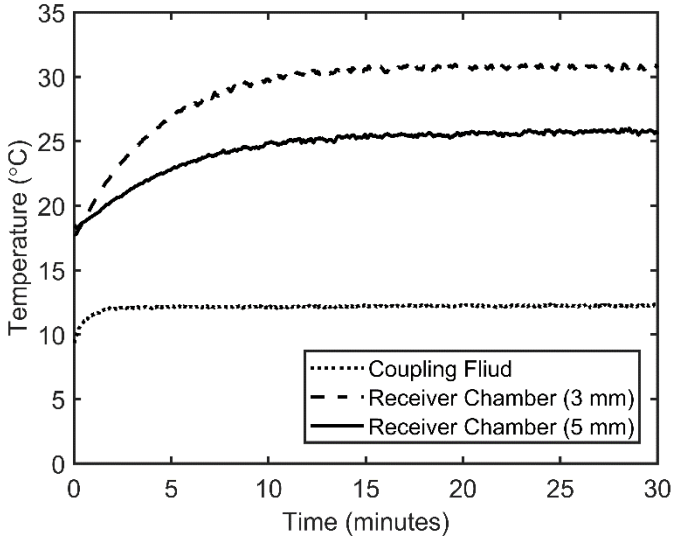

Fig. B-13 Receiver chamber temperatures during 30 minutes of sonoporation (55 W/cm^2) for transducer distances of 3 mm and 5 mm. Coupling fluid temperature is also shown.

B.3.5 Foil Pitting Experiments

Foil pitting experiments were used to determine the influence of transducer to skin distance on the inertial cavitation activity at the skin aperture. With the coupling fluid circulating, each piece of aluminium foil was exposed to ultrasound for 2 s at an intensity of 55 W/cm^2. When the transducer was 3 mm from the skin aperture, the mean number of pits was 35 (Fig. B-14). When the distance was increased to 5 mm, the mean number of pits was 16 – representing a 56 *%* decrease (p<0.05). The mean then decreased by a further 93 *%* when the distance was increased to 7 mm.

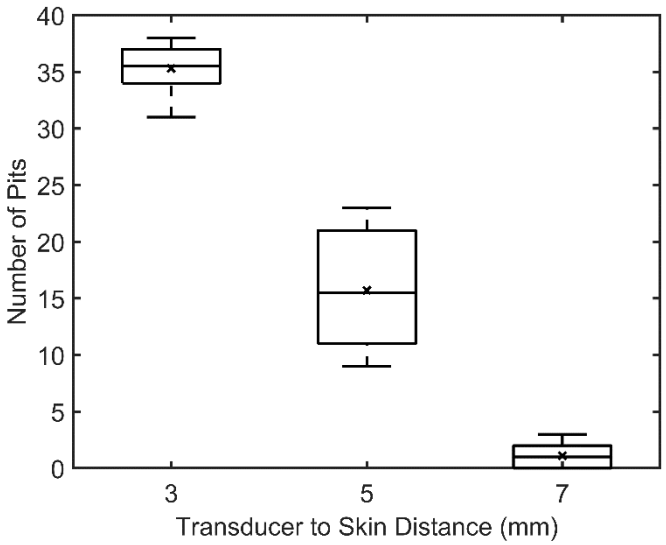

Fig. B-14 Number of pits in aluminium foil as a function of transducer to skin distance. Ultrasound was applied for 2 s at an ultrasound of 55 W/cm^2 (n=10)

B.4 Discussion

The purpose of this study was to find a combination of sonoporation parameters that could be used to enhance post-sonoporation calcein transport in the coupling fluid temperature study (Chapter 2). Of the five combinations of sonoporation parameters investigated

(outlined in Table B-1), only two combinations resulted in significant (p<0.05) increases in the mean receiver concentration (and therefore skin permeability) relative to the control case. The greatest increase was achieved with an application time of 30 minutes, an intensity of 55 W/cm^2 and a transducer to skin distance of 3 mm. A lesser, but still significant, increase was achieved with an application time of 10 minutes, an intensity of 55 W/cm^2 and a transducer to skin distance of 3 mm. A comparison of these two datasets shows that increasing the ultrasound application time increased the mean skin permeability enhancement by 88 % (significant at p=0.38). This is due to inertial cavitation activity – the longer the skin was exposed to the ultrasound field, the more inertial cavitation events impacted the SC. An increase in permeability enhancement with increasing ultrasound application time was also found in the study by Mitragotri, et al. (2000a). In that study, the skin conductivity enhancement achieved with an effective ultrasound time of 6 minutes was approximately twice that achieved with an effective time of 3 minutes. Similarly, Terahara, et al. (2002a) found that the mannitol permeability enhancement achieved with 6 minutes of effective ultrasound pre-treatment time was almost twice that achieved with 1.5 minutes.

Relative to the protocols at 3 mm, the three sonoporation protocols that involved a distance of 5 mm all resulted in insignificant increases in the mean receiver calcein concentration. Therefore, decreasing the transducer to skin distance (from 5 mm to 3 mm) increased the skin permeability enhancement. An increase in skin permeability enhancement with decreasing transducer distance was also found in the sonoporation study by Herwadkar, et al. (2012). In that study, the transdermal transport of ketoprofen following 2 minutes of sonoporation with the transducer 3 mm from the skin was almost 5 times the transport following sonoporation at 6 mm. Similarly, Terahara, et al. (2002a) found that the skin

conductivity (an established proxy for permeability to mass transport) achieved after 12 minutes of ultrasound application at 2.5 mm was 4 times that achieved after application at 10 mm. The increase in ultrasound enhancement that occurs with decreasing transducer to skin distance is due to the greater number of inertial cavitation events which occur closer to the transducer tip. This was shown with foil pitting experiments in the study by Terahara, et al. (2002a) – the number of pits after ultrasound application at 40 mm was only 12 *%* of that after application at 5 mm. Foil pitting experiments showed that an increase in pitting occurs with decreasing distance in the present circulating setup too. When the transducer was 3 mm from the skin, the mean number of pits after 2 s of ultrasound application (at 55 W/cm^2) was 35. The mean number of pits then decreased as the transducer distance increased (Fig. B-14) – the mean at 5 mm was only 44 *%* of that at 3 mm, while the mean at 7 mm was only 3 *%* of that at 3 mm. From these pitting results it can be concluded that the inertial cavitation activity at the skin aperture increases with decreasing transducer distance in the present circulating setup. This explains the increased post-sonoporation transport with decreasing transducer distance.

An increase in receiver chamber temperature with decreasing transducer distance may also have contributed to the increase in post-sonoporation transport with decreasing transducer distance. In the study by Akomeah, et al. (2004), the transdermal transport of methyl paraben after 4 hours with the diffusion cell in a water bath at 45 °C was shown to be 3.5 times that after 4 hours in a water bath at 23 °C. This difference was attributed, in part, to temperature induced changes in the lipid structure of the stratum corneum – changes which are known to influence the skin's permeability to mass transfer (Gay, et al. 1994, Potts and Francoeur 1990). To quantify the influence of transducer distance on receiver chamber temperature in the

present study, a thermocouple was positioned in the receiver fluid, 2 mm below the skin surface. Measurements with this thermocouple showed that, regardless of the application time, the receiver chamber temperature during sonoporation at 3 mm was a maximum of 5 °C greater than the receiver temperature during sonoporation at 5 mm. Considering the strict control of the fluid on the SC side, a receiver temperature difference of 5 °C would have had a near negligible influence on the skin permeability. Therefore, an increase in receiver chamber temperature with decreasing transducer distance did not contribute to the increase in post-sonoporation transport with decreasing distance. This reinforces the conclusion that it was increased inertial cavitation activity impacting the skin that resulted in greater transport following sonoporation at 3 mm.

Given the benefits of moving the transducer closer to the skin surface it would be logical to reduce the distance to 0.58 mm – the very edge of the far field according to Eq. (3.1). However, the minimum transducer to skin distance was limited by the design of the donor chamber (shown in Fig. B-1). The thickness of the polypropylene at the base of the donor chamber was 2 mm. Therefore, 3 mm was considered to be the minimum transducer to skin distance as a 1 mm gap was required between the transducer tip and the donor chamber base so that the cooled coupling fluid could flow freely over the skin surface.

Of the five combinations of experimental parameters investigated in this study, that which involved an application time of 10 minutes, an intensity of 55 W/cm^2 and a transducer to skin distance of 3 mm was deemed most appropriate for use in the coupling fluid temperature study (Chapter 2). This combination of parameters resulted in a significant transport enhancement after only a short ultrasound application. An application time of 30 minutes

resulted in a greater skin permeability enhancement, however, as 42 individual transport experiments were needed for the study in Chapter 2, this was deemed to be an unnecessarily long application time.

Future, *in vitro*, *in vivo* or clinical studies that want to obtain a greater permeability increase by using an application time of 30 minutes, 1 hour, or more should note that the ability of the circulating temperature control system is not time dependent. When an application time of 30 minutes was used in the present study, the coupling fluid temperature was constant over the entire duration (Fig. B-13). Therefore, constant ultrasound application can be used, regardless of the application time, without any concern for coupling fluid temperature increase. This long duration temperature control capability enables far greater ultrasound application times that have previously been feasible. Previously, when a 10 % duty cycle was used to control thermal effects, 30 minutes of ultrasound would have taken 5 hours to administer. This duration would be impractical in a clinical setting and tedious in a laboratory setting. With the present system, a 30 minute or 1 hour application time is now far more practical as duty cycles are no longer required.

B.5 Conclusions

The purpose of this study was to find a combination of sonoporation parameters that could be used to enhance post-sonoporation calcein transport in the coupling fluid temperature study (Chapter 2). A calibration curve was produced so that the concentration of calcein in the receiver fluid could be calculated from the fluorescent intensity measured by the spectrofluorometer. The concentration of calcein in the receiver fluid following a control case

with no ultrasound was then compared to the concentration following sonoporation with five different combinations of experimental parameters. The combination that was deemed most appropriate for the coupling fluid temperature study involved an application time of 10 minutes, an intensity of 55 W/cm^2 and a transducer to skin distance of 3 mm. Relative to the control case, this combination of parameters resulted in a in a 3.8-fold increase (significant at $p<0.05$) in mean receiver chamber concentration and a 2.8-fold increase in the median. Although the present study did not directly address any of the thesis objectives, it does contain the first known example of calcein transport enhancement using continuous sonoporation with coupling fluid temperature control. The present study also shows that, in a sonoporation setup with circulating coupling fluid temperature control, post-sonoporation transport decreases with increasing transducer to skin distance and increases with increasing ultrasound application time.

Given this positive relationship between application time and transport, future researchers and clinicians will find it beneficial to use long application times. Prior to the introduction of the circulating temperature control system presented in this thesis, 30 minutes of sonoporation would have taken up to 5 hours to administer, due to the need for duty cycles to minimise thermal effects. Such a timeframe is tedious in an experimental setting and impractical in a clinical setting. With temperature control, duty cycles and fluid replacement are no longer required. It is now possible to apply long durations (≥30 minutes) of ultrasound in a reasonable, clinically practical time.

Appendix C Hydrophone Calibration Data

This appendix contains the complete calibration information for the hydrophone (2.0 mm Needle Hydrophone, Precision Acoustics Ltd., Dorchester, Dorset, UK) used in Chapters 3 and 4, and Appendix A. This calibration was performed by Neptune Sonar Ltd (East Yorkshire, UK).

NEPTUNE SONAR LTD

ACOUSTIC CALIBRATION LABORATORY

TEST CERTIFICATE

PROJECT REF:	6131
SERIAL NUMBER:	SM2526
TRANSDUCER TYPE:	Needle Hydrophone
DESCRIPTION:	
TEST SPECIFICATION:	6061-10-01-01
ISSUE DATE:	31 October 2016

Ref Projector:	D/11_18685	**Ref Projector:**	D/26_22807
Ref Projector:	D/70_29325	**Ref Projector:**	D/140_29348
Ref Projector:	D/HF_24505		

TABULATED RESULTS **(8 pages)**
HYDROPHONE SENSITIVITY GRAPH **(2 pages)**

Calibration Engineer

.....

P. Jones

Quality Executive

.....

N. P. Dearing

Issued by:

Neptune Sonar Ltd
Kelk Lake
Kelk
Driffield
East Yorkshire
TEL: +44(0) 1262 490234
FAX: +44(0) 1262 490485
Email: info@neptune-sonar.co.uk

Customer:

Precision Acoustics
Hampton Farm Business Park
Higher Brockhampton
Dorchester
DT2 8QH

The reported expanded uncertainty is based on a standard uncertainty multiplied by a coverage factor k = 2, providing a level of confidence of approximately 95%

NEPTUNE SONAR LTD

ACOUSTIC CALIBRATION LABORATORY

CALIBRATION DATE: 31 October 2016 at 12:01
TRANSDUCER TYPE: Needle Hydrophone
SERIAL NUMBER: SM2526
CALIBRATED BY: I. Griffiths

PROJECT No.: 6131
DESCRIPTION:
TEST SPECIFICATION: 6061-10-01-01
WATER TEMPERATURE: 12°C (±0.5)
CABLE: 20m

REMARKS: Measured at end of 20m cable
Using customer supplied power supply DCPS536

FREQUENCY (kHz) (±0.005%)	HYDROPHONE SENSITIVITY (dBre1V/µPa)	UNCERTAINTY (dB)
5.000	-241.9	±1.0
6.000	-241.6	±1.2
7.000	-241.6	±1.0
8.000	-240.5	±1.0
9.000	-238.9	±1.0
10.000	-240.6	±1.0
11.000	-239.5	±1.0
12.000	-237.8	±1.0
13.000	-239.5	±1.0
14.000	-237.3	±1.0
15.000	-237.3	±1.0
16.000	-236.2	±1.0
17.000	-237.2	±1.0
18.000	-237.1	±1.2
19.000	-236.4	±1.2
20.000	-236.4	±1.1
21.000	-236.5	±1.2
22.000	-235.6	±1.1
23.000	-236.7	±1.0
24.000	-236.7	±1.0
25.000	-235.5	±1.0
26.000	-235.7	±1.0
27.000	-235.8	±1.0
28.000	-235.7	±1.0
29.000	-236.4	±1.0
30.000	-236.7	±1.0
31.000	-236.3	±1.0
32.000	-235.1	±1.0
33.000	-234.6	±1.0
34.000	-233.5	±1.0

NEPTUNE SONAR LTD

ACOUSTIC CALIBRATION LABORATORY

CALIBRATION DATE: 31 October 2016 at 12:01
TRANSDUCER TYPE: Needle Hydrophone
SERIAL NUMBER: SM2526
CALIBRATED BY: I. Griffiths

PROJECT No.: 6131
DESCRIPTION:
TEST SPECIFICATION: 6061-10-01-01
WATER TEMPERATURE: 12°C (±0.5)
CABLE: 20m

REMARKS: Measured at end of 20m cable
Using customer supplied power supply DCPS536

FREQUENCY (kHz) (±0.005%)	HYDROPHONE SENSITIVITY (dBre1V/µPa)	UNCERTAINTY (dB)
35.000	-232.8	±1.0
36.000	-232.4	±1.0
37.000	-231.8	±1.0
38.000	-231.1	±1.0
39.000	-232.0	±1.0
40.000	-232.2	±1.0
41.000	-231.9	±1.0
42.000	-230.2	±1.0
43.000	-230.3	±1.0
44.000	-230.4	±1.0
45.000	-233.6	±1.0
46.000	-236.1	±1.0
47.000	-236.6	±1.0
48.000	-236.0	±1.0
49.000	-236.0	±1.0
50.000	-235.7	±1.0
51.000	-236.1	±1.0
52.000	-235.8	±1.0
53.000	-235.7	±1.0
54.000	-235.2	±1.0
55.000	-234.9	±1.0
56.000	-234.5	±1.0
57.000	-234.7	±1.0
58.000	-234.4	±1.0
59.000	-234.4	±1.0
60.000	-234.7	±1.0
61.000	-234.9	±1.0
62.000	-234.4	±1.0
63.000	-234.5	±1.0
64.000	-234.8	±1.0

NEPTUNE SONAR LTD

ACOUSTIC CALIBRATION LABORATORY

CALIBRATION DATE: 31 October 2016 at 12:01
TRANSDUCER TYPE: Needle Hydrophone
SERIAL NUMBER: SM2526
CALIBRATED BY: I. Griffiths

PROJECT No.: 6131
DESCRIPTION:
TEST SPECIFICATION: 6061-10-01-01
WATER TEMPERATURE: 12°C (±0.5)
CABLE: 20m

REMARKS: Measured at end of 20m cable
Using customer supplied power supply DCPS536

FREQUENCY (kHz) (±0.005%)	HYDROPHONE SENSITIVITY (dBre1V/µPa)	UNCERTAINTY (dB)
65.000	-235.0	±1.0
66.000	-234.8	±1.0
67.000	-234.3	±1.0
68.000	-234.1	±1.0
69.000	-233.8	±1.0
70.000	-234.2	±1.0
71.000	-234.4	±1.0
72.000	-234.6	±1.0
73.000	-234.2	±1.0
74.000	-234.7	±1.0
75.000	-234.5	±1.0
76.000	-234.9	±1.0
77.000	-235.1	±1.0
78.000	-235.3	±1.0
79.000	-234.6	±1.0
80.000	-233.8	±1.0
81.000	-233.6	±1.0
82.000	-233.7	±1.0
83.000	-234.2	±1.0
84.000	-234.2	±1.0
85.000	-234.0	±1.0
86.000	-233.7	±1.0
87.000	-233.5	±1.0
88.000	-233.5	±1.0
89.000	-233.8	±1.0
90.000	-234.0	±1.0
91.000	-234.0	±1.0
92.000	-233.5	±1.0
93.000	-234.1	±1.0
94.000	-234.4	±1.0

NEPTUNE SONAR LTD

ACOUSTIC CALIBRATION LABORATORY

CALIBRATION DATE: 31 October 2016 at 12:01
TRANSDUCER TYPE: Needle Hydrophone
SERIAL NUMBER: SM2526
CALIBRATED BY: I. Griffiths

PROJECT No.: 6131
DESCRIPTION:
TEST SPECIFICATION: 6061-10-01-01
WATER TEMPERATURE: 12°C (±0.5)
CABLE: 20m

REMARKS: Measured at end of 20m cable
Using customer supplied power supply DCPS536

FREQUENCY (kHz) (±0.005%)	HYDROPHONE SENSITIVITY (dBre1V/µPa)	UNCERTAINTY (dB)
95.000	-234.9	±1.0
96.000	-233.7	±1.0
97.000	-233.3	±1.0
98.000	-232.9	±1.0
99.000	-233.3	±1.0
100.000	-233.5	±1.0
101.000	-233.5	±1.0
102.000	-233.0	±1.0
103.000	-232.9	±1.0
104.000	-232.9	±1.0
105.000	-232.7	±1.0
106.000	-232.8	±1.0
107.000	-232.6	±1.0
108.000	-232.4	±1.0
109.000	-232.2	±1.0
110.000	-232.5	±1.0
111.000	-232.4	±1.0
112.000	-232.4	±1.0
113.000	-231.4	±1.0
114.000	-231.0	±1.0
115.000	-231.7	±1.0
116.000	-233.4	±1.0
117.000	-234.8	±1.0
118.000	-234.4	±1.0
119.000	-233.1	±1.0
120.000	-231.9	±1.0
125.000	-229.5	±1.0
130.000	-230.3	±1.0
135.000	-231.5	±1.0
140.000	-230.1	±1.0

NEPTUNE SONAR LTD

ACOUSTIC CALIBRATION LABORATORY

CALIBRATION DATE: 31 October 2016 at 12:01
TRANSDUCER TYPE: Needle Hydrophone
SERIAL NUMBER: SM2526
CALIBRATED BY: I. Griffiths

PROJECT No.: 6131
DESCRIPTION:
TEST SPECIFICATION: 6061-10-01-01
WATER TEMPERATURE: 12°C (±0.5)
CABLE: 20m

REMARKS: Measured at end of 20m cable
Using customer supplied power supply DCPS536

FREQUENCY (kHz) (±0.005%)	HYDROPHONE SENSITIVITY (dBre1V/μPa)	UNCERTAINTY (dB)
145.000	-229.3	±1.0
150.000	-230.1	±1.0
155.000	-226.8	±1.0
160.000	-226.4	±1.0
165.000	-227.9	±1.0
170.000	-228.5	±1.0
175.000	-227.1	±1.0
180.000	-227.3	±1.0
185.000	-226.9	±1.0
190.000	-225.8	±1.0
195.000	-225.8	±1.0
200.000	-225.1	±1.0
205.000	-225.7	±1.0
210.000	-225.8	±1.0
215.000	-225.8	±1.0
220.000	-225.7	±1.0
225.000	-226.7	±1.0
230.000	-224.9	±1.0
235.000	-225.5	±1.0
240.000	-226.9	±1.0
245.000	-226.3	±1.0
250.000	-227.0	±1.0
255.000	-226.4	±1.0
260.000	-225.6	±1.0
265.000	-226.8	±1.0
270.000	-226.2	±1.0
275.000	-225.5	±1.0
280.000	-227.2	±1.0
285.000	-226.1	±1.0
290.000	-226.0	±1.0

NEPTUNE SONAR LTD

ACOUSTIC CALIBRATION LABORATORY

CALIBRATION DATE: 31 October 2016 at 12:01
TRANSDUCER TYPE: Needle Hydrophone
SERIAL NUMBER: SM2526
CALIBRATED BY: I. Griffiths

PROJECT No.: 6131
DESCRIPTION:
TEST SPECIFICATION: 6061-10-01-01
WATER TEMPERATURE: 12°C (±0.5)
CABLE: 20m

REMARKS: Measured at end of 20m cable
Using customer supplied power supply DCPS536

FREQUENCY (kHz) (±0.005%)	HYDROPHONE SENSITIVITY (dBre1V/µPa)	UNCERTAINTY (dB)
295.000	-226.2	±1.0
300.000	-225.6	±1.0
310.000	-227.3	±1.0
320.000	-226.2	±1.0
330.000	-225.1	±1.0
340.000	-226.7	±1.0
350.000	-226.0	±1.0
360.000	-225.0	±1.0
370.000	-225.8	±1.0
380.000	-227.4	±1.0
390.000	-223.1	±1.0
400.000	-224.6	±1.0
410.000	-225.8	±1.0
420.000	-225.4	±1.0
430.000	-223.3	±1.0
440.000	-224.5	±1.0
450.000	-228.3	±1.0
460.000	-225.0	±1.0
470.000	-224.9	±1.0
480.000	-227.6	±1.0
490.000	-226.1	±1.0
500.000	-224.6	±1.0
510.000	-231.0	±1.0
520.000	-226.7	±1.0
530.000	-229.9	±1.0
540.000	-229.4	±1.0
550.000	-228.4	±1.0
560.000	-224.5	±1.0
570.000	-229.8	±1.0
580.000	-221.4	±1.0

NEPTUNE SONAR LTD

ACOUSTIC CALIBRATION LABORATORY

CALIBRATION DATE: 31 October 2016 at 12:01
TRANSDUCER TYPE: Needle Hydrophone
SERIAL NUMBER: SM2526
CALIBRATED BY: I. Griffiths

PROJECT No.: 6131
DESCRIPTION:
TEST SPECIFICATION: 6061-10-01-01
WATER TEMPERATURE: 12°C (±0.5)
CABLE: 20m

REMARKS: Measured at end of 20m cable
Using customer supplied power supply DCPS536

FREQUENCY (kHz) (±0.005%)	HYDROPHONE SENSITIVITY (dBre1V/µPa)	UNCERTAINTY (dB)
590.000	-226.0	±1.0
600.000	-222.8	±1.0
610.000	-223.1	±1.0
620.000	-226.6	±1.0
630.000	-224.1	±1.0
640.000	-223.6	±1.0
650.000	-225.9	±1.0
660.000	-222.7	±1.0
670.000	-223.2	±1.0
680.000	-226.0	±1.0
690.000	-223.4	±1.0
700.000	-226.7	±1.0
710.000	-223.6	±1.0
720.000	-227.4	±1.0
730.000	-225.8	±1.0
740.000	-224.6	±1.0
750.000	-226.1	±1.0
760.000	-226.7	±1.0
770.000	-224.7	±1.0
780.000	-230.2	±1.0
790.000	-225.2	±1.0
800.000	-228.7	±1.0
810.000	-227.0	±1.0
820.000	-227.1	±1.0
830.000	-228.0	±1.0
840.000	-227.1	±1.0
850.000	-227.3	±1.0
860.000	-227.3	±1.0
870.000	-226.6	±1.0
880.000	-227.5	±1.0

NEPTUNE SONAR LTD

ACOUSTIC CALIBRATION LABORATORY

CALIBRATION DATE: 31 October 2016 at 12:01
TRANSDUCER TYPE: Needle Hydrophone
SERIAL NUMBER: SM2526
CALIBRATED BY: I. Griffiths

PROJECT No.: 6131
DESCRIPTION:
TEST SPECIFICATION: 6061-10-01-01
WATER TEMPERATURE: 12°C (±0.5)
CABLE: 20m

REMARKS: Measured at end of 20m cable
Using customer supplied power supply DCPS536

FREQUENCY (kHz) (±0.005%)	HYDROPHONE SENSITIVITY (dBre1V/μPa)	UNCERTAINTY (dB)
890.000	-226.3	±1.0
900.000	-227.5	±1.0
910.000	-226.0	±1.0
920.000	-227.3	±1.0
930.000	-226.1	±1.0
940.000	-226.0	±1.0
950.000	-227.3	±1.0
960.000	-226.7	±1.0
970.000	-226.2	±1.0
980.000	-228.6	±1.0
990.000	-226.1	±1.0
1000.000	-227.8	±1.0

NEPTUNE SONAR LTD

ACOUSTIC CALIBRATION LABORATORY

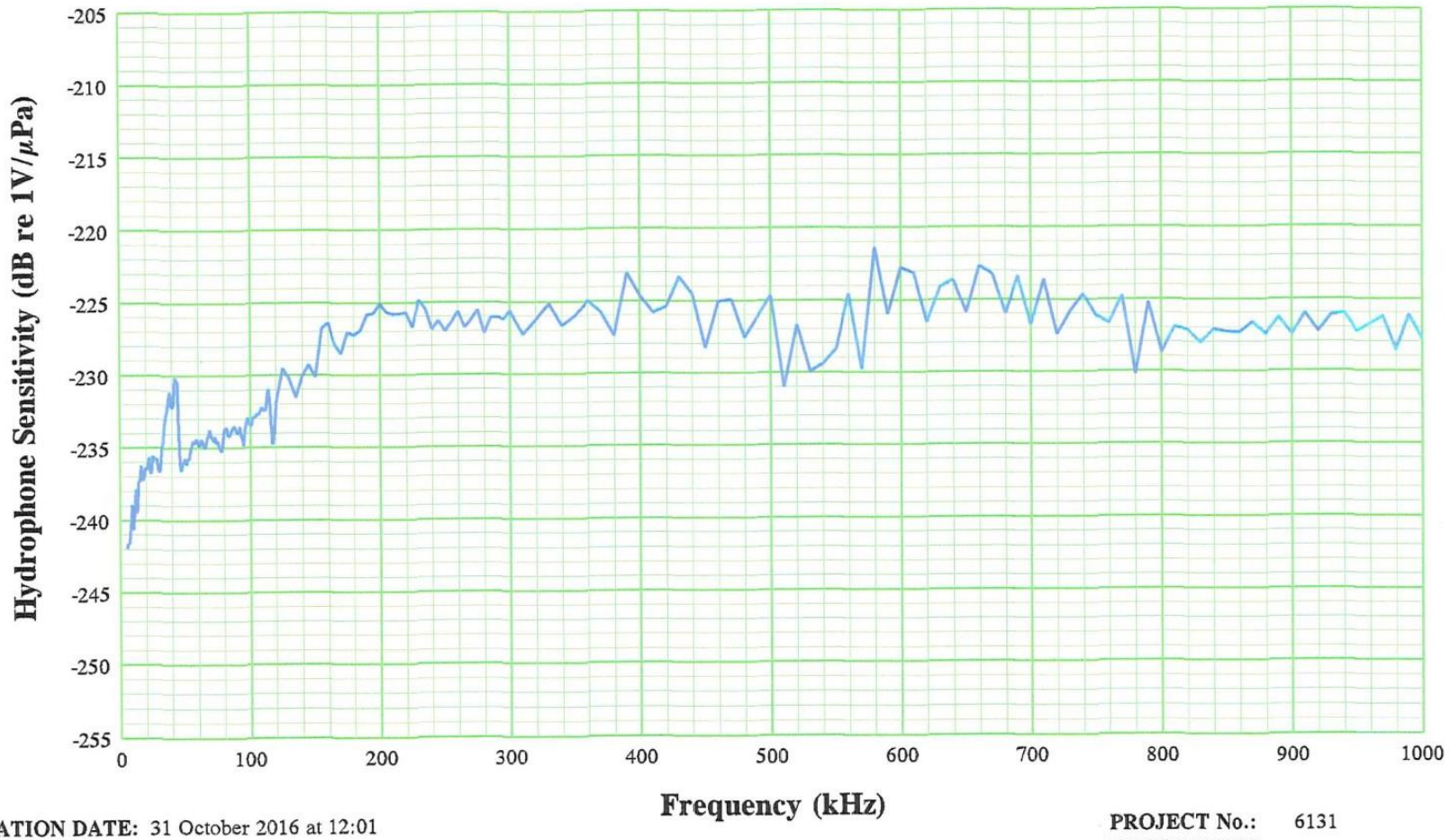

CALIBRATION DATE: 31 October 2016 at 12:01
TRANSDUCER TYPE: Needle Hydrophone
SERIAL NUMBER: SM2526
CALIBRATED BY: I. Griffiths
REMARKS: Measured at end of 20m cable
Using customer supplied power supply DCPS536

PROJECT No.: 6131
DESCRIPTION:
TEST SPEC: 6061-10-01-01
WATER TEMP: 12°C (±0.5)
CABLE: 20m

Ref:-MSSM2526:13:02:39

NEPTUNE SONAR LTD

ACOUSTIC CALIBRATION LABORATORY

CALIBRATION DATE: 31 October 2016 at 12:01
TRANSDUCER TYPE: Needle Hydrophone
SERIAL NUMBER: SM2526
CALIBRATED BY: I. Griffiths
REMARKS: Measured at end of 20m cable
Using customer supplied power supply DCPS536

PROJECT No.: 6131
DESCRIPTION:
TEST SPEC: 6061-10-01-01
WATER TEMP: 12°C (±0.5)
CABLE: 20m

Ref:-MSSM2526:13:02:31

This thesis involved the purchase, construction and assembly of an entire laboratory setup from scratch; 176 transdermal transport experiments (plus the same amount again to learn how); 279 spectrofluorometer measurements (double that for mistakes); 68 HPLC measurements (triple that for mistakes); 156 foil pitting experiments (plus another 100 with a transducer that didn't work); approximately 79 million hydrophone data points; approximately 25 hours of temperature data (double that for development of temperature control); 1 broken water tank which caused a small flood; about 10 2.5 hour round trips to the abattoir; approximately 150 pigs' ears; and at least 3 instances of pigs' blood squirting into my mouth/eyes while dermatoming.

*

A final note to the reader, and to the author as well,

Only now that I have done it, that I have attempted it once, do I finally understand how it must be done. There is a cruel irony in this, and a wonderful lesson.

JPR

Relevant Journal Papers and Conference Contributions

Robertson, J. and Becker, S., *Influence of Acoustic Reflection on the Inertial Cavitation Dose in a Franz Diffusion Cell*. Ultrasound Med Biol 2018; 44:1100-09.

Robertson, J. and Becker, S., *Passive Cavitation Detection During Skin Sonoporation*, IUTAM Symposium on Recent Advances in Moving Boundary Problems in Mechanics, Christchurch, New Zealand, 2018. Contribution – Peer Reviewed Conference Paper and Oral Presentation.

Robertson, J. and Becker, S., *Temperature Control in a Franz Diffusion Cell Skin Sonoporation Setup*, 70th Annual Meeting of the APS Division of Fluid Dynamics, Denver, Colorado, 2017. Contribution – Conference Abstract and Oral Presentation.

Robertson, J. and Becker, S., *The Effects of Acoustic Reflection on the Inertial Cavitation Behaviour in a Novel in vitro Skin Insonation Setup,* Fluids in New Zealand, Christchurch, New Zealand, 2017. Contribution – Conference Abstract and Oral Presentation.

Robertson, J. and Becker, S., *Custom Experimental Apparatus Design for the Investigation of Ultrasound as an Active Enhancement Method in Transdermal Drug Delivery*, 1st Word Congress on Electroporation, Portorož, Slovenia, 2015. Contribution – Peer Reviewed Conference Paper and Poster Presentation.

Robertson, J. and Becker, S., *Motivations for a Custom Apparatus for Sonophoresis Experimentation*, 9th IFAC Symposium on Biological and Medical Systems, Berlin, Germany, 2015. Contribution – Peer Reviewed Conference Paper and Poster Presentation.

Robertson, J. and Becker, S., *Motivations for a Custom Apparatus for Sonophoresis Experimentation*, Health Research Society of Canterbury 2015 Poster Expo, Christchurch, New Zealand, 2015. Contribution – Poster Presentation.

Four additional full length journal papers based off of the work in Chapter 2, Chapter 3, Appendix A, and Appendix B are in preparation.

References

Agache P, Monneur C, Leveque J, De Rigal J. Mechanical properties and Young's modulus of human skin in vivo. Archives of dermatological research 1980; 269:221-32.

Ahmadi F, McLoughlin IV, Chauhan S, ter-Haar G. Bio-effects and safety of low-intensity, low-frequency ultrasonic exposure. Prog Biophys Mol Bio 2012; 108:119-38.

Akomeah F, Nazir T, Martin GP, Brown MB. Effect of heat on the percutaneous absorption and skin retention of three model penetrants. European Journal of Pharmaceutical Sciences 2004; 21:337-45.

Alonso A, Meirelles NC, Tabak M. Effect of hydration upon the fluidity of intercellular membranes of stratum corneum: an EPR study. Biochimica et Biophysica Acta (BBA) - Biomembranes 1995; 1237:6-15.

Alvarez-Román R, Merino G, Kalia YN, Naik A, Guy RH. Skin Permeability Enhancement by Low Frequency Sonophoresis: Lipid Extraction and Transport Pathways. J Pharm Sci 2003; 92:1138-46.

Ashburn MA, Ogden LL, Zhang J, Love G, Basta SV. The pharmacokinetics of transdermal fentanyl delivered with and without controlled heat. The Journal of Pain 2003; 4:291-97.

Bacon DR, Carstensen EL. Increased heating by diagnostic ultrasound due to nonlinear propagation. The Journal of the Acoustical Society of America 1990; 88:26-34.

Bader KB, Raymond JL, Mobley J, Church CC, Felipe Gaitan D. The effect of static pressure on the inertial cavitation threshold. The Journal of the Acoustical Society of America 2012; 132:728-37.

Baji S, Hegde AR, Kulkarni M, Raut SY, Manikkath J, Reddy MS, Mutalik S. Skin permeation of gemcitabine hydrochloride by passive diffusion, iontophoresis and sonophoresis: In vitro and in vivo evaluations. Journal of Drug Delivery Science and Technology 2018; 47:49-54.

Barati AH, Mokhtari-Dizaji M, Mozdarani H, Bathaie Z, Hassan ZM. Effect of exposure parameters on cavitation induced by low-level dual-frequency ultrasound. Ultrason Sonochem 2007; 14:783-89.

Barnett S. Conclusions and recommendations on thermal and non-thermal mechanisms for biological effects of ultrasound. 1996.

Barry BW. Novel mechanisms and devices to enable successful transdermal drug delivery. European Journal of Pharmaceutical Sciences 2001; 14:101-14.

Becker S, Zorec B, Miklavčič D, Pavšelj N. Transdermal transport pathway creation: Electroporation pulse order. Math Biosci 2014; 257:60-68.

Benson HA. Transdermal drug delivery: penetration enhancement techniques. Current drug delivery 2005; 2:23-33.

Bian S, Seth A, Daly D, Carlisle R, Stride E. A multimodal instrument for real-time in situ study of ultrasound and cavitation mediated drug delivery. Review of Scientific Instruments 2017; 88:034302.

Bommannan D, Potts RO, Guy RH. Examination of Stratum Corneum Barrier Function In Vivo by Infrared Spectroscopy. Journal of Investigative Dermatology 1990; 95:403-08.

Boucaud A, Garrigue MA, Machet L, Vaillant Lc, Patat F. Effect of sonication parameters on transdermal delivery of insulin to hairless rats. J Control Release 2002; 81:113-19.

Boucaud A, Machet L, Arbeille B, Machet MC, Sournac M, Mavon A, Patat F, Vaillant L. In vitro study of low-frequency ultrasound-enhanced transdermal transport of fentanyl and caffeine across human and hairless rat skin. Int J Pharm 2001; 228:69-77.

Boucaud A, Montharu J, Machet L, Arbeille B, Machet MC, Patat F, Vaillant L. Clinical, histologic, and electron microscopy study of skin exposed to low-frequency ultrasound. The Anatomical Record: An Official Publication of the American Association of Anatomists 2001; 264:114-19.

Boyd BW, Becker S. Numerical modelling of an acoustically-driven bubble collapse near a solid boundary. Fluid Dynamics Research 2018.

Brabec K, Mornstein V. Detection of ultrasonic cavitation based on low-frequency analysis of acoustic signal. Cent Eur J Biol 2007; 2:213-21.

Bull V, Civale J, Rivens I, ter Haar G. A comparison of acoustic cavitation detection thresholds measured with piezo-electric and fiber-optic hydrophone sensors. Ultrasound Med Biol 2013; 39:2406-21.

Cancel L, Tarbell J, Ben-Jebria A. Fluorescein permeability and electrical resistance of human skin during low frequency ultrasound application. J Pharm Pharmacol 2004; 56:1109-18.

Cevc G. Drug delivery across the skin. Expert opinion on investigational drugs 1997; 6:1887-937.

Chang PP, Chen W-S, Mourad PD, Poliachik SL, Crum LA. Thresholds for inertial cavitation in albunex suspensions under pulsed ultrasound conditions. IEEE Trans Ultrason Ferroelectr Freq Control 2001; 48:161-70.

Chen B, Wei J, Iliescu C. Sonophoretic enhanced microneedles array (SEMA)—Improving the efficiency of transdermal drug delivery. Sensors and Actuators B: Chemical 2010; 145:54-60.

Chen W-S, Brayman AA, Matula TJ, Crum LA. Inertial cavitation dose and hemolysis produced in vitro with or without Optison. Ultrasound Med Biol 2003; 29:725-37.

Choi J, C Carlisle R, Coviello C, Seymour L, Coussios C-C. Non-invasive and real-time passive acoustic mapping of ultrasound-mediated drug delivery, 2014.

Clarys P, Alewaeters K, Jadoul A, Barel A, Manadas RO, Préat V. In vitro percutaneous penetration through hairless rat skin: influence of temperature, vehicle and penetration enhancers. European Journal of Pharmaceutics and Biopharmaceutics 1998; 46:279-83.

Cleveland RO, Sapozhnikov OA, Bailey MR, Crum LA. A dual passive cavitation detector for localized detection of lithotripsy-induced cavitation in vitro. The Journal of the Acoustical Society of America 2000; 107:1745-58.

Coussios CC, Roy RA. Applications of Acoustics and Cavitation to Noninvasive Therapy and Drug Delivery. Annu Rev Fluid Mech 2008; 40:395-420.

Cracknell AP. Ultrasonics. London: Wykeham Publication, 1980.

Dahlan A, Alpar HO, Murdan S. An investigation into the combination of low frequency ultrasound and liposomes on skin permeability. Int J Pharm 2009; 379:139-42.

Dick IP, Scott RC. Pig Ear Skin as an In-vitro Model for Human Skin Permeability. J Pharm Pharmacol 1992; 44:640-45.

Dunne A, Crampton D, Egaña M. Effect of post-exercise hydrotherapy water temperature on subsequent exhaustive running performance in normothermic conditions. Journal of Science and Medicine in Sport 2013; 16:466-71.

El Jastimi R, Lafleur M. A dual-probe fluorescence method to examine selective perturbations of membrane permeability by melittin. Biospectroscopy 1999; 5:133-40.

Farny CH, Holt RG, Roy RA. The Correlation Between Bubble-Enhanced HIFU Heating and Cavitation Power. IEEE Trans Biomed Eng 2010; 57:175-84.

Fernandez P, Martin M, Gonzalez A, Pablos F. HPLC determination of catechins and caffeine in tea. Differentiation of green, black and instant teas. Analyst 2000; 125:421-25.

Francoeur ML, Golden GM, Potts RO. Oleic Acid: Its Effects on Stratum Corneum in Relation to (Trans)Dermal Drug Delivery. Pharm Res 1990; 7:621-27.

Franeta J, Agbaba D, Eric S, Pavkov S, Aleksic M, Vladimirov S. HPLC assay of acetylsalicylic acid, paracetamol, caffeine and phenobarbital in tablets. Il Farmaco 2002; 57:709-13.

Frölich M, Giannotti A, Modell JH. Opioid overdose in a patient using a fentanyl patch during treatment with a warming blanket. Anesthesia & Analgesia 2001; 93:647-48.

Gaitan DF, Crum LA, Church CC, Roy RA. Sonoluminescence and bubble dynamics for a single, stable, cavitation bubble. The Journal of the Acoustical Society of America 1992; 91:3166-83.

Gateau J, Aubry J-F, Pernot M, Fink M, Tanter M. Combined passive detection and ultrafast active imaging of cavitation events induced by short pulses of high-intensity ultrasound. IEEE Trans Ultrason Ferroelectr Freq Control 2011; 58:517-32.

Gay CL, Guy RH, Golden GM, Mak VHW, Francoeur ML. Characterization of Low-Temperature (i.e., <65° C) Lipid Transitions in Human Stratum Corneum. Journal of Investigative Dermatology 1994; 103:233-39.

Golden GM, Guzek DB, Harris RR, McKie JE, Potts RO. Lipid Thermotropic Transitions in Human Stratum Corneum. Journal of Investigative Dermatology 1986; 86:255-59.

Golden GM, Guzek DB, Kennedy AE, McKie JE, Potts RO. Stratum corneum lipid phase transitions and water barrier properties. Biochemistry 1987; 26:2382-88.

Gyöngy M, Coussios C-C. Passive cavitation mapping for localization and tracking of bubble dynamics. The Journal of the Acoustical Society of America 2010; 128:EL175-EL80.

Hallow DM, Mahajan AD, McCutchen TE, Prausnitz MR. Measurement and correlation of acoustic cavitation with cellular bioeffects. Ultrasound Med Biol 2006; 32:1111-22.

Han T, Das DB. Permeability Enhancement for Transdermal Delivery of Large Molecule Using Low-Frequency Sonophoresis Combined with Microneedles. J Pharm Sci 2013; 102:3614-22.

Hao J, Ghosh P, Li SK, Newman B, Kasting GB, Raney SG. Heat effects on drug delivery across human skin. Expert Opinion on Drug Delivery 2016; 13:755-68.

Harding CR. The stratum corneum: structure and function in health and disease. Dermatologic therapy 2004; 17:6-15.

Helga F, Sunali B, Miklós G, Constantin CC. Cavitation-enhanced delivery of insulin in agar and porcine models of human skin. Phys Med Biol 2015; 60:2421.

Henry S, McAllister D, Allen M, Prausnitz M. 1998a Micromachined needles for the transdermal delivery of drugs. *Micro Electro Mechanical Systems, 1998. MEMS 98. Proceedings., The Eleventh Annual International Workshop on*: IEEE, 494-98.

Henry S, McAllister DV, Allen MG, Prausnitz MR. Microfabricated microneedles: a novel approach to transdermal drug delivery. J Pharm Sci 1998b; 87:922-25.

Herwadkar A, Sachdeva V, Taylor LF, Silver H, Banga AK. Low frequency sonophoresis mediated transdermal and intradermal delivery of ketoprofen. Int J Pharm 2012; 423:289-96.

Heymans SV, Martindale CF, Suler A, Pouliopoulos AN, Dickinson RJ, Choi JJ. Simultaneous Ultrasound Therapy and Monitoring of Microbubble-Seeded Acoustic Cavitation Using a Single-Element Transducer. IEEE Trans Ultrason Ferroelectr Freq Control 2017; 64:1234-44.

Hockham N, Coussios CC, Arora M. A real-time controller for sustaining thermally relevant acoustic cavitation during ultrasound therapy. IEEE Trans Ultrason Ferroelectr Freq Control 2010; 57:2685-94.

Hubert M, Vandervieren E. An adjusted boxplot for skewed distributions. Computational statistics & data analysis 2008; 52:5186-201.

Jacobi U, Kaiser M, Toll R, Mangelsdorf S, Audring H, Otberg N, Sterry W, Lademann J. Porcine ear skin: an in vitro model for human skin. Skin Research and Technology 2007; 13:19-24.

Jelenc J, Jelenc J, Miklavcic D, Lebar AM. Low-Frequency Sonoporation in vitro: Experimental System Evaluation. Strojniški vestnik 2012; 58:319-26.

Johnson M, Mitragotri S, Patel A, Blankschtein D, Langer R. Synergistic effects of chemical enhancers and therapeutic ultrasound on transdermal drug delivery. J Pharm Sci 1996; 85:670-79.

Kendall M, Rishworth S, Carter F, Mitchell T. Effects of Relative Humidity and Ambient Temperature on the Ballistic Delivery of Micro-Particles to Excised Porcine Skin. Journal of Investigative Dermatology 2004; 122:739-46.

Khokhlova VA, Bailey MR, Reed JA, Cunitz BW, Kaczkowski PJ, Crum LA. Effects of nonlinear propagation, cavitation, and boiling in lesion formation by high intensity focused ultrasound in a gel phantom. The Journal of the Acoustical Society of America 2006; 119:1834-48.

King DA, Malloy MJ, Roberts AC, Haak A, Yoder CC, O'Brien Jr WD. Determination of postexcitation thresholds for single ultrasound contrast agent microbubbles using double passive cavitation detection. The Journal of the Acoustical Society of America 2010; 127:3449-55.

Kinoshita M, Hynynen K. Key factors that affect sonoporation efficiency in in vitro settings: The importance of standing wave in sonoporation. Biochem Biophys Res Commun 2007; 359:860-65.

Kirjavainen M, Mönkkönen J, Saukkosaari M, Valjakka-Koskela R, Kiesvaara J, Urtti A. Phospholipids affect stratum corneum lipid bilayer fluidity and drug partitioning into the bilayers. J Control Release 1999; 58:207-14.

Kodama T, Tomita Y. Cavitation bubble behavior and bubble-shock wave interaction near a gelatin surface as a study of in vivo bubble dynamics. Applied Physics B: Lasers & Optics 2000; 70:139.

Kost J, Pliquett U, Mitragotri S, Yamamoto A, Langer R, Weaver J. Synergistic effect of electric field and ultrasound on transdermal transport. Pharm Res 1996; 13:633-38.

Krzywinski M, Altman N. 2014 Points of significance: visualizing samples with box plots: Nature Publishing Group.

Kushner J, Blankschtein D, Langer R. Experimental demonstration of the existence of highly permeable localized transport regions in low-frequency sonophoresis. J Pharm Sci 2004; 93:2733-45.

Kushner J, Blankschtein D, Langer R. Evaluation of hydrophilic permeant transport parameters in the localized and non-localized transport regions of skin treated simultaneously with low-frequency ultrasound and sodium lauryl sulfate. J Pharm Sci 2008; 97:906-18.

Kushner J, Blankschtein D, Langer R. Heterogeneity in skin treated with low-frequency ultrasound. J Pharm Sci 2008; 97:4119-28.

Lai C-Y, Wu C-H, Chen C-C, Li P-C. Quantitative relations of acoustic inertial cavitation with sonoporation and cell viability. Ultrasound Med Biol 2006; 32:1931-41.

Lanke SSS, Kolli CS, Strom JG, Banga AK. Enhanced transdermal delivery of low molecular weight heparin by barrier perturbation. Int J Pharm 2009; 365:26-33.

Lauterborn W, Ohl C-D. Cavitation bubble dynamics. Ultrason Sonochem 1997; 4:65-75.

Lavon I, Grossman N, Kost J. The nature of ultrasound–SLS synergism during enhanced transdermal transport. J Control Release 2005; 107:484-94.

Lawrie A, Brisken A, Francis S, Cumberland D, Crossman D, Newman C. Microbubble-enhanced ultrasound for vascular gene delivery. Gene therapy 2000; 7:2023.

Le L, Kost J, Mitragotri S. Combined effect of low-frequency ultrasound and iontophoresis: applications for transdermal heparin delivery. Pharm Res 2000; 17:1151-54.

Lee KL, Zhou Y. Quantitative evaluation of sonophoresis efficiency and its dependence on sonication parameters and particle size. J Ultrasound Med 2015; 34:519-26.

Lee S, Newnham RE, Smith NB. Short ultrasound exposure times for noninvasive insulin delivery in rats using the lightweight cymbal array. IEEE Trans Ultrason Ferroelectr Freq Control 2004a; 51:176-80.

Lee S, Snyder B, Newnham RE, Barrie Smith N. Noninvasive ultrasonic transdermal insulin delivery in rabbits using the light-weight cymbal array. Diabetes technology & therapeutics 2004b; 6:808-15.

Lee SE, Choi KJ, Menon GK, Kim HJ, Choi EH, Ahn SK, Lee SH. Penetration Pathways Induced by Low-Frequency Sonophoresis with Physical and Chemical Enhancers: Iron Oxide Nanoparticles versus Lanthanum Nitrates. J Invest Dermatol 2010; 130:1063-72.

Liao A-H, Lu Y-J, Hung C-R, Yang M-Y. Efficacy of transdermal magnesium ascorbyl phosphate delivery after ultrasound treatment with microbubbles in gel-type surrounding medium in mice. Materials Science and Engineering: C 2016; 61:591-98.

Lindeque BGPMD, Shuler FDMDP, Bates CMMD. Skin Temperatures Generated Following Plaster Splint Application. Orthopedics (Online) 2013; 36:364-67.

Liu J, Lewis T, Prausnitz M. Non-Invasive Assessment and Control of Ultrasound-Mediated Membrane Permeabilization. Pharm Res 1998; 15:918-24.

Makoto O, Shunichi S, Masahiko K, Hitoshi W, Satoko K, Miya I, Makoto K, Masahiko Y, Hiroshi A, Minoru O. Transdermal Delivery of Photosensitizer by the Laser-Induced Stress Wave in Combination with Skin Heating. Japanese Journal of Applied Physics 2002; 41:L814.

Marjukka Suhonen T, A. Bouwstra J, Urtti A. Chemical enhancement of percutaneous absorption in relation to stratum corneum structural alterations. J Control Release 1999; 59:149-61.

Maruani A, Boucaud A, Perrodeau E, Gendre D, Giraudeau B, Machet L. Low-frequency ultrasound sonophoresis to increase the efficiency of topical steroids: A pilot randomized study of humans. Int J Pharm 2010; 395:84-90.

Maruani A, Vierron E, Machet L, Giraudeau B, Halimi JM, Boucaud A. Tolerance of low-frequency ultrasound sonophoresis: a double-blind randomized study on humans. Skin Research and Technology 2012; 18:151-56.

Maxwell AD, Wang T-Y, Yuan L, Duryea AP, Xu Z, Cain CA. A tissue phantom for visualization and measurement of ultrasound-induced cavitation damage. Ultrasound Med Biol 2010; 36:2132-43.

McDannold N, Vykhodtseva N, Hynynen K. Targeted disruption of the blood–brain barrier with focused ultrasound: association with cavitation activity. Physics in Medicine & Biology 2006; 51:793.

McLean J, Mortimer A. A cavitation and free radical dosimeter for ultrasound. Ultrasound in Medicine and Biology 1988; 14:59-64.

Menon GK, Cleary GW, Lane ME. The structure and function of the stratum corneum. Int J Pharm 2012; 435:3-9.

Merino G, Kalia YN, Delgado-Charro MB, Potts RO, Guy RH. Frequency and thermal effects on the enhancement of transdermal transport by sonophoresis. J Control Release 2003; 88:85-94.

Miller DL. Overview of experimental studies of biological effects of medical ultrasound caused by gas body activation and inertial cavitation. Prog Biophys Mol Bio 2007; 93:314-30.

Mitragotri S, Blankschtein D, Langer R. Ultrasound-mediated transdermal protein delivery. Science 1995a; 269:850-53.

Mitragotri S, Blankschtein D, Langer R. Transdermal Drug Delivery Using Low-Frequency Sonophoresis. Pharm Res 1996; 13:411-20.

Mitragotri S, Edwards DA, Blankschtein D, Langer R. A mechanistic study of ultrasonically-enhanced transdermal drug delivery. J Pharm Sci 1995b; 84:697-706.

Mitragotri S, Farrell J, Tang H, Terahara T, Kost J, Langer R. Determination of threshold energy dose for ultrasound-induced transdermal drug transport. J Control Release 2000a; 63:41-52.

Mitragotri S, Kost J. Low-frequency sonophoresis: a noninvasive method of drug delivery and diagnostics. Biotechnology progress 2000; 16:488-92.

Mitragotri S, Kost J. Low-frequency sonophoresis: A review. Adv Drug Deliv Rev 2004; 56:589-601.

Mitragotri S, Ray D, Farrell J, Tang H, Yu B, Kost J, Blankschtein D, Langer R. Synergistic effect of low-frequency ultrasound and sodium lauryl sulfate on transdermal transport. J Pharm Sci 2000b; 89:892-900.

Montes H, Hynynen K. A system for the simultaneous delivery of intraoperative radiation and ultrasound hyperthermia. International Journal of Hyperthermia 1995; 11:109-19.

Morimoto Y, Mutoh M, Ueda H, Fang L, Hirayama K, Atobe M, Kobayashi D. Elucidation of the transport pathway in hairless rat skin enhanced by low-frequency sonophoresis based on the solute–water transport relationship and confocal microscopy. J Control Release 2005; 103:587-97.

Moritz AR, Henriques FC. Studies of Thermal Injury: II. The Relative Importance of Time and Surface Temperature in the Causation of Cutaneous Burns. The American Journal of Pathology 1947; 23:695-720.

Mueller H, Kassack MU, Wiese M. Comparison of the usefulness of the MTT, ATP, and calcein assays to predict the potency of cytotoxic agents in various human cancer cell lines. Journal of Biomolecular Screening 2004; 9:506-15.

Mutoh M, Ueda H, Nakamura Y, Hirayama K, Atobe M, Kobayashi D, Morimoto Y. Characterization of transdermal solute transport induced by low-frequency ultrasound in the hairless rat skin. J Control Release 2003; 92:137-46.

Newshan G. Heat-related toxicity with the fentanyl transdermal patch. Journal of pain and symptom management 1998; 16:277.

Nour WMN, Dulias U, Schneider J, Gahr KHZ. The effect of surface finish and cavitating liquid on the cavitation erosion of alumina and silicon carbide ceramics, 2007.

O'Brien Jr WD. Ultrasound–biophysics mechanisms. Prog Biophys Mol Bio 2007; 93:212-55.

Ogiso T, Hirota T, Iwaki M, Hino T, Tanino T. Effect of temperature on percutaneous absorption of terodiline, and relationship between penetration and fluidity of the stratum corneum lipids. Int J Pharm 1998; 176:63-72.

Ogura M, Paliwal S, Mitragotri S. Low-frequency sonophoresis: Current status and future prospects. Adv Drug Deliv Rev 2008; 60:1218-23.

Oh J-H, Park H-H, Do K-Y, Han M, Hyun D-H, Kim C-G, Kim C-H, Lee SS, Hwang S-J, Shin S-C. Influence of the delivery systems using a microneedle array on the permeation of a hydrophilic molecule, calcein. European journal of pharmaceutics and biopharmaceutics 2008; 69:1040-45.

Ohara N, Takayama K, Nagai T. Combined Effect of d-Limonene Pretreatment and Temperature on the Rat Skin Permeation of Lipophilic and Hydrophilic Drugs, 1995.

Owen CM, Pal L, Mumford SL, Freeman R, Isaac B, McDonald L, Santoro N, Taylor HS, Wolff EF. Effects of hormones on skin wrinkles and rigidity vary by race/ethnicity: four-year follow-up from the ancillary skin study of the Kronos Early Estrogen Prevention Study. Fertility and sterility 2016; 106:1170-75. e3.

Paliwal S, Menon GK, Mitragotri S. Low-Frequency Sonophoresis: Ultrastructural Basis for Stratum Corneum Permeability Assessed Using Quantum Dots. J Invest Dermatol 2006; 126:1095-101.

Papir YS, Hsu K-H, Wildnauer RH. The mechanical properties of stratum corneum: I. The effect of water and ambient temperature on the tensile properties of newborn rat stratum corneum. Biochimica et Biophysica Acta (BBA) - General Subjects 1975; 399:170-80.

Park D, Ryu H, Kim HS, Kim Y-s, Choi K-S. Sonophoresis using ultrasound contrast agents for transdermal drug delivery: an in vivo experimental study. Ultrasound Med Biol 2012; 38:642-50.

Park D, Yoon J, Park J, Jung B, Park H, Seo J. Transdermal drug delivery aided by an ultrasound contrast agent: an in vitro experimental study. Open Biomed Eng J 2010; 4:56.

Park EJ, Werner J, Smith N. Ultrasound Mediated Transdermal Insulin Delivery in Pigs Using a Lightweight Transducer. Pharm Res 2007; 24:1396-401.

Pathan IB, Setty CM. Chemical penetration enhancers for transdermal drug delivery systems. Tropical Journal of Pharmaceutical Research 2009; 8.

Petronilli V, Miotto G, Canton M, Brini M, Colonna R, Bernardi P, Di Lisa F. Transient and long-lasting openings of the mitochondrial permeability transition pore can be monitored directly in intact cells by changes in mitochondrial calcein fluorescence. Biophys J 1999; 76:725-34.

Polat BE, Deen WM, Langer R, Blankschtein D. A physical mechanism to explain the delivery of chemical penetration enhancers into skin during transdermal sonophoresis — Insight into the observed synergism. J Control Release 2012; 158:250-60.

Polat BE, Figueroa PL, Blankschtein D, Langer R. Transport pathways and enhancement mechanisms within localized and non-localized transport regions in skin treated with low-frequency sonophoresis and sodium lauryl sulfate. J Pharm Sci 2011a; 100:512-29.

Polat BE, Hart D, Langer R, Blankschtein D. Ultrasound-mediated transdermal drug delivery: Mechanisms, scope, and emerging trends. J Control Release 2011b; 152:330-48.

Potts RO, Francoeur ML. Lipid biophysics of water loss through the skin. Proceedings of the National Academy of Sciences of the United States of America 1990; 87:3871-73.

Potts RO, Golden GM, Francoeur ML, Mak VHW, Guy RH. Mechanism and enhancement of solute transport across the stratum corneum. J Control Release 1991; 15:249-60.

Prausnitz MR. A practical assessment of transdermal drug delivery by skin electroporation. Adv Drug Deliv Rev 1999; 35:61-76.

Prausnitz MR, Bose VG, Langer R, Weaver JC. Electroporation of mammalian skin: a mechanism to enhance transdermal drug delivery. Proceedings of the National Academy of Sciences 1993; 90:10504-08.

Prausnitz MR, Langer R. Transdermal drug delivery. Nature Biotechnol 2008; 26:1261-68.

Prausnitz MR, Mitragotri S, Langer R. Current status and future potential of transdermal drug delivery. Nature reviews Drug discovery 2004; 3:115.

Price GJ, Lenz EJ. The use of dosimeters to measure radical production in aqueous sonochemical systems. Ultrasonics 1993; 31:451-56.

Prodduturi S, Sadrieh N, Wokovich AM, Doub WH, Westenberger BJ, Buhse L. Transdermal delivery of fentanyl from matrix and reservoir systems: effect of heat and compromised skin. J Pharm Sci 2010; 99:2357-66.

Qiu Y, Luo Y, Zhang Y, Cui W, Zhang D, Wu J, Zhang J, Tu J. The correlation between acoustic cavitation and sonoporation involved in ultrasound-mediated DNA transfection with polyethylenimine (PEI) in vitro. J Control Release 2010; 145:40-48.

Rangsimawong W, Obata Y, Opanasopit P, Ngawhirunpat T, Takayama K. Enhancement of Galantamine HBr Skin Permeation Using Sonophoresis and Limonene-Containing PEGylated Liposomes. AAPS PharmSciTech 2018; 19:1093-104.

Rich KT. 2017 Characterization of cavitation effects in therapeutic ultrasound: sonophoresis experiments and quantitative emission measurements: University of Cincinnati.

Rich KT, Hoerig CL, Rao MB, Mast TD. Relations between acoustic cavitation and skin resistance during intermediate-and high-frequency sonophoresis. J Control Release 2014; 194:266-77.

Rifai B, Arvanitis CD, Bazan-Peregrino M, Coussios C-C. Cavitation-enhanced delivery of macromolecules into an obstructed vessel. The Journal of the Acoustical Society of America 2010; 128:EL310-EL15.

Robertson J, Becker S. Influence of Acoustic Reflection on the Inertial Cavitation Dose in a Franz Diffusion Cell. Ultrasound Med Biol 2018; 44:1100-09.

Rodrigues CI, Marta L, Maia R, Miranda M, Ribeirinho M, Máguas C. Application of solid-phase extraction to brewed coffee caffeine and organic acid determination by UV/HPLC. Journal of Food Composition and Analysis 2007; 20:440-48.

Salgaonkar VA, Datta S, Holland CK, Mast TD. Passive cavitation imaging with ultrasound arrays. The Journal of the Acoustical Society of America 2009; 126:3071-83.

Sarheed O, Abdul Rasool BK. Development of an Optimised Application Protocol For Sonophoretic Transdermal Delivery of a Model Hydrophilic Drug. Open Biomed Eng J 2011; 5:14-24.

Sarheed O, Frum Y. Use of the skin sandwich technique to probe the role of the hair follicles in sonophoresis. Int J Pharm 2012; 423:179-83.

Schoellhammer CM. 2015 Use of Physical Enhancers for Gastrointestinal and Transdermal Drug Delivery. *Chemical Engineering*. Cambridge, USA: Massachusetts Institute of Technology.

Schoellhammer CM, Polat BE, Mendenhall J, Maa R, Jones B, Hart DP, Langer R, Blankschtein D. Rapid skin permeabilization by the simultaneous application of dual-frequency, high-intensity ultrasound. J Control Release 2012; 163:154-60.

Seto JE, Polat BE, Lopez RFV, Blankschtein D, Langer R. Effects of ultrasound and sodium lauryl sulfate on the transdermal delivery of hydrophilic permeants: Comparative in vitro studies with full-thickness and split-thickness pig and human skin. J Control Release 2010; 145:26-32.

Shahzad Y, Louw R, Gerber M, du Plessis J. Breaching the skin barrier through temperature modulations. J Control Release 2015; 202:1-13.

Shomaker TS, Zhang J, Ashburn MA. Assessing the Impact of Heat on the Systemic Delivery of Fentanyl Through the Transdermal Fentanyl Delivery System. Pain Medicine 2000; 1:225-30.

Silva CL, Nunes SCC, Eusébio MES, Pais AACC, Sousa JJS. Thermal Behaviour of Human Stratum Corneum. Skin Pharmacology and Physiology 2006; 19:132-39.

Smith N, Lee S, Maione E, Roy RB, McElligott S. Ultrasound-mediated transdermal transport of insulin in vitro through human skin using novel transducer designs. Ultrasound Med Biol 2003; 29:311-17.

Smith NB. Perspectives on transdermal ultrasound mediated drug delivery. Int J Nanomedicine 2007; 2:585-94.

Souza J, Meira A, Volpato NM, Mayorga P, Gottfried C. Effect of phonophoresis on skin permeation of commercial anti-inflammatory gels: sodium diclofenac and ketoprofen. Ultrasound Med Biol 2013; 39:1623-30.

Spitzer M, Wildenhain J, Rappsilber J, Tyers M. BoxPlotR: a web tool for generation of box plots. Nature methods 2014; 11:121.

Sprawls P. The Physical Principles of Medical Imaging. Wisconsin: Medical Physics Publishing, 1995.

Sundaram J, Mellein BR, Mitragotri S. An Experimental and Theoretical Analysis of Ultrasound-Induced Permeabilization of Cell Membranes. Biophys J 2003; 84:3087-101.

Tachibana K, Tachibana S. Transdermal delivery of insulin by ultrasonic vibration. J Pharm Pharmacol 1991; 43:270-71.

Tang H, Blankschtein D, Langer R. Effects of Low-Frequency Ultrasound on the Transdermal Permeation of Mannitol: Comparative Studies with In Vivo and In Vitro Skin. J Pharm Sci 2002b; 91:1776-94.

Tang H, Mitragotri S, Blankschtein D, Langer R. Theoretical Description of Transdermal Transport of Hydrophilic Permeants: Application to Low-Frequency Sonophoresis. J Pharm Sci 2001; 90:545-68.

Tang H, Wang CCJ, Blankschtein D, Langer R. An Investigation of the Role of Cavitation in Low-Frequency Ultrasound-Mediated Transdermal Drug Transport. Pharm Res 2002a; 19:1160-69.

Terahara T, Mitragotri S, Kost J, Langer R. Dependence of low-frequency sonophoresis on ultrasound parameters; distance of the horn and intensity. Int J Pharm 2002a; 235:35-42.

Terahara T, Mitragotri S, Langer R. Porous resins as a cavitation enhancer for low-frequency sonophoresis. J Pharm Sci 2002b; 91:753-59.

Tezel A, Dokka S, Kelly S, Hardee GE, Mitragotri S. Topical delivery of anti-sense oligonucleotides using low-frequency sonophoresis. Pharm Res 2004; 21:2219-25.

Tezel A, Mitragotri S. Interactions of Inertial Cavitation Bubbles with Stratum Corneum Lipid Bilayers during Low-Frequency Sonophoresis. Biophys J 2003a; 85:3502-12.

Tezel A, Paliwal S, Shen Z, Mitragotri S. Low-frequency ultrasound as a transcutaneous immunization adjuvant. Vaccine 2005; 23:3800-07.

Tezel A, Sens A, Mitragotri S. Investigations of the role of cavitation in low-frequency sonophoresis using acoustic spectroscopy. J Pharm Sci 2002; 91:444-53.

Tezel A, Sens A, Mitragotri S. Description of transdermal transport of hydrophilic solutes during low-frequency sonophoresis based on a modified porous pathway model. J Pharm Sci 2003b; 92:381-93.

Tezel A, Sens A, Tuchscherer J, Mitragotri S. Frequency Dependence of Sonophoresis. Pharm Res 2001; 18:1694-700.

Tominaga K, Tojo K. Effect of Environmental Temperature on Transdermal Drug Penetration. Biological and Pharmaceutical Bulletin 2010; 33:1983-87.

Trommer H, Neubert R. Overcoming the stratum corneum: the modulation of skin penetration. Skin pharmacology and physiology 2006; 19:106-21.

Ueda H, Mutoh M, Seki T, Kobayashi D, Morimoto Y. Acoustic cavitation as an enhancing mechanism of low-frequency sonophoresis for transdermal drug delivery. Biological and Pharmaceutical Bulletin 2009; 32:916-20.

Ueda H, Ogihara M, Sugibayashi K, Morimoto Y. Change in the electrochemical properties of skin and the lipid packing in stratum corneum by ultrasonic irradiation. Int J Pharm 1996; 137:217-24.

Van Duzee BF. Thermal Analysis Of Human Stratum Corneum. Journal of Investigative Dermatology 1975; 65:404-08.

Vanakoski J, Seppälä T, Sievi E, Lunell E. Exposure to high ambient temperature increases absorption and plasma concentrations of transdermal nicotine. Clinical Pharmacology & Therapeutics 1996; 60:308-15.

Vanbever R, Preat V. In vivo efficacy and safety of skin electroporation. Adv Drug Deliv Rev 1999; 35:77-88.

Verdier-Sévrain S, Bonté F. Skin hydration: a review on its molecular mechanisms. Journal of cosmetic dermatology 2007; 6:75-82.

Vichare V, Mujgond P, Tambe V, Dhole S. Simultaneous spectrophotometric determination of paracetamol and caffeine in tablet formulation. International Journal of PharmTech Research 2010; 2:2512-16.

Weimann LJ, Wu J. Transdermal delivery of poly-l-lysine by sonomacroporation. Ultrasound Med Biol 2002; 28:1173-80.

Whyte WA, Orlando DA, Hnisz D, Abraham BJ, Lin CY, Kagey MH, Rahl PB, Lee TI, Young RA. Master transcription factors and mediator establish super-enhancers at key cell identity genes. Cell 2013; 153:307-19.

Williamson C, Scholtz JR. Time-Temperature Relationships in Thermal Blister Formation*. Journal of Investigative Dermatology 1949; 12:41-47.

Wolff E, Pal L, Altun T, Madankumar R, Freeman R, Amin H, Harman M, Santoro N, Taylor HS. Skin wrinkles and rigidity in early postmenopausal women vary by race/ethnicity: baseline characteristics of the skin ancillary study of the KEEPS trial. Fertility and sterility 2011; 95:658-62. e3.

Wolloch L, Kost J. The importance of microjet vs shock wave formation in sonophoresis. J Control Release 2010; 148:204-11.

Wong T-W, Chen C-H, Huang C-C, Lin C-D, Hui S-W. Painless electroporation with a new needle-free microelectrode array to enhance transdermal drug delivery. J Control Release 2006; 110:557-65.

Wu J, Chappelow J, Yang J, Weimann L. Defects generated in human stratum corneum specimens by ultrasound. Ultrasound in Medicine and Biology 1998; 24:705-10.

Wu KS, van Osdol WW, Dauskardt RH. Mechanical properties of human stratum corneum: Effects of temperature, hydration, and chemical treatment. Biomaterials 2006; 27:785-95.

Xie Y, Xu B, Gao Y. Controlled transdermal delivery of model drug compounds by MEMS microneedle array. Nanomedicine: Nanotechnology, Biology and Medicine 2005; 1:184-90.

Yao-Sheng T, Choi JJ, Konofagou EE. Identifying the Inertial Cavitation Pressure Threshold and Skull Effects in a Vessel Phantom Using Focused Ultrasound and Microbubbles. AIP Conf Prec 2010; 1215:186-89.

Yin L, Qin FH, Zhou Y, Qi X. Enhancing percutaneous permeability of sinomenine hydrochloride using dual-frequency sonophoresis. Journal of Drug Delivery Science and Technology 2016; 36:62-67.

Zell K, Sperl J, Vogel M, Niessner R, Haisch C. Acoustical properties of selected tissue phantom materials for ultrasound imaging. Physics in Medicine & Biology 2007; 52:N475.

Zhai H, Ebel JP, Chatterjee R, Stone KJ, Gartstein V, Juhlin KD, Pelosi A, Maibach HI. Hydration vs. skin permeability to nicotinates in man. Skin Research and Technology 2002; 8:13-18.

Zhou Y, Cui J, Deng CX. Dynamics of Sonoporation Correlated with Acoustic Cavitation Activities. Biophys J 2008; 94:L51-L53.

Zorec B, Becker S, Reberšek M, Miklavčič D, Pavšelj N. Skin electroporation for transdermal drug delivery: The influence of the order of different square wave electric pulses. Int J Pharm 2013; 457:214-23.

Zorec B, Jelenc J, Miklavčič D, Pavšelj N. Ultrasound and electric pulses for transdermal drug delivery enhancement: Ex vivo assessment of methods with in vivo oriented experimental protocols. Int J Pharm 2015; 490:65-73.